

Spatio-Temporal Modelling of Land Use/Land Cover and Climate Change Effects on Surface Runoff and River Discharge in the Klang River Basin

Majid Azari

**Thesis submitted to the University of Nottingham for the
degree of Doctor of Philosophy**

ABSTRACT

Urbanisation, climate change, and their impacts on hydrological processes are a growing concern in urban watersheds around the world. This research examined the complex relationship between land use and land cover (LULC) change, precipitation variability, and their combined spatio-temporal impacts on surface runoff and river discharge in the Klang River basin, Malaysia.

The research utilised an integrated approach, combining outputs from LULC and climate models with a hydrological model. Trend analysis of LULC, precipitation, and temperature were also carried out, to detect trends in these parameters.

The maximum likelihood algorithm and The Decision Forest – Markov Chain models were used for LULC classification and LULC change modelling. Mann-Kendall and Sen’s Slope statistical methods were used for trend analysis. Lastly, the Soil and Water Assessment Tool (SWAT) was used for the hydrological modelling of surface runoff and river discharge.

The results of the study, reveal a significant trend in LULC, mostly attributed to the increasing trend in urban land, where urban areas increased by 147.5 km² (11.8 %), and natural vegetation decreased by 73.4 km² (5.9%) in the period 1999 to 2017. Similarly, increasing trends

were observed in precipitation intensity and frequency in urban areas. An increasing trend was also detected in temperature, specifically land surface temperature.

The hydrological modelling results demonstrate the relationship between these changes and increased surface runoff and river discharge. The results also illustrate that LULC changes have a more significant impact on hydrological processes compared to climate change, especially in urbanised regions.

However, the magnitude and contribution of these changes are still uncertain in many watersheds in Malaysia. Hence, this study addressed the gap in research by integrating the impact of both LULC change and climate change variables on hydrological processes, where previous studies only considered one or the other.

The outcome of the quantitative analysis of this study can help policymakers prioritise the protection and conservation of urban green spaces and forests, implement green and climate-resilient infrastructure, and consider the potential future impacts of both LULC and climate change on hydrological processes in urban planning and decision making.

Keywords: Land use change, hydro-meteorological trends, hydrological modelling, SWAT, surface runoff.

ACKNOWLEDGEMENT

First and foremost, I would like to express my sincere gratitude to my supervisors, Prof. Andy Chan, and Dr. Lawal Billa, for their invaluable advice, continuous support, and patience during my PhD study. Their immense knowledge and experience have encouraged me throughout the completion of this research and thesis.

I would like to extend my gratitude to the staff at the Department of Irrigation and Drainage (DID) Malaysia and the Meteorological Department (MET) Malaysia, for the valuable information they provided for this research.

Lastly, I would like to thank my family, my brothers Saeid and Masoud, and my sister Rayhaneh for always being there for me supporting me and encouraging me throughout the completion of my research. And most importantly, I would like to thank my mother for all she has done for me and for always being there for me.

Finally, I would like to dedicate this thesis to the memory of my late father, who will always be remembered and be my inspiration.

PUBLICATIONS

Journal

- Azari, M., Billa, L., & Chan, A. (2022). Multi-temporal analysis of past and future land cover change in the highly urbanised state of Selangor, Malaysia. *Ecological Processes*, 11(2).
- Li-An, C., Billa, L., & Azari M. (2018). Anthropocene climate and landscape change that increases flood disasters. *International Journal of Hydrology*, 2(4), 487-491.

Conference Proceeding

- Azari, M., Billa, L., & Chan, A. (2020). Modeling of land-use/land-cover change and its impact on the local climate of Klang River Basin. *IOP Conference Series: Earth and Environmental Science*, 489, 012017.

Table of Contents

ABSTRACT	1
ACKNOWLEDGEMENT	3
PUBLICATIONS	4
LIST OF FIGURES	9
LIST OF TABLES	10
LIST OF ABBREVIATION	12
CHAPTER 1: INTRODUCTION	16
1.1 BACKGROUND	16
1.2 PROBLEM STATEMENT	20
1.3 AIM AND OBJECTIVES	24
1.4 RESEARCH QUESTIONS	24
1.5 SIGNIFICANCE OF THE STUDY	25
1.6 SCOPE	27
1.7 THESIS OUTLINE	28
CHAPTER 2: LITERATURE REVIEW	31
2.1 GENERAL FACTORS AFFECTING SURFACE RUNOFF AND RIVER DISCHARGE	31
2.2 LAND USE AND LAND COVER CHANGE IMPACTS ON SURFACE RUNOFF AND RIVER DISCHARGE	33
2.2.1 <i>SURFACE RUNOFF AND RIVER DISCHARGE DYNAMICS IN RESPONSE TO LAND USE AND LAND COVER CHANGES IN MALAYSIA</i>	36
2.3 LAND USE AND LAND COVER CHANGE IMPACTS ON CLIMATE VARIABLES	39
2.3.1 <i>IMPACTS ON BIOGEOCHEMICAL CYCLES</i>	39
2.3.2 <i>IMPACTS ON BIOGEOPHYSICAL PROCESSES</i>	40
2.3.2.1 <i>IMPACT OF URBANISATION ON PRECIPITATION</i>	45
2.3.3 <i>IMPACTS OF LAND USE AND LAND COVER CHANGE ON LOCAL CLIMATE IN MALAYSIA</i>	48
2.4 IMPACT OF CLIMATE VARIABILITY ON SURFACE RUNOFF AND RIVER DISCHARGE	49
2.4.1 <i>IMPACT OF PRECIPITATION CHANGES ON SURFACE RUNOFF AND RIVER DISCHARGE IN MALAYSIA</i>	50
2.5 TRENDS IN LAND USE AND LAND COVER, PRECIPITATION AND TEMPERATURE	52
2.5.1 <i>GLOBAL TRENDS IN LAND USE AND LAND COVER</i>	52

2.5.1.1 LAND USE AND LAND COVER TRENDS IN MALAYSIA	53
2.5.2 GLOBAL TRENDS IN PRECIPITATION AND TEMPERATURE	56
2.5.2.1 PRECIPITATION AND TEMPERATURE TRENDS IN MALAYSIA	59
2.5.2.2 INDICES FOR TREND ANALYSIS	62
2.6 LAND USE AND LAND COVER, HYDROLOGICAL AND CLIMATE MODELLING METHODS	62
2.6.1 LAND USE AND LAND COVER MODELLING METHODS	62
2.6.2 HYDROLOGICAL MODELLING METHODS	65
2.6.2.1 MAIN HYDROLOGICAL MODEL CLASSIFICATION	66
2.6.2.1.1 STOCHASTIC MODELS	66
2.6.2.1.2 DETERMINISTIC MODELS	67
2.6.2.2 HYDROLOGICAL MODEL CLASSIFICATION BASED ON STRUCTURE	70
2.6.3 CLIMATE MODELLING METHODS	74
2.6.3.1 GLOBAL CLIMATE MODELS	74
2.6.3.2 REPRESENTATIVE CONCENTRATION PATHWAYS	76
2.6.3.3 GLOBAL CLIMATE MODEL DOWNSCALING	79
2.6.3.4 CLIMATE MODELLING IN MALAYSIA	80
2.7 SUMMARY OF LITERATURE REVIEW	83
CHAPTER 3: METHODOLOGY	86
3.1 INTRODUCTION	86
3.2 STUDY AREA	87
3.2.1 CLIMATE	88
3.2.2 GEOLOGY AND SOIL	89
3.2.3 DRAINAGE AND WATER RESOURCES	90
3.3 DATA ACQUISITION	91
3.3.1 LAND USE AND LAND COVER DATA	91
3.3.2 HYDRO-CLIMATIC DATA	92
3.3.3 HYDROLOGICAL MODELLING DATA	95
3.3.3.1 DIGITAL ELEVATION MAP	95
3.3.3.2 SLOPE	95
3.3.3.3 SOIL	96
3.3.3.4 LAND USE AND LAND COVER	98
3.3.3.5 WEATHER	98
3.3.3.6 STREAMFLOW DATA	101
3.4 METHODOLOGY	101
3.4.1 ANALYSIS OF SPATIO-TEMPORAL TRENDS IN LAND-USE AND LAND COVER	101
3.4.1.1 LAND USE AND LAND COVER CLASSIFICATION	103
3.4.1.1.1 ACCURACY ASSESSMENT	103
3.4.1.2 LAND USE AND LAND COVER CHANGE MODELLING	103
3.4.1.2.1 CHANGE ANALYSIS	105
3.4.1.2.2 TRANSITION POTENTIAL MODELLING	105
3.4.1.2.3 CHANGE PREDICTION	106
3.4.1.2.4 VALIDATION	107

3.4.2 ANALYSIS OF SPATIO-TEMPORAL TRENDS IN PRECIPITATION AND TEMPERATURE	108
3.4.2.1 DATA PREPROCESSING	109
3.4.2.1.1 NORMALITY AND AUTOCORRELATION	109
3.4.2.1.2 OUTLIER DETECTION	110
3.4.2.1.3 FILLING MISSING DATA	111
3.4.2.1.4 VALIDATION OF ERA5 DATA	111
3.4.2.1.5 DOWNSCALING OF THE GCM MODELS	113
3.4.2.2 SELECTED INDICES FOR PRECIPITATION AND TEMPERATURE ANALYSIS	114
3.4.2.3 MANN-KENDALL TREND STATISTICS	115
3.4.2.3.1 SEN'S SLOPE	117
3.4.2.4 LAND SURFACE TEMPERATURE TREND ANALYSIS	118
3.4.3 DEVELOPMENT OF SPATIO-TEMPORAL HYDROLOGICAL MODEL	123
3.4.3.1 SWAT MODEL DESCRIPTION	123
3.4.3.2 MODEL SETUP	126
3.4.3.3 SENSITIVITY ANALYSIS	128
3.4.3.4 CALIBRATION AND VALIDATION	129
3.4.3.4.1 OBJECTIVE FUNCTIONS	131
3.4.3.5 HYDROLOGICAL MODELLING FOR FUTURE SCENARIOS	132
3.4.4 SUMMARY OF METHODOLOGY	133
CHAPTER 4: RESULTS AND DISCUSSION	135
4.1 ANALYSIS OF SPATIO-TEMPORAL TRENDS IN LAND-USE AND LAND COVER	135
4.1.1 LAND USE AND LAND COVER CLASSIFICATION	135
4.1.2 LAND USE AND LAND COVER CHANGE MODELLING	139
4.1.2.1 MODEL VALIDATION	140
4.1.3 DISCUSSION	142
4.2 ANALYSIS OF SPATIO-TEMPORAL TRENDS IN PRECIPITATION, TEMPERATURE AND RIVER DISCHARGE	150
4.2.1 PRECIPITATION TRENDS	150
4.2.1.1 ANNUAL TREND	150
4.2.1.2 SEASONAL TREND	157
4.2.2 TEMPERATURE TRENDS	166
4.2.2.1 LAND SURFACE TEMPERATURE	170
4.2.3 TRENDS IN FUTURE SCENARIOS	173
4.2.3.1 PRECIPITATION TREND	173
4.2.3.2 TEMPERATURE TREND	176
4.2.4 RIVER DISCHARGE TRENDS	179
4.2.5 DISCUSSION	181
4.3 QUANTITATIVE ANALYSIS OF SPATIO-TEMPORAL HYDROLOGICAL MODELLING	190
4.3.1 SWAT MODEL PARAMETER SENSITIVITY ANALYSIS	190
4.3.2 SWAT MODEL CALIBRATION AND VALIDATION	191
4.3.3 IMPACTS OF LAND USE AND LAND COVER AND PRECIPITATION CHANGES ON SURFACE RUNOFF	193

4.3.3.1 IMPACTS UNDER FUTURE SCENARIOS	196
4.3.4 IMPACTS OF LAND USE AND LAND COVER AND PRECIPITATION CHANGES ON RIVER DISCHARGE UNDER FUTURE SCENARIOS	200
4.3.5 DISCUSSION	202
4.4 SUMMARY OF RESULTS AND DISCUSSION	206
CHAPTER 5: CONCLUSION	209
<hr/>	
5.1 CONCLUSION	209
5.2 STUDY LIMITATIONS	212
5.3 RECOMMENDATIONS	213
5.3.1 RECOMMENDATIONS FOR FUTURE RESEARCH	213
5.3.2 RECOMMENDATIONS FOR POLICY MAKERS AND STAKEHOLDERS	214
REFERENCES	216
<hr/>	
APPENDIX	257
<hr/>	
APPENDIX A – DEFINITION OF THE ETCCDI INDICES.	257
APPENDIX B - LULC MODELLING DRIVER VARIABLES	260
APPENDIX C – THE GAINS AND LOSSES AND NET GAIN FOR THE YEAR 1999-2006 AND 2006-2017	263
APPENDIX D – AVERAGE MONTHLY PRECIPITATION	264

LIST OF FIGURES

Figure 2.3-1: Aerosol-Enhanced Conditional Instability Increasing Rainfall Levels In Sichuan. Acronyms: MSE (Moist Static Energy), SW (Shortwave Radiation), SH (Surface Sensible Heat Flux), And LH (Surface Latent Heat Flux) (Fan et al., 2015)..... 47

Figure 2.5-1: Yearly Surface Temperature Compared To The 20th-Century Average From 1880-2020. Blue Bars Indicate Cooler-Than-Average Years; Red Bars Show Warmer-Than-Average Years (NOAA, 2021). 57

Figure 2.5-2: Precipitation Worldwide, 1901-2019 (Blunden et al., 2020) 58

Figure 2.5-3: Annual Mean Temperature Trend For Four Meteorological Stations In Malaysia. (Malaysian Meteorological Department, 2009)..... 60

Figure 2.6-1: The Classification Of Hydrological Models (Dwarakish and Ganasri, 2015). 66

Figure 3.1-1: The Summary Flowchart Of The Overall Methodology. 87

Figure 3.2-1: Map Of The Klang River Basin..... 88

Figure 3.2-2: (a) Northeast Monsoon And (b) Southwest Monsoon (Bakar et al., 2020)..... 89

Figure 3.3-1: Location Of Selected Hydro-Climatic Stations. 93

Figure 3.3-2: A.Elevation Map, B.Slope Map And C.Soil Map Of The Study Area..... 97

Figure 3.3-3: Ground Stations And CHIRPS Locations For Precipitation Data. 101

Figure 3.4-1: Summary Flowchart Of The Land-Use And Land Cover Modelling. 102

Figure 3.4-2: Summary Flowchart Of The Hydro-Climatic Trend Analysis. 108

Figure 3.4-3: ERA5 grid for the study area, from which temperature data is collected..... 113

Figure 3.4-4: Summary Flowchart Of The Land Surface Temperature Modelling. 119

Figure 3.4-5: Summary Flowchart Of The Hydrological Modelling Using SWAT Model. 124

Figure 4.1-1: Lulc Map Of Year 1999, 2006 And 2017..... 136

Figure 4.1-2: The Simulated LULC Map For Year 2030..... 140

Figure 4.1-3: The Area Under The Curve Of The Total Operating Characteristic, Showcasing The Validation Of The Model. 141

Figure 4.1-4: The Quantity And Allocation Disagreement, Showcasing The Validation Of The Simulated Map With The Reference Map..... 142

Figure 4.1-5: The Increase Of Built-Up Areas For The Period 1999 To 2030..... 147

Figure 4.1-6: Urban Expansion Into Forest Areas In Bukit Jelutong (Image Obtained From Google Earth, In Year 2022)..... 148

Figure 4.2-1: Average Annual Precipitation In Klang River Basin. 152

Figure 4.2-2: The Annual Precipitation Trend For Klang River Basin (Significance Level Taken At 0.01 And 0.05)..... 153

Figure 4.2-3: The Graph Of Average Annual Precipitation For Stations Located Within Built Up Areas..... 154

Figure 4.2-4: The SDII Seasonal Trend Map For NWM, SWM, Intm1 And Intm2. 159

Figure 4.2-5: The R10mm Seasonal Trend Map For NWM, SWM, Intm1, And Intm2. 161

Figure 4.2-6: The R30mm Seasonal Trend Maps For NEM, SWM, Intm1 And Intm2..... 163

Figure 4.2-7: The R95p Seasonal Trend Maps For NEM, SWM, Intm1 And Intm2. 165

Figure 4.2-8: The Average Annual ERA5 Temperature For The Period 1979-2018. 167

Figure 4.2-9: Land Surface Temperature For Year 1999, 2006 And 2017. 172

Figure 4.2-10: Mean Annual Temperature For Klang River Basin (2006-2099), Under Different RCP Scenarios. 177

Figure 4.2-11: Average Annual And Monthly River Discharge At Stations Sungai Batu And Jambatan Sulaiman..... 180

Figure 4.3-1: SWAT Model Calibration 95PPU..... 192

Figure 4.3-2: SWAT Model Validation 95PPU..... 193

Figure 4.3-3: Surface Runoff For The Land-Use And Land Cover Maps Of 1999, 2006 And 2017..... 195

Figure 4.3-4: Simulated Surface Runoff For LULC 2030 Scenario. 197

Figure 4.3-5: Simulated Surface Runoff For Climate Change Scenarios RCP4.5 And RCP8.5.	198
Figure 4.3-6: Simulated Surface Runoff For Combined LULC 2030 And RCP4.5 Scenario, And LULC 2030 And RCP8.5 Scenario.	200

LIST OF TABLES

Table 1.2-1: List Of Flood Events In Malaysia.	21
Table 2.6-1: Comparison Of The Basic Structure Of Rainfall-Runoff Models (Devi et al., 2015).	72
Table 2.7-1: Summary Of Literature Review.	83
Table 3.3-1: Landsat Image Information Used In Study.	91
Table 3.3-2: Station Name, ID, Coordinates, And Period Of Data, For Selected Stations.	93
Table 3.3-3: Details Of The Global Climate Models Used In The Study.	94
Table 3.3-4: FAO Soil Code And Soil Classification.	98
Table 3.3-5: LULC Classification And SWAT Code.	98
Table 3.4-1: Statistics Comparing ERA5 Data With Observed Data.	112
Table 3.4-2: Rainfall intensity categories according to Department of Irrigation and Drainage.	115
Table 3.4-3: Summary Of Methodology.	133
Table 4.1-1: LULC Area For Each Classification, For The Years 1999, 2006, And 2017.	137
Table 4.1-2: The Producer's And User's Accuracy For The LULC Classification Maps Of Years 1999,2006, And 2017, Showing The Accuracy Of The LULC Maps.	137
Table 4.1-3: Error Matrix For The LULC Maps Of 1999, 2006, And 2017, Showing Accuracy Of The LULC Maps.	138
Table 4.1-4: LULC Area And Changes Between Years 2017 And 2030.	140
Table 4.2-1: Trends For Annual Precipitation.	155
Table 4.2-2: Annual Trend For SDII, R10mm, R30mm, And R95p.	156
Table 4.2-3: Seasonal Trend For SDII.	159
Table 4.2-4: Seasonal Trend For R10mm.	161
Table 4.2-5: Seasonal Trend For R30mm.	163
Table 4.2-6: Seasonal Trend For R95p.	165
Table 4.2-7: The Annual And Seasonal Mean Temperature Trend.	168
Table 4.2-8: The Annual And Seasonal Txx Trend.	169
Table 4.2-9: The Annual And Seasonal Tnx Trend.	169
Table 4.2-10: Annual Precipitation Trend For Future Climate Scenarios For The Period 2006-2099.	174
Table 4.2-11: Monthly Precipitation Trend For Future Climate Scenarios For The Period 2006-2099.	174
Table 4.2-12: SDII Trend For Future Climate Scenarios.	176
Table 4.2-13: R95p Trend For Future Climate Scenarios.	176
Table 4.2-14: Change In Mean, Maximum, And Minimum Temperatures Under Different RCP Scenarios For All Time Periods Relative To Historical Data.	177
Table 4.2-15: Average Annual Temperature Trend For Future Climate Scenarios For The Period 2006-2099.	178
Table 4.2-16: Annual Maximum Temperature Trend For Future Climate Scenarios For The Period 2006-2099.	179
Table 4.2-17: Annual Minimum Temperature Trend For Future Climate Scenarios For The Period 2006-2099.	179
Table 4.2-18: Annual And Monthly River Discharge Trends For Stations 3116430 And 3116434.	181
Table 4.3-1: Sensitivity Ranking Of Parameters Used In Simulation Of Water Discharge.	190

Table 4.3-2: SWAT Model Parameters Used To Calibrate Streamflow.....	191
Table 4.3-3: The Calibration And Validation Fitting Metrics.....	192
Table 4.3-4: Trend For Simulated River Discharge For Future LULC And Climate Change Scenarios.....	201
Table 4.3-5: Simulated Average Annual River Discharge For Future LULC And Climate Change Scenarios At Sg. Batu Sentul Station.....	201
Table 4.4-1: Summary Of Results And Discussion.....	206

LIST OF ABBREVIATION

95PPU	95% Prediction Uncertainty
AAT	All-At-a-Time
AFOLU	Agriculture, Forestry and Other Land Use
AGCM	Atmospheric General Circulation Models
ANN	Artificial Neural Network
AR5	Fifth Assessment Report
AUC	Area Under the Curve
BT	Brightness Temperature
CA	Cellular Automata
CCD	Cold Cloud Duration
CFS	Climate Forecast System
CH ₄	Methane
CHIRPS	Climate Hazards Group InfraRed Precipitation with Station
CO ₂	Carbon Dioxide
CRU	Climate Research Unit
DEM	Digital Elevation Map
DID	Department of Irrigation and Drainage
DT	Decision Trees
ECMWF	European Centre for Medium-Range Weather Forecasts
ET	Evapotranspiration
ETCCDI	Expert Team for Climate Change Detection and Indices
EU	European Union
FP6	6th Research Framework Program
GCM	Global Climate Model

GHG	Greenhouse Gase
GIS	Geographic Information System
GKL	Greater Kuala Lumpur
GLUE	Generalised Likelihood Uncertainty Estimation
GMST	Global Mean Surface Temperatures
GPCC	Global Precipitation Climatology Centre
HRU	Hydrological Response Unit
IntM1	Inter- Monsoon 1
IntM2	Inter- Monsoon 2
IPCC	Intergovernmental Panel on Climate Change
ISI-MIP5	Inter-Sectoral Impact Model Intercomparison Project
LCM	Land Change Modeller
LH	Latin Hypercube
LSE	Land Surface Emissivity
LST	Land Surface Temperature
LULC	Land use and land cover
MAE	Mean Absolute Error
MCMC	Markov Chain Monte Carlo
MET	Malaysian Meteorological Department
MK	Mann-Kendall
ML	Machine Learning
MLP	Multi-Layer Perceptron
NCDC	National Climate Data Center
NDVI	Normal Difference Vegetation Index
NEM	Northeast Monsoon
N ² O	Nitrous Oxide

NS	Nash-Sutcliffe
OAT	One-At-a-Time
ParaSol	Parameter Solution
POWER	Prediction of Worldwide Energy Resources
PSO	Particle Swarm Optimisation
R	Pearson's Correlation Coefficient
R2	Correlation Coefficient
R ²	Coefficient of Determination
R10mm	Number of Heavy Rainfall Days
R95p	Very Wet Day
RCP	Representative Concentration Pathways
RCM	Regional Climate Model
RF	Random Forest
RMSE	Root Mean Square Error
SCS-CN	Soil Conservation Service Curve Number
SDII	Simple Daily Intensity Index
SDIR	Short Duration Intense Rainfall
SNHT	Standard Normal Homogeneity Test
SRES	Special Report on Emission Scenarios
SRTM	Shuttle Radar Topography Mission
SUFI-2	Sequential Uncertainty Fitting
SUHII	Surface Urban Heat Island Intensity
SVM	Support Vector Machine
SWAT	Soil and Water Assessment Tool
SWM	Southwest Monsoon
TNx	Monthly Maximum Value of Daily Minimum Temperature

TOA	Top Of the Atmosphere
TOC	Total Operating Characteristics
TP	Time Periods
TXx	Monthly Maximum Value of Daily Maximum Temperature
UHI	Urban Heat Island
UHII	Urban Heat Island Intensity
UN	United Nations
USDA-ARS	USDA Agriculture Research Service
WATCH	Water and Global Change
WRF	Weather Research and Forecasting

CHAPTER 1: INTRODUCTION

1.1 BACKGROUND

Water is an important part of sustainable development, as it is an essential natural resource for human activity. Land use and land cover (LULC) change and changes in precipitation properties are two major factors that greatly affect water resources and the hydrological cycle. Surface runoff and river discharge are among the major parameters of the hydrological cycle that are directly affected by LULC and precipitation changes.

The combination of LULC and precipitation change can potentially have a significant effect on surface runoff and river discharge. Therefore, to effectively manage water resources it is essential to develop an integrated spatio-temporal model that assesses the impacts of LULC and precipitation changes on runoff and river discharge at basin level.

The interrelated relationship between LULC and precipitation changes and their effects on surface runoff and river discharge can be complex. The changes in LULC can impact the amount and timing of runoff, while changes in precipitation like shift in patterns and intensity can exacerbate these effects. LULC change can occur because of urban and agricultural expansion, deforestation, and mining activities. When LULC changes occurs, it can alter the biogeochemical cycles and

biogeophysical processes between the surface and atmosphere (Zhou *et al.*, 2020).

LULC change can impact biogeochemical cycles like the carbon cycle by altering carbon sinks and carbon dioxide (CO²) emissions (Li *et al.*, 2020), and affects biogeophysical process like surface albedo, roughness, and evapotranspiration (Lejeune *et al.*, 2017; Winckler *et al.*, 2017; Hirsch *et al.*, 2018), and hence alter the energy budget, water budget and atmospheric variables like temperature and precipitation.

Urbanisation can greatly affect surface properties, like an increase in imperviousness due to roads, pavements, and buildings, which can significantly reduce infiltration and increase surface runoff. Urbanisation can also lead to deforestation and reduction in vegetation cover, which can further reduce evapotranspiration, interception by plants and increase soil compaction, hence leading to increase in surface runoff.

Several studies have shown the changes to surface properties due to urbanisation can alter and induce precipitation over urban areas (Pielke *et al.*, 2002; Shepherd, 2005; Liang and Ding, 2017; Niyogi *et al.*, 2017; Liu and Niyogi, 2019; Singh and Qin, 2020; Yu *et al.*, 2020). Past studies have shown that the combination of increasing temperature and cloud nucleating aerosols in urban areas has greatly affected precipitation properties, where increase in precipitation amount and intensity has

been observed as a result (Seino *et al.*, 2018; Varentsov *et al.*, 2018; M. Wu *et al.*, 2019; Schmid and Niyogi, 2017; Zhong *et al.*, 2017).

Other land-use changes like agricultural expansion and mining can also greatly affect surface properties, like increasing soil erosion, which can increase sediment loading in rivers and reduce the water holding capacity of soils, and removal of vegetation cover, which all can lead to an increase in surface runoff.

LULC change around the world has seen significant rise in the past few decades, because of increasing population, demand for agricultural land, increasing economic growth, and urbanisation. More than 70% of the global ice-free land surface is directly affected by anthropogenic actions (IPCC, 2019), and in the past five decades, the driving force behind these LULC changes has been the increase in agricultural land, and since 1992 rapid urbanisation has also added to the ever-growing change in LULC (Díaz *et al.*, 2019).

To understand the effects of LULC change on surface runoff and river flow, it's important to first carry out land use change modelling, with its results being used as input into hydrological models. Land use change modelling provides a systematic method for quantifying and simulating these changes and helps in estimating future scenarios. Furthermore, the output from land use and climate change models can be integrated

with hydrological models, which allows for greater understanding of these complex interactions between LULC, climate and hydrological processes. Researchers can examine how different land use scenarios affect surface runoff and river flow under different climate conditions using various statistical, empirical, or process-based models.

There are several types of models with which LULC change modelling can be carried out. There are statistical models like Markov Chain (MC), empirical models like logistic regression, dynamic models like Cellular Automata (CA), and integrated models. The Decision Forest – Markov Chain (DF-MC) model used in this research is an integrated model where the Random Forest machine learning algorithm is integrated with MC.

DF-MC is largely used for land use classification; however, a few studies have shown its effectiveness in land use change modelling too. Al-sharif and Pradhan, (2015); Samardžić-petrović et al., (2015); Karimi et al., (2019) all used DF-MC to model land use change, and the studies concluded that it is an effective method in predicting future scenarios of land use change.

The DF-MC model has several advantages over other models. The DF model is easy to understand and interpret, it is highly flexible and adaptable to various types of data, it can capture non-linear relationships between input variables and land use change outcomes, it

can handle missing data effectively, which is a common issue in land use change modeling due to data availability and quality, and decision forest is an ensemble of random trees which improves performance and reduces overfitting (Bruch et al, 2020; Colkesen and Kavzoglu, 2019).

The Klang River basin is an important source of water for Kuala Lumpur and its surrounding area. The basin has experienced significant environmental challenges, including land use changes, shift in local weather parameters like precipitation and temperature. These changes have had an impact on the hydrological cycle, water quantity and quality of the basin. However, the contribution and magnitude of these changes are still uncertain in many basins in Malaysia and in the Klang River basin, with most previous studies focusing only on either land use change or climate change.

Understanding the role of LULC change and changes in climate parameters in the hydrological cycle, and the effects in future scenarios, is important in the mitigation and implementation of land use policies and planning, and helps policy makers, and stake holders to better tackle the future issues related to LULC change.

1.2 PROBLEM STATEMENT

Changes in land use and land cover coupled with changes in precipitation have the potential to greatly alter hydrological processes and pose

significant threats to water resources in river basins. LULC change can alter surface properties like permeability which can affect infiltration, surface runoff and river discharge. It can also affect surface albedo and evapotranspiration, which can lead to changes in precipitation, and these changes to surface properties can hence increase risk of flooding.

Malaysia has seen a rapid change in LULC in the last 50 years, due to population and economic growth. Agricultural land has been the dominant land use change in Malaysia, however, since the early 1990s, urbanisation has seen an accelerated increase. The Malaysian government in 1991 implemented the Vision 2020 with the goal to achieve a fully developed and industrialised economy by 2020, and this has led to accelerated LULC change and urbanisation. The state of Selangor has seen the greatest increase in population and urbanisation in this period, and as of 2010 the federal territories of Kuala Lumpur and Putrajaya are 100% urbanised (Hasan and Nair, 2014).

Flooding has been a major issue in Malaysia, and the country has experienced significant flooding events in recent years, which have resulted in loss of life and economic damage (**Table 1.2-1**).

Table 1.2-1: List Of Flood Events In Malaysia.

Year	Cost (millions)	Victims	Deaths
1926	/	/	45
1967	>60 MYR	>250000	/
1971	>84.7 MYR	180000	24
1996	300 USD	39687	241

2000	/	100000	15
2001	0.65 USD	>10000	14
2003	/	31046	5
2005	240 MYR	99405	14
2007	605 USD	137533	17
2007	316 MYR	36143	22
2008	21 USD	34000	28
2010	8 USD	50000	4
2013	/	34000	3
2014	2900 MYR	>500000	25

(Bell *et al.*, 2020)

Selangor has faced several major flooding and extreme weather events during the last two decades, for example, the floods on 30th April 2000, 26th April 2001, 29th October 2001, 11th June 2002, 10th June 2003, and 10th June 2007 (Samsuri *et al.*, 2018), and in recent years areas like Kajang Town faced flash floods in 2002, 2008, 2011 and three times in 2014, resulting in damages and economic loss to the people in the area. It is estimated that during floods there is around 51.5% in economic loss due to businesses being unable to operate, and about 46% loss due to damages to goods and commodities (Bari *et al.*, 2021).

Despite numerous studies on the effects of land use changes and climate change on hydrological processes, the combined effects of these factors on surface runoff and river flow dynamics are poorly understood.

There have been few past studies that have analysed the combined effects of LULC and climate change on hydrological process in Malaysia. For instance, the study by (Tan *et la.*, 2015) investigated separate and

combined impacts of land use and climate variability on hydrological components in the Johor River Basin, however the study did not consider future LULC and climate scenarios. Most of the past studies in Malaysia have been concentrating on either LULC impacts or climatic impacts, therefore there is still gaps in knowledge on the combined effects of LULC and climate change.

For example, the study by Kabiri *et al.*, (2015) examined the effects of climate change on river discharge in the Klang River basin, where the study used global climate models for emission scenarios A2 and B2 for the period 2001 -2100. However, this study did not consider land use change and the effects of land use change on river discharge.

Therefore, this research aims to bridge the gap in existing knowledge by assessing the combined effects of LULC and precipitation changes on hydrological processes, with a focus on surface runoff and river discharge in the Klang River basin. Importantly, the research will analyse the potential impacts of LULC changes, especially urban expansion, coupled with projected precipitation and temperature change scenarios on hydrological processes in the Klang River basin. To achieve this aim, the study will integrate future LULC and climate scenarios into the analysis, which will provide an overall understanding of the potential threats to water resources, particularly in the face of increasing flood events.

The study will contribute to both the scientific understanding of these complex interactions and provide valuable insights for policymakers and urban planners. Ultimately, this research aims to provide valuable information, to help in sustainable land use planning and water resource management in the Klang River basin.

1.3 AIM AND OBJECTIVES

The aim of this research is to assess the combined spatio-temporal impacts of land use and land cover (LULC) changes and precipitation variations on surface runoff and river discharge within the Klang River basin, while also projecting these effects under future scenarios.

The objectives are:

1. To analyse spatio-temporal trends in land use and land cover, precipitation, and temperature.
2. To develop an integrated spatio-temporal hydrological model, with land use and climate models.
3. To measure quantitative effects of both LULC and precipitation changes on surface runoff and river discharge.

1.4 RESEARCH QUESTIONS

The following research questions will be used to address and achieve the objectives of the study.

1. What is the magnitude of the spatio-temporal changes in LULC for the period 1999 to 2017 in Klang River basin?
2. What are the future patterns of change in LULC as projected by DT-Markov Chain model?
3. What is the intensity and frequency of the trends detected in precipitation and temperature data, for the Klang River basin?
4. What are the quantitative effects of both LULC change and precipitation change under different scenarios on the surface runoff and river discharge in Klang River basin?

1.5 SIGNIFICANCE OF THE STUDY

Southeast Asia is one of the most populated regions in the world, with a large number of the population living within urban areas located close to major water resources like rivers, lakes, and coastal lines. LULC and climate change have greatly affected the hydrological cycle and water resources in this part of the world, where natural disasters like extreme weather events and flooding occur regularly.

Although the effects of LULC and climate change can be observed at different scales, it is at local and watershed levels that these effects are significant. It is therefore important to assess these effects, which play an important part in policy making discussions and urban planning at the local level.

The Klang River basin located in the state of Selangor, is a highly urbanised and populated basin. In the past few decades, the basin has experienced major LULC change, in particular urban expansion, which has resulted in areas like the federal territories of Kuala Lumpur and Putrajaya becoming 100% urbanised. Current studies have shown that LULC change has played an integral role in impacting hydrological processes and increasing the risk of flooding in the Klang River basin.

Research on precipitation and temperature trends has shown that these climate variables can also impact the hydrological cycle and water resources of the basin. However, in most of these studies the combined effects of LULC change and changes in precipitation variables were not considered. As both LULC and precipitation changes play a significant role in surface runoff and river discharge, it is important to study and understand the relationship and impacts of both on hydrological processes in the Klang River basin and how these processes could be affected under future scenarios.

Therefore, a quantitative assessment of the potential consequences of LULC change and climate change on hydrological processes at the watershed level in the Klang River basin, is of utmost importance. The results of this study can help to better understand the implications of LULC change and climate change in the real-world environment, which

can help policy makers and urban planners to incorporate the effects of LULC change and climate change into policies and decisions.

1.6 SCOPE

The focus of the study is to assess the combined effects of land use and land cover and precipitation change on surface runoff and river discharge in the Klang River basin. The first step in the study is to determine the spatio-temporal changes in LULC and to establish the pattern of change, with a particular interest in expansion of urban land for an 18-year period from 1999 to 2017. This is followed by modelling future LULC change scenarios for the year 2030, based on past trends, and variables that bring about change. Secondly, the study will analyse climatic variables, in particular precipitation and temperature for a 40-year period from 1975 to 2015, to showcase the spatio-temporal trends, and compare these trends with future climate scenarios from climate models. Lastly, the study will integrate the LULC change and climate models with the SWAT hydrological model to analyse the spatio-temporal quantitative effects of LULC and precipitation changes on surface runoff and river discharge in the Klang River basin.

The study has certain limitations, with one of the limitations being that the LULC change modeling is only up to the year 2017, as the study began in year 2017 and satellite data were only available up to the year

2017. The other limitation is that the study only covers the Klang River basin, since modelling hydrological processes is complex and time consuming, therefore the neighboring basins were not considered for this study. Availability and quality of overserved data was another limitation to the study.

1.7 THESIS OUTLINE

The thesis comprises of five chapters; each chapter is briefly described below:

Chapter 1 includes the introduction of the thesis, which gives a general introduction of the research topic. It also includes the problem statement, aims and objectives, research questions, scope, and importance of the study in the Klang River basin.

Chapter 2 explores the impacts of land use and land cover change on climate and hydrological processes, and the various methodologies in land use, climate, and hydrological modelling, by reviewing previous studies. The aim of this chapter is to review previous studies and journal papers on the effects of land use and climate change on hydrological processes, to identify gaps in knowledge, and identify the strengths and weaknesses of the various methodologies used.

Chapter 3 describes the methodology used in this research. This chapter consists of two parts, the first part describes the study area and

characteristics, such as climate, geology, soil, and drainage. In the second part, the various data and methods used in land use change modelling, trend analysis and hydrological modelling are described. Three hydro-metrological time series data are utilised in the trend analysis method, these are precipitation, temperature, and river discharge, the Mann-Kendall test and Sen's slope are used to detect trends in these data. For land use change modelling, a Decision Forest - Markov Chain model is utilised, and for hydrological modelling the SWAT model is used. This chapter also presents the full description of the methods used for land use change modelling, trend analysis and hydrological modelling.

Chapter 4 presents the results and discussions of the study. It demonstrates the spatio-temporal trends and changes in LULC and hydro-climatic variables like precipitation and temperature, in the Klang River basin. The LULC maps are classified and changes in land use are modelled for future scenarios. The Mann-Kendall test is used to analyse the annual and seasonal trend in precipitation intensity and frequency, mean, maximum and minimum temperature and river discharge. Landsat satellite images are utilised to generate LSTs. Finally, in this chapter, the separate and combined effects of LULC change and climate change are modelled using the SWAT hydrological model, to assess the changes in river discharge and runoff.

Chapter 5 presents the conclusions arrived through the study and includes the limitations the study faces, while also giving recommendations for future studies and for policymakers.

CHAPTER 2: LITERATURE REVIEW

Land use and land cover (LULC) change can have several impacts on the environment, these include loss of biodiversity (Powers and Jetz, 2019), reduction in water quality (Calijuri *et al.*, 2015; Hua, 2017; Namugize *et al.*, 2018), impact on the hydrological cycle which can lead to increase in flooding (Apollonio *et al.*, 2016; Welde and Gebremariam, 2017; Patil and Nataraja, 2020), regional climate change (Salazar *et al.*, 2015; Findell *et al.*, 2017), air quality change (Sun *et al.*, 2016), and soil erosion (Borrelli *et al.*, 2017). This chapter will review the literature on the impacts of LULC, precipitation and temperature on surface runoff and river discharge. The chapter will also review the global and local trends in LULC, precipitation and temperature, and the modelling methods used to analyse the impacts of these changes and trends on hydrological processes.

2.1 GENERAL FACTORS AFFECTING SURFACE RUNOFF AND RIVER DISCHARGE

There are several factors that affect surface runoff and river discharge, which can be natural or human induced. Among these factors precipitation plays a significant role, which can determine the amount of surface runoff and river discharge. Precipitation properties like volume, intensity, and duration can greatly impact surface runoff and river discharge.

Intense and prolonged precipitation, particularly when the soil is saturated or impermeable, can result in an increase of surface runoff and river discharge. On the other hand, drought and low precipitation events can result in decrease of surface runoff and river discharge, leading to low soil moisture and, in extreme cases, drying of rivers.

Other climate and weather factors that can also impact surface runoff and river discharge, include temperature, evaporation rates, and prevailing wind patterns, which can affect water availability and influence the timing and intensity of runoff events (Depetris, 2021).

LULC change is another significant factor that can affect surface runoff and river discharge. Urbanisation, deforestation, agricultural practices, and other land use changes can impact the flow of water within a watershed. Paved surfaces and buildings increase surface runoff by preventing water from infiltrating into the ground and disrupting the natural drainage patterns. Similarly, irrigation and reservoir management can modify river discharge.

Besides LULC change, other human activities, and land modifications, like building of dams, levees, and reservoirs can highly impact surface runoff and river discharge, by changing the natural flow patterns of rivers and streams. For example, dams regulate flow and storage of water, which then affects downstream discharge.

The physical characteristic of a watershed also influences the movement of water within a watershed and ultimately affects surface runoff and river discharge. Watershed size, shape, slope, and soil properties can determine the rate and flow path of water, for example steep slopes and smaller watersheds tend to generate more surface runoff, impermeable soils can result in higher surface runoff compared to well-draining soils.

2.2 LAND USE AND LAND COVER CHANGE IMPACTS ON SURFACE RUNOFF AND RIVER DISCHARGE

Water is a vital component of the ecosystem, but its availability and quality are threatened by the increasing demands and pressures from the growing global population and economy. The hydrological processes that govern the water cycle, such as surface runoff, evapotranspiration, and infiltration, are sensitive to changes in land use and land cover (LULC) (Dwarakish and Ganasri, 2015).

One of the major drivers of LULC change is agriculture, which can have profound effects on the hydrological cycle. For instance, deforestation for agricultural expansion and irrigation can alter the global evapotranspiration (ET) fluxes, which in turn can influence the regional climate (Gordon *et al.*, 2008).

Zou et al., (2017) found that in Northwest China, agricultural practices had a larger impact on ET than climate change, accounting for 60.93%

of the ET increase from 1984 to 2014, while climate change contributed 28.01%. Another aspect of the hydrological cycle that is strongly affected by LULC change is runoff. The conversion of forests and natural vegetation to agricultural and urban land can reduce the soil infiltration capacity and increase the surface runoff generation.

Munoth and Goyal, (2020) demonstrated that in the Upper Tapi River Sub-Basin, India, the LULC change from 1975 to 2016, which involved an 18% increase in agricultural land, a 7% decrease in forest and a 10% decrease in rangeland, resulted in a 32% increase in runoff. Similarly, Bradshaw *et al.*, (2007) reported that a 10% decrease in natural forest area across 56 developing countries from 1990 to 2000 was associated with a 4%-28% increase in flood frequency and a 4%-8% increase in flood duration.

Urbanisation is a global phenomenon that has altered the hydrological cycle by replacing the natural vegetation and soil, which play a key role in intercepting, storing, and releasing rainwater, with impervious surfaces such as buildings, roads, and sidewalks. These surfaces reduce the infiltration and evapotranspiration of rainwater and increase the surface runoff into streams, leading to higher peak discharge, volume, and frequency of floods (Bonneau *et al.*, 2017).

Zang *et al.*, (2019) showed that in the upper reaches of the Minjing River in China, the urbanisation of forest and grassland areas decreased the actual ET, soil water content, percolation, and groundwater contribution to streamflow, while increasing the surface runoff, water yield and annual runoff. In contrast, natural areas such as forests and grasslands have a greater capacity to regulate the rainwater through vegetation and soil processes and generate subsurface flow when the storage capacity is exceeded (Konrad, 2003).

Zope *et al.*, (2016) illustrated that in the Oshiwara river basin in Mumbai, India, the rapid urbanisation from 1966 to 2009, which involved a 74.84% increase in urban land and a 42.8% decrease in open spaces, resulted in a significant increase in runoff volume, with the 2-year return period exceeding the 100-year return period, and an expansion of flood risk areas by 64.29%. These studies all reach a common conclusion, where agricultural and urban land uses are the two most significant land uses that have great impact on hydrological processes, in particular surface runoff.

The future implication of LULC change on hydrological processes is an important issue to consider, and several studies have delved into the possible effects of future land use change on runoff and river discharge. For example, two recent studies by Mohammady *et al.*, (2017) and Sinha and Eldho, (2018) assessed the effects of land use change on

runoff for different time periods, both studies simulated land use change for the year 2030 and past years and compared the runoff of each year. Mohammady *et al.*, (2017) looked at the Baghsalian watershed in Iran, where land use maps for the years 1986, 2012 and 2030 are used. The results showed that the main land use change is from forest and rangeland to agricultural and urban areas. Similarly, Sinha and Eldho, (2018) used land use maps for years 1972, 1979, 1991, 2000, 2012, and 2030 for the Netravati River basin in India, which showed urban areas, agriculture and water bodies increased and forests, grassland and bare lands decreased from 1972 to 2030. In both studies, runoff simulation software is used to calculate runoff volumes, and in both studies the results showed an increase in runoff volume due to land-use change, in the case of Sinha and Eldho, (2018) there is also a continues increase of 7.88% in stream flow.

2.2.1 SURFACE RUNOFF AND RIVER DISCHARGE DYNAMICS IN RESPONSE TO LAND USE AND LAND COVER CHANGES IN MALAYSIA

In Malaysia, the increase in agricultural land and urbanisation, have had great impact on water resources and the hydrological process, which have increased the risk of extreme flooding. LULC change is a major contributor to flooding in states like Selangor, Johor, and Kelantan, where there has been extensive change in LULC. For example, in Sungai Layang catchment in Johor, the increase of agricultural and urban land

between the years 2000 and 2010, resulted in 47.9% loss in forest cover, and increased water yield by 35.46%, due to changes in infiltration rate and evapotranspiration, which can affect surface runoff (Baiya and Hashim, 2020).

In the Kelantan River basin, correlation between deforestation, agricultural land, and runoff volume was observed for the period 1984 to 2013. In this period forest areas were converted to agricultural land (palm oil, rubber, and paddy), urban land and grass land, which resulted in increased peak discharge and runoff (Abdulkareem *et al.*, 2019, Saadatkah *et al.*, 2016,).

Similarly in the Hulu Kelang basin in Selangor, the direct runoff volume from agricultural and urban land increased by 10%, and decreased by 5% for forest land, in the period between 1994 to 2013 (Nader and Azman, 2017). In Hulu Langat basin, Memarian *et al.*, (2014) analysed the impacts of LULC changes on water discharge and sediment load using the SWAT model, for past, present, and future land use scenarios. The study used land use maps of 1984, 1990, 1997 and 2002 as past land use scenarios, land use map of 2006 as present land use scenario and a simulated land use map of 2020 for future land use scenario. The results showed an increasing trend in discharge and surface runoff from the years 1984 -2020, due to an increase in urban land use.

In the Klang River basin, a study by Abas & Hashim, (2014) examined the relationship between urban growth and surface runoff in the Klang and Langat River basins for the period 2000 to 2010. The study used the Soil Conservation Service Curve Number (SCS CN) method and calculated the runoff coefficient for the land use maps of the years 2000, 2006 and 2010. The results showed increasing runoff coefficient with an increase in urban area, and an average of 5% increase in runoff from 2002 -2010.

Similar results were found at Sungai Kayu Ara a sub basin in the Klang River basin, where the impact of rainfall duration, ARI (magnitude) and land use development on peak discharge and volume was examined under different land development conditions (Alaghmand *et al.*, 2012). The result of the study shows, land development had more impact on runoff peak discharge and runoff volume compared to rainfall duration and magnitude, with ultimate land development condition where imperviousness is at 90%, having the largest increase in runoff peak discharge (91%) and runoff volume (45%) compared to other conditions.

It is clear from all these studies, that land use change has a significant impact on hydrological processes in watersheds across Malaysia, and in particular, urban land use has the largest impact. However, in all these studies the combined impacts of LULC and precipitation changes on

hydrological processes were not analysed, with only few studies like Alaghmand *et al.*, (2012) and Ebrahimian *et al.*, (2017) which assessed the combined effects of LULC and climate change on hydrological processes. Therefore, there is still a gap in knowledge and understanding of the relationship between LULC and climatic changes on hydrological processes in Malaysia and the Klang River basin.

2.3 LAND USE AND LAND COVER CHANGE IMPACTS ON CLIMATE VARIABLES

2.3.1 IMPACTS ON BIOGEOCHEMICAL CYCLES

Land is both a source and a sink of greenhouse gases (GHGs), therefore land use and land cover change have major impact on the biogeochemical cycles, in particular the carbon cycle. In the last 50 years, 82% of total global carbon emissions is caused by fossil fuel burning, and 18% by land use change (Friedlingstein *et al.*, 2019). According to a 2019 report by IPCC in the period 2007- 2016, about 13% of CO₂, 44% of methane (CH₄), and 82% of nitrous oxide (N₂O) emissions were due to Agriculture, Forestry and Other Land Use (AFOLU) activities, which accounted for 23% of total net anthropogenic emissions of GHGs (IPCC, 2019).

The increase in CO₂ and other GHGs can affect global temperatures, carbon cycling can affect vegetation cover, which can directly affect albedo hence resulting in the increase or decrease of surface

temperatures. On the other hand, the GHGs and aerosols in the atmosphere can affect the incoming solar radiation and the outgoing longwave radiation by absorbing or reflecting the radiation (Megonigal and Neubauer, 2019). The change of LULC from forest to agricultural land and pasture can decrease the soil carbon concentration mainly by the reduction of detritus, the acceleration of soil organic matter decomposition, and the destruction of the physical protection of organic matter due to agricultural practices (Yang *et al.*, 2003).

Climate modelling for the period 1850 to 2300, shows carbon loss of 490 Pg C due to land conversion, which is larger than the 230 Pg C caused by climate change, and 40% of the carbon loss due to LULC change is due to direct human modification of land surface (Mahowald *et al.*, 2017). Other GHGs have also been increasing due to LULC change, for example, global N₂O has increased since 1750 from a pre-industrial concentration of 270 ppbv to 330 ppbv in 2017, and the main source of N₂O is agriculture (IPCC, 2019).

2.3.2 IMPACTS ON BIOGEOPHYSICAL PROCESSES

LULC change also affects the biogeophysical processes of earth's surface, like surface albedo, roughness, and evapotranspiration, which can impact local, regional, and even global climate. The changes in the biogeophysical processes leads to changes in the energy and moisture

budget of the land surface, which hence alters the flow of heat, water, and dynamics of near-surface atmosphere and influences properties of the atmosphere (Deng *et al.*, 2013).

Surface albedo is the fraction of the sunlight reflected by the earth's surface and is a main part of the energy budget. The change in surface albedo can result in an increase or decrease in temperature, which can hence affect other climate variables like precipitation, by affecting the amount of water vapor the atmosphere can hold, which affects the planet's cloudiness, which in turn again affects the albedo, and hence the cycle starts again (Perkins, 2019).

During 1750–2011, the global albedo effect had an estimated radiative forcing of about $-0.15 \pm 0.10 \text{ Wm}^{-2}$, which is a small amount due to LULC change being highly regionalised, however the effects of local LULC change on albedo can be significant (Zhang and Liang, 2018). Different land use types and land covers have different albedos, for example, fresh snow covering sea ice has a 85% reflective rate, whereas ocean waters can have 7% reflective rate (Perkins, 2019).

Forests for example, usually have low albedo but have higher evapotranspiration rates, compared to open vegetation, therefore this can lead to warming through higher absorption of shortwave radiation, however this is encountered by the cooling effect from the loss of latent

heat due to evapotranspiration (Prevedello *et al.*, 2019). Forests and other vegetation like grassland, also have impact on spatial and seasonal variations in albedo and temperature. For example, deforestation and afforestation in Europe have varying effects on albedo and temperature at different latitudes, and seasons.

A climate modeling study by Tölle *et al.*, (2018) used the COSMO-CLM (v5.09) regional climate model to study the sensitivity of temperature to albedo parametrisation in Europe for the period 1986-2015. The results showed afforestation in the mid-latitudes has a strong warming effect during winter due to lower albedo, however, during summer afforestation has a small effect on warming, due to the cooling effects of evapotranspiration. On the other hand, the warming effect due to deforestation in the summer is 3°C higher than the warming from afforestation, and in the high latitudes the high conversion of forest to grassland, which results in high snow cover during winter has cooling effect of about -0.5°C.

A similar study by Huang *et al.*, (2020) also looked at the effects of LULC changes on temperature and humidity in Europe for the period 1992-2015. The study came to similar conclusions, where revegetation of abandoned agricultural land in Eastern Europe resulted in a warming effect, due to reduction of surface albedo and soil moisture-temperature

feedback, and Southern, Central and Western parts of Europe experienced an average cooling of -0.12°C .

However, deforestation and afforestation in the tropical and temperate regions show the opposite effect, where deforestation has a warming effect and afforestation has a cooling effect (Li *et al.*, 2015, Li *et al.*, 2016; Alkama and Cescatti, 2016). From 2000-2010 deforestation in the tropics and temperate regions caused an average warming of 0.38°C and 0.16°C respectively, whereas afforestation resulted in cooling of about -0.18°C and -0.19°C in these same regions. The tropical regions have the highest sensitivity to forest changes, where losses of about 50% in forest cover resulted in 1.08°C increase in land surface temperature (LST), and a similar forest cover gain reduced LST by -1.11°C (Prevedello *et al.*, 2019).

Urbanisation also has low albedo, and high absorption rate, due to the darker color materials used in urban areas, like asphalt and concrete (Li *et al.*, 2013). For example, Trlica *et al.*, (2017) studied the variations in albedo and surface temperatures across an urbanised landscape, and the study found that with increasing urbanisation, surface albedo decreased and surface temperature increased. The combination of low albedo, vegetation cover, and moisture plus the added heat from anthropogenic activities in urban areas, results in a phenomenon known as Urban Heat Island (UHI) effect, where urban areas have higher

temperature than the surrounding rural areas (Lo and Quattrochi, 2003).

UHI effect is generally very localised and is dependent on local vegetation cover, albedo, and climate variables like wind, cloud cover, and the proximity to sea (IPCC, 2007). A study on surface urban heat island intensity (SUHII) effect across 419 global big cities, showed an average annual increase of 1.5°C for daytime SUHII, and an increase of 1.1°C for nighttime SUHII. The study found a negative correlation between daytime SUHII and urban vegetation cover (Peng *et al.*, 2012).

In South East Asia, urbanisation has been increasing at a rapid rate, where currently half of the population live in urban areas, and by 2025 about 70 million more people will be living in urban areas (Rahman *et al.*, 2020). A study by Estoque *et al.*, (2017) examined the relationship between LST with impervious surface and green spaces, in the metropolitan cities of Bangkok (Thailand), Jakarta (Indonesia), and Manila (Philippines). The study found a strong significant positive correlation between LST and density of impervious surfaces, and a negative correlation with green spaces, where the mean LST of imperviousness surfaces is about 3°C higher than that of green spaces.

The changes in evapotranspiration (ET) and surface roughness due to LULC change also affect the climate and go hand in hand with the effects

of albedo. ET is the combined process of evaporation from the soil and transpiration from the vegetation mainly through the leaves (Boulet *et al.*, 2020). ET is a major part of Earth's energy balance, and influences the planetary boundary layer, mesoscale circulation patterns, and weather, it is also a large part of the hydrological cycle and accounts for 60% of continental precipitation (Liang *et al.*, 2012), and 70% of total global precipitation (Good *et al.*, 2015). ET is influenced by atmospheric variables (radiation, wind speed, temperature, and vapor pressure deficit), vegetation type, and available soil moisture (Wang *et al.*, 2018; Ajami, 2021).

Surface roughness can have a major control on atmospheric responses to LULC changes, where it can impact vertical wind speed, air temperature, mesoscale and global momentum exchange, energy exchange between land and atmosphere, and turbulent air mixing (June *et al.*, 2018). For example, a decrease in surface roughness can increase the boundary layer wind speed (Laban *et al.*, 2019), deforestation can result in reduction of surface roughness which can alter precipitation (Khanna and Medvigy, 2014; Khanna *et al.*, 2017).

2.3.2.1 IMPACT OF URBANISATION ON PRECIPITATION

The biogeophysical processes can also play a major role in precipitation variability, changes due to urbanisation can alter precipitation over an

urban area. The increase in urban areas results in the increasing of surface roughness, rise in air temperature, increase in aerosols which then provide a source for cloud condensation nuclei, and the urban canopy can result in diverting of precipitating systems (Shepherd, 2005). Several studies on the impact of urbanisation on precipitation show an increase in precipitation amounts and intensity over urban areas attributed to an increase in temperature (Seino *et al.*, 2018; Varentsov *et al.*, 2018; Wu *et al.*, 2019), cloud nucleating aerosols (Schmid and Niyogi, 2017), and a combination of temperature increase and aerosol effect (Zhong *et al.*, 2017).

The increase in greenhouse gases and aerosols due to urbanisation, industrialisation, and biomass burning, creates a mechanism called aerosol-enhanced conditional instability. The burning of fossil fuels and biomass produces a pollutant called 'black carbon', which when suspended in the atmosphere absorbs the sun's radiation. During the daytime, this process stabilises the atmosphere and suppresses local storms, subsequently the wind transports heavy warm moist air to mountainous regions, which is lifted, generating strong convection and extremely heavy precipitation in the evening (**Figure 2.3-1**). Simulations by Fan *et al.*, (2015), at northwest of the Sichuan basin in China, showed that heavy air pollution trapped in the basin significantly enhanced the rainfall intensity over the mountainous areas through the

aerosol-enhanced conditional instability, which resulted in catastrophic flooding in the Sichuan basin on 8-9 July 2013.

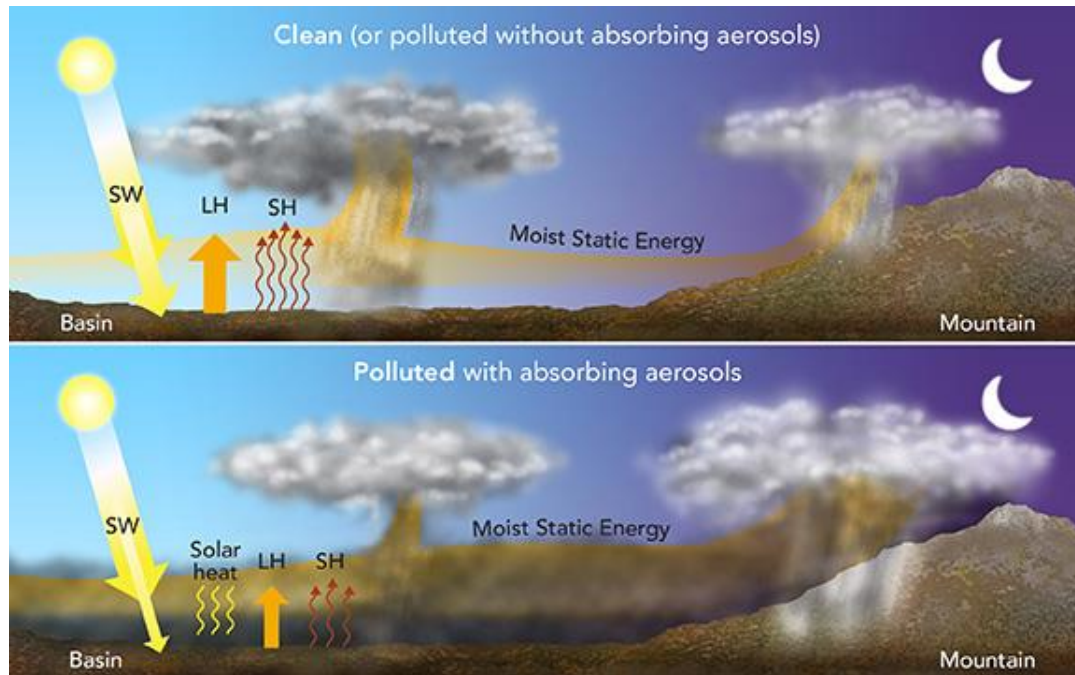


Figure 2.3-1: Aerosol-Enhanced Conditional Instability Increasing Rainfall Levels In Sichuan. Acronyms: MSE (Moist Static Energy), SW (Shortwave Radiation), SH (Surface Sensible Heat Flux), And LH (Surface Latent Heat Flux) (Fan et al., 2015)

In Northern Taiwan, heat from anthropogenic activities has shown to influence precipitation formation, where climate modeling shows precipitation to be stronger on urban areas compared to non-urban areas (Lin et al., 2011). In another study by Yang et al., (2017), it is observed that there is a relationship between urban heat island intensity (UHII) and short duration intense rainfall (SDIR) in Beijing. The study found that SDIR occurred more frequently in urban areas compared to

rural areas and mostly in the summer, it also showed that UHII is at its highest before the start of SDIR events.

2.3.3 IMPACTS OF LAND USE AND LAND COVER CHANGE ON LOCAL

CLIMATE IN MALAYSIA

Malaysia is one of the most urbanised countries in East Asia (Plecher, 2020), in 2020 the urban population in Malaysia was at 75%, with projections estimating by 2040, it will reach 85% (Samat *et al.*, 2020). This has resulted in expansion of urban areas at the expense of other land covers, by 2010 the federal territories of Kuala Lumpur and Putrajaya were 100% urbanised, and the state of Selangor was 91.4% urbanised (Hasan and Nair, 2014). The effects of urbanisation on UHI in Selangor and in particular the Greater Kuala Lumpur (GKL) area have been studied as early as 1972 by (Sani, 1972), who used in-situ data collection using temperature traverse technique, and determined that temperatures are higher at the city center compared to its surrounding rural areas.

More recent studies have been carried out to analyse UHI in GKL, for example, Elsayed, (2012) modified the methods used by Sani in 1972 and analysed UHI in GKL, whereas several studies used geographic information system (GIS) and remote sensing methods to study UHI (Shaharuddin *et al.*, 2014; Yusuf *et al.*, 2014; Amanollahi *et al.*, 2016),

and some studies used climate models like ADMS-Urban (Wang *et al.*, 2019) and Weather Research and Forecasting (WRF) Model (Morris *et al.*, 2015, 2017). The consensus from all these studies is that UHII is higher in urban areas compared to its surrounding rural areas, and the intensity ranges between 4°C – 6°C in most studies, with some studies showing intensity as high as 8°C.

2.4 IMPACT OF CLIMATE VARIABILITY ON SURFACE RUNOFF AND RIVER DISCHARGE

Climate variability, in particular precipitation changes can significantly impact hydrological processes in a watershed (Zhang *et al.*, 2016). To better plan and manage water resources, it is important to understand the impacts of changes in climate parameters on hydrological processes within a watershed (Amisigo *et al.*, 2015). The changes in climate parameters can have a direct impact on the spatial and temporal dynamics of the water cycle. These changes can affect precipitation patterns, intensity, and duration, evaporation rates and overall water availability in a watershed (Konapala *et al.*, 2020).

The changes in climate parameters can cause several hydrological issues, including altering of river flow, surface runoff, impacts on groundwater recharge, and overall changes in the water balance of a watershed. Climate change can also increase the frequency and

magnitude of extreme hydrological events such as droughts and floods. Döll and Schmied, (2012) carried out a global scale analysis of the impacts of climate change on mean annual runoff and mean annual discharge of freshwater resources, under A2 and B2 climate change scenarios until 2050. The study estimated that the mean annual runoff, discharge, and high flows are projected to increase by more than 10% on about half of the global land area by the year 2050.

2.4.1 IMPACT OF PRECIPITATION CHANGES ON SURFACE RUNOFF AND RIVER DISCHARGE IN MALAYSIA

Malaysia like many parts of the world, has been affected by climate change. The changes in global climate have impacted local weather, in particular precipitation and temperature, which in turn have affected hydrological processes. There has been increasing occurrences of extreme weather event in the past few decades in Malaysia, which are characterised by high temperatures, high rainfall, dry spells, thunderstorms, and strong winds (Tang, 2019).

In a study by *Amin et al.*, (2019), a regional climate model was used to assess the impact of climate change in the 21st century on precipitation, air temperature, soil water storage and annual mean flows. Based on Coupled Model Intercomparison Project phase 3 (CMIP3) datasets, the study dynamically downscaled 15 future climate projections from 3

GCMs covering 4 emission scenarios (SRES B1, A1FI, A1B, A2), for the whole Peninsular Malaysia covering 10 watersheds and 12 coastal regions.

The results showed, change in the 30-year mean annual precipitation for the period 2070-2100 to be 36.3% compared to the period 1970-2000 which is 17.1%, among the 10 watersheds and 45.4% and 22.9% respectively, among the coastal regions. However, for annual mean flow, the results show variation among the 10 watersheds, although the 30-year average mean flow does increase during the 21st century, with the period 2070-2100 showing the highest range in average change between 19.1% to 45.8%.

In the Klang River basin, changes in precipitation and temperature have had a significant impact on hydrological processes. In a study for Klang River basin conducted by Kabiri *et al.*, (2015), hydrological modelling was carried out using output data from the Hadley Centre Third Generation—GCM model for emission scenarios A2 and B2. The results showed that the mean annual discharge is predicted to decrease by 9.4%, 4.9%, and increase by 3.4% for the A2 and decrease by about 17.3%, 14.3% and 6.2% for the B2 scenario, respectively, in the 2020s, 2050s, and 2080s.

The review of past literature shows that there is spatial and temporal variability in precipitation patterns, frequency, and intensity, which results in variability in hydrological processes like river discharge and runoff. On the other hand, the impacts of LULC change are consistently similar among past studies, where increase in urbanisation and agricultural land, has resulted in increase in runoff and river discharge.

However, there is an important factor missing from many of the previous studies, where the combined effect of LULC change and climatic change on hydrological processes is not assessed. Since both LULC and climate parameters are interlinked and have significant impact on hydrological processes, it's important to consider both factors in hydrological studies.

2.5 TRENDS IN LAND USE AND LAND COVER, PRECIPITATION AND TEMPERATURE

2.5.1 GLOBAL TRENDS IN LAND USE AND LAND COVER

About 100 million km² (70%) of Earth's ice free surface has been directly affected by human activities (Arneeth and *et al.*, 2019), around 30% of this has been changed from forests to agricultural and urban land (Luyssaert *et al.*, 2014). The Global South has strong decrease in forest cover and increase in agricultural land, whereas the Global North (including China) has increase in forest cover and decrease in agricultural land between 1960-2019, with tropical forests experiencing

the highest deforestation rates (Winkler *et al.*, 2021). The agricultural abandonment in Europe and US, and reforestation programs in China have contributed to the forest gain in the Global North, whereas the increase in production of beef and agricultural products in Brazil has increased deforestation in the Amazon, and the increase in palm oil production has resulted in an increase of deforestation in Southeast Asia and West Africa (Winkler *et al.*, 2021).

However, in recent times the rate of deforestation has reduced in some tropical areas, for example, from 2015-2020 the rate of deforestation in South America and Asia was half of the rate in the 1990s, whereas in Africa deforestation rates continue to be high. Although the deforestation rate has reduced in South America and Asia, there are still large parts of forests being converted to other land types, like agriculture and urban land. For example, palm plantations have more than doubled between 1990 and 2020, from 4.20 million ha to 9.34 million ha, with Asia having most of the increase, and mainly in Malaysia where palm oil plantations increased from 2.35 million ha to 6.36 million ha (FAO, 2020).

2.5.1.1 LAND USE AND LAND COVER TRENDS IN MALAYSIA

Palm oil production, was the main contributor to the Malaysian economy until 1987, when manufacturing took over as the main contributor to

the economy as the government shifted its development policy to the manufacturing sector, and by the year 2000 other sectors like infrastructure and commercial development started growing, giving rise to urbanisation (Abdullah and Hezri, 2008). However, palm oil remains a major part of the Malaysian economy and continues to expand. Between 1990 and 2017 agricultural land increased by 55.7% with 98.2% of this area being plantations (Yan *et al.*, 2020). And as of 2017 palm oil plantations occupied 17.62% of the land mass in Malaysia, which has led to 20% loss in forests (Ezechi and Muda, 2019).

For example, a study by Masum *et al.*, (2017) looked at land use change and forest management of hill forest areas in Penang, and the study found the annual rate of deforestation since 1991 is at 1.4%, which is higher than the rate across Southeast Asia. Deforestation has occurred in many parts of Malaysia between 1988 and 2017, about 16% (189,423 ha) of forest cover in Perak and more than 9% (33,391 ha) of forest cover in Kedah is lost to anthropogenic activities (Mohd Jaafar *et al.*, 2020). In Selangor, forest and peat swamps decreased by 2.5% and 12.7% respectively, from 1989 to 2011 (Aisyah *et al.*, 2015), in another study it is shown that, the district of Gombak experienced an increase of 44.53% in urban land from 1999-2014, and a decrease of 34.6% in rubber plantation (Asnawi and Choy, 2016).

Urbanisation has seen a rapid increase, and Malaysia is one of the most urbanised countries in East Asia (Plecher, 2020). 50.4% of the population lived in urban areas in 1991, this number reached to 65% in 2010, and as of 2020 the number of the population living in urban areas has reached 75%, with projections estimating by 2040 it will reach 85% (Samat *et al.*, 2020). This has resulted in expansion of urban areas at the expense of other land cover, urban areas increased from 1793.2 ha in 1992 to 3235.4 ha in 2002 and in 2010 urban areas reached to 3987.8 ha (Mohammed *et al.*, 2016). Selangor and Penang have historically been the most urbanised states in Malaysia and the rate of urbanisation continued to rise over the years, by 2010 the federal territories of Kuala Lumpur and Putrajaya were 100% urbanised and the state of Selangor was 91.4% urbanised (Hasan and Nair, 2014).

Projection for future global land use scenarios show an increase in cropland by 2.1 million km² and pasture land by 1.6 million km² by 2050, and built-up areas are expected to increase by 0.5 million km² (80%), with these expansions expected to be mostly occurring in Sub-Saharan Africa, Latin America, South Asia and Southeast Asia (Van der Esch *et al.*, 2017). In Malaysia, a study by Mahamud *et al.*, (2019) projected the future LULC scenario in Kelantan for the year 2025, the study showed expected increase in built-up areas (181.69 km), oil palm (2142.48 km), and rubber plantation (3076.24 km). And in Seremban,

projections show decrease in agricultural land by 337 km² and increase in urban areas by 278 km² by the year 2030 (Aburas *et al.*, 2018). In terms of projecting future land use change, there have been few studies carried out, especially in Malaysia, therefore there is need for more studies in future LULC change scenarios.

2.5.2 GLOBAL TRENDS IN PRECIPITATION AND TEMPERATURE

The Intergovernmental Panel on Climate Change (IPCC) has predicted a rise in global mean temperatures between 1.4 - 5.8°C by the year 2100 (Haines *et al.*, 2006; McMichael *et al.*, 2006; Ullah *et al.*, 2021). Past trends show a significant rise in global temperatures since the early 20th century, and some of the evidence includes the melting of polar ice caps and rising sea levels (Foster and Rahmstorf, 2011). In recent years, the global mean surface temperatures (GMST) recorded have been extremely high. The year 2020 is the second warmest year on record based on National Oceanic and Atmospheric Administration's (NOAA) temperature data, which is 0.98°C warmer than the twentieth century average temperature of 13.9°C, and just 0.04°C less than the 2016 temperatures which is the warmest year on record, and the 10 warmest years on record have all occurred since 2005 (**Figure 2.5-1**) (NOAA, 2021). However, on a regional scale, many regions have already experienced greater warming, with increases of 1.5°C in at least one season (Allen *et al.*, 2018).

GLOBAL AVERAGE SURFACE TEMPERATURE

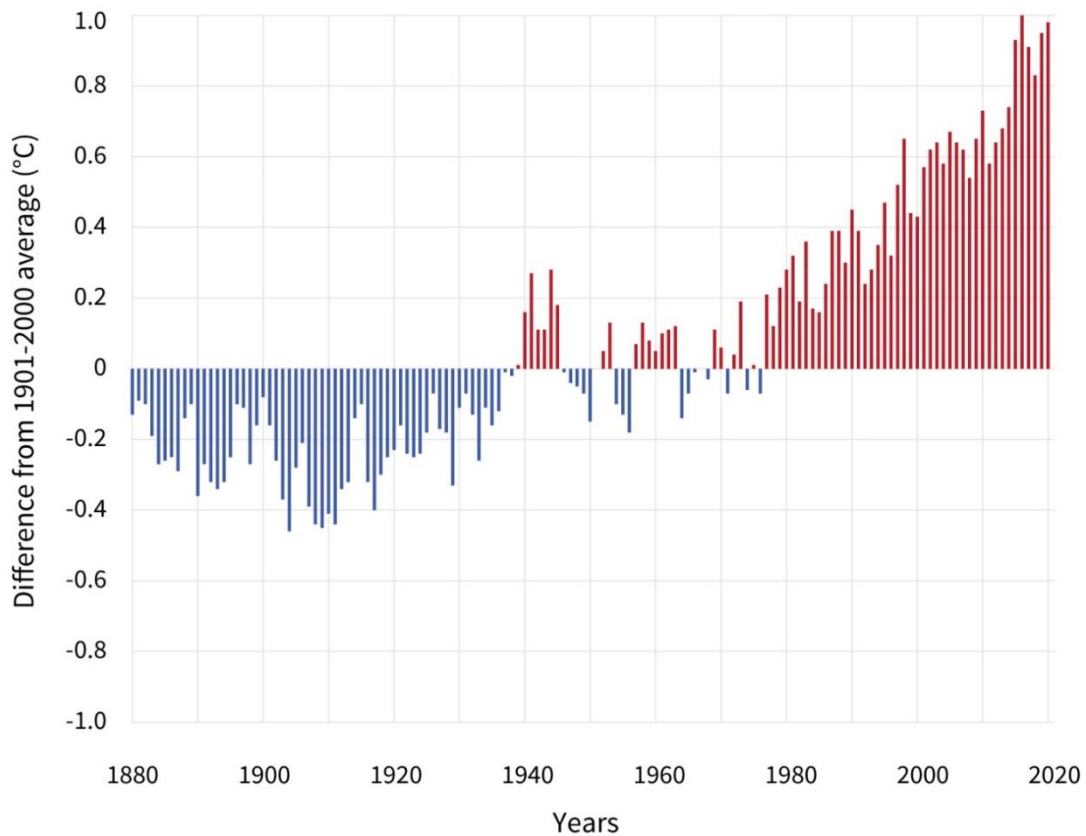


Figure 2.5-1: Yearly Surface Temperature Compared To The 20th-Century Average From 1880-2020. Blue Bars Indicate Cooler-Than-Average Years; Red Bars Show Warmer-Than-Average Years (NOAA, 2021).

The increase in global average surface temperatures results in an increase in evaporation, which in turn, increases overall global precipitation. The atmospheric water vapor, which supplies the water for precipitation increases in proportion to the saturation concentrations at a rate of about 6%–7% per degree rise in temperature (Tabari, 2020). It is expected that a warming climate will increase precipitation in many areas. However, because climate change causes shifts in wind patterns

and ocean currents that drive the world's climate system, it results in some areas warming more than others and some areas cooling, which also means precipitation patterns vary across the world. For example, observed trends in the period 1900 to 2005 show a significant increase in precipitation in eastern parts of North and South America, northern Europe, and northern and central Asia, whereas precipitation declined in the Sahel, the Mediterranean, southern Africa and parts of southern Asia (IPCC, 2007). Overall, the global precipitation since 1901 has increased at an average rate of 0.10 inches per decade (**Figure 2.5-2**), and in the same period global surface temperature has increased by 0.17°F per decade (Blunden *et al.*, 2020).

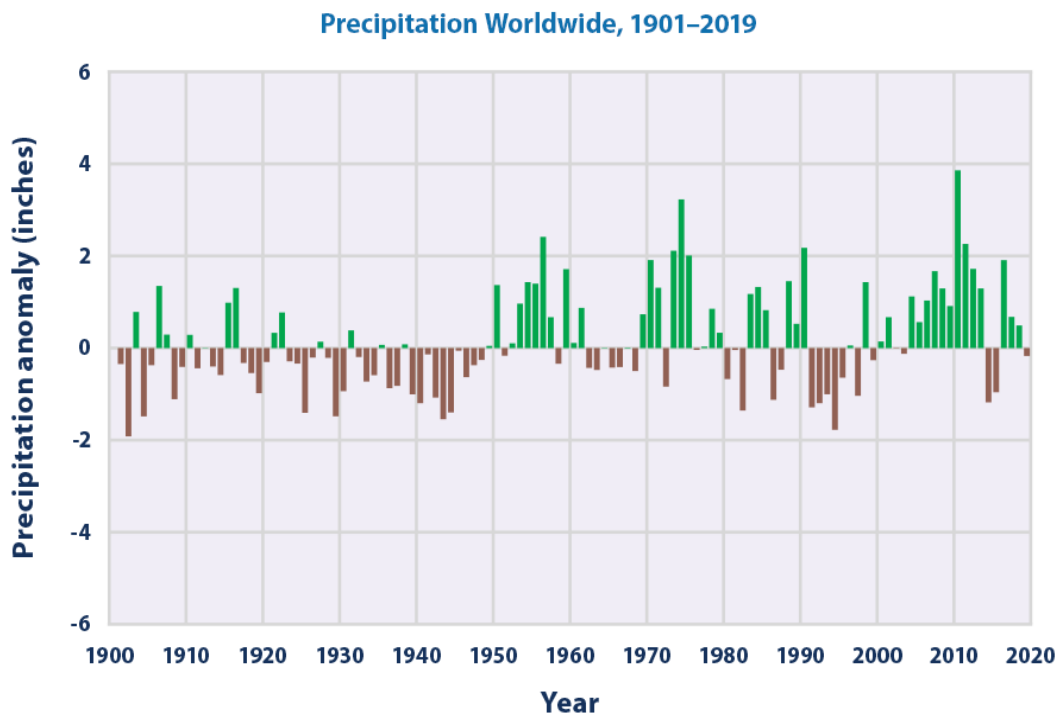


Figure 2.5-2: *Precipitation Worldwide, 1901-2019* (Blunden *et al.*, 2020) .

Southeast Asia and Asia as a whole has also faced rising temperature over the past few decades. Choi *et al.*, (2009) looked at the changes in mean and extreme temperature and rainfall events of 10 Asia Pacific countries from 1955-2007, the study found that the annual average maximum and minimum temperatures have increased by 0.17°C/decade and 0.24°C/decade respectively since the 1950s which are greater than the average global rates.

2.5.2.1 PRECIPITATION AND TEMPERATURE TRENDS IN MALAYSIA

The trend in temperature across Malaysia for the period 1956-2018, shows an increasing trend across all parts of Malaysia, with western Peninsular Malaysia having the highest trend, and the year 2015 – 2016 having the strongest spike in temperatures due to El Nino (Tang, 2019). This is akin to the findings in the report by Malaysian Meteorological Department (MET), for the 40-year period from 1968 to 2007. For the analysis, four meteorological stations namely Kuching, Kota Kinabalu, Kuantan and Petaling Jaya, are chosen which represent Sarawak, Sabah, East and West Peninsular Malaysia respectively. All stations showed an increase in temperature trend, with Petaling Jaya station located in Selangor showing the highest increase in temperature as shown in **Figure 2.5-3** (Malaysian Meteorological Department, 2009).

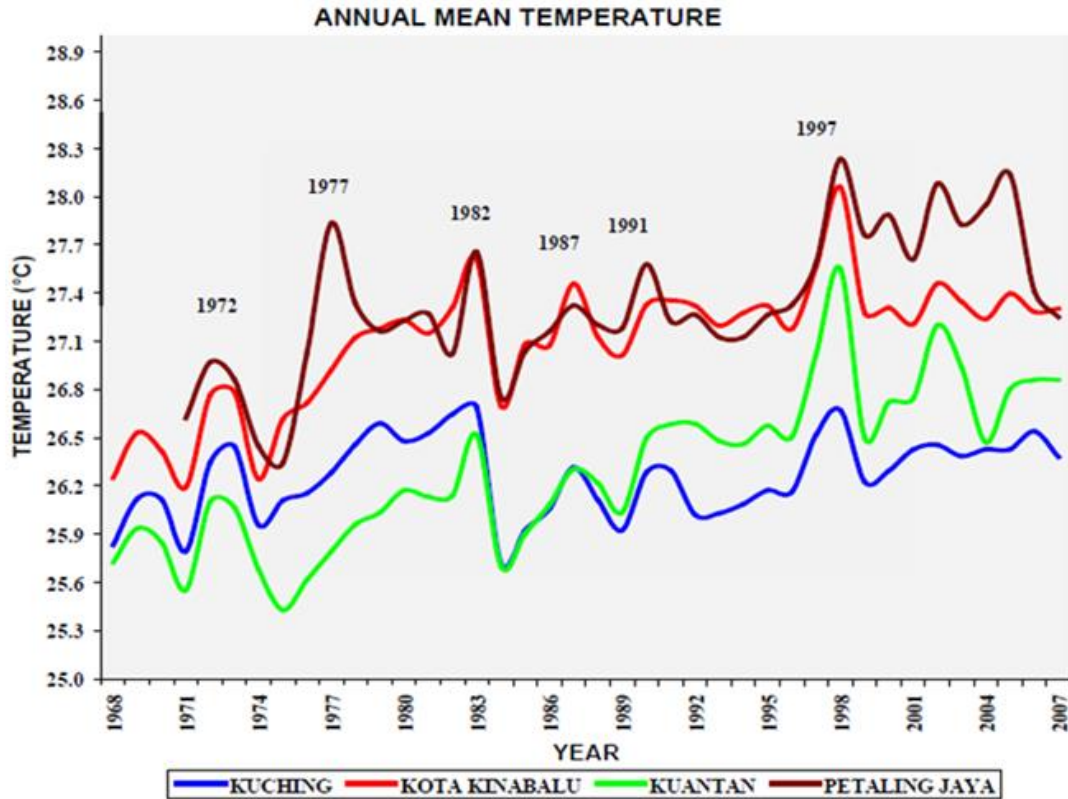


Figure 2.5-3: Annual Mean Temperature Trend For Four Meteorological Stations In Malaysia. (Malaysian Meteorological Department, 2009).

The report also looked at the precipitation trend, where data from 1951 to 2005 is gathered from meteorological stations, and El Nino and La Nina events in this period are also considered too. The results show high variability in rainfall trend, with a fall in rainfall from 1975 to 2005 with more intense and frequent dry spells compared to the period from 1951 to 1975, with the El Nino events having resulted in dry events in Peninsular Malaysia. However, the La Nina events resulted in wet years except for 1955 and 1998, and the wettest years were 1984, 1988 and 1999. Although the dry years are more frequent, the intensity of rainfall

increase during the wet years is comparable with the intensity of dry years (Malaysian Meteorological Department, 2009).

However, the main drawback of this study is that only one meteorological station was used for each of the 4 regions in Malaysia, and this may not give a proper representation of the climatic factors in those regions. Because, both temperature and precipitation can have great spatial variability within local climatic scales. Therefore, adding more meteorological stations will give a better representation of the spatial and temporal variation in climatic factors.

In terms of seasonal climate, the Northeast monsoon (NEM) has a greater influence on annual precipitation compared to the Southwest monsoon (SWM), especially in the eastern parts of Peninsular Malaysia, on the other hand there is a high variability in monthly rainfall in Southwest and Western regions during the NEM (Wong *et al.*, 2016). In eastern Peninsular Malaysia, significant increase in annual, and seasonal precipitation during the period 1971-2010 is detected, at a rate of 12.8 mm/year for annual precipitation, and the Northeast monsoon rainfall increased at a rate of 2.7 mm/year (Mayowa *et al.*, 2015). In Selangor, rainfall trend analysis carried out for the Langat river basin by Palizdan *et al.*, (2014); and Amirabadizadeh *et al.*, (2015), show increasing trend in annual and NEM precipitations, with the rate of increase in annual precipitation being greater than that of the seasonal precipitation.

2.5.2.2 INDICES FOR TREND ANALYSIS

To detect and analyse trends in precipitation and temperature the list of indices recommended by the Expert Team for Climate Change Detection and Indices (ETCCDI) is commonly used (Klein Tank *et al.*, 2009). The ETCCDI indices are easy to calculate and understand, and provide statistically sound measures of daily variability of extreme events derived from daily precipitation and temperature data (Shawul and Chakma, 2020). The list consists of 27 indices for precipitation and temperature as shown in **Appendix A**.

There are several advantages of using the ETCCDI indices, for example SDII considers the total amount of precipitation throughout the year and considers the changes in daily precipitation. As for the benefit of using percentile thresholds like R95p, is that they take the edges of the time series into account, and therefore the number of days exceeding percentile thresholds is more evenly distributed in space and is meaningful in every region.

2.6 LAND USE AND LAND COVER, HYDROLOGICAL AND CLIMATE MODELLING

METHODS

2.6.1 LAND USE AND LAND COVER MODELLING METHODS

Land use change models are great tools for researchers and professionals to explore the dynamics and drivers that bring about

change in LULC (Agarwal *et al.*, 2002). LULC change models are capable of capturing (reproducing) these complex dynamics of LULC change and be used to extrapolate future land use scenarios (Soesbergen, 2016), which can help to inform policies affecting such change. A broad array of models and modelling methods are available to researchers, and each type has certain advantages and disadvantages depending on the objective of the research.

There are statistical and empirical models like logistic regression and Markov chain, dynamic models like Cellular Automata (CA) and integrated models (Al-sharif and Pradhan, 2014). The Markov chain and CA are the most commonly used methods in LULC change and many studies use an integration of CA-Markov method (Hamad *et al.*, 2018; Karimi *et al.*, 2018; Khawaldah *et al.*, 2020; Mansour *et al.*, 2020; Huang *et al.*, 2020).

In recent years, several machine learning (ML) methods have been commonly used in LULC change modelling, like artificial neural network (ANN), support vector machine (SVM) and random forest (RF). For example, Mirici *et al.*, (2017) used a Multi-Layer Perceptron (MLP), ANN and Markov chain approach to simulated future land use change. Whereas Samardžić-Petrović *et al.*, (2016) used the SVM method to model urban land use change.

GIS and remote sensing are also commonly used methods for land use and land cover change modelling. Remotely sensed, multispectral, multiresolution, and temporal satellite images are used by processing and extracting information about land use and land cover changes with the use of GIS tools. Studies like (Hegazy and Kaloop, 2015; Rawat and Kumar, 2015; Haque and Basak, 2017) all used GIS and remote sensing methods to assess land use change.

GIS and remote sensing are user friendly, handle data processing easier and less expertise is needed to analyse data, therefore making these methods popular. Another advantage of using GIS and remote sensing is that it allows support data to help in interpretation and analysis of land use data, but on the other hand GIS and remote sensing also have some disadvantages for example, the different quality of data from various sources can degrade the results of land use and land cover detection (Lu *et al.*, 2004), some of the data used may require large storage space, and processing the data can be time consuming.

In Malaysia, there have been several studies that have used LULC models, GIS, and Remote Sensing to study LULC changes, with these studies having varied spatial scope. For example, Gambo *et al.*, (2018); and Razaai *et al.*, (2020) utilised LULC change modelling to study the changes within and around protected areas. Whereas studies by Verburg *et al.*, (2002); Memarian *et al.*, (2012); Ibrahim and Ludin, (2016);

Kamarudin *et al.*, (2018); and Majid *et al.*, (2018) all studied LULC change at the basin level, and other studies like Boori *et al.*, (2015); Almdhun *et al.*, (2018); and Samat *et al.*, (2020) studied land use change in cities/towns. In Selangor, several studies have carried out LULC change modelling, for example, Boori *et al.*, (2015); Nourqolipour *et al.*, (2015a); Nourqolipour *et al.*, (2015b) and Nourqolipour *et al.*, (2016) analysed LULC change for several areas in Selangor.

2.6.2 HYDROLOGICAL MODELLING METHODS

Hydrological process, like infiltration, stream flow, and surface runoff are an important component of the hydrological cycle. LULC can greatly affect the amount of runoff flowing into rivers and lakes, which depends on soil properties, land cover, elevation, vegetation type and weather variables like precipitation amount, duration and intensity (Sitterson *et al.*, 2017). Hydrological models are powerful tools that help researchers to better understand these processes of the hydrological cycle and their interactions with the land and atmosphere.

There are a wide range of hydrological models available for various types of hydrological studies. These hydrological models can be classified into 2 main categories, stochastic models and deterministic models, based on the presence of random variables, their distribution in space, and temporal variation (Dwarakish and Ganasri, 2015). Hydrological models

can furthermore be classified based on if the hydrological processes are described as conceptual, empirical, or fully physically based as shown in Error! Reference source not found..

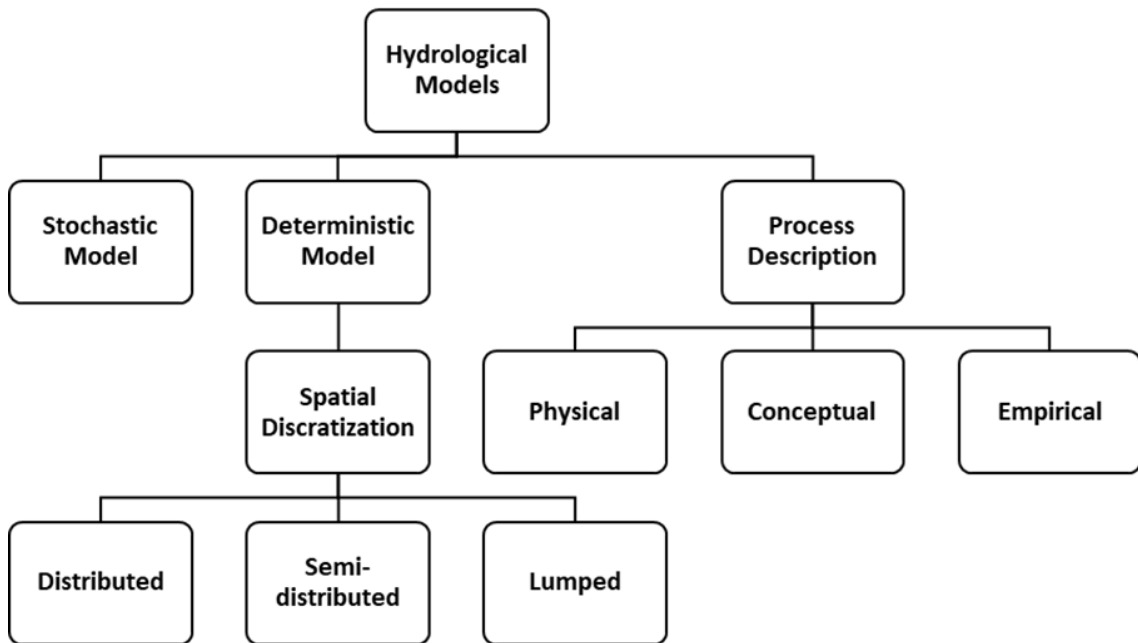


Figure 2.6-1: *The Classification Of Hydrological Models* (Dwarakish and Ganasri, 2015).

2.6.2.1 MAIN HYDROLOGICAL MODEL CLASSIFICATION

2.6.2.1.1 STOCHASTIC MODELS

Stochastic models are mathematical models, which use random variables to represent process uncertainty and generate different results from one set of input data and parameter values when they run under “externally seen” identical conditions. A particular set of inputs will

produce an output according to a statistical distribution. This allows some randomness or uncertainty in the possible outcome due to uncertainty in input variables, boundary conditions, or model parameters.

On the other hand, in deterministic models' randomness is not considered, therefore a given input always produces the same output, where a single set of data and parameter values in a simulation will produce a single result. Stochastic-deterministic models can also be created by introducing stochastic error models to the deterministic models. For example, in a deterministic rainfall-runoff model stochastic rainfall could be used as an input (Pechlivanidis *et al.*, 2011).

2.6.2.1.2 DETERMINISTIC MODELS

Deterministic models can be classified in to 3 classes, lumped models, semi-distributed models, and distributed models.

1. Lumped models are simple models developed based on the water balance equation. They use basin-averaged meteorological inputs and consider the whole basin as a single unit, flow is generated at the basin outlet by homogenising the model parameters throughout the basin, which can often cause over or under estimation (Beven, 2012). The weakness of a lumped model is that it assumes all data including input,

output, and parameters to be uniform both spatially and temporally over the watershed. However, in real world there is variability over space and time, for example rainfall can vary significantly both spatially and temporally (Sitterson *et al.*, 2017).

2. Semi-distributed models, on the other hand, are developed to consider spatial variability of the watershed characteristics. The semi-distributed models are popular models used in hydrological studies, where the models divide the watershed to smaller subbasins, and hydrological computation is carried out separately for each subbasin. There are different ways models divide the watershed, some models like HEC-HMS use natural watershed divides as the criterion for dividing a watershed, whereas other models use the hydrological response unit (HRU), which is based upon the LULC, soil and slope, for example SWAT and HSPF models (Paudel, 2010). A benefit of using semi-distributed models compared to disturbed models is they use less computational time and less data and fewer parameters (Pechlivanidis *et al.*, 2011).
3. Distributed models consider the spatial heterogeneity in input data and parameters, therefore making them the most complex models. Fully distributed models divide the watershed

into homogenous grids, which routes flow through the basin from grid to grid (Brirhet and Benaabidate, 2016). The hydrological process within each grid is calculated separately, however the model incorporates interaction with neighboring grids. This hence can provide greater detail of processes at specific parts of the watershed, and since distributed models are structured like physically based models, they provide modelling which is closer to actual hydrological processes in the watershed. Distributed models require large number of spatially and temporally distributed data, the data include land use maps, DEM, topography, gridded precipitation, soil characteristics and their change over time, and watershed characteristics like dimension and boundaries. Therefore, the disadvantage of using distributed models is, they require long computational time, dependence on input data, catchment size and computational constraints. Secondly, distributed models require distributed data and calibrated parameters for each grid cell. And these models can also be limited spatially by model resolution or input grid size (Vaze *et al.*, 2012).

2.6.2.2 HYDROLOGICAL MODEL CLASSIFICATION BASED ON STRUCTURE

Hydrological models can also be classified based on their structure, into 3 classes, empirical models, conceptual models and physical models (Sitterson *et al.*, 2017).

1. Empirical models, also called data driven models, have no physical transformation function to relate input to output, and hence do not consider the features and process of the hydrological system. Therefore, simple equations are used that relate drivers of runoff response to flow at the watershed outlet. Empirical models often use regression relationship, where there is always a non-linear statistical relationship between input and output, based on hydro-meteorological data, like rainfall and runoff (Vaze *et al.*, 2012). Empirical models, are best suited for ungauged watershed where there is less availability of data, as very few parameters are needed to run the model (Pechlivanidis *et al.*, 2011).
2. Conceptual models describe all the components of the hydrological processes that convert rainfall to runoff. These models use conceptual storage (reservoirs) that interconnect to represent the physical elements in the catchment, whereby they are recharged by rainfall, infiltration and percolation and emptied by evaporation, runoff, and drainage. Mathematical

equations are used to estimate the components of the water balance equation, which determine the movement of water between these storages and in and out of the model. The general equations for conceptual models are versions of the water balance equation which control surface water and storage fluctuations, as shown below.

$$\frac{ds}{dt} = P - ET - Q_s \pm GW \quad (1)$$

Where ds/dt is the change in storage, P is precipitation, ET is evapotranspiration, Q_s is surface runoff and GW is groundwater. One of the drawbacks of conceptual models is, that they require large amount of meteorological and hydrological data for calibration, and the calibration involves curve fitting, which make interpreting the model difficult, therefore effects of land use change cannot be predicated with much accuracy (Devi *et al.*, 2015).

3. Physical models, also referred to as mechanistic models, are based on the physics of hydrological processes, and physically based equations to describe these processes and control watershed responses. Some of the equations used in physically based models, include the water balance equation, conservation of mass and energy, momentum, and kinematics equation (Sitterson *et al.*, 2017). Physical models use variables

that can be measured and are functions of both time and space. Physical models do not require large number of meteorological and hydrological data to calibrate the model, but they do require evaluation of a large number of parameters that describe the physical characteristics of the watershed (Devi et al., 2015).

A comparison and examples of empirical, conceptual, and physical models is shown in **Table 2.6-1**.

Table 2.6-1: Comparison Of The Basic Structure Of Rainfall-Runoff Models (Devi et al., 2015).

	Empirical	Conceptual	Physical
Method	Non-linear relationship between inputs and outputs, black box concept	Simplified equations that represent water storage in catchment	Physical laws and equations based on real hydrologic responses
Strengths	Small number of parameters needed, can be more accurate, fast run time	Easy to calibrate, simple model structure	Incorporates spatial and temporal variability, very fine scale
Weaknesses	No connection between physical catchment, input data distortion	Does not consider spatial variability within catchment	Large number of parameters and calibration needed, site specific
Best Use	In ungauged watersheds, runoff is the only output needed	When computational time or data are limited.	Have great data availability on a small scale
Examples	Curve Number, Artificial Neural Networks	HSPF, TOPMODEL, HBV, Stanford	MIKE-SHE, KINEROS, VIC, PRMS

Semi-distributed physical models are some of the most popular hydrological models used in research studies. One of the most used models is the Soil and Water Assessment Tool (SWAT) that is developed

by USDA Agriculture Research Service (USDA-ARS). SWAT is a river basin or watershed scale, semi-distributed physically based continuous model, which has been extensively used around the world in hydrological studies for various purposes, for example in research on agricultural practices and their effects on hydrological process (Jang *et al.*, 2017; Briak *et al.*, 2019; Chen *et al.*, 2021; Rumph Frederiksen and Molina-Navarro, 2021), or research on water quality (Khwairakpam *et al.*, 2019; Nazari-Sharabian *et al.*, 2019; Y. Wu *et al.*, 2019; Noori *et al.*, 2020) and research on the effects of land use change or climate change on hydrological processes (Shiferaw *et al.*, 2018; Tamm *et al.*, 2018; Bhatta *et al.*, 2019; Ndhlovu and Woyessa, 2020; Saade *et al.*, 2021).

Some of the strengths of the SWAT model, is its ability to integrate different aspects of hydrological modelling, from land use management practices to climate change scenarios, and water quality and quantity studies. Another advantage of using the SWAT model is that it can model yearly, monthly, daily, and even sub-daily simulations over a long period of time. On the other hand, one of the main weaknesses of the SWAT model is, HRUs are not spatially represented in the subbasins, this keeps the model simple, but ignores flow and pollutant routing between HRUs. The other disadvantage of the SWAT model is, it requires a wide range

of different data to run the model and many parameters to modify during calibration, which makes it time consuming (Glavan and Pintar, 2012).

Another widely used method by researchers is the Soil Conservation Service Curve Number (SCS-CN), which is an empirical method used to calculate runoff or infiltration from excess rainfall. The SCS-CN is developed by the Soil Conservation Services of the U.S Department of Agriculture which is first published in Section 4 of the National Engineering Handbook in 1956. SCS-CN takes in to account the soil type, land-use, hydrologic conditions, and antecedent moisture conditions, it is primarily developed for small agricultural watersheds, but over the years it has been used for rural, forest and urban watersheds (Mishra *et al.*, 2012). The popularity of SCS-CN is down to its simplicity to use, easy to understand and that it considers most of the runoff variables. The SCS-CN method is available in many of the hydrological models, like the HEC-HMS and SWAT models.

2.6.3 CLIMATE MODELLING METHODS

2.6.3.1 GLOBAL CLIMATE MODELS

Global climate models (GCM) also sometimes called general circulation models have evolved from atmospheric general circulation models (AGCMs) that used physics only, and mostly predicted daily weather, to more complex models that simulate other aspects of the climate

systems: atmospheric chemistry, aerosols, interaction of land surface, land and sea ice, carbon cycle and biogeochemical processes. GCMs simulate present and project future climate under various scenarios of CO² increase in the atmosphere (Idso *et al.*, 2013). GCMs solve mathematical equations, that account for conservation of energy, mass and momentum and the exchange of these components in the climate systems, based on well documented physical processes (Flato *et al.*, 2013).

In GCMs the Earth's surface is divided into three-dimensional grid cells, and the results of each process modelled in each cell are transferred to neighboring cells, which allows temporal modelling of energy and matter. The resolution of GCMs depend on the grid cell size, the smaller the grid size the higher the resolution of the model, and the more details the model will have (Elias, 2021). However, high resolution models require much higher computing power, which is why there are only several institutions around world capable of carrying out high resolution global climate modelling.

GCMs however have some limitations which can result in uncertainties in the model:

- To produce viable future projections, GCMs must incorporate many physical, chemical, and biological processes that influence climate

over time, however some of these processes are missing or inadequately represented in some GCMs.

- Limitations in computing power is another drawback that GCMs face. This reduces the ability of some GCMs to model important climate processes. Therefore, low-resolution models often fail to capture many important phenomena of regional and lesser scales.

Uncertainty in some GCMs can also arise, due to the failure to account properly for certain “multiplier effects” that could significantly amplify the initial impacts of certain biospheric processes.

2.6.3.2 REPRESENTATIVE CONCENTRATION PATHWAYS

In climate change studies to model and project future climate, assumptions are made based on socio-economic and physical changes within the environment that can affect climate change, and provide possible description of future scenarios with respect to changes in a range of variables like socio-economic, technology, energy, land use and emissions of greenhouse gases and air pollutants (van Vuuren *et al.*, 2011). These assumptions are used as input in climate models to explore potential impacts of anthropogenic climate change and the vulnerability associated with these changes and help provide adaptive policies in decision making under these uncertainties.

In the past several sets of scenarios were created by IPCC like the IS92 scenarios and the Special Report on Emission Scenarios (SRES) scenarios. However, as the need for more detailed scenarios has increased in recent years, with interest in scenarios that consider the impact of different climate policies, a new set of scenarios is developed known as the representative concentration pathways (RCPs). The RCPs are four greenhouse gas concentration (not emissions) trajectories adopted by the IPCC for its Fifth Assessment Report (AR5). The four RCPs, RCP 2.6, RCP 4.5, RCP 6.0, and RCP 8.5, are named after a possible range of radiative forcing values in the year 2100 (van Vuuren *et al.*, 2011).

Each of the RCPs represents a target level of radiative forcing produced by the end of 2100. Radiative forcing is described as the extra heat in the lower atmosphere that will be retained due to additional greenhouse gases, it is measured in Watts per square meter (W/m^2). The RCP2.6 represents the best-case scenario pathway, where greenhouse gas emissions are greatly reduced, resulting in a best estimate global average temperatures rise of $1.6^{\circ}C$ by 2100 compared to the pre-industrial period. On the other hand, RCP8.5 is the worst-case scenario or the business-as-usual scenario, where greenhouse gas emissions continue to grow unregulated, leading to a best estimate global average temperature rise of $4.3^{\circ}C$ by 2100. And the RCP4.5 and RCP6.0 are two

medium stabilisation pathways, with varying levels of mitigation (van Vuuren *et al.*, 2011).

The comparison between SRES scenarios and RCP scenarios, shows the SRES scenarios are slightly higher for CO² concentration. And in terms of CO² concentrations and global temperature change the SRES A1F1 is similar to RCP8.5; SRES A1B to RCP6.0 and SRES B1 to RCP4.5. However, the RCP2.6 scenario show much lower CO² and temperatures values compared to any SRES scenario, this is because it includes the option of using policies to achieve net negative CO² emissions before the end of century, while SRES scenarios do not (IPCC, 2014).

The RCP scenarios have some advantages over SRES scenarios. The major difference between SRES and RCP scenarios is that RCP scenarios start with atmospheric concentrations of greenhouse gases (GHG), whereas SRES scenarios start with socio-economic processes. This reduces uncertainty in modelling, because every modelling step from a socio-economic scenario to climate change impact adds uncertainty. Therefore, by starting with concentrations there are fewer steps to impacts and hence less uncertainty in impact assessment (Jubb *et al.*, 2013; Sanderson *et al.*, 2017).

The other advantage of RCP scenarios is, they consider climate change mitigation policies to limit emissions, whereas the SRES scenarios do not have explicate carbon emission controls.

2.6.3.3 GLOBAL CLIMATE MODEL DOWNSCALING

Downscaling is the process of creating higher spatial resolution data from the coarse global climate models, to have climate data in closer agreement with station level data. There are 2 methods of downscaling GCM models, dynamic downscaling, and statistical downscaling. Statistical downscaling creates high resolution dataset, by developing statistical relationship between the GCMs parameters and locally observed data. It uses historical observations to calibrate statistical models, which then generate future climate data by using the GCMs output for future scenarios on regional scale (Rashid and Hossain, 2018).

On the other hand, dynamic downscaling uses a mesoscale high resolution or regional climate model (RCM) coupled with a GCM to estimate local scale climate (Gaur and Simonovic, 2019). In dynamic downscaling RCMs take the large-scale atmospheric output from GCMs at the lateral boundaries and incorporate detailed surface properties, like topography, land-sea contrast, and surface heterogeneities, to generate realistic high resolution climate data. One weakness of

dynamic downscaling is, because they are nested in GCMs, they are affected by the accuracy of the large scale forcing of GCMs and their biases, therefore there is a need for bias correction with dynamic downscaling (Trzaska and Schnarr, 2014).

2.6.3.4 CLIMATE MODELLING IN MALAYSIA

There are several climate change modelling studies in Malaysia that have assessed the impacts of climate change in various topics, like agriculture, hydrology, and policy mitigation.

For example, a study by the Malaysian Meteorological Department, (2009) used nine coupled Atmosphere-Ocean General Circulation Models (AOGCMs) to study future climate conditions in Malaysia up to year 2100, under the SRES A1B scenario. The results of the ensemble mean temperature and precipitation show, an increase of 2.5°C in mean temperature for both Peninsular and East Malaysia. However, precipitation shows no clear trend due to the high variability, with an increase of 6%-10% in west coast of peninsular Malaysia and Sarawak, 10% increase in Sabah and 4%-6% decrease over central Pahang and coastal Kelantan, relative to the 1990-1999 annual precipitation values.

The study also used the Regional Climates for Impacts Studies (PRECIS) RCM model, to project regional climate under A2 and B2 scenarios at 50 km scale. The average annual temperature from the RCM for all the

regions are consistent with GCM, however there is some deviation from the GCM for the period 2080 to 2089, where significant reduction 0.4°C to 0.5°C is projected by the RCM. As for precipitation the RCM simulates general reduction in annual average precipitation for all regions. However, the decrease in precipitation is more evident in Sabah. The significant decrease in precipitation during years 2028, 2048, 2061 and 2079 simulated by the RCM, is consistent with the corresponding significant decrease in temperature projected for the same 4 years. However, this study assessed the wider sub regional climate in Malaysia, and the study used the older SRES scenarios.

In a similar study by Ngai *et al.*, (2020) seven RCMs under RCP4.5 and RCP8.5 are used to assess precipitation at six sub regions in Malaysia. The results show expected decrease in precipitation frequencies over Malaysia by the end of the century under both scenarios, with western Peninsular Malaysia experiencing 4% to 8% decrease in frequency compared to historic data. However, precipitation intensity and extremes are expected to decrease over Peninsular Malaysia during winter and increase over east Malaysia during summer and autumn.

At watershed level there are only a hand full of studies that have carried out climate change modelling to assess the impact of climate change on hydrological process. For example, Syahmi Armain *et al.*, (2021) used statistical downscaling to downscale the CanESM2 climate model to the

Kelantan River basin scale, and assessed the impact of precipitation change on river discharge under the RCP8.5 climate scenario for two time periods, 2041-2070 and 2071-2100. The study found monthly precipitation is expected to decrease by 30% and river discharge by 50% during both time periods.

Tan, *et al.*, (2019) used climate projections from four Coordinated Regional Climate Downscaling Experiments–Southeast Asia (CORDEX-SEA) models under RCP4.5 and RCP8.5 scenarios to assess the future hydro-meteorological droughts in Johor River basin. The study found that annual precipitation is expected to vary between -44.2% to 24.3% among the 4 models, and maximum and minimum temperatures are expected to increase between 0.8°C-3.7°C and 0.7°C-4.7°C respectively, like precipitation annual stream flow is expected to vary between -88.7% to 42.2%. Overall, it is expected Johor River basin will experience more frequent dry conditions in the future.

As for Klang River basin, climate modelling is carried out by one study only, where Kabiri *et al.*, (2013), used the HadCM3 global climate model for the Klang River basin. The study assessed the future climate change precipitation under the SRES A2 scenario, for 3 time slices the 2020s, 2050s and 2080s. The results show increasing precipitation by the end of the century. However, projections show decrease in mean

precipitation in 2020s by 7% and in 2050s by 0.6%, whereas there is increase in precipitation in 2080s by 12.4%.

However, in majority of these studies, LULC change was not considered when assessing climate change impact on hydrological process. It's important to integrate LULC change into hydro-meteorological studies, as LULC change has direct impact on hydrological process, and on local climate conditions. Therefore, in this study, the combined effects of both LULC change and climate change on hydrological process in the Klang River basin is assessed.

2.7 Summary of Literature Review

The summary of each literature review section highlighting the key findings is presented in **Table 2.7-1**.

Table 2.7-1: Summary Of Literature Review.

Section	Key Findings
1. General Factors Affecting Surface Runoff and River Discharge	<ul style="list-style-type: none"> • Precipitation including its volume, intensity and duration play a significant role in affecting surface runoff and river discharge. • Other factors like urbanisation, deforestation and temperature also have significant impact on hydrological processes.
2. Land Use and Land Cover Change Impacts on Surface Runoff and River Discharge	<ul style="list-style-type: none"> • Agricultural activities, deforestation, and urbanisation significantly impact the hydrological cycle. • Urbanisation replaces natural vegetation and soil with impervious surfaces, increasing surface runoff and the risk of flooding. • Strong correlation between LULC changes and increased runoff volume observed in Malaysia, with urban expansion and agricultural land

having significant impact on hydrological processes.

3. Land Use and Land Cover Change Impacts on Climate Variables

- Biogeophysical processes, such as surface albedo, roughness, and evapotranspiration, are influenced by LULC change and have cascading effects on climate.
- Surface albedo changes can lead to temperature fluctuations that influence other climate variables like precipitation.
- ET and surface roughness affect the energy and moisture budget of the land surface, impacting climate.
- Urbanisation lowers albedo, raises temperatures, and contributes to the Urban Heat Island (UHI) effect.
- UHI can result in higher precipitation intensity over urban areas due to aerosol-enhanced conditional instability.
- The increase in urban areas in Malaysia, particularly in the Greater Kuala Lumpur (GKL) area, has led to significant UHI effects, with temperatures often 4°C - 6°C higher in urban areas compared to rural surroundings.

4. Impact of Climate variability on Surface runoff and River Discharge

- Climate variability, particularly changes in precipitation, has a significant impact on hydrological processes within watersheds.
- Climate change can alter the spatial and temporal dynamics of the water cycle, affecting precipitation patterns, intensity, and duration.
- These changes can lead to alterations in river flow, surface runoff, groundwater recharge, and the overall water balance in a watershed.
- Climate change can also exacerbate the occurrence of extreme hydrological events like droughts and floods.
- Global analyses suggest that mean annual runoff and discharge are projected to increase by more than 10% on about half of the global land area by 2050.
- Research in Malaysia indicates that future climate change is expected to lead to significant increases in mean annual precipitation.
- Climate modelling for the Klang River basin reveals mean annual discharge showing variations and trends based on emission scenarios.

5. Trends In Land-use and Land Cover, Precipitation and Temperature

- Tropical forests have experienced the highest deforestation rates.
- Factors contributing to deforestation include agricultural practices, urbanisation, and mining.
- Palm plantations in Malaysia more than doubled between 1990 and 2020.
- Urbanisation has rapidly increased in Malaysia, making it one of the most urbanised countries in East Asia.
- Temperature trends show a significant increase across Malaysia, with western Peninsular Malaysia experiencing the highest trend.
- Precipitation trends indicate high variability, with periods of increased rainfall and more intense dry spells.
- Seasonal climate is influenced by monsoons, with Northeast monsoon (NEM) having a greater impact on annual precipitation.

6. Land Use and Land Cover, Hydrological and Climate Modelling Methods

- Various LULC models, including statistical, dynamic, and integrated models, are available.
- Markov chain and Cellular Automata (CA) are commonly used methods for LULC change.
- Machine learning methods like Artificial Neural Networks (ANN), Support Vector Machine (SVM), and Random Forest (RF) are increasingly used.
- Hydrological models can be grouped into empirical, conceptual, or physical models.
- Hydrological models can further be grouped as stochastic or deterministic, lumped, semi-distributed, or distributed.
- SWAT is a popular semi-distributed model.
- Global Climate Models (GCMs) help study climate change, with varying spatial resolutions.
- Representative Concentration Pathways (RCPs) provide scenarios for future climate conditions.
- Downscaling methods (dynamic and statistical) are used to refine GCM output for regional-scale studies.
- In Malaysia, various studies have examined climate change impacts on temperature, precipitation, and hydrological processes.
- Few studies have integrated both LULC change and climate change impacts on hydrological processes.

CHAPTER 3: METHODOLOGY

3.1 INTRODUCTION

The following chapter will provide an in-depth explanation of each of the methods used within this study, outlining step-by-step procedures, and data sources used to analyse the impacts of land use and land cover change and precipitation changes on surface runoff and river discharge.

The summary of the overall methodology and data used is presented in

Figure 3.1-1.

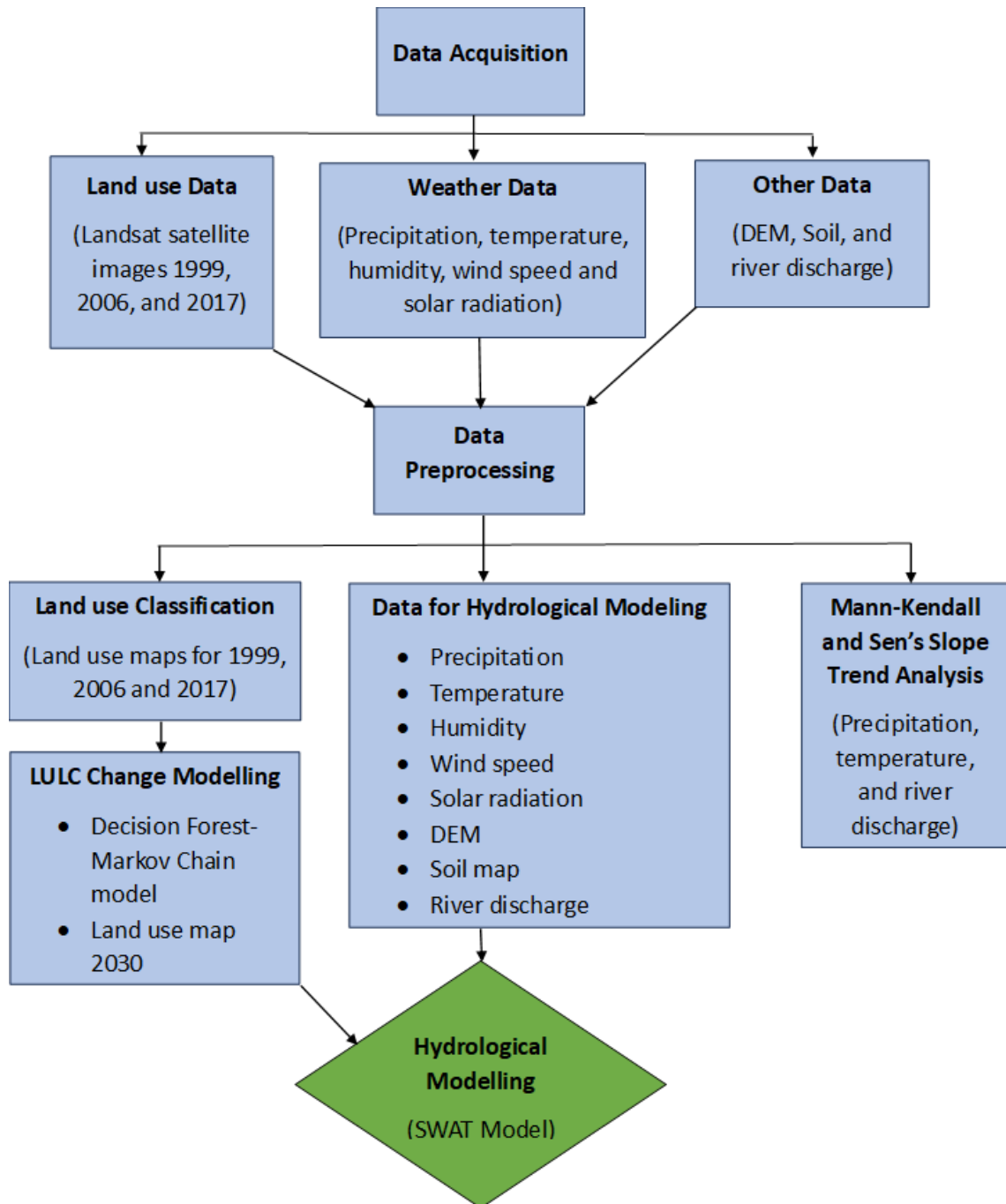


Figure 3.1-1: The Summary Flowchart Of The Overall Methodology.

3.2 STUDY AREA

The Klang River basin is located in West Coast of Peninsular Malaysia in the state Selangor, at latitudes 2°35'-3°60' N and longitudes 100°45'-

102°00' E. **Figure 3.2-1** shows the geographical location of the Klang River basin. Upstream of the basin, elevation is around 1400 m above sea level, and downstream of the basin elevation is between -115 m to 15 m. The federal territory of Kuala Lumpur is located within the Klang River basin, with majority of the 6.5 million inhabitants of Selangor living within the Klang River basin.

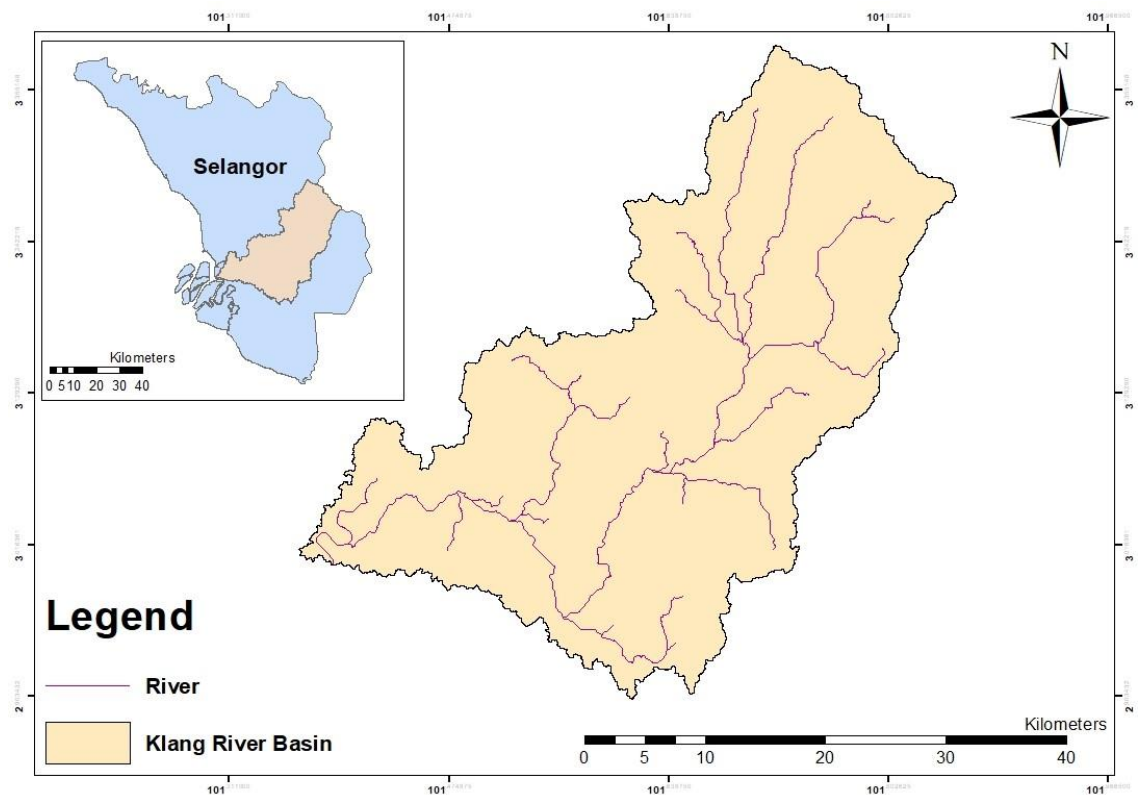


Figure 3.2-1: Map Of The Klang River Basin.

3.2.1 CLIMATE

The Klang River basin receives widespread heavy and prolonged rainfall during the summer (May–September) and winter (November–March) seasons, associated with the SWM and NEM monsoon winds,

respectively (**Figure 3.2-2**), with 2 inter- monsoon periods occurring in April (IntM1) and October (IntM2). At the same time, because of its nearness to the equator, heavy localised rainfalls of shorter duration, associated with severe convective thunderstorms created by unstable weather conditions, occur throughout the year. The average annual rainfall ranges from 1900 mm to over 2600 mm. The mean monthly temperature in the basin ranges from 26-28°C, with a daily mean humidity of about 80%-85%.

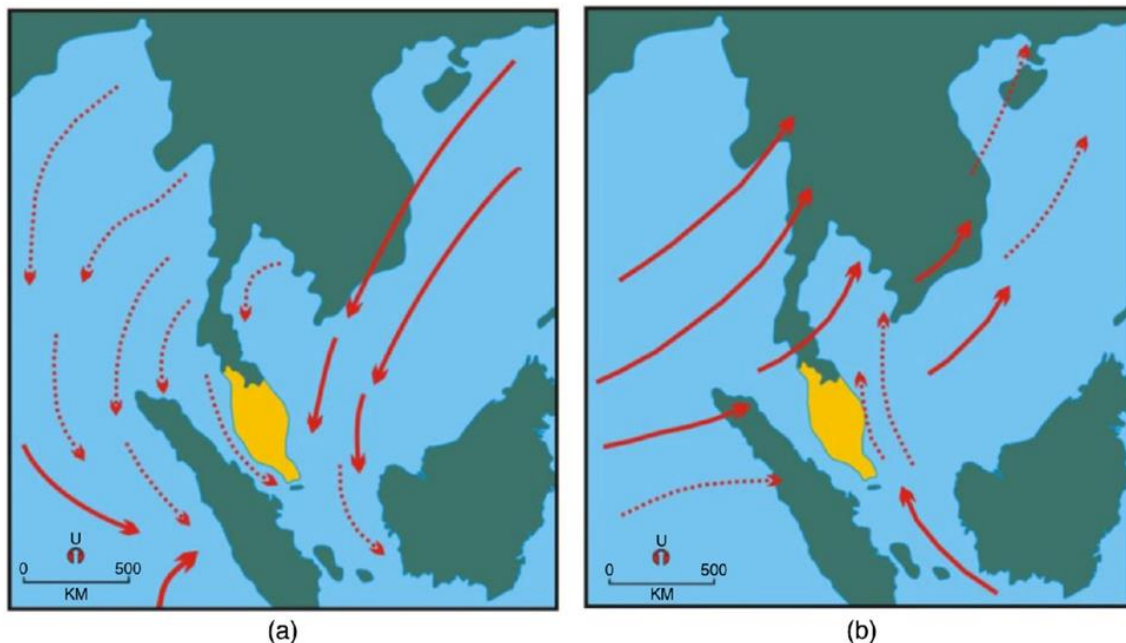


Figure 3.2-2: (a) Northeast Monsoon And (b) Southwest Monsoon (Bakar et al., 2020).

3.2.2 GEOLOGY AND SOIL

The upper part of the Klang River basin consists of mostly igneous rocks, in particular granite with some dacite, rhyolite, and micro granodiorite.

The Northwest of the Klang River basin is made up of mostly granitic rocks and vein quartz of the Mesozoic age, with some parts of the Northwest being covered by schist of Kajang formation. The central parts of the basin is underlain by limestone of the Kuala Lumpur limestone formation, and schist underlies the land between Kelang and Gombak River, while most of the Ampang area is underlain by granite (Balamurugan, 1991).

The soils in the Klang River basin consist of a wide range, which vary from very thin sandy regolith covering quartzite ridges to the extremely deep weathering profile on the most gentle granite slopes. The soils are mostly formed from igneous, sedimentary, and metamorphic rocks, and marine and river alluvium. Like most sedentary soil in Western Malaysia, the soils in the Klang River basin are highly weathered, leached, and low in nutrient, with a strong influence from parent rock materials. Slope also plays a large part in the formation of soils in the Klang River basin, where soils on hill tops are generally shallow and young compared to those in the lower slopes (Balamurugan, 1991).

3.2.3 DRAINAGE AND WATER RESOURCES

The Klang River is 120 km in length, and consists of several tributaries, namely, Batu River, Gombak River, Kerayong River, Damansara River, Keroh River, Kuyoh River, PENCHALA River and Ampang River. The Klang

River originates upstream on the eastern part of the basin and flows through KL and eventually drains into the Malacca strait to the west of the basin. The basin area is approximately 1285 km², which is mostly urbanised, with the upstream of the basin having tropical rain forests.

3.3 DATA ACQUISITION

3.3.1 LAND USE AND LAND COVER DATA

The study used Landsat 5 TM (1999 & 2006) and Landsat 8 OLI (2017) satellite images (**Table 3.3-1**) obtained from United State Geological Services (USGS) at (<http://earthexplorer.usgs.gov/>). The Shuttle Radar Topography Mission (SRTM) digital elevation map is also obtained from USGS website, the ancillary data like, road network and rivers are obtained from open street website at (<https://www.openstreetmap.org>) which are used for land use change modelling. The slope map is created from the DEM and using the slope tool in ArcGIS.

Table 3.3-1: Landsat Image Information Used In Study.

Date	Satellite	Resolution	Date Acquired
1999	Landsat 5 Thematic Mapper	30m	11th February 1999
2006	Landsat 5 Thematic Mapper	30m	2nd March 2006
2017	Landsat 8 Operational Land Imager	30m	27th March 2017

Landsat images are chosen because, the Landsat images have a wider spatial coverage at 30 m resolution, compared to other satellites like Sentinel, therefore there is less need for image mosaicking. Another reason for choosing Landsat, is that for the study area Landsat images

have less cloud cover compared to other satellite images, and the images for the years 1999, 2006 and 2017 are chosen, as they have less than 10% cloud cover.

The LULC maps, are compared with the LULC maps from the Department of Town and Country Planning Malaysia (JPBD). Although, the LULC maps from JPBD has more land use classes under urban and agricultural classes, the overall classification does match the LULC classifications in this study.

3.3.2 HYDRO-CLIMATIC DATA

The climate data consists of precipitation and temperature data, and the hydrological data consists of river discharge. For precipitation, daily data from 8 stations obtained from the Department of Irrigation and Drainage (DID) and 2 stations from the MET is used. The location of each station is shown in **Figure 3.3-1**, and the station details are shown in **Table 3.3-2**. The period for the rainfall data for the DID stations is from 1975-2015, however for station 3117070 it's from 1975-2019, and for station 3116006 from 1977-2019, as for the 2 stations for MET, the data period is from 1995-2018.

For temperature, due to insufficient data, the ERA 5 reanalysis daily mean, maximum and minimum 2m temperature data from the European Centre for Medium-Range Weather Forecasts (ECMWF) at 0.25° by

0.25° spatial resolution for the period 1979 to 2018 is used, the data is obtained from ClimateEngine.org.

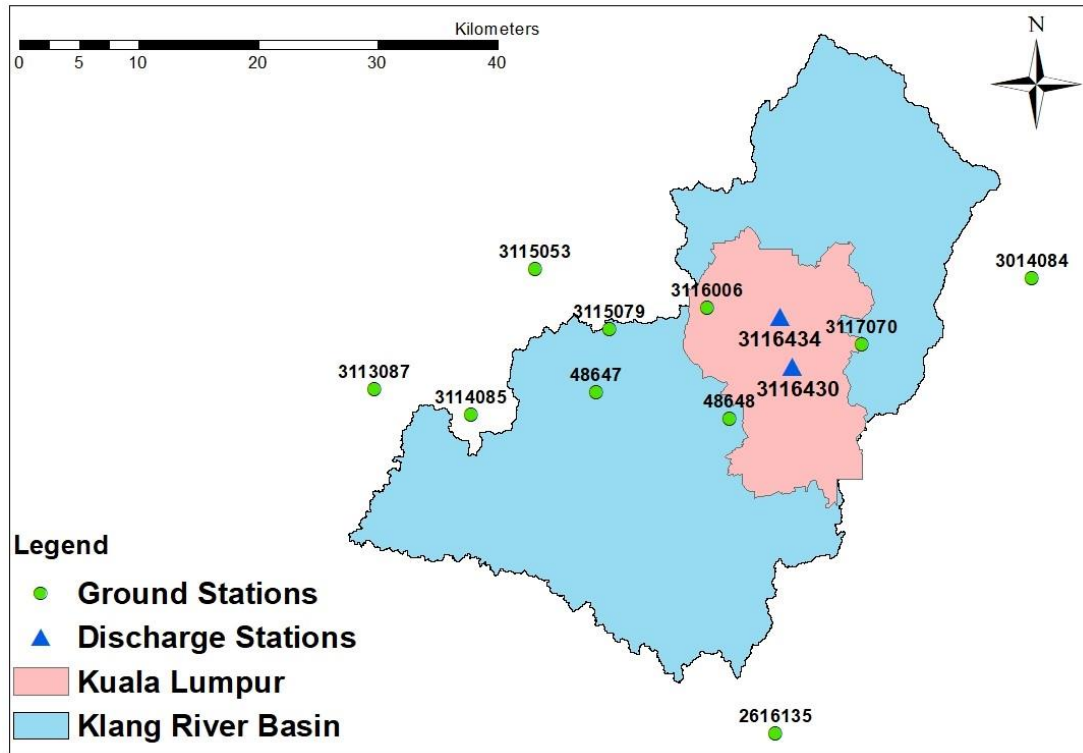


Figure 3.3-1: Location Of Selected Hydro-Climatic Stations.

Table 3.3-2: Station Name, ID, Coordinates, And Period Of Data, For Selected Stations.

Station ID	Station Name	Latitude	Longitude	Data Period
2616135	Ldg. Telok Merbau	2.86	101.68	1975 - 2015
3014084	Pejabat JPS Klang	3.21	101.88	1975 - 2015
3113087	Ldg. Sg. Kapar	3.12	101.38	1975 - 2015
3115079	Pusat Penyelidikan Getah Sg.Bul	3.17	101.56	1975 - 2015
3114085	Setia Alam	3.1	101.46	1975 - 2015
3115053	Ldg. Elmina A	3.21	101.5	1975 - 2015
48648	Petaling Jaya	3.1	101.65	1995 - 2018
48647	Subang	3.12	101.55	1995 - 2018
3117070	Pusat Penyelidikan at JP Ampang	3.16	101.75	1975 - 2019
3116006	Ldg. Edinburgh	3.18	101.63	1977 - 2019
3116430	Jambatan Sulaiman	3.14	101.70	1973 - 2017
3116434	Batu Sentul	3.18	101.69	1970 - 2018

An ensemble of 5 GCMs, each with 4 RCPs scenarios supported by Inter-Sectoral Impact Model Intercomparison Project (ISI-MIP5) for daily precipitation, maximum and minimum temperature is used for future climate change analysis. This daily data covers the period 1950 to 2099, and the data is obtained from 2w2e.com, where the data is reformatted from NetCDF into SWAT-readable text files. The 5 GCM models used to analyse the future climate are; HadGEM2-ES, IPSL-CM5A-LR, MIROC-ESM-CHEM, GFDL-ESM2M, and NorESM1-MThe (**Table 3.3-3**), and the 4 RCPs scenarios used are RCP2.6, RCP4.5, RCP6 and RCP8.5 (Abbaspour *et al.*, 2019).

Table 3.3-3. Details Of The Global Climate Models Used In The Study.

Data Type	Resolution	Period of Data	Source
GCM 1	0.5°	(1960-2099)	GFDL-ESM2M, daily, RCP (2.6, 4.5, 6.0, 8.5), NOAA/Geophysical Fluid Dynamics Laboratory
GCM 2	0.5°	(1960-2099)	HadGEM2-ES, daily, RCP (2.6, 4.5, 6.0, 8.5), Met Office Hadley Center
GCM3	0.5°	(1960-2099)	IPSL-CM5A-LR, daily, RCP (2.6, 4.5, 6.0, 8.5), L'Institut Pierre-Simon Laplace
GCM4	0.5°	(1960-2099)	MIROC, daily, RCP (2.6, 4.5, 6.0, 8.5), AORI, NIES and JAMSTEC
GCM5	0.5°	(1960-2099)	NorESM1-M, daily, RCP (2.6, 4.5, 6.0, 8.5), Norwegian Climate Center

The data used from the GCMs consist of historic data from 1960-2005 and future data from 2006-2099. In this study we used 3 future time periods (TP) to analyse the future climate variables, the time periods used are TP1 (2006-2039), TP2 (2040-2069) and TP3 (2070-2099).

3.3.3 HYDROLOGICAL MODELLING DATA

SWAT requires large geospatial input data to drive watershed dynamics. These data include topography (Digital Elevation Map), weather data, soil physical parameters and LULC map. The accuracy of model prediction depends on data availability and quality. All the input maps are projected to the WGS 1984 UTM Zone 47N projection.

3.3.3.1 DIGITAL ELEVATION MAP

SRTM digital elevation map (DEM) with the resolution of 90 m by 90 m for the study area (**Figure 3.3-2A**) obtained from USGS (<https://earthexplorer.usgs.gov/>) is used in this study.

3.3.3.2 SLOPE

Slope represents the rate of change of elevation for each DEM cell. The slope map (**Figure 3.3-2B**) is created from the DEM using the slope tool in ArcGIS.

3.3.3.3 SOIL

FAO-UNESCO soil map of the World, which is based on the FAO-UNESCO soil map of the world, is obtained from Food and Agriculture Organisation (FAO). The soil map is at 1:5.000.000 scale. The soil map for the study area is shown in (**Figure 3.3-2C**) and the soil code and its classification are shown in **Table 3.3-4**.

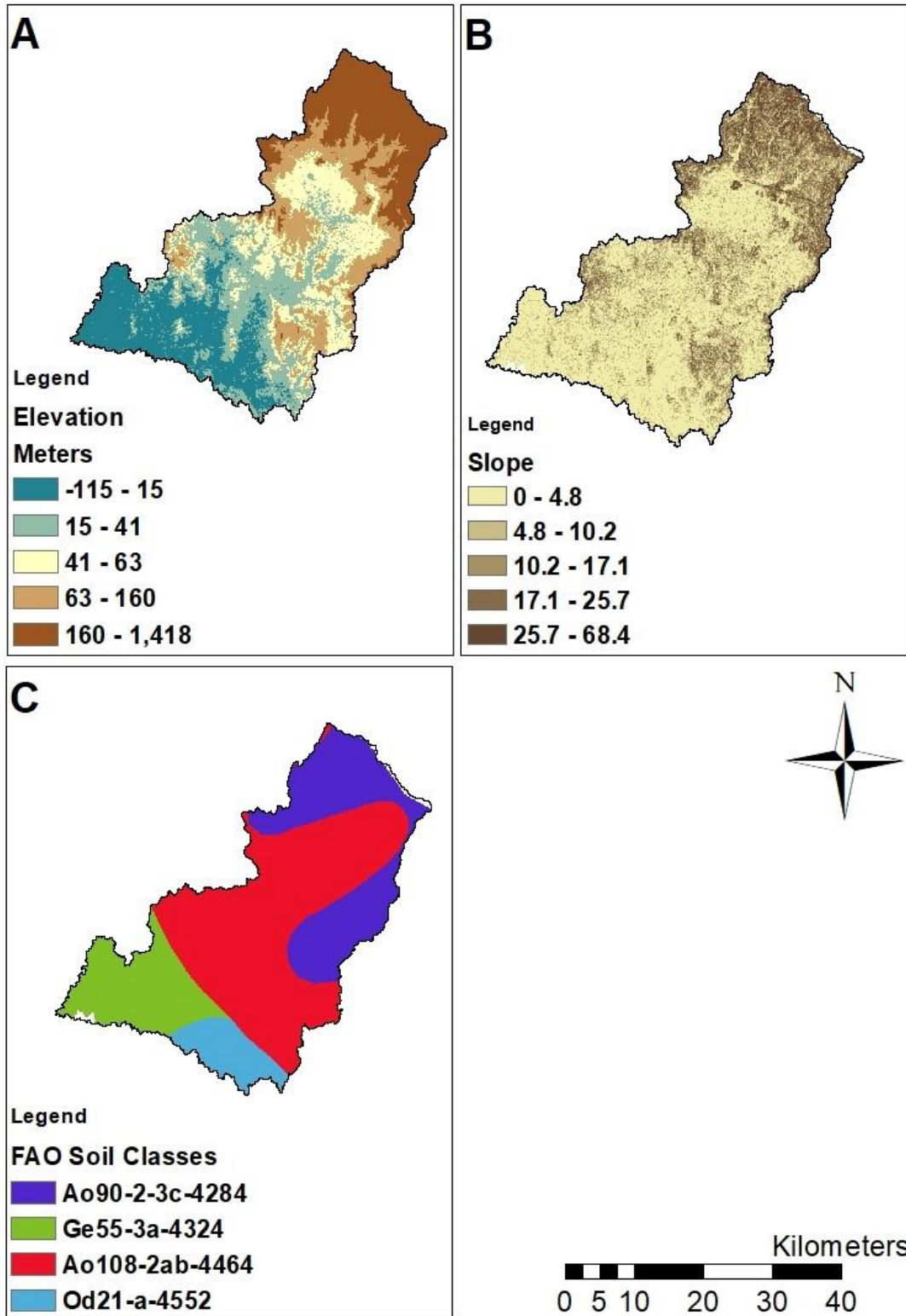


Figure 3.3-2: A. Elevation Map, B. Slope Map And C. Soil Map Of The Study Area.

Table 3.3-4: *FAO Soil Code And Soil Classification.*

Soil Classification				
FAO Soil Code	Dominant Soil Unit	Soil Association	Textural Class	Slope Class
Ao108-2ab	Orthic Acrisols	Ferric Acrisols and Dystric Nitrosols	Medium texture	Level to undulated and rolling to hilly
Ao90-2-3c	Orthic Acrisols	Humic Acrisols, Dystric Cambisols and Lithosols	Medium and fine texture	Steeply dissected to mountainous
Ge55-3a	Eutric Gleysols	Gleyic Cambisols and Thionic Fluvisols	Fine texture	Level to undulated
Od21-a	Dystric Histosols	Humic Gleysols and Thionic Fluvisols	-	Level to undulated

3.3.3.4 LAND USE AND LAND COVER

The classified land use maps for the years 1999, 2006, 2017 (**Figure 4.1-1**) and 2030 (**Figure 4.1-2**) are used as the land use inputs. The land use maps consist of 5 classes; Water, Natural Vegetation, Agriculture, Built Up and Cleared Land. The SWAT LULC codes and their representative LULC types are shown in (**Table 3.3-5**).

Table 3.3-5: *LULC Classification And SWAT Code.*

LULC SWAT Code	LULC Classification	SWAT Definition
WATR	Water	Water
FRSE	Natural Vegetation	Evergreen Forest
AGRL	Agriculture	Agricultural Generic
URHD	Built Up	Urban High Density
BARR	Cleared Land	Bare Ground

3.3.3.5 WEATHER

The weather data is an important input in hydrological modelling; therefore, the lack of weather data and the poor quality of data can increase modelling uncertainty and bring about limitations to the study,

which is a common issue in hydrological studies. To compensate for the lack of data, many hydrological studies use other sources of data like reanalysis and satellite data. Hence in this study we incorporate reanalysis and satellite data with observed data to improve the quality of weather input data and compensate for lack of data. The weather variables used in this study are daily precipitation, daily maximum and minimum temperature, relative humidity, solar radiation, and wind speed.

For precipitation, data from 8 stations obtained from DID and 2 stations obtained from MET, located within and around the watershed is used (**Figure 3.3-3**). To increase the coverage of the precipitation data over the basin, the study integrated the Climate Hazards Group InfraRed Precipitation with Station data (CHIRPS) precipitation data with observed data. CHIRPS is a 35+ year quasi-global rainfall data set with a resolution 0.05° ranging from 1981 to near-present.

The CHIRPS product is an integration of various datasets: the monthly precipitation climatology (CHPclim) that is created using rain gauge stations collected from FAO and GHCN, the Cold Cloud Duration (CCD) information based on thermal infrared data archived from CPC and NOAA National Climate Data Centre (NCDC), the Version 7 TRMM 3B42 data, the Version 2 atmospheric model rainfall field from the NOAA

Climate Forecast System (CFS), and the rain gauge stations data from multiple sources.

Several studies have shown the CHIRPS dataset to perform well in hydrological modelling and having better agreement with observed data compared to other datasets (Tuo *et al.*, 2016; Dhanesh *et al.*, 2020; Pang *et al.*, 2020; Zhang *et al.*, 2020).

For temperature, data are only available from 2 MET stations, therefore due to lack of data, ERA5 reanalysis data is integrated with the 2 MET station data. As for relative humidity, wind speed, and solar radiation there is no observed data available, therefore the ERA5 reanalysis data is also used for wind speed and for relative humidity data from NASA's The Prediction of Worldwide Energy Resources (POWER) project dataset is used at resolution of $1/2^\circ$ by $5/8^\circ$. For solar radiation simulated data within SWAT model is used.

All the weather datasets used for the hydrological modelling are for the period 1995-2018.

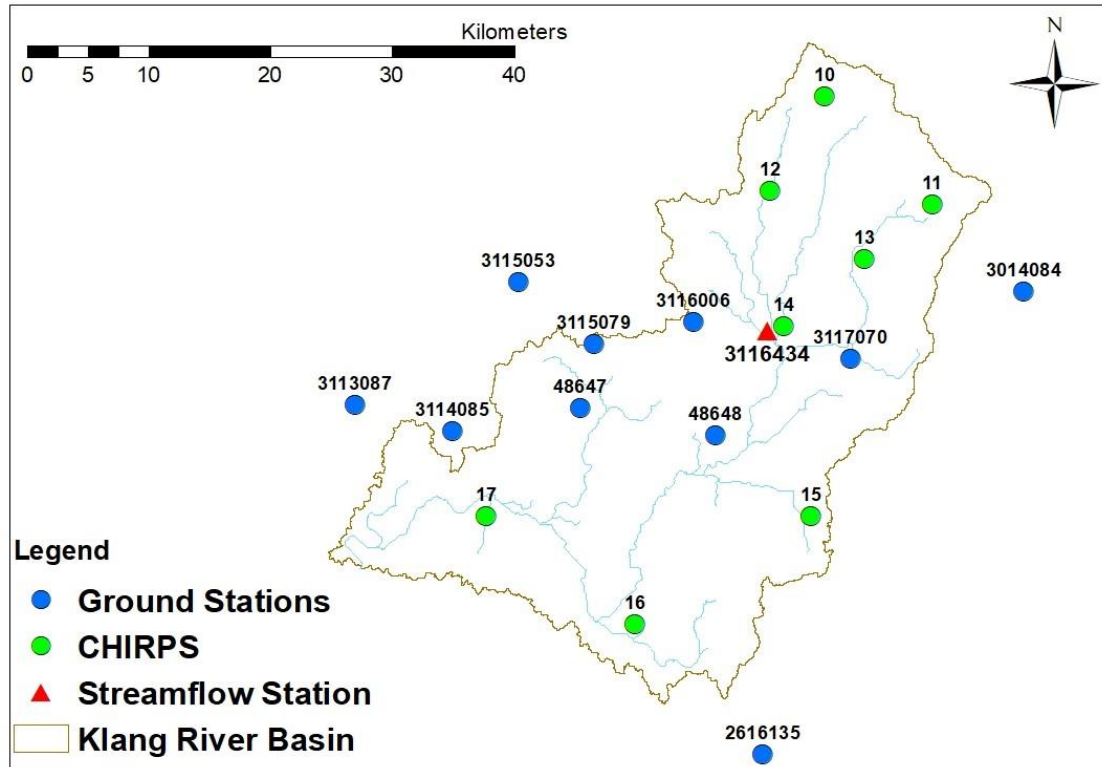


Figure 3.3-3: Ground Stations And CHIRPS Locations For Precipitation Data.

3.3.3.6 STREAMFLOW DATA

River discharge data is obtained from DID, for stations Jambatan Sulaiman (3116430) and Batu Sentul (3116434) as shown in **Figure 3.3-1** under **Section 3.3.2** for the periods 1973 to 2017 and 1970 to 2018 respectively.

3.4 METHODOLOGY

3.4.1 ANALYSIS OF SPATIO-TEMPORAL TRENDS IN LAND-USE AND LAND

COVER

The **Figure 3.4-1** shows the flowchart of the methods used in the land use and land cover modelling.

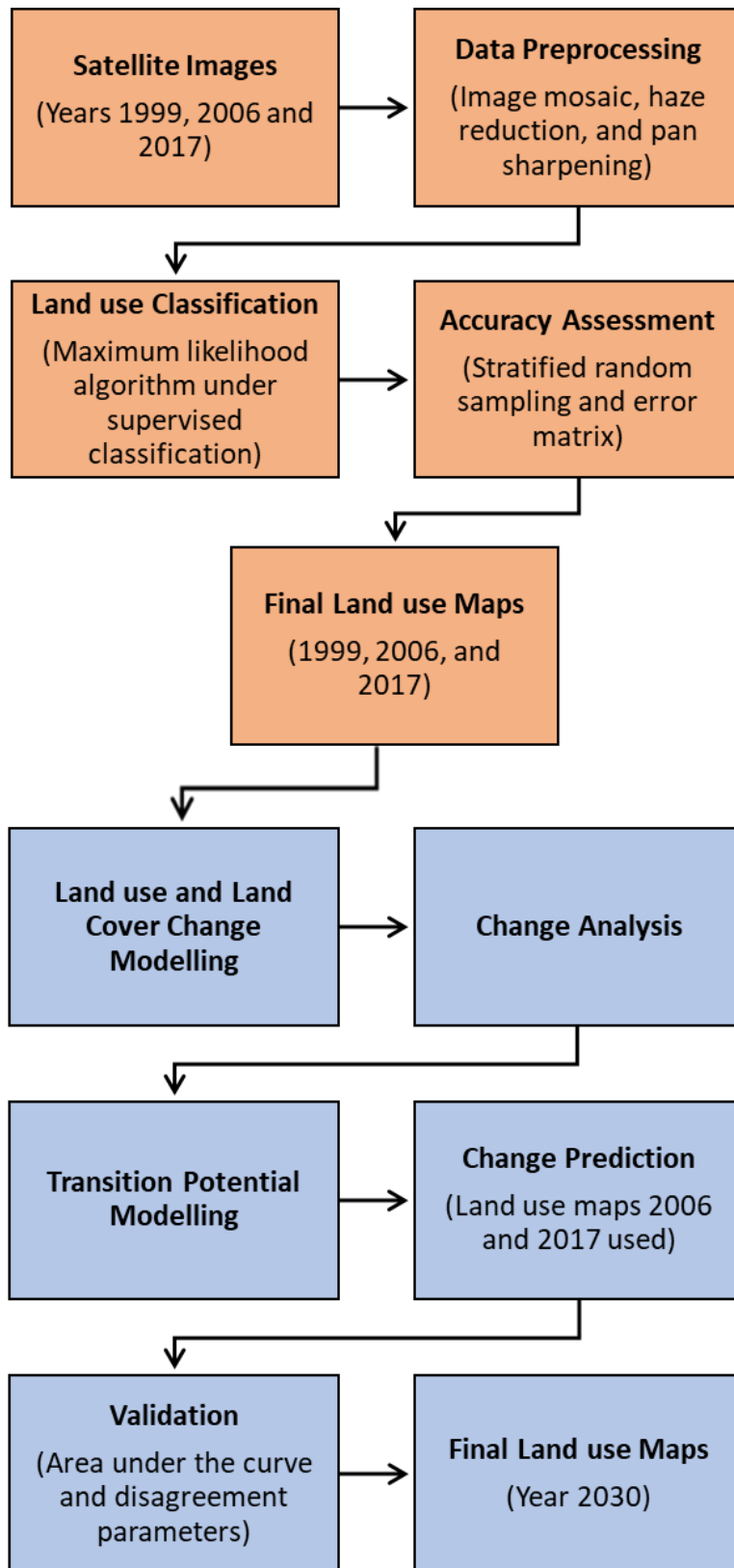


Figure 3.4-1: Summery Flowchart Of The Land-Use And Land Cover Modelling.

3.4.1.1 LAND USE AND LAND COVER CLASSIFICATION

Image mosaic is carried out to merge images which give the full extent of the study area, followed by haze reduction process to remove, or reduce any haze in all the images, and for the 2017 image the panchromatic band of Landsat 8 is used to pan sharpen the image and improve its spatial resolution from 30 m to 15 m, for better interpretation and classification of land use.

The maximum likelihood algorithm under supervised classification which is a commonly used method for classification is performed to classify Landsat images of 1999, 2006, and 2017. The following 5 land use classes are generated; Water, Natural Vegetation, Agriculture, Built-up and Cleared Land.

3.4.1.1.1 ACCURACY ASSESSMENT

For accuracy assessment, error matrix which is a commonly used method is calculated, using stratified random sampling. 150 sample points are generated for the study area for each map, and ground truth data obtained from Google Earth is used as reference points.

3.4.1.2 LAND USE AND LAND COVER CHANGE MODELLING

To simulate a future land use map, an integrated Decision Forest - Markov Chain (DF-MC) model is used. The DF-MC method uses the Random Forest machine learning algorithm, which consists of an

ensemble of Decision Trees (DT). This method has only been used in few land use change modelling studies in recent times (Al-sharif and Pradhan, 2015; Samardžić-petrović *et al.*, 2015; Karimi *et al.*, 2019). However, the Random Forest algorithm has shown to have several advantages over other machine learning methods. It is faster and easier to understand and interpret, the algorithm is completed at a fixed number of operations, it can process large volumes of data, a small quantity of parameters is needed to be adjusted during modelling, and has higher accuracy compared to other machine learning algorithms, as shown in studies by (Kamusoko and Gamba, 2015; Legdou *et al.*, 2020; Mao *et al.*, 2020).

The Land Change Modeller (LCM) in TerrSet software developed by Clack Labs, is used for the modelling. The LCM is based on historical land use data, transition potential maps and Markov matrices, to simulate future LULC change. The LCM consists of 3 main steps, change analysis, transition potential modelling, and change prediction. The data used in this study are the land use maps of the years 1999, 2006 and 2017, and the parameters used in the land use change are, distance to roads, distance to rivers, distance to urban areas, digital elevation map and slope.

3.4.1.2.1 CHANGE ANALYSIS

The change analysis step calculates the nature and extent of land use change between time 1 and time 2 and between 2 land use maps, the changes that are identified are transitions from one land use state to another. The change analysis evaluates gains and losses, detect net gains, and create change maps.

3.4.1.2.2 TRANSITION POTENTIAL MODELLING

In this step the potential of land to transition are identified, and transition potential maps for each transition is created. The transition potential maps that have same underlying driver variables, are grouped within an empirically evaluated transition sub-model. A transition sub-model can consist of a single land use transition or a group of transitions that are thought to have the same underlying driver variables. These driver variables are used to model the historical change process.

The driver variables used in this study are, distance to roads, distance to rivers, distance to urban, DEM and slope (**Appendix B**). The driver variables are selected based on literature review and authors knowledge of the study area. The transition potential maps are created using Decision Forest algorithm, which is implementation of the Random Forest method.

3.4.1.2.3 CHANGE PREDICTION

In the final step, the historical change of rates calculated in the change analysis step and the transition potential maps, are used to predict a future scenario for a specified future date. The Markov Chain determines the amount of change using the earlier and later land cover maps along with the date specified. The procedure determines exactly how much land would be expected to transition from the later date to the prediction date based on a projection of the transition potentials into the future and creates a transition probabilities file. The transition probabilities file is a matrix that records the probability that each land cover category will change to every other category.

To validate the model, the LULC maps of 1999 and 2006 are first used to simulate a LULC map of 2017, which is then validated against the reference LULC map of 2017. Then in the next step the future land use map of 2030 is simulated using the 2006 and 2017 LULC maps. The year 2030 is chosen for future LULC map, to reflect the Malaysian Government Shared Prosperity Vision 2030, with one of its visions being sustainability, which aims to achieve national development which is eco-friendly and gives emphasis on conserving and preserving natural resources. This is also in line with the United Nations (UN) 2030 Agenda for Sustainable Development (SDG 2030) and the Selangor structural Plan 2035.

The gains and losses and net gain for the year 1999-2006 and 2006-2017 from the change analysis step is shown in (**Appendix C**).

3.4.1.2.4 VALIDATION

For the validation of the model the Area under the Curve (AUC) of Total Operating Characteristic (TOC) and disagreement parameters (allocation disagreement and quantity disagreement) methods are used. TOC method indicates how well the model is predicting change, while the allocation and quantity disagreement provides detailed information on the accuracy of predicted change and persistence of each land cover class.

Quantity disagreement (quantification error) is when the quantity of cells of a class in the simulated map is different from the quantity of cells of the same class in the reference map. On the other hand, allocation disagreement (location error) is when the location of a class in the simulated map is different from location of that class in the reference map. These metrics of disagreement are recommended by (Pontius and Millones, 2011; Pontius *et al.*, 2011) as an alternative to Kappa statistics, since Kappa indices attempt to compare accuracy to a baseline of randomness, but randomness is not a reasonable alternative for map construction.

The accuracy of the model is based on four components of disagreement namely, hits (accuracy of observed versus predicted change), misses (error due to observed change predicted as persistence), false alarms (error due to observed persistence predicted as change) and correct rejections (accuracy of observed versus predicted persistence) (Kushwaha *et al.*, 2021).

3.4.2 ANALYSIS OF SPATIO-TEMPORAL TRENDS IN PRECIPITATION AND TEMPERATURE

The summary flowchart of hydro-climatic trend analysis is shown in

Figure 3.4-2.

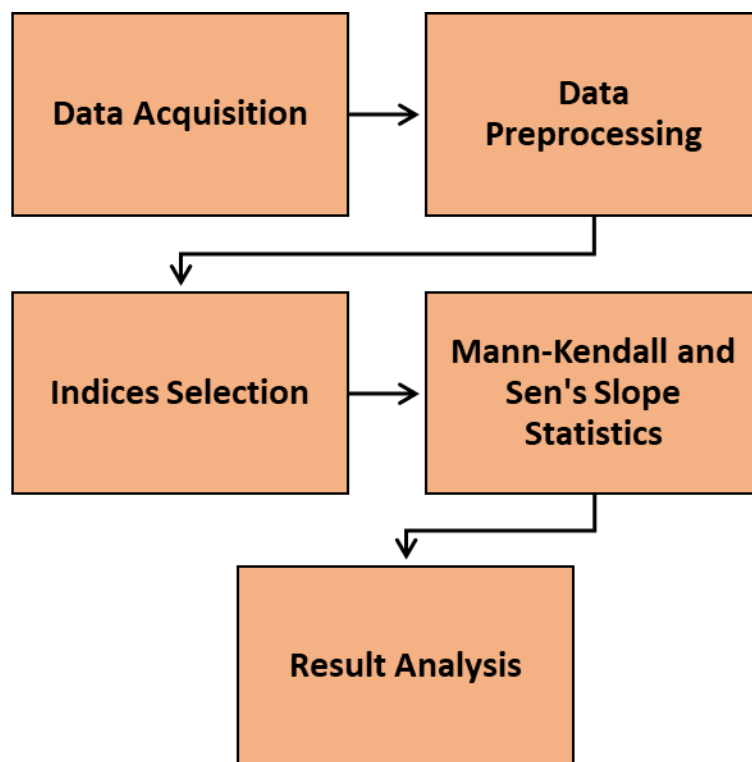


Figure 3.4-2: Summary Flowchart Of The Hydro-Climatic Trend Analysis.

3.4.2.1 DATA PREPROCESSING

3.4.2.1.1 NORMALITY AND AUTOCORRELATION

Before carrying out the trend analysis, normality, and autocorrelation tests are conducted for the data of each station. For normality, four tests are used, the Shapiro-Wilk test, the Anderson-Darling test, the Lilliefors test, and the Jarque-Bera test, and for autocorrelation, the Durbin Watson test is used.

The Durbin Watson measures autocorrelation (also called serial correlation) in residual from regression analysis. Autocorrelation occurs when there are similarities of a time series data over successive time intervals, which can lead to underestimates of the standard error and can result in insignificant predictors to appear as significant. The Durbin Watson test always assumes values between 0 and 4, where:

2 is no autocorrelation.

0 to <2 is positive autocorrelation (common in time series data).

>2 to 4 is negative autocorrelation (less common in time series data).

Test statistic values in the range of 1.5 to 2.5 are commonly considered as relatively normal, and hence no autocorrelation is present, on the other hand values outside of this range could be cause for concern. The Durbin-Watson statistics can also be tested for significance using the

Durbin-Watson Table. For each value of alpha (.01 or .05) and each value of the sample size n (from 6 to 2000) and each value of the number of independent variables k (from 1 to 20), the table contains a lower and upper critical value (d_L and d_U). The test value d greater than d_U indicates there is no autocorrelation, values below d_L indicate there is autocorrelation and values between d_L and d_U indicate the test is inconclusive.

The data for all stations are found to be normally distributed, and there is no autocorrelation found in the data.

3.4.2.1.2 OUTLIER DETECTION

The method suggested by (Crochemore *et al.*, 2019) is used to detect the outliers in river discharge. In this method the outlier detection is based on the median and standard deviation of the data, while the median is not sensitive to outliers, the standard deviation is sensitive to the existence of outliers. First the data is standardised by subtracting the median from the data. Then all the values greater than five times the standard deviation ($5SD$) is flagged as outliers, and finally the outliers are visually inspected to differentiate with peak flows, where outliers are considered as events instead of single days, where one outlier consists of consecutive days above the threshold ($5SD$).

3.4.2.1.3 FILLING MISSING DATA

The precipitation stations with less than 10 percent of missing data are chosen for the study. And since Mann-Kendall test has a low sensitivity to abrupt breaks and missing values (Sa'adi *et al.*, 2019), the missing data are ignored, and not considered in the trend analysis.

As for the river discharge data, since there is lack of neighboring stations to carry out linear interpolation regression method and multiple imputation method did not give accurate representation of the data, therefore the dates with missing value are ignored in trend analysis. And after visual inspection of the data, it is found that data from 2014-2018 for station Batu Sentul (3116434) has irregular pattern, where for the 5-year period all daily discharge is less than or equal to 1m/s, which indicates an issue with the instrument or an unknown element in the river upstream of the station resulting in the reduced flow. Therefore, this 5-year period is removed from the analysis.

3.4.2.1.4 VALIDATION OF ERA5 DATA

The ERA 5 reanalysis temperature data are compared and validated with temperature data from stations 48648 and 48647, using correlation coefficient (R^2), mean absolute error (MAE), root mean square error (RMSE), and Pearson's correlation coefficient (R) as shown in **Table 3.4-1**.

The correlation of coefficient (R²) is the measure of how strong the linear relationship is between 2 variables, the R² values range between -1 to 1, a correlation value of -1 shows a perfect correlation but negative and a value of 1 show a perfect positive correlation, and a correlation coefficient 0 shows no correlation. The correlation coefficient R² is similar to Pearson’s correlation coefficient R, where R² is square of the Pearson’s coefficient R. The RMSE on the other hand is used to measure the difference between predicted values from a model and observed values. Root Mean Square Error (RMSE) is the standard deviation of the residuals (prediction errors). And the residuals are a measure of how far from the regression line data points are; RMSE is a measure of how spread out these residuals are. Whereas the MAE is the mean of the amount of error in the measurements. The MAE measures the average magnitude of the errors in a set of predictions, without considering their direction.

The ERA5 data covers grids of 0.25 by 0.25 therefore for temperature trend analysis, data for each grid covering the study area is used **(Figure 3.4-3)**.

Table 3.4-1: Statistics Comparing ERA5 Data With Observed Data.

	Station 48647	Station 48648
Root Mean Square Error (RMSE)	0.995	1.075
Correlation Coefficient (R ²)	0.636	0.654
Pearson's correlation coefficient(R)	0.798	0.809

Mean Absolute Error (MAE)	0.83	0.887
----------------------------------	------	-------

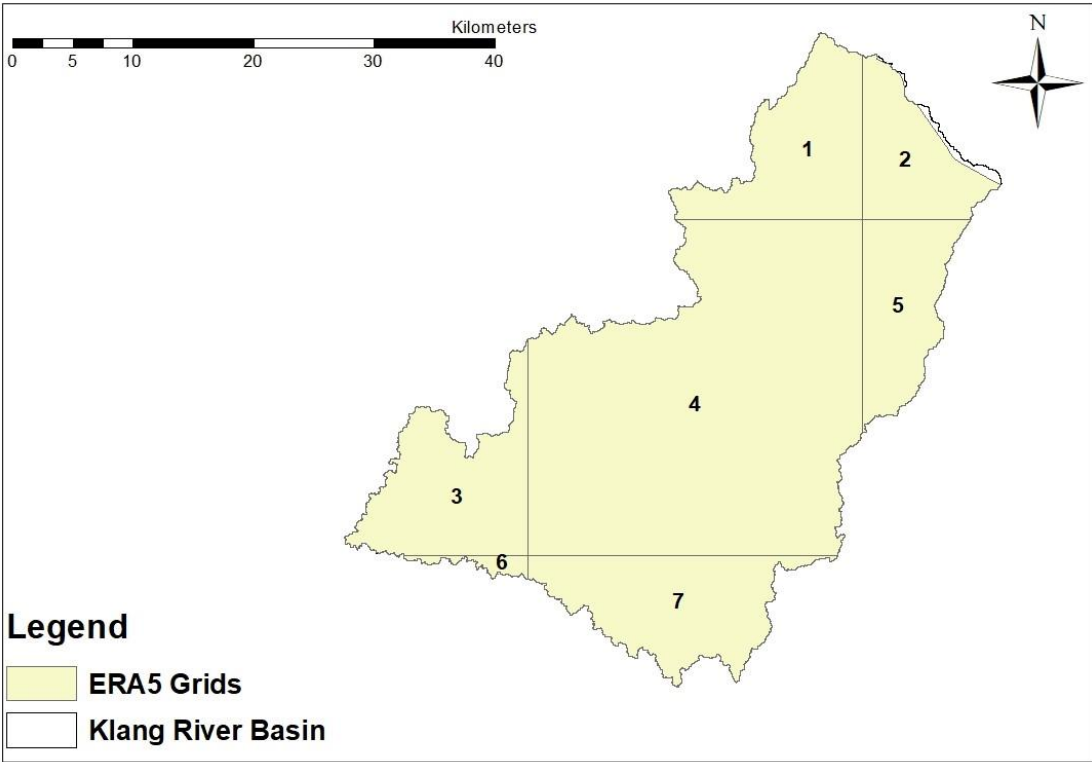


Figure 3.4-3: ERA5 grid for the study area, from which temperature data is collected.

3.4.2.1.5 DOWNSCALING OF THE GCM MODELS

The Water and global change (WATCH) forcing data is a 20th century meteorological forcing dataset for land surface and hydrological models, which is generated as part of the European Union’s (EU) 6th Research Framework Program (FP 6). The 5 GCM models are downscaled using the 0.5° grid WATCH Forcing Data, the period 1960 to 1999 is used as the reference period to downscale the GCM models.

WATCH is a combination of the ERA-40 daily data, which is the 40-year reanalysis of the European Centre for Medium-Range Weather Forecasts, and the Climate Research Unit TS2.1 dataset (CRU). The WATCH Forcing Data combines the daily statistics of ERA-40 with the monthly mean characteristics of CRU and Global Precipitation Climatology Centre (GPCC) datasets and represents a complete gridded observational dataset for bias correction of global climate data (Abbaspour *et al.*, 2019).

3.4.2.2 SELECTED INDICES FOR PRECIPITATION AND TEMPERATURE

ANALYSIS

The indices selected for the trend analysis of precipitation and temperature are chosen from the list recommended by the Expert Team for Climate Change Detection and Indices (ETCCDI). For precipitation 4 indices were selected, the R10mm and Rnnmm indices represented precipitation frequency, whereas the R95p and SDII represented the intensity of precipitation. For temperature 2 indices were selected, the TXx and TNx.

The Department of Irrigation and Drainage (DID) has categorised rainfall intensity into 4 categories (**Table 3.4-2**). In this study we used R10mm index to represent the light rainfall intensity and for Rnnmm

index we used rainfall amount $\geq 30\text{mm}$ which represents heavy rainfall intensity.

Table 3.4-2: Rainfall intensity categories according to Department of Irrigation and Drainage.

Categorisation of Rainfall Intensity (in one hour.)	
Light	1-10(mm)
Moderate	11-30(mm)
Heavy	30-60(mm)
Very Heavy	> 60(mm)

3.4.2.3 MANN-KENDALL TREND STATISTICS

Trend analysis is important when studying climate variables as it shows significant changes in these variables over time. The Mann-Kendall test (Mann, 1945; Kendall, 1975) is used to analyse the trend in annual and seasonal precipitation and precipitation intensity. The Mann-Kendall (MK) test is a non-parametric test, therefore the data does not need to fit a normal distribution, and it can identify if there are linear or non-linear trends in the time series data. The null hypothesis of the Mann-Kendall test is that there is no trend in the data, whereas the alternative hypothesis is that there is a trend in the data, and this trend can be positive, negative, or non-null.

The Mann-Kendall test statistic S is calculated using the formula.

$$S = \sum_{k=1}^{n-1} \sum_{j=k+1}^n \text{sgn}(X_j - X_k) \quad (2)$$

Where x_j and x_k are the annual values in years' j and k , $j > k$, respectively, and

$$\mathit{sgn}(X_j - X_k) = \begin{cases} 1 & \text{if } X_j - X_k > 0 \\ 0 & \text{if } X_j - X_k = 0 \\ -1 & \text{if } X_j - X_k < 0 \end{cases}$$

As suggested by (Salmi *et al.*, 2002) if n is 9 or less, the absolute value of S is compared directly to the theoretical distribution of S derived by Mann and Kendall. The two-tailed test is used for four different significance levels α : 0.1, 0.05, 0.01, and 0.001. At a certain probability level, the null hypothesis is rejected in favor of the alternative hypothesis if the absolute value of S equals or exceeds a specified value $S_{\alpha/2}$, where $S_{\alpha/2}$ is the smallest S which has a probability less than $\alpha/2$ to appear in case of no trend. A positive (negative) value of S indicates an upward (downward) trend. If n is at least 10, the normal approximation test is used. However, if there are several tied values (i.e., equal values) in the time series, it may reduce the validity of the normal approximation when the number of data values is close to 10. First, the variance of S is computed by the following equation which considers that ties may be present:

$$\mathit{VAR}(S) = \frac{1}{18} \left[n(n-1)(2n+5) - \sum_{p=1}^q t_p(t_p-1)(2t_p+5) \right] \quad (3)$$

Here q is the number of tied groups and t_p is the number of data values in the p th group.

The values of S and $\mathit{VAR}(S)$ are used to compute the test statistic Z as follows:

$$z = \begin{cases} \frac{S-1}{\sqrt{VAR(S)}} & \text{if } S > 0 \\ \mathbf{0} & \text{if } S = 0 \\ \frac{S+1}{\sqrt{VAR(S)}} & \text{if } S < 0 \end{cases} \quad (4)$$

The Z value indicates a significant trend, where a positive (negative) value of Z indicates an upward (downward) trend, and the statistic Z has a normal distribution. To test for either an upward or downward monotone trend (a two-tailed test) at a level of significance, H0 is rejected if the absolute value of Z is greater than $Z_{1-\alpha/2}$, where $Z_{1-\alpha/2}$ is obtained from the standard normal cumulative distribution tables. In this research, we used the MAKESENS excel templet which is developed by the Finnish Meteorological Institute to calculate the Mann-Kendall test, and the significance is considered at 0.01 and 0.05 levels of significance.

3.4.2.3.1 SEN'S SLOPE

Sen's slope estimator Q is used to measure the magnitude of change. Sen's nonparametric method is used to estimate the true slope of an existing trend (as change per year), which is developed by Sen (Sen, 1968). The Sen's slope estimator Q is calculated by:

$$Qi = \frac{X_j - X_k}{j - k} \quad (5)$$

where $j > k$.

If there are n values X_j in the time series, we get as many as $N = n(n-1)/2$ slope estimates Q_i . Sen's estimator of the slope is the median of these N values of Q_i . The N values of Q_i are ranked from the smallest to the largest and the Sen's estimator is:

$$Q = Q_{\left[\frac{N+1}{2}\right]}, \text{ if } N \text{ is odd.}$$

or (6)

$$Q = \frac{1}{2} (Q_{\left[\frac{N}{2}\right]} + Q_{\left[\frac{N+2}{2}\right]})$$

A $100(1-\alpha)\%$ two-sided confidence interval about the slope estimate is obtained by the nonparametric technique based on the normal distribution. The method is valid for n as small as 10 unless there are many ties.

3.4.2.4 LAND SURFACE TEMPERATURE TREND ANALYSIS

The Land Surface Temperature (LST) trend analysis summary flowchart is shown in **Figure 3.4-4**.

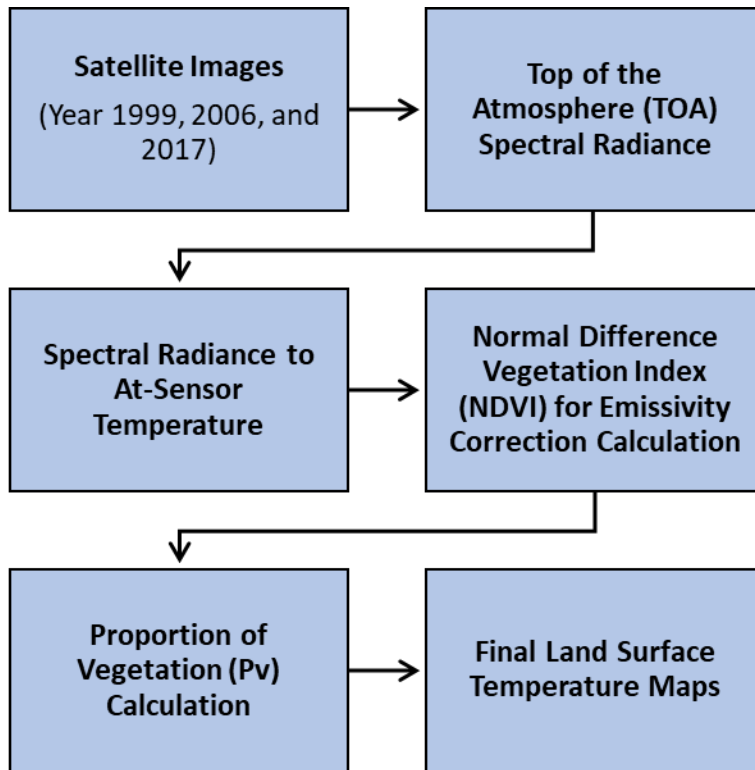


Figure 3.4-4: Summary Flowchart Of The Land Surface Temperature Modelling.

The Land Surface Temperature (LST) is calculated for the year 2017 using the thermal band (band 10) and bands 6 and 5 of the Landsat images, and for LST for years 1999 and 2006 only the thermal band (band 6) is used. To obtain the LST map of 2017 from Landsat 8 image, methods used in (Avdan and Jovanovska, 2016) are used. The first step is to calculate the top of the atmosphere (TOA) spectral radiance with the equation:

$$L\lambda = M_L * Q_{cal} + A_L - O_i \quad (7)$$

Where M_L represents the band-specific multiplicative rescaling factor, Q_{cal} is the Band 10 image, A_L is the band-specific additive rescaling

factor, and O_i is the correction for Band 10. All these data are available in the metadata of the image.

The second step is to convert the spectral radiance to At-sensor temperature, using the thermal constants provided in the metadata. The following equation is used to get the brightness temperature (BT).

$$BT = \frac{K_2}{\ln[(K_1/L\lambda)+1]} - 273.15 \quad (8)$$

Where K_1 and K_2 stand for the band-specific thermal conversion constants obtained from the metadata. To convert the results from Kelvin to Celsius, the absolute zero (-273.15°C) is added to the equation.

The next step is to calculate Normal Difference Vegetation Index (NDVI) for emissivity correction. To calculate NDVI, the visible and near-infrared bands are used. The calculation of NDVI is essential since the amount of vegetation present is an important factor, and NDVI is used to calculate proportion of vegetation (P_v). The following equation is used to calculate NDVI.

$$NDVI = \frac{NIR(\text{band } 5) - R(\text{band } 4)}{NIR(\text{band } 5) + R(\text{band } 4)} \quad (9)$$

Where NIR represents the near-infrared band (Band 5) and R represents the red band (Band 4).

The next step is to calculate the proportion of vegetation (P_v) using the equation (10).

$$P_v = \left(\frac{NDVI - NDVI_{min}}{NDVI_{max} - NDVI_{min}} \right)^2 \quad (10)$$

Where $NDVI_{min}$ is the minimum value of NDVI obtained from equation (9) and $NDVI_{max}$ is the maximum value of NDVI.

This is then followed by calculating the Land Surface Emissivity (LSE), which is important in calculating LST, since the LSE is a proportionality factor that scales blackbody radiance (Planck's law) to predict emitted radiance, and it is the efficiency of transmitting thermal energy across the surface into the atmosphere. LSE is calculated using equation (11), which is suggested by (Sobrino, Jiménez-Muñoz and Paolini, 2004).

$$\varepsilon = 0.004P_v + 0.986 \quad (11)$$

The final step is to calculate the LST or the emissivity corrected land surface temperature T_s , using the equation (12).

$$T_s = \frac{BT}{\{1 + [(\lambda BT / \rho) \ln \varepsilon]\}} \quad (12)$$

Where, T_s is the LST in Celsius, BT is at-sensor BT ($^{\circ}C$), λ is the wavelength of emitted radiance (for which the peak response and the average of the limiting wavelength ($\lambda = 10.895$) will be used), ε is the emissivity calculated in equation (11), and

$$\rho = h\sigma^c = 1.438 * 10^{-2}mK \quad (13)$$

Where σ is the Boltzmann constant (1.38×10^{-23} J/K), h is Planck's constant (6.626×10^{-34} J s), and c is the velocity of light (2.998×10^8 m/s).

For LST for years 1999 and 2006, obtained from Landsat 5, the steps and equations from the Landsat hand book is used (Ihlen and Zanter, 2019).

For Landsat 5, band 6 which is the thermal band is used to obtain LST. First the Digital Number (DN) is converted to spectral radiance (L_λ) using the equation (14)

$$L_\lambda = \left(\frac{LMAX_\lambda - LMIN_\lambda}{QCALMAX - QCALMIN} \right) * (QCAL - QCSLMIN) + LMIN_\lambda \quad (14)$$

Where, L_λ is the Spectral radiance at the sensor's aperture in (Watts/ ($m^2 * sr * \mu m$)), QCAL is band 6, LMIN λ is Spectral radiance scaled to QCALMIN in (Watts/ ($m^2 * sr * \mu m$)), LMAX λ is the Spectral radiance scaled to QCALMAX in (Watts/ ($m^2 * sr * \mu m$)), QCALMIN is Minimum quantized calibrated pixel value (corresponding to LMIN λ) in DN and QCALMAX is the Maximum quantized calibrated pixel value (corresponding to LMAX λ) in DN. All these values are found in the metadata of Landsat 5.

The next step is to calculate LST, by using the equation (15).

$$T = \frac{K2}{\ln\left(\frac{K1}{L_\lambda} + 1\right)} - 273.15 \quad (15)$$

Where, T is the Effective at-satellite temperature in Kelvin, K2 is the Calibration constant 2, K1 is the Calibration constant 1 and L_λ is Spectral radiance in (Watts/ (m² * sr * μ m)) which is calculated in equation (14). The K1 and K2 constants are found in the metadata of Landsat 5. Finally, the LST is converted from Kelvin to Celsius by adding the absolute zero (-273.15°C) to the equation.

3.4.3 DEVELOPMENT OF SPATIO-TEMPORAL HYDROLOGICAL MODEL

3.4.3.1 SWAT MODEL DESCRIPTION

The summary of the SWAT model setup is presented in the **Figure**

3.4-5.

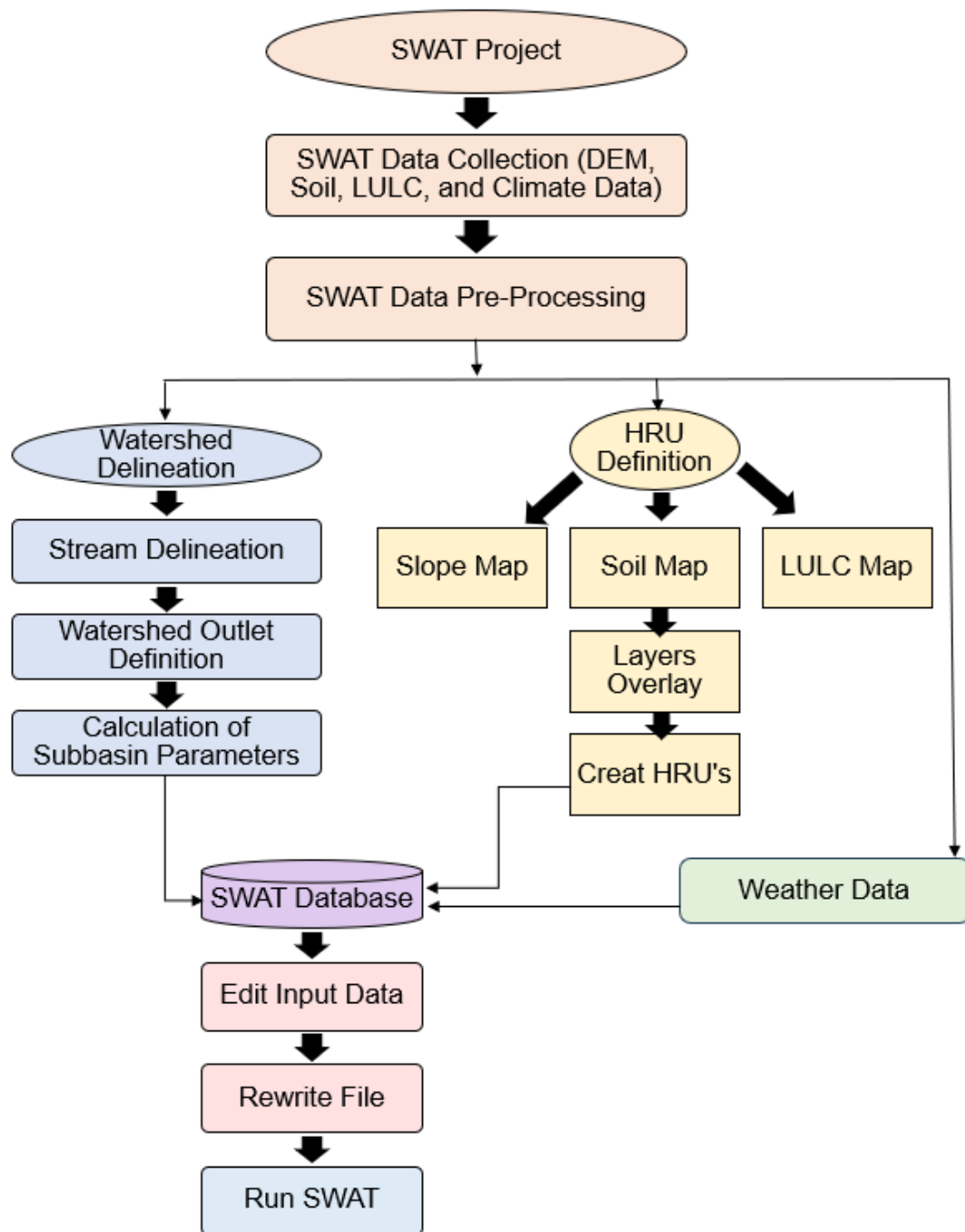


Figure 3.4-5: Summary Flowchart Of The Hydrological Modelling Using SWAT Model.

The Soil and Water Assessment Tool (SWAT) (Arnold *et al.*, 1993; Arnold *et al.*, 1998), is a long-term, continuous simulation watershed model.

SWAT is a public domain model that is developed by the USDA Agricultural Research Service (USDA-ARS) and Texas A&M AgriLife Research. Its main aim is to predict the impact of land management practices on water, sediment and agricultural chemical yields with reasonable accuracy in a large, complex, ungauged watersheds with varying soil, land use and management conditions over long periods of time (Neitsch *et al.*, 2000a; Neitsch *et al.*, 2000b). SWAT is a physically based model that can run at various time steps including daily, monthly and yearly (Gassman *et al.*, 2007).

The major components used in the model include weather, hydrology, soil properties, plant growth, pesticides, and land management (Arnold *et al.*, 2012). The model divides the watershed in to sub watersheds, which are further divided into Hydrologic Response Units (HRUs) that represent areas of homogeneous land use, management, topographical and soil characteristics (Neitsch *et al.*, 2011). The output from each HRU is routed to the stream within the sub watershed, and the model does not simulate the interaction among HRUs (Srinivasan *et al.*, 2005).

Water balance is the moving force behind all the processes in SWAT, as it affects plant growth and movement of sediments, nutrients, pesticides, and pathogens. Watershed hydrology is divided into a land phase and a water phase. The land phase deals with sediment and nutrient loading in to the main channel in each sub basin, and the water

phase (in-stream or routing phase) deals with movement of water and sediment through the channel network of the sub basin to the outlet (Arnold *et al.*, 2012).

There are several hydrological components that SWAT is able to manage, for example surface runoff, stream flow and subsurface flow, evaporation from the soil, evapotranspiration from plant canopy and aquifer recharge (Neitsch *et al.*, 2000). SWAT uses the modified USDA-SCS Curve Number (CN) method (USDA Soil Conservation Service, 1972) to estimate runoff volumes from daily rainfall, and uses Modified Universal Soil Loss Equation to estimate sediment yield for each sub-watershed or HRU (Williams, 1995).

3.4.3.2 MODEL SETUP

The study is conducted using SWAT 2012 with ArcSWAT 10.1.18 interface which is an extension of ArcGIS. The first step in the model setup is watershed delineation, where the basin and sub-basin boundaries plus stream networks are delineated using the DEM map. This was then followed by adding reservoirs to the watershed, and in the Klang River basin there are 2 reservoirs, the Batu dam, and the Klang Gates dam.

To simulate the reservoir outflow, the targeted release method is used since release data from the dams are not available. In this method, a

target storage is set, and the water released from the reservoir is a function of the target storage. This method is a simplistic method, and does not consider all decision criteria, however it does follow the general release rules used by reservoir operators and reasonably simulates major outflows and low-flow periods (Memarian *et al.*, 2014).

The HRUs are then defined based on unique land use, soil, and slope combinations. The land use, soil and slope maps are overlaid together creating the HRUs. The slope consisted of 3 classes 0-5%, 5-15%, and 15-9999%. This is then followed by defining the HRUs, default values for land-use (20%), soil (10%) and slope (20%) as suggested by (Winchell *et al.*, 2007) to be adequate for most applications is used in this study. Once the HRUs are created, the weather data is then imported into the model and input tables are generated. The SWAT weather generator within the model is used in filling missing weather data.

The modified Soil Conservation Service Curve Number (SCS-CN) method, which uses land use, soil, and the antecedent moisture condition to estimate surface runoff from daily precipitation is used for this study, the Green-Ampt method which estimates infiltration is another method available in SWAT to determine surface runoff and infiltration.

As for channel routing, there are 2 options available in SWAT, the variable storage method, and the Muskingum method. For this study the Muskingum method is used.

The final step before calibration involves model simulation and reading output files, which are then used for calibration. The model is simulated on a daily time step from January 1999 to December 2018, with 4 years of warm up from January 1995 to December 1998.

3.4.3.3 SENSITIVITY ANALYSIS

The process of calculating the rate of change in model output with respect to changes to model inputs (parameters) is known as sensitivity analysis (Arnold *et al.*, 2012). SWAT uses many parameters, therefore the first step in calibration is to determine the most sensitive parameters that have the greatest impact on the output. In this study sensitivity analysis is done by using the SWAT-CUP software (Abbaspour, 2012) an ArcSWAT interface tool. Sensitivity analysis is important for 2 main reasons, firstly the parameters in the model represent the processes in the hydrological system, and sensitivity analysis provides information on the most important processes in the study region. Secondly, sensitivity analysis eliminates the parameters identified as not sensitive, therefore reducing the number of parameters needed for calibration.

There are 2 methods of sensitivity analysis in SWAT-CUP, the one-at-a-time (OAT) or local sensitivity analysis, and all-at-a-time (AAT) or global sensitivity analysis. In OAT method, all parameters are held constant while changing one to determine its effect on model output, whereas AAT all parameters are changing. In AAT parameter sensitivities are determined by calculating a multiple regression system to get the statistics of the parameter sensitivity. A t-test is then used to identify the relative significance of a parameter, and t-stat and p-values are used to rank each parameter according to its sensitivity. Parameters with p-values of <0.05 and larger t-stat values are considered more sensitive (Abbaspour *et al.*, 2017).

3.4.3.4 CALIBRATION AND VALIDATION

Calibration is the process of reducing the prediction uncertainty to try and get a more accurate output, by better parameterising the model to a given set of local conditions. Calibration is achieved by comparing model predictions (output) for a given set of assumed conditions with observed data for the same conditions, and carefully selecting values for model input parameters within their respective uncertainty ranges (Arnold *et al.*, 2012).

There are several calibration and validation methods available for SWAT, within SWAT-CUP there is the algorithm SUFI-2 (Sequential Uncertainty

Fitting), generalised likelihood uncertainty estimation (GLUE), parameter solution (ParaSol), Markov chain Monte Carlo (MCMC), and particle swarm optimisation (PSO) which can all be utilised in calibration and validation of SWAT models (Abbaspour *et al.*, 2004; Abbaspour *et al.*, 2007).

The SUFI-2 algorithm which is a built-in function of SWAT-CUP, that takes into consideration all the sources of uncertainties such as parameters, conceptual model, input, and driving variables, is a popular method used in hydrological studies. The degree to which all uncertainties are accounted for is quantified by a measure referred to as the p-factor, which is the percentage of measured data bracketed by the 95% prediction uncertainty (95PPU).

The 95PPU is calculated at the 2.5% and 97.5% levels of the cumulative distribution of an output variable obtained through Latin Hypercube (LH) sampling, disallowing 5% of very bad simulations. The r-factor on the other hand is the ratio of the average width of the 95PPU band and the standard deviation of the measured variable. Theoretically, the value of the p-factor ranges between 0 and 100%, while that of r-factor ranges between 0 and infinity. A p-factor of 1 and r-factor of zero is a simulation that exactly corresponds to measured data. Generally, a value greater than 0.7 for p-factor and a value less than 1.5 for r-factor is considered acceptable for calibration and validation of discharge (Abbaspour *et al.*,

2015). In this study the SUFI-2 method is used to calibrate and validate the model, with observed data from Batu Sentul station.

Model Validation is the process where a given site-specific model can show the ability to make sufficiently accurate simulations, although sufficiently accurate can vary based on project goals (Moriasi *et al.*, 2012). In SWAT validation involves using the parameters that are determined during calibration to run the model, then comparing the simulated data with observed data that is not used in calibration. In this study, observed stream flow data from the station, for the period of 1999 to 2002 is used for calibration and the period 2006 to 2008 is used for validation.

3.4.3.4.1 OBJECTIVE FUNCTIONS

To evaluate the hydrological goodness of fit of a hydrological model, objective functions are used. In SWAT-CUP there are several objective functions that can be used in calibration and validation of the model. Two of the most common objective functions used are the Nash-Sutcliffe efficiency (NS) and the coefficient of determination (R^2), which are used for this study. The NS is a normalised statistic that determines the relative magnitude of the residual variance ("noise") compared to the measured data variance ("information") (Nash and Sutcliffe, 1970). NS ranges between $-\infty$ and 1, where 1 being the optimal value. Generally,

values between 0 and 1 are considered acceptable, with values greater than 0.5 being satisfactory (Moriasi *et al.*, 2007). NS is calculated with following equation:

$$NS = 1 - \frac{\sum_{i=1}^n (Q_o - Q_p)^2}{\sum_{i=1}^n (Q_o - Q_{avg})^2} \quad (16)$$

Where Q_o and Q_p are the observed and simulated data, respectively, Q_{avg} is the average of the observed data and n is the total number of data records.

The R^2 describes the degree of collinearity or the proportion of variance measured between simulated and measured data. R^2 ranges from 0 – 1, with values greater than 0.5 considered acceptable (Santhi *et al.*, 2001; Van Liew *et al.*, 2003). R^2 is calculated with the following equation.

$$R^2 = 1 - \frac{\sum (Y_i - \hat{Y}_i)^2}{\sum (Y_i - \bar{Y})^2} \quad (17)$$

Y_i denotes the value of the i th dependent variable, \bar{Y} is the mean of the dependent variable and \hat{Y}_i is the i th fitted value.

3.4.3.5 HYDROLOGICAL MODELLING FOR FUTURE SCENARIOS

After calibration and validation of the model and simulation of hydrological processes for the years 1999, 2006 and 2017, the model is used to simulate hydrological processes for future LULC and climate

scenarios. All the input parameters are unchanged, except for land use map, precipitation, and temperature data, where future data is used. For land use map, the modelled land use map of 2030 is used, and for weather data precipitation and temperature data from the GCMs for the RCP4.5 and RCP8.5 scenarios for the TP1, TP2 and TP3 time periods is used. First, simulation is carried out for LULC 2030 separately, then for RCP4.5 and RCP8.5 scenarios separately, and finally simulation is carried out for combined LULC 2030 and RCP scenarios.

3.4.4 SUMMARY OF METHODOLOGY

The summary of all the methods and the criteria for assessment of the methods used in this research is presented in **Table 3.4-3**.

Table 3.4-3: Summary Of Methodology.

Methodology	Summary	Criteria for Testing
Land use and land cover classification	<ul style="list-style-type: none"> • Landsat satellite images for years 1999, 2006 and 2017 used. • Maximum likelihood algorithm supervised classification used. • Maps classified into 5 classes namely: Water, Natural Vegetation, Agriculture, Built-up, Cleared land. 	<ul style="list-style-type: none"> • Accuracy assessment carried out. • Error matrix method used. • Stratified random sampling used, with 150 random samples. • Ground truth data obtained from Google Earth for reference points. • Producer accuracy and user accuracy criteria used for accuracy assessment.
Land use and land cover change modelling	<ul style="list-style-type: none"> • Integrated Decision Forest - Markov Chain (DF-MC) model used. 	<ul style="list-style-type: none"> • Criteria for accuracy assessment used are, Area under the Curve (AUC) of Total

	<ul style="list-style-type: none"> • Change analysis step is carried out, which calculates the changes between 2 land use maps. • The transition potential modelling is carried out, where potential of land to transition are identified, and transition potential maps for each transition is created. • Variables for LULC change used are distance to roads, distance to rivers, distance to urban, DEM and slope. • Markov chain model with the transition potential and rate of changed used to model future LULC map for year 2030, based on LULC maps of 2006 and 2017. 	<p>Operating Characteristic (TOC) and disagreement parameters.</p> <ul style="list-style-type: none"> • Accuracy of the model is based on four components of disagreement namely, hits, misses, false alarms, and correct rejections.
<p>Spatio-temporal trend analysis</p>	<ul style="list-style-type: none"> • Mann-Kendall and Sen's slope statistics used. • Normality, autocorrelation, outlier detection tests used. • 4 indices for precipitation (SDII, R95p, R10mm and R30mm) and 2 indices for temperature (TXx and TNx) used. • Land Surface Temperature (LST) calculated from thermal band of satellite images for years 1999, 2006 and 2017. 	<ul style="list-style-type: none"> • Criteria for data preprocessing include data must be normally distributed, data must not have autocorrelation, must detect, and remove outliers, fill missing data or if few missing data ignore.
<p>Hydrological modelling (SWAT)</p>	<ul style="list-style-type: none"> • The SWAT model used for the hydrological modelling of the Klang River basin. 	<ul style="list-style-type: none"> • Sensitivity analysis must be carried out to determine most sensitive parameters. • The p-factor and r-factor are important in model validation. • NS and R2 should also be considered.

CHAPTER 4: RESULTS AND DISCUSSION

4.1 ANALYSIS OF SPATIO-TEMPORAL TRENDS IN LAND-USE AND LAND COVER

4.1.1 LAND USE AND LAND COVER CLASSIFICATION

The spatio-temporal land use and land cover (LULC) classification maps for the years 1999, 2006, and 2017 are presented in **Figure 4.1-1**. There have been notable trends detected in LULC change within the study area over the period 1999- 2017. Built-up land has seen a significant increase by 147.5 km² constituting to an 11.8% rise, while water bodies have seen a slight expansion of 4.31 km². in contrast agricultural land decreased by 36.71 km² (2.9 %), natural vegetation by 73.4 km² (5.9%), and cleared land by 41.79 km² (3.3%).

In terms of spatial trend, changes are primarily located in the lower parts of the Klang River basin where substantial areas of cleared land have been transformed into urban land. On the other hand, the upper parts of the basin remain largely unchanged and are predominantly covered by natural vegetation. **Table 4.1-1** provides the breakdown of changes in land area for each land use classification for the period 1999 -2017.

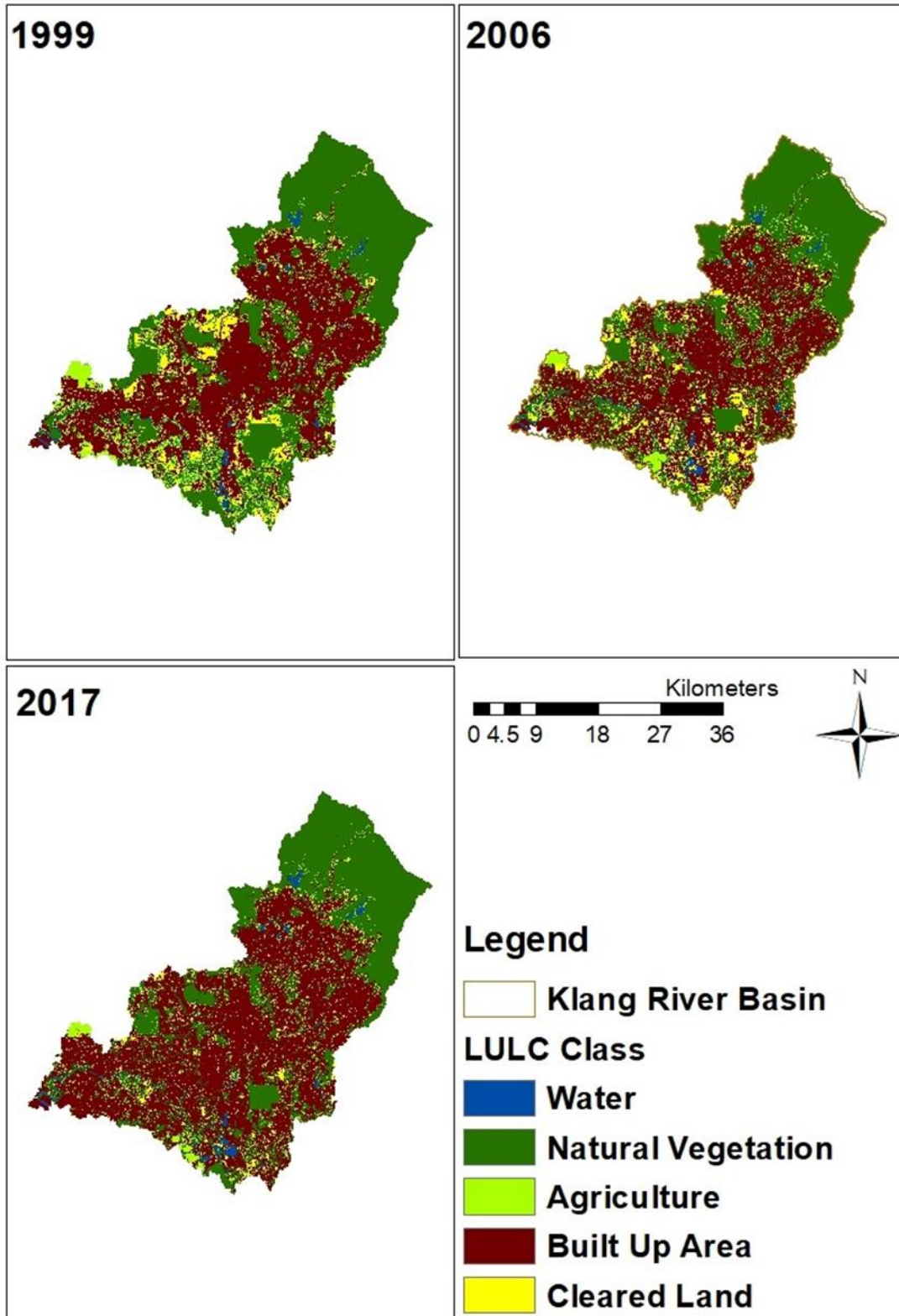


Figure 4.1-1: Lulc Map Of Year 1999, 2006 And 2017.

Table 4.1-1: LULC Area For Each Classification, For The Years 1999, 2006, And 2017.

	Area						Change	
	1999		2006		2017		1999-2017	
	Area (km ²)	Area (%)						
Water	19.38	1.6	22.27	1.8	23.69	1.9	4.31	0.3
Natural Vegetation	516.3	41.3	488.9	39.1	442.9	35.4	-73.4	-5.9
Agriculture	98.46	7.9	79.53	6.4	61.75	4.9	-36.71	-2.9
Built Up	538.7	43.1	570	45.6	686.2	54.9	147.5	11.8
Cleared Land	76.86	6.2	88.92	7.1	35.07	2.8	-41.79	-3.3

The overall accuracy of the LULC maps for the years 1999, 2006, and 2017 stands at 84%, 92.74%, and 88.67%, respectively. More details of the accuracy assessment are provided in **Table 4.1-2**.

Table 4.1-2: The Producer's And User's Accuracy For The LULC Classification Maps Of Years 1999,2006, And 2017, Showing The Accuracy Of The LULC Maps.

	1999		2006		2017	
	Producers Accuracy	Users Accuracy	Producers Accuracy	Users Accuracy	Producers Accuracy	Users Accuracy
Water	50.00%	100.00%	100.00%	100.00%	50.00%	50.00%
Natural Vegetation	97.14%	80.95%	98.18%	91.53%	96.49%	83.33%
Agriculture	70.00%	89.74%	88.64%	92.86%	86.27%	91.67%
Built-Up	82.61%	90.48%	85.00%	100.00%	84.85%	96.55%
Cleared Land	60.00%	60.00%	100.00%	80.00%	71.43%	100.00%

However, for the 1999 and 2017 LULC maps, the class water exhibits low producer and user accuracy, both at 50%. This can be attributed to the limited number of random samples available for the class water during the accuracy assessment, with only 2 random samples selected for the class water in each year. In both cases, the model incorrectly classified one sample point as another class, leading to the 50%

producer and user accuracy scores, as further illustrated in the error matrix in **Table 4.1-3**.

Table 4.1-3: Error Matrix For The LULC Maps Of 1999, 2006, And 2017, Showing Accuracy Of The LULC Maps.

Error Matrix of 1999		Reference Data				
Classified Data	Water	Natural Vegetation	Agriculture	Built-Up	Cleared Land	Row Total
Water	1	0	0	0	0	1
Natural Vegetation	1	68	14	1	0	84
Agriculture	0	2	35	2	0	39
Built Up	0	0	0	19	2	21
Cleared Land	0	0	1	1	3	5
Column Total	2	70	50	23	5	150

Error Matrix of 2006		Reference Data				
Classified Data	Water	Natural Vegetation	Agriculture	Built-Up	Cleared Land	Row Total
Water	27	0	0	0	0	27
Natural Vegetation	0	54	4	1	0	59
Agriculture	0	1	39	2	0	42
Built Up	0	0	0	17	0	17
Cleared Land	0	0	1	0	4	5
Column Total	27	55	44	20	4	150

Error Matrix of 2017		Reference Data				
Classified Data	Water	Natural Vegetation	Agriculture	Built-Up	Cleared Land	Row Total
Water	1	0	1	0	0	2
Natural Vegetation	1	55	6	3	1	66
Agriculture	0	2	44	2	0	48
Built Up	0	0	0	28	1	29

Cleared Land	0	0	0	0	5	5
Column Total	2	57	51	33	7	150

4.1.2 LAND USE AND LAND COVER CHANGE MODELLING

The simulated LULC map of 2030 is presented in **Figure 4.1-2**. The projection of future changes shows several significant changes in LULC between 2017 and 2030. Built-up land is estimated to increase by 120.6 km² (9.7%), and agricultural land to marginally increase by 9.11 km² (0.7%). On the other hand, natural vegetation is projected to decrease by 109.5 km² (8.7%), and a marginal decrease in water bodies by 20.94 km² (1.7%). A detailed summary of these changes is provided in **Table 4.1-4**.

The trends in the projected model between 2017 to 2030 shows similarities to the trends in LULC change between 1999 and 2017. In both the past and projected future model, Built-up land exhibits increasing trend in both spatial and temporal context. Whereas, in both cases natural vegetation and cleared land show decreasing trend. The magnitude of change in both past and future projected models are similar, showing continuous rate of change into the future with current development conditions.

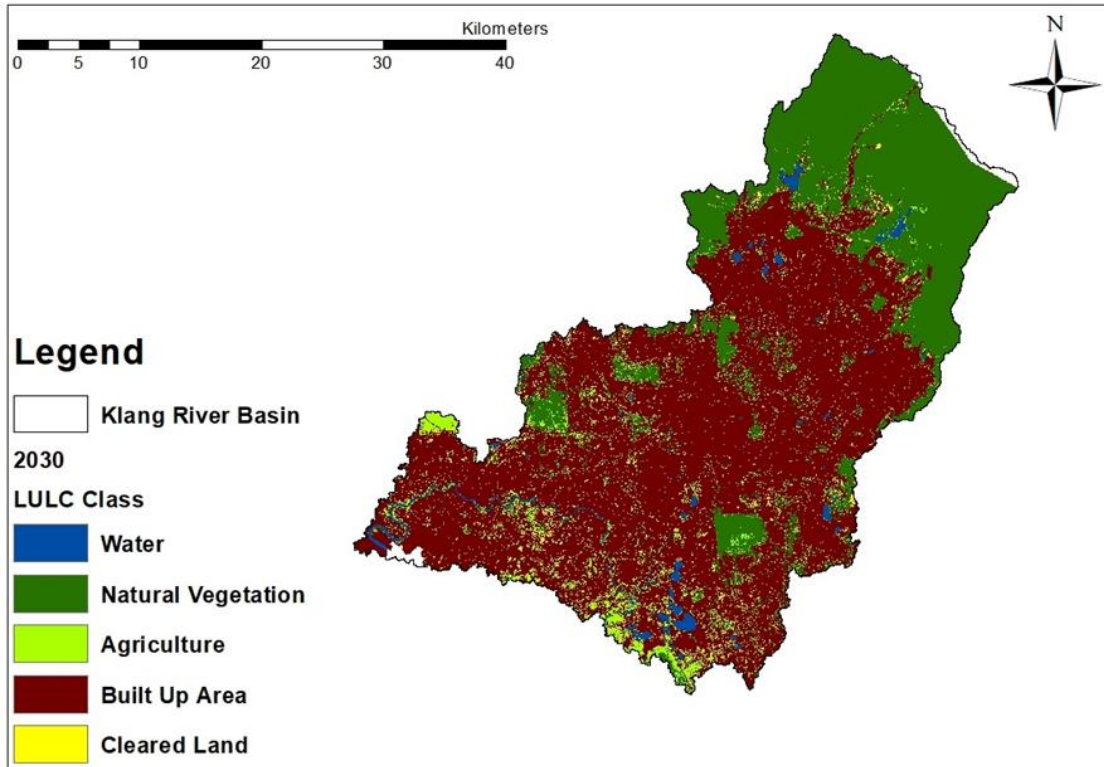


Figure 4.1-2: The Simulated LULC Map For Year 2030.

Table 4.1-4: LULC Area And Changes Between Years 2017 And 2030.

	2030		Change from 2017-2030	
	Area (km ²)	Area (%)	Area (km ²)	Area (%)
Water	23.6	1.9	-0.09	0.0
Natural Vegetation	333.4	26.7	-109.5	-8.7
Agriculture	70.86	5.7	9.11	0.7
Built Up	806.8	64.6	120.6	9.7
Cleared Land	14.13	1.1	-20.94	-1.7

4.1.2.1 MODEL VALIDATION

The model validation is presented by the Area Under the Curve (AUC) of the Total Operating Characteristic (TOC) as shown in **Figure 4.1-3**. An AUC value of 0.84 for model validation was obtained.

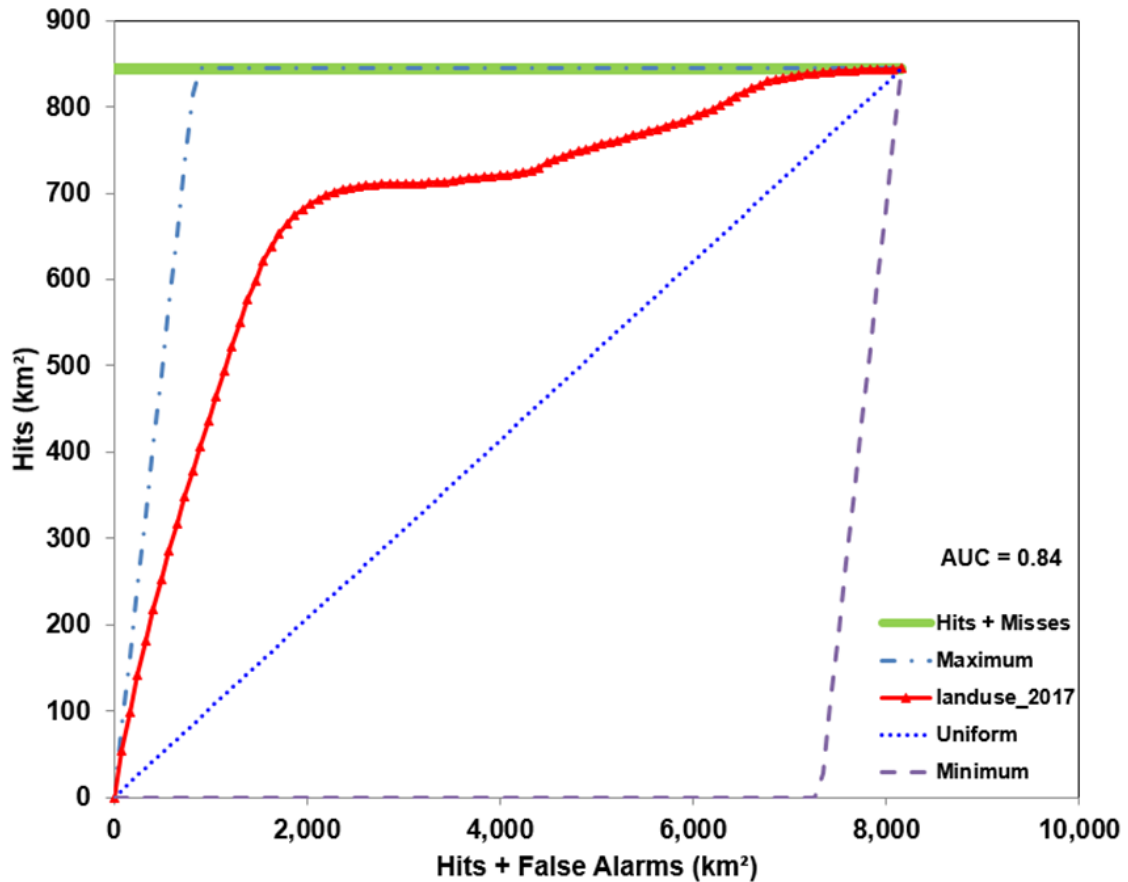


Figure 4.1-3: The Area Under The Curve Of The Total Operating Characteristic, Showcasing The Validation Of The Model.

The cross-tabulation matrix in **Figure 4.1-4** presents a breakdown of hits, misses, false alarms, wrong hits, and correct rejections in the model validation process. The overall components of agreement amount to 71.1%, derived from the sum of Hits (3.1%) and Correct Rejections (68%). In contrast, the components of disagreement total to 28.9%, resulting from the sum of Misses (14.9%), False Alarms (9.4%), and Wrong Hits (4.7%). This comprehensive assessment contributes to our understanding of the model's performance and accuracy.

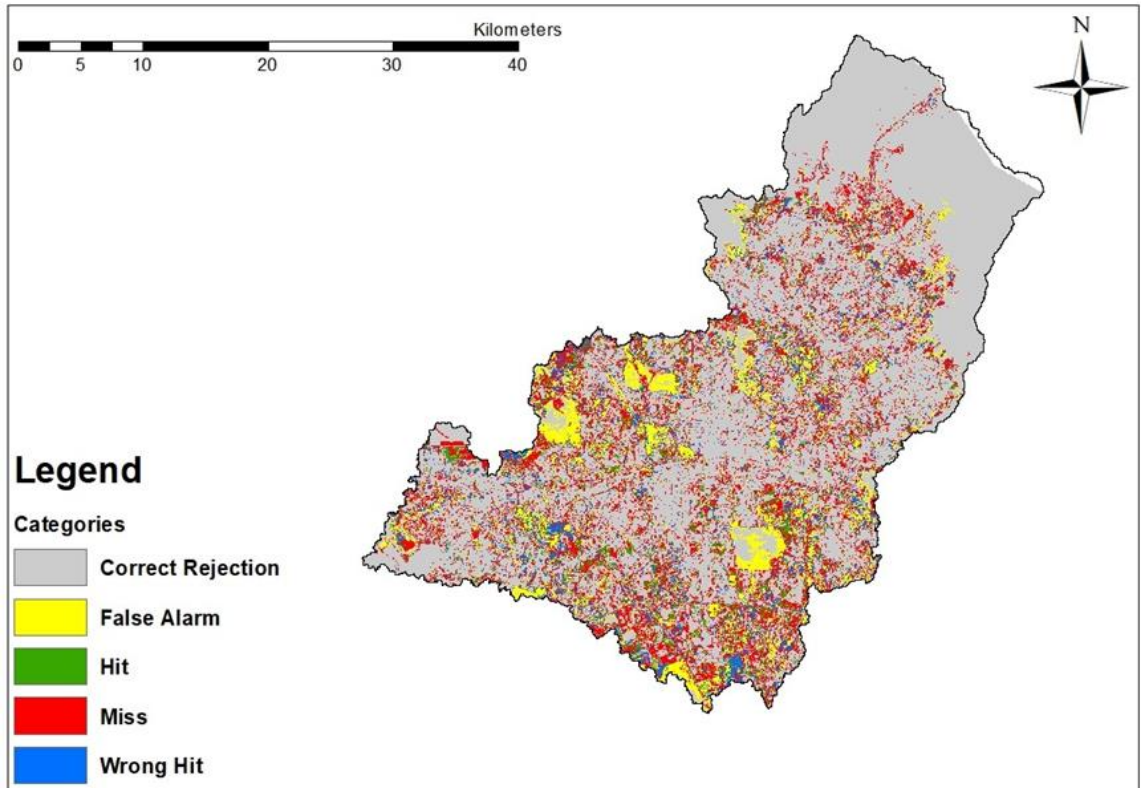


Figure 4.1-4: *The Quantity And Allocation Disagreement, Showcasing The Validation Of The Simulated Map With The Reference Map.*

4.1.3 DISCUSSION

Land use and land cover change modelling provides valuable information on changing landscape dynamics and their potential impact on hydrological processes. To understand the impacts of these change on hydrological processes, it is important to first analyse and understand the trends in LULC, and to showcase the magnitude of change both in terms of spatial and temporal trend, then project future changes in LULC. To accomplish this, the study utilised the maximum likelihood algorithm under the supervised classification and the integrated

Decision Forest – Markov Chain model methods, to classify and analyse the spatio-temporal trends in LULC. The model used Landsat satellite images for land use classification and input for the land use change model.

An important step in LULC change modelling is to assess the goodness of the model in use. The overall accuracy assessment of the LULC maps as shown in **Table 4.1-2**, presents satisfactory outcome in land use classification. Additionally, the Area Under the Curve (AUC) value of 0.84, and the higher total components of agreement (71.1%) over total components of disagreement (28.9%) in the DT-MC model validation affirm the reliability and suitability of the model for simulating future land use scenarios. These validation results are in accordance with prior research conducted by Samardžić-petrović et al. (2015), which obtained similar AUC values (0.7 to 0.8). Therefore, highlighting the effectiveness of the DT-MC model in modeling LULC changes.

The analysis of the spatio-temporal trends in LULC change, discovered several significant trends. The observed LULC trend for the period 1997 to 2017 illustrates the magnitude of change in LULC, with an increase of 147.5 km² (11.8%) in built-up areas, increasing at a rate of 7.76 km² (0.62%) per year was observed (**Figure 4.1-5**). This expansion is primarily concentrated in the central part of the Klang River basin highlighting the spatial trend. Although the average annual urban

growth rate of 0.6% for Klang River basin is lower than the Malaysian average annual urban growth rate of 1.5% for the period 2000 to 2010 (World Bank Group, 2015), this is still a significant increase in urban land in the Klang River basin, considering around 43% of the basin was already urbanised in the year 1999.

The increase in urban land is mostly attributed to the urban sprawl of the densely populated federal territory of Kuala Lumpur (KL) and its surrounding urban areas. This urban sprawl phenomenon aligns with the findings of previous studies (Rosni et al., 2016; and Almdhun et al., 2018), underscoring the growth of KL and its consequential impact on the wider basin landscape.

The LULC change beyond 2017 and up to 2030, illustrates continuous increasing trend in built-up land, with an estimated increase of 120.6 km² (9.7%). The spatial trend shows that urban expansion will primarily encroach within urban green spaces and the remaining forests located in the middle and lower regions of the basin. This is attributed to the proximity to existing urban areas and road networks, with the lower-lying and accessible terrains in these areas being especially attractive for urban development. On the other hand, natural vegetation and forests in the upper basin are expected to remain largely unaffected, due to lack of accessibility and steeper slopes.

This is supported by the findings in the study by Othman *et al.*, (2009) that examined land use and land cover changes in the Langat-Dengkil sub-catchment within the Klang-Langat catchment from 1990 to 2001, with a forecast for 2020. During this period, there was a significant decrease of 9.5% (4,303 ha) in forested land and a 17.3% (11,598 ha) reduction in agricultural land, while urban land expanded substantially by almost six times (18,860 ha), primarily at the expense of agriculture and forests in the Langat-Dengkil sub-catchment. In the wider Klang-Langat catchment, deforestation encompassed 36,351 ha, including 12,244 ha of Permanent Forest Reserve.

The analysis identified key factors contributing to deforestation: proximity to major access points within 1000m, proximity to towns within 2000m, lower altitudes below 100m, and gentle slopes less than 5°. The study's projections for 2020 indicated that if the Permanent Forest Reserve is strictly protected, deforestation could be reduced to 22,340 ha or 22%. However, without such protection, deforestation is expected to be much more extensive, covering 50,851 ha or 50% of the area. This illustrates the vulnerability of urban green spaces and protected forests to LULC change, which is important in control and reduction of surface runoff and risk of flooding.

Unfortunately, urban expansion into these Forest Reserves is already taking place. For example, the large forest area at Bukit Jelutong in the

southern part of Klang River basin is experiencing urban encroachment as of 2022, as shown in **Figure 4.1-6**. Similarly, the northern part of Selangor is estimated to undergo urban expansion by about 33% from 2015 to 2033 with distance to road and distance to build up areas, being the major variables in the urban expansion (Camara et al., 2020). Further highlighting the role of accessibility in driving land use changes. The increase of transportation networks is a major factor in the expansion of urban areas in Malaysia. For example, in George Town, Northern Malaysia, it is estimated by 2030 urban land to expand from 925.77 km² to 1253.95 km², with the North-South highway and the second bridge between Georg Town and Penang island playing a major role in this expansion (Samat et al., 2020). This illustrates that availability of road network and accessibility increases the speed and magnitude of LULC change and urban expansion.

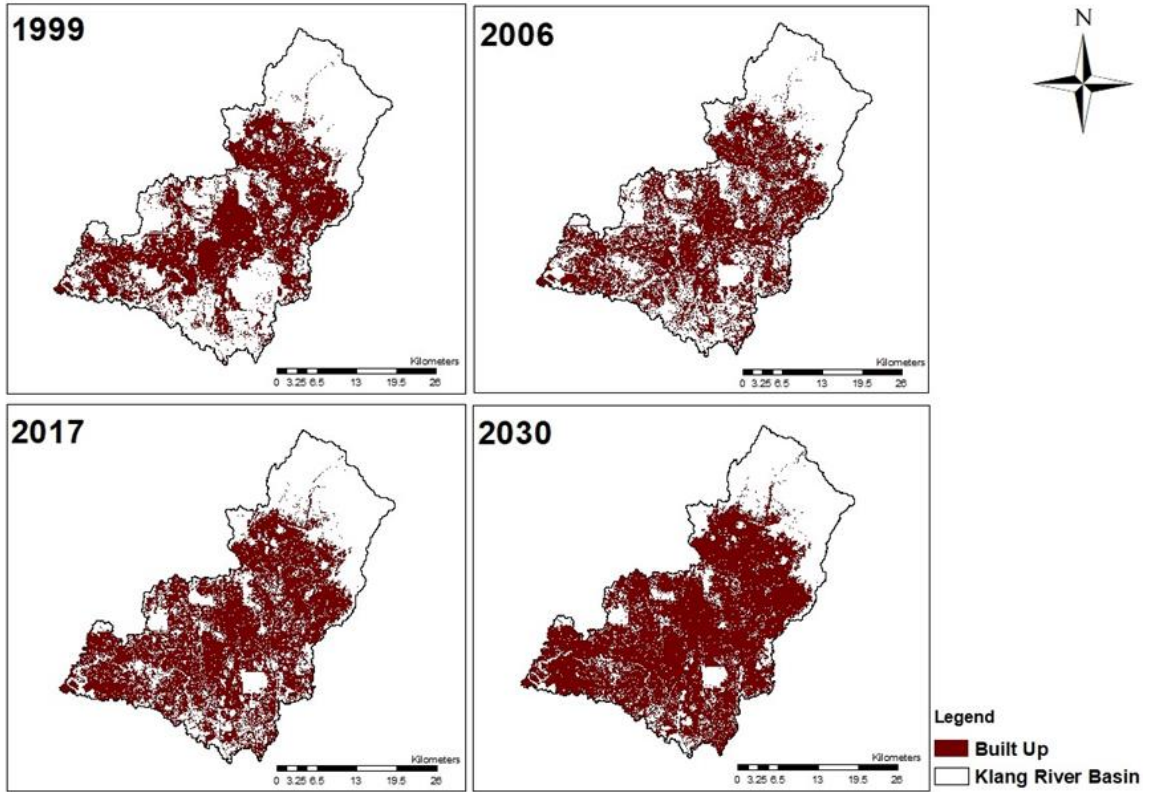


Figure 4.1-5: The Increase Of Built-Up Areas For The Period 1999 To 2030.

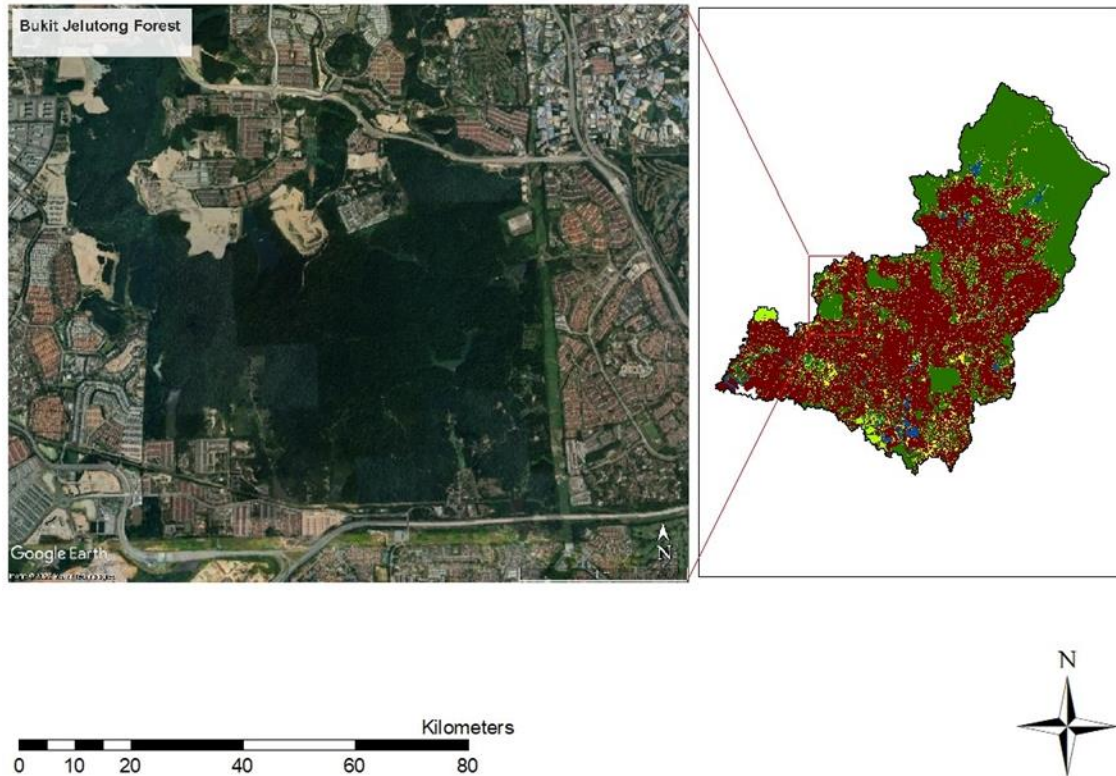


Figure 4.1-6: *Urban Expansion Into Forest Areas In Bukit Jelutong (Image Obtained From Google Earth, In Year 2022).*

The decrease in natural vegetation and agricultural land for the period 1999 to 2017 by 73.4 km² (5.9%) and 36.71 km² (2.9%) respectively, and increase in built-up areas, resulted in increase in imperviousness of the land surface and therefore reducing infiltration capacity of land, as shown by previous studies, hence increasing surface runoff, river discharge and risk of flooding.

The regions most affected by the decreasing trend in natural vegetation, agricultural land and cleared land are the Southern and Western parts of the basin. The future projections, estimates a continuous decrease in

natural vegetation and cleared land until 2030, at a yearly rate of 7.82 km² (0.62%) and 1.5 km² (0.12%) respectively, with agricultural land projected to increase slightly.

As the population and the economy of Selangor continues to grow, and with the aim of reaching the goals of Malaysia Shared Prosperity Vision 2030 and Selangor Structural Plan 2030, demand for urban and agricultural land increases, hence more of the protected areas and urban green spaces will be used to meet these demands. This is evident in past cases where the government de-gazette forest reserves for urban expansion.

For example, 106.65 ha of the Ampang forest reserve was de-gazette in 2014 to construct an expressway, and in 2016 around 30 ha of Sungai Puteh North and South Forest Reserves were de-gazette for a highway, and 28.3 ha of Bukit Lagong Forest Reserve was de-gazette for a housing project. In a more recent case, the government has proposed to de-gazette 985 ha (97%) of the Kuala Langat North Forest Reserve for urban development (Ravindran and Rajendra, 2020).

If the rapid increase in urbanisation and uncontrolled urban expansion is allowed to continue, it will have a negative impact on the basin. The Klang River basin and in particular KL experience regular flooding events, and this is largely attributed to urban development (Bhuiyan *et*

al., 2018). The combined impact of the uncontrolled urban expansion and changing precipitation can have devastating effect on the hydrological processes in the Klang River basin, that is already experiencing regular flooding events.

4.2 ANALYSIS OF SPATIO-TEMPORAL TRENDS IN PRECIPITATION, TEMPERATURE AND RIVER DISCHARGE

4.2.1 PRECIPITATION TRENDS

4.2.1.1 ANNUAL TREND

The interpolated mean annual precipitation map of the Klang River basin is presented in **Figure 4.2-1**, while the annual precipitation trend map of the 10 stations is presented in **Figure 4.2-2**. The mean annual precipitation analysis exhibits a distinct pattern across the Klang River basin. The central regions of the basin experienced higher mean annual precipitation, ranging from 3010mm to 3368mm, in contrast the Southern regions of the basin recorded the lowest mean annual precipitation, varying between 2024mm and 2388mm. This demonstrates that there is spatial variability in precipitation distribution in the Klang River basin.

The annual precipitation trend map highlights an overall increasing trend in precipitation, with only one station displaying a decreasing trend. A significant trend in precipitation was noticeable at stations located in the

central part of the Klang River basin. The mean annual precipitation amounts for the period 1999 to 2017 for the 5 stations located in the central part of the basin as shown in **Figure 4.2-3**, illustrates a gradual increase in precipitation over this period. Notably, the year 2006 stands out as the year with the highest annual precipitation amount for 3 out of the 5 stations.

Spatial variability is present in mean annual precipitation for the period 1999 to 2017, as the 5 stations in the basin exhibit higher precipitation amounts compared to the 5 stations located outside the basin. Station 48648 had the highest mean annual precipitation at 3369 mm, whereas station 2616135 located outside the basin had the lowest mean annual precipitation at 1708 mm.

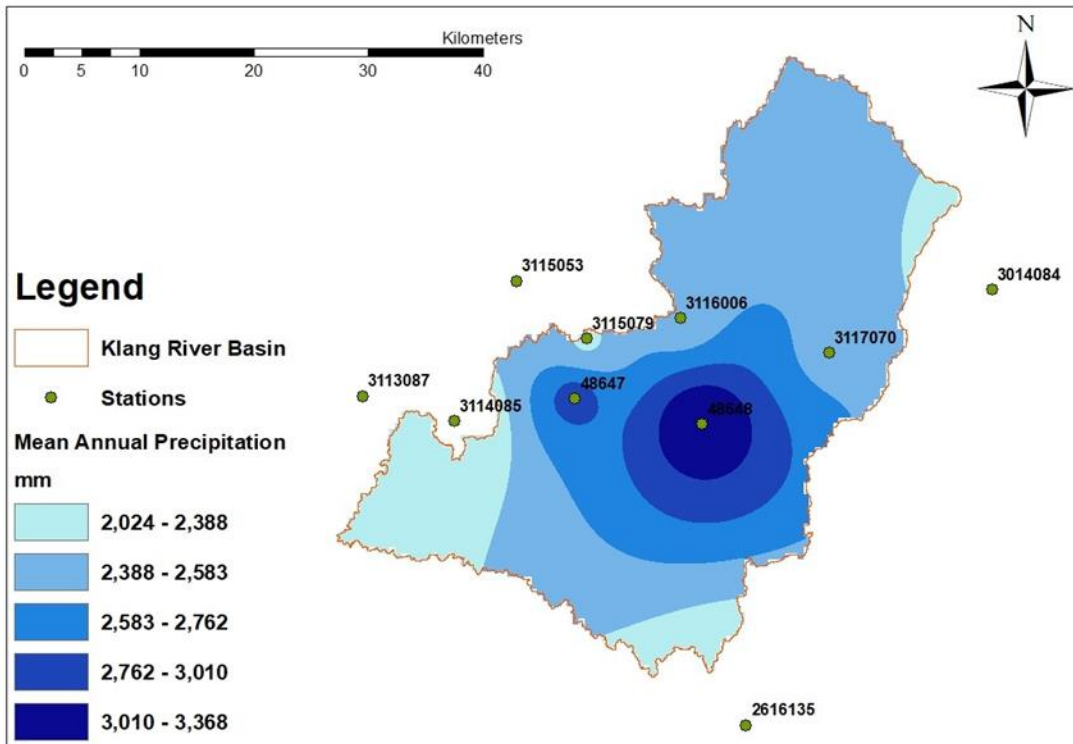


Figure 4.2-1: Average Annual Precipitation In Klang River Basin.

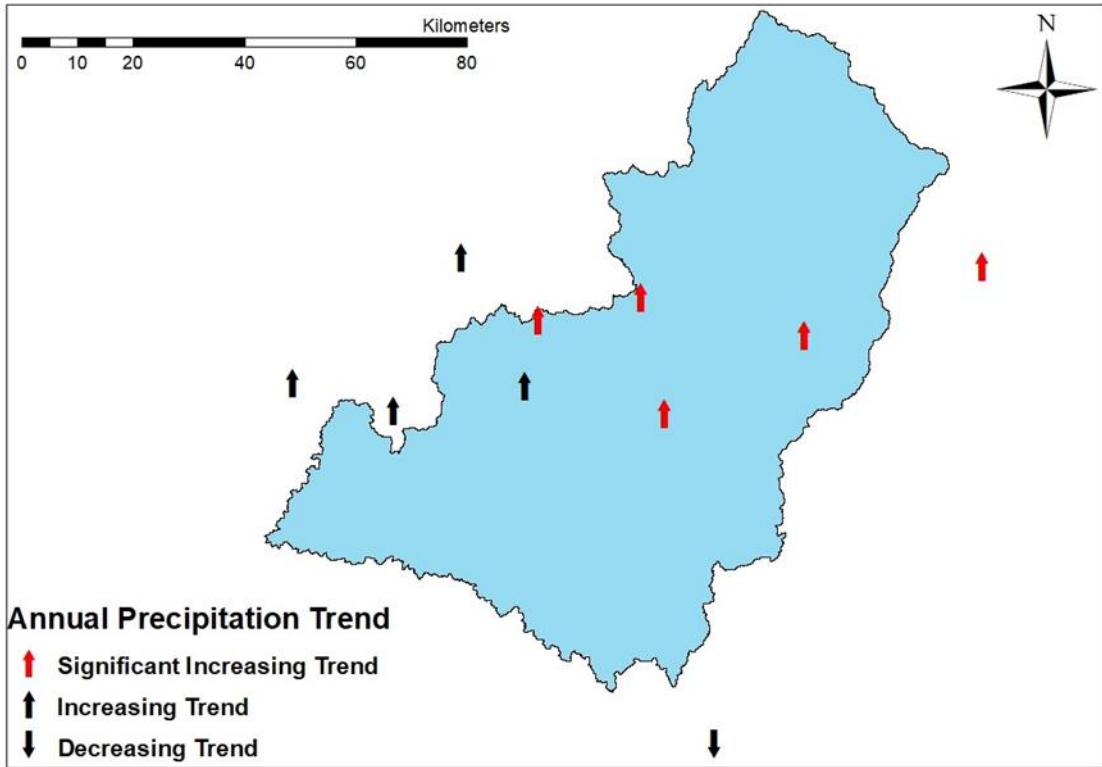


Figure 4.2-2: The Annual Precipitation Trend For Klang River Basin (Significance Level Taken At 0.01 And 0.05).

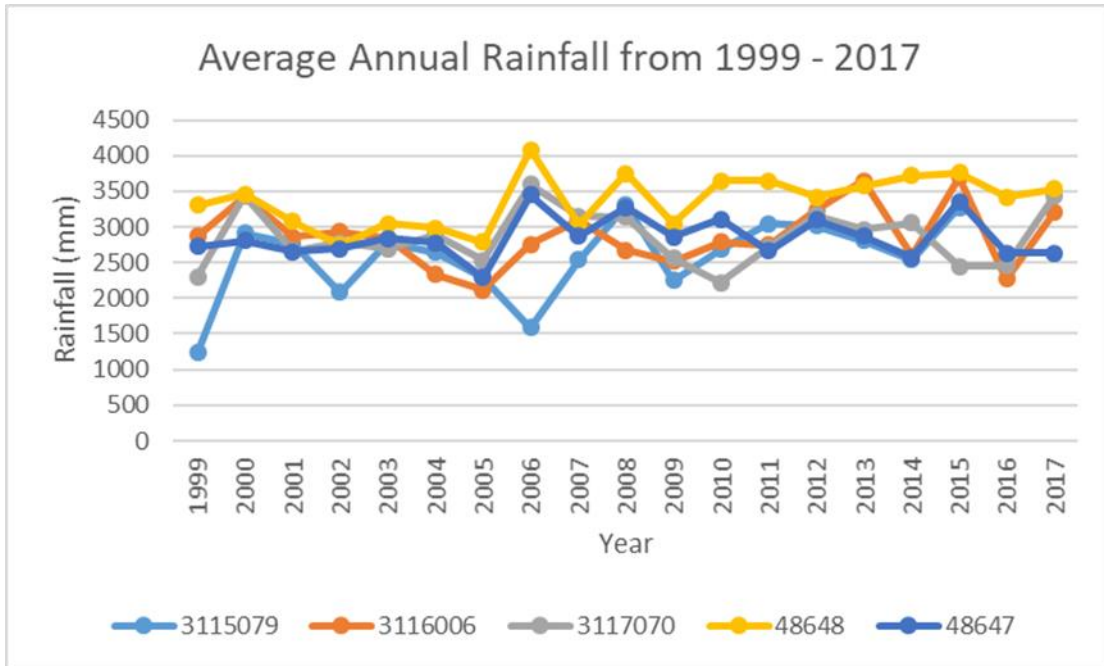


Figure 4.2-3: The Graph Of Average Annual Precipitation For Stations Located Within Built Up Areas.

The significance level and rate of change in annual precipitation trend is shown in **Table 4.2-1**. Among the 10 stations negative trend was detected at only station 2616135, while only half of the stations had significant trend. The rate of change, which is represented by the Sen's slope, was found to be highest at station 3116006, with a rate of 28.46 mm/year. The results of the Sen's slope indicate that rate of change is higher at the stations located in the central region of the Klang River basin.

Table 4.2-1: Trends For Annual Precipitation.

Stations	Annual Precipitation	
	Test Z	Sen's Slope
2616135	-1.02	-3.94
3014084	2.50*	15.76
3113087	1.56	9.67
3115079	3.16**	21.61
3114085	0.26	0.82
3115053	0.33	2.53
48648	2.06*	26.27
48647	1.56	15.41
3117070	2.01*	11.68
3116006	3.43**	28.46

** if trend at $\alpha = 0.01$ level of significance, * if trend at $\alpha = 0.05$ level of significance, + if trend at $\alpha = 0.1$ level of significance, if the cell is blank, the significance level is greater than 0.1.

Shifting the focus to the annual trends of key precipitation indices, namely SDII, R10mm, R30mm, and R95p (**Table 4.2-2**), it is evident that there is spatial and temporal variability in trends among the indices. While some stations show decreasing trends in SDII, the stations located in the central part of the Klang River basin consistently display positive trends across all four indices. Many of these trends are statistically significant, emphasising the dynamic nature of precipitation patterns in this region.

Table 4.2-2: Annual Trend For SDII, R10mm, R30mm, And R95p.

Stations	SDII		R10mm		R30mm		R95p	
	Test Z	Sen's Slope	Test Z	Sen's Slope	Test Z	Sen's Slope	Test Z	Sen's Slope
2616135	-2.28*	-0.14	-1.32	-0.11	-1.48	-0.11	-0.43	-1.35
3014084	-3.25**	-0.14	1.64	0.29	0.87	0.08	1.92+	6.43
3113087	0.3	0.01	0.54	0.09	1.77+	0.15	2.10*	6.82
3115079	4.84**	0.12	3.19**	0.55	4.33**	0.37	2.75**	9.87
3114085	-4.01**	-0.19	-2.44*	-0.44	-0.91	-0.06	0.46	1.51
3115053	-0.01	0	-0.33	-0.08	0.2	0	0.51	1.69
48648	2.41*	0.12	2.90**	0.65	1.94+	0.38	1.36	7.54
48647	0.92	0.07	1.15	0.25	1.15	0.25	1.07	8.1
3117070	1.32	0.04	2.11*	0.27	2.10*	0.17	1.75+	8.87
3116006	2.55*	0.08	3.81**	0.8	2.55*	0.28	3.01**	16.53

** if trend at $\alpha = 0.01$ level of significance, * if trend at $\alpha = 0.05$ level of significance, + if

trend at $\alpha = 0.1$ level of significance, if the cell is blank, the significance level is greater than 0.1.

On the other hand, the Sen's slope estimator for the R95p index, shows notably high rate of increase for stations within urban areas of the Klang River basin. Station 3116006 exhibits the highest rate of change at 16.53 mm per year for R95p compared to other stations. Whereas, for SDII stations with decreasing significant trends exhibited higher rate of change. The station 3114085 located in the Southern part of the basin recorded the highest rate of change at -0.19 mm/day per year.

The Sen's slope for R10mm and R30mm, at stations 48648 and 3115079, both situated in urban areas, demonstrates the highest rates of change. Station 48648 has the highest rate of change at 0.65 days per year for R10mm and 0.38 days per year for R30mm. This illustrates that there is higher frequency of heavy and moderate precipitation over

urban areas, whereas the intensity of heavy precipitation is highest over urban areas, but intensity of moderate to low precipitation is low and decreasing over certain areas in the South, West and Eastern part of the basin.

4.2.1.2 SEASONAL TREND

The analysis of the average monthly precipitation presented in **Appendix D**, provides crucial insights into the seasonal variability of precipitation across our study area. The highest average precipitation was observed in the month of November across all the stations, which correspond to the North-East Monsoon. The urban stations situated within the Klang River basin exhibit notably higher average precipitation in November compared to stations located outside the basin. Among these urban stations, station 48648 registers the highest November precipitation at 416 mm. On the other hand, the month of June, corresponding to the South-West Monsoon (SWM) season, emerges as the driest month for most of the stations, with an average precipitation amount of merely 139 mm.

➤ *SIMPLE DAY INTENSITY INDEX (SDII)*

The analysis of the SDII trend shows spatial variability, with a mixture of increasing and decreasing trend detected among the stations, as highlighted in **Figure 4.2-4**. With 6 out of 10 stations, the SWM has the

most stations with significant trend, as shown in **Table 4.2-3**. Overall, the 5 urban stations showcase an increasing trend, except for station 3117070 during IntM1. Meanwhile, stations located outside the basin boundaries consistently display a decreasing trend. This highlights the spatial and seasonal variability in moderate to low precipitation intensity, which echoes the annual patterns.

The Sen's slope estimator reveals that the rate of change in SDII is most pronounced during SWM and IntM2, with station 48648 registering the highest rate at 0.29 mm/day per year. Among all the stations, the stations 3014084 and 3114085 show consistent significant negative trend, with an average seasonal rate of change at -0.14 mm/day per year and -0.2 mm/day per year respectively.

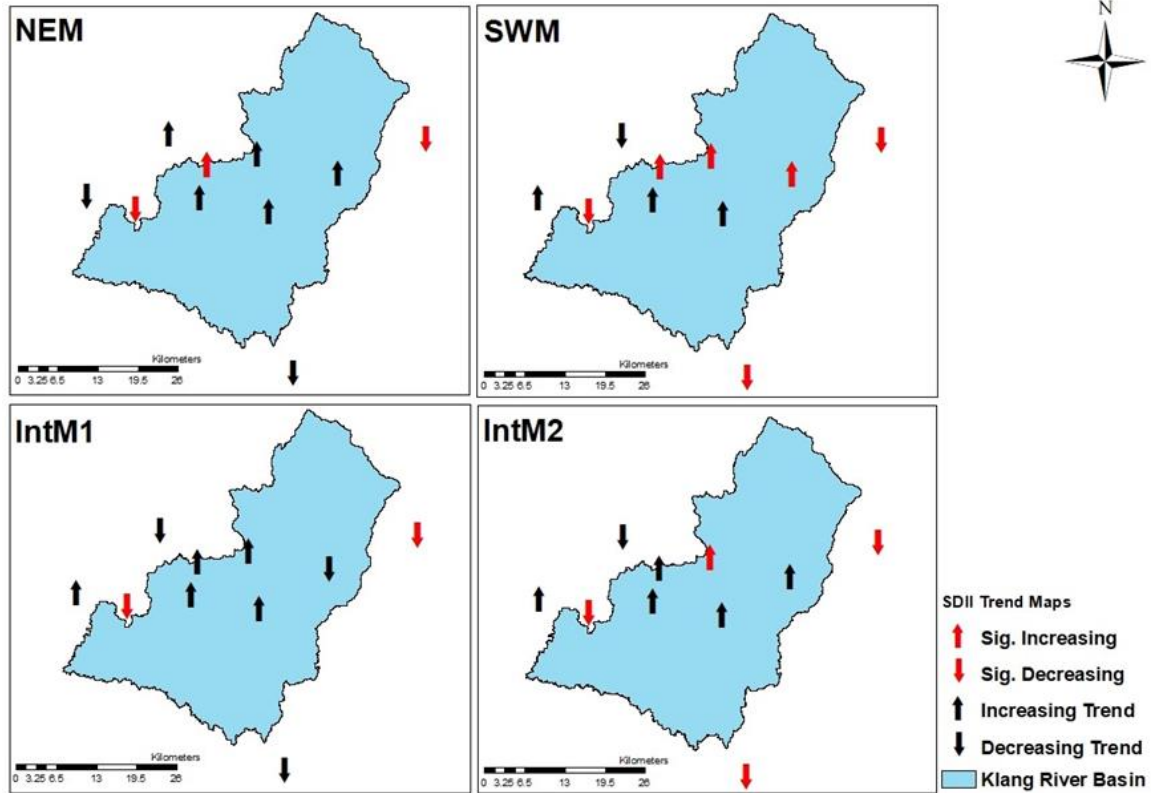


Figure 4.2-4: The SDII Seasonal Trend Map For NEM, SWM, Intm1 And Intm2.

Table 4.2-3: Seasonal Trend For SDII.

Stations	NEM		SWM		IntM1		IntM2	
	Test Z	Sen's Slope	Test Z	Sen's Slope	Test Z	Sen's Slope	Test Z	Sen's Slope
2616135	-1.70+	-0.1	-2.48*	-0.16	-1.07	-0.09	-2.56*	-0.26
3014084	-2.53*	-0.12	-2.32*	-0.13	-2.13*	-0.13	-2.33*	-0.19
3113087	-0.03	-0.01	0.82	0.04	0.13	0.03	0.76	0.06
3115079	4.03**	0.15	3.25**	0.11	0.51	0.02	1.38	0.08
3114085	-4.10**	-0.21	-2.85**	-0.19	-2.14*	-0.22	-2.33*	-0.18
3115053	0.57	0.04	-1	-0.05	-0.59	-0.05	-0.51	-0.04
48648	0.67	0.05	1.61	0.11	1.07	0.09	0.92	0.29
48647	0.92	0.07	1.76+	0.1	0.22	0.04	0.97	0.15
3117070	1.14	0.04	2.20*	0.06	-0.41	-0.03	1.35	0.08
3116006	1.32	0.05	3.01**	0.11	0.7	0.07	3.53**	0.23

** if trend at $\alpha = 0.01$ level of significance, * if trend at $\alpha = 0.05$ level of significance, + if trend at $\alpha = 0.1$ level of significance, if the cell is blank, the significance level is greater than 0.1.

➤ *R10mm*

The analysis of R10mm, which quantifies the frequency of days with precipitation exceeding 10 mm, shows a mix of increasing and decreasing trends (**Figure 4.2-5**). Notably, significant trends are only detected during the NEM season, and only for urban stations within our study area (**Table 4.2-4**). Examining Sen's slope, we find that the highest rate of change in R10mm occurs during the NEM season, with stations 3116006 and 3115079 in urban areas registering the most substantial increases at 0.4 and 0.38 days per year, respectively. Among all the stations only station 3114085 exhibits negative trend for all the seasons. The overall positive trend in R10mm indicates an increase in frequency of occurrence of moderate rainfall events, especially in the NEM period.

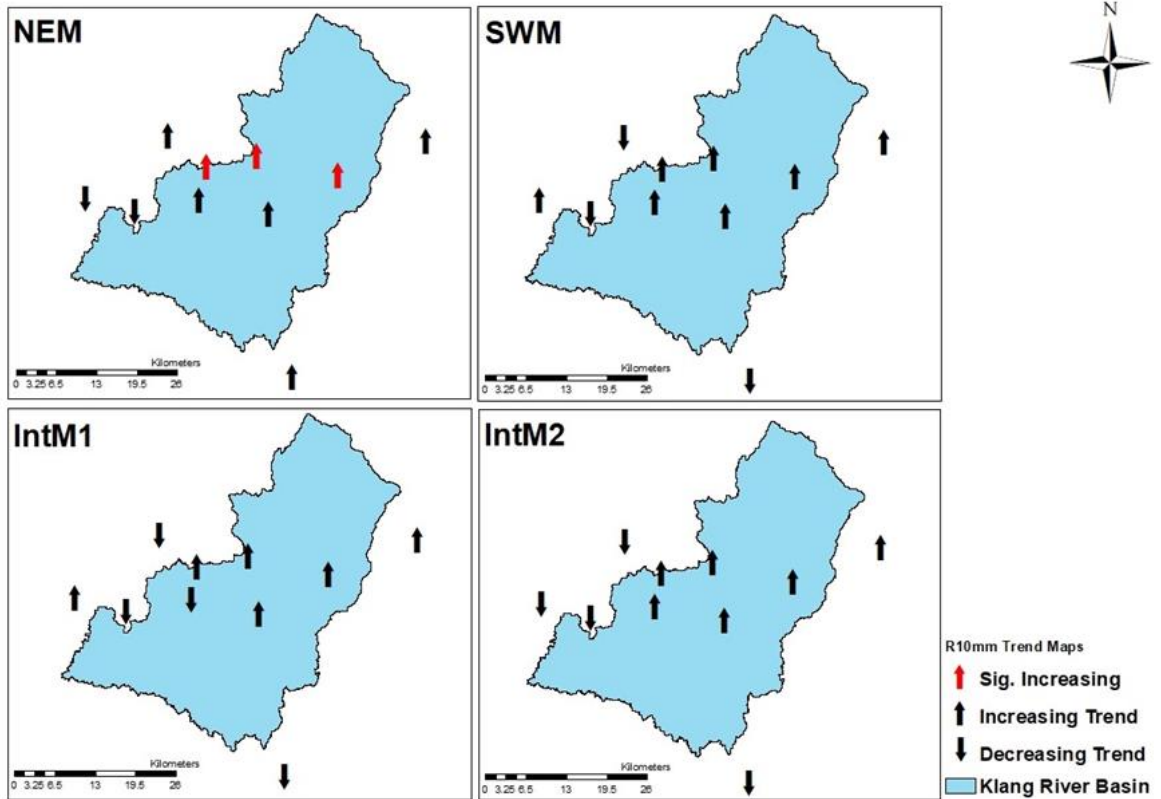


Figure 4.2-5: The R10mm Seasonal Trend Map For NEM, SWM, Intm1, And Intm2.

Table 4.2-4: Seasonal Trend For R10mm.

Stations	NEM		SWM		IntM1		IntM2	
	Test Z	Sen's Slope						
2616135	0.51	0.04	-1.65+	-0.1	-1.36	-0.03	-0.99	-0.03
3014084	1.76+	0.23	1.21	0.08	1	0.03	1.56	0.05
3113087	-0.09	0	0.19	0	0.96	0	-0.16	0
3115079	3.61**	0.38	1.34	0.1	0.58	0	0.87	0.04
3114085	-1.70+	-0.17	-1.16	-0.09	-1.02	-0.04	-1.46	-0.06
3115053	0.8	0.11	-1.37	-0.11	-1.06	-0.04	-0.66	-0.01
48648	1.47	0.26	1.27	0.29	1.23	0.09	0.8	0.06
48647	1.15	0.25	0.52	0.09	-1.24	-0.09	0.1	0
3117070	2.15*	0.19	0.64	0.06	0.71	0	0.7	0
3116006	3.33**	0.4	1.41	0.17	1.58	0.07	1.29	0.06

** if trend at $\alpha = 0.01$ level of significance, * if trend at $\alpha = 0.05$ level of significance, + if trend at $\alpha = 0.1$ level of significance, if the cell is blank, the significance level is greater than 0.1.

➤ *R30mm*

Similarly, the analysis of R30mm, which characterises the frequency of extreme rainfall events, reveals an overall increase in trends (**Figure 4.2-6**). However, statistically significant trends are primarily confined to the urban stations 3117070, 3116006, and 3115079 during the NEM season and station 3115079 during the SWM season, with no significant decreasing trends observed (**Table 4.2-5**).

Sen's slope analysis underscores the prominence of change during the NEM and SWM periods, with stations 3116006 and 3115079 again exhibiting the highest rate of change at 0.15 and 0.25 days per year, respectively. On the other hand, the rate of change for the IntM1 and IntM2 were very low and at many stations the rate of change is 0, indicating no increase in number of extreme rainfall events for most of the locations.

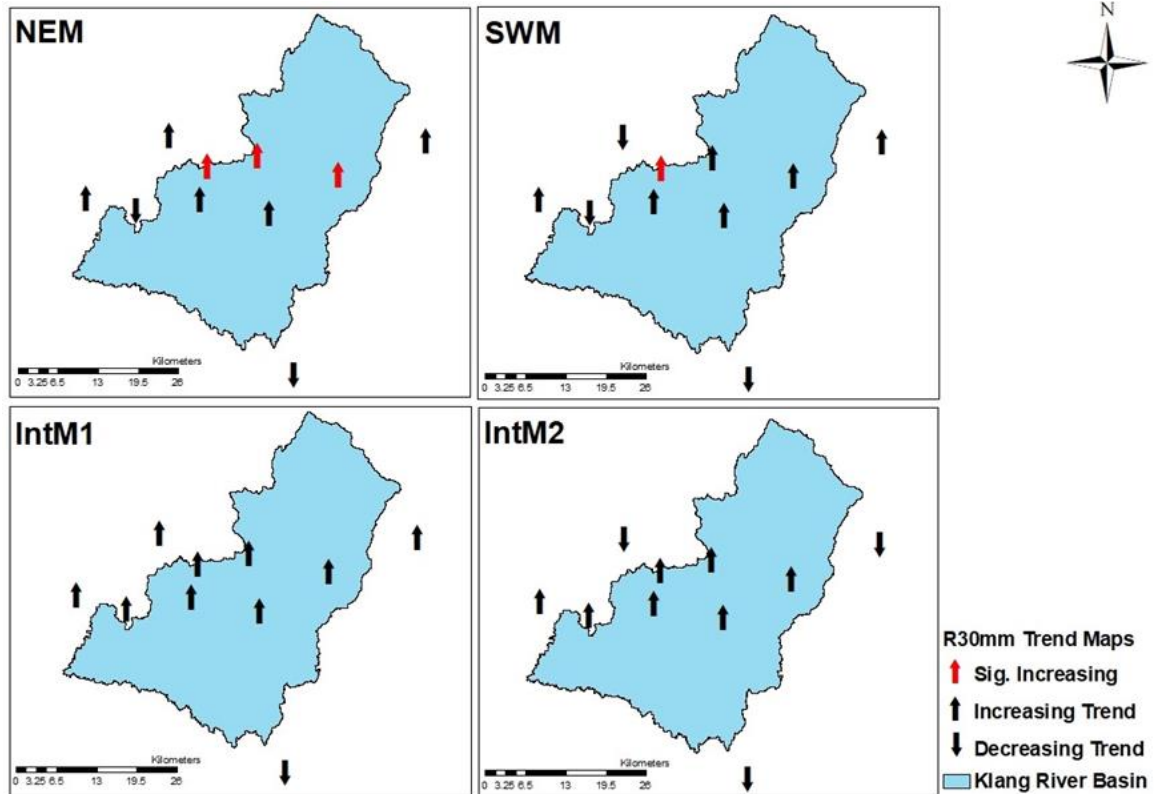


Figure 4.2-6: The R30mm Seasonal Trend Maps For NEM, SWM, Intm1 And Intm2.

Table 4.2-5: Seasonal Trend For R30mm.

Stations	NEM		SWM		IntM1		IntM2	
	Test Z	Sen's Slope						
2616135	-1.09	-0.03	-0.84	-0.04	-0.82	0	-0.99	-0.03
3014084	0.81	0.04	0.96	0.04	0.64	0	-0.16	0
3113087	1.63	0.08	1.28	0.06	0.91	0	0.8	0
3115079	4.04**	0.25	2.66**	0.11	0.31	0	0.83	0
3114085	-1.82+	-0.07	-0.59	0	0.13	0	0.38	0
3115053	1.58	0.11	-0.79	-0.03	0.06	0	-0.83	0
48648	0.95	0.12	1	0.12	0.26	0	1.16	0.07
48647	0.6	0.07	0.52	0.09	0.64	0	0.08	0
3117070	2.20*	0.11	1.33	0.04	0.58	0	0.3	0
3116006	2.30*	0.15	1.88+	0.09	1.04	0	0.73	0

** if trend at $\alpha = 0.01$ level of significance, * if trend at $\alpha = 0.05$ level of significance, + if trend at $\alpha = 0.1$ level of significance, if the cell is blank, the significance level is greater than 0.1.

➤ *R95p*

Lastly, the study examined R95p, a metric that reflects the intensity of heavy precipitation events. A consistent increase in trends is observed during NEM, except for station 2616135 (**Figure 4.2-7**). Whereas, during SWM period station 2616135 did not show any trend. The inter-monsoon periods generally exhibited increasing trend, apart from stations 2616135, 3014084, 3114085, and 3115053. However, statistically significant trends are observed only at stations 3117070, 3116006, and 3115079 (**Table 4.2-6**), highlighting the importance of extreme precipitation on urban areas within the Klang River basin.

Sen's slope calculations reveal that the highest rate of change in R95p is observed at Station 48648, located in the central part of the basin, with an increase of 7.87 mm per year during the SWM season. Overall, the highest rate of change in extreme precipitation intensity was detected at the 5 urban stations particularly during NEM and SWM. Indicating an increase in intensity of extreme precipitation events over urban areas.

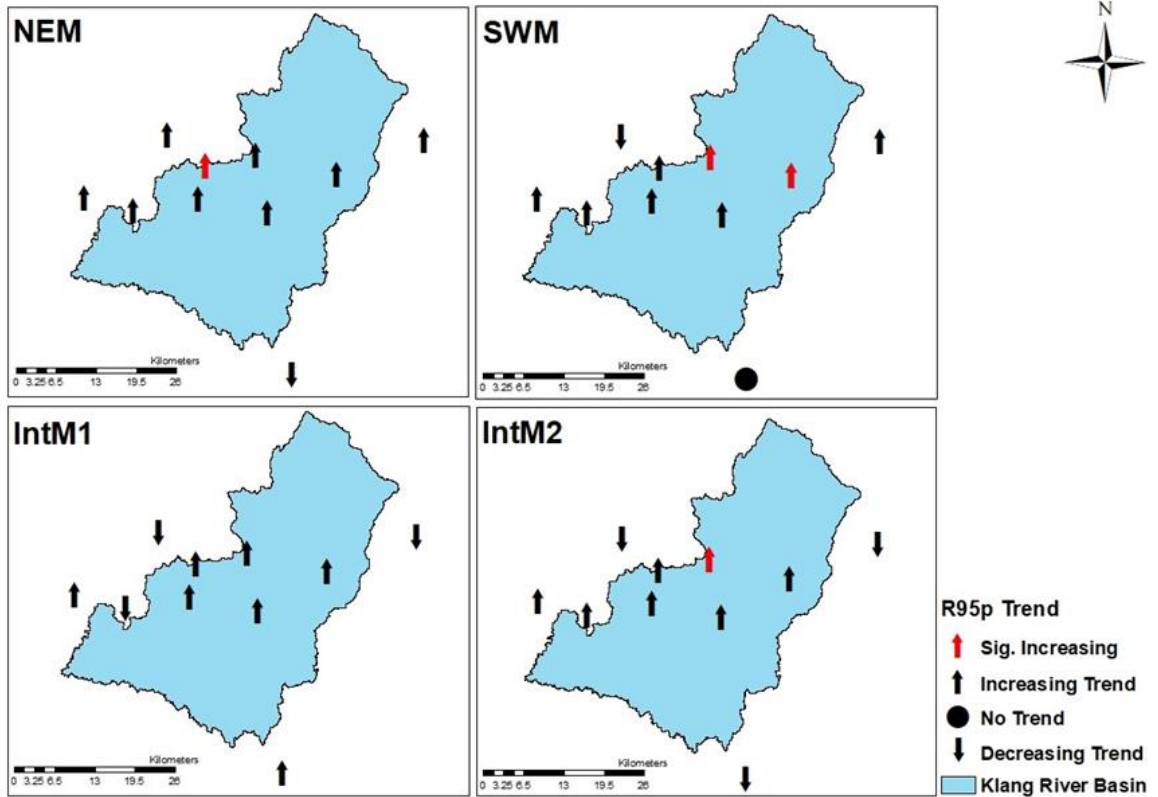


Figure 4.2-7: The R95p Seasonal Trend Maps For NEM, SWM, Intm1 And Intm2.

Table 4.2-6: Seasonal Trend For R95p.

Stations	NEM		SWM		IntM1		IntM2	
	Test Z	Sen's Slope						
2616135	-0.97	-1.11	0	0	1.54	0.46	-0.83	-1.17
3014084	1.84+	3.35	1.37	2.28	-0.14	-0.05	-0.13	-0.05
3113087	1.44	2.57	1.19	2.08	0.72	1	0.7	0.23
3115079	2.92**	6.18	1.63	2.98	0.63	0.12	0.36	0.07
3114085	1.36	1.52	0.1	0	-0.05	-0.03	0.16	0.12
3115053	1.21	2.45	-0.38	-0.42	-0.42	-0.18	-0.55	-0.19
48648	1.22	5.54	1.22	7.87	0.15	0	0.3	0
48647	0.02	0.97	1.94+	6.37	0.55	0.1	1.6	1.42
3117070	1.33	3.24	2.03*	4.41	0.01	0	1.1	0.6
3116006	1.67+	4.39	3.00**	7.74	0.24	0	1.96*	1.54

4.2.2 TEMPERATURE TRENDS

The annual mean, maximum, and minimum 2-meter air temperatures, depicted in **Figure 4.2-8**, convey a comprehensive overview of the temperature regime. The annual average temperature ranges from 24.8°C to 28°C, while the average annual minimum temperature spans from 21.4°C to 25.7°C, and the average annual maximum temperature ranges between 28.2°C to 32.4°C. Notably, the highest annual mean and minimum temperatures are situated downstream of the Klang River, predominantly in the southern region of our study area. On the other hand, the lowest temperatures are observed upstream, in the Northern segment of the basin. The highest annual maximum temperatures are primarily concentrated in the central part of the basin, corresponding to the urban areas.

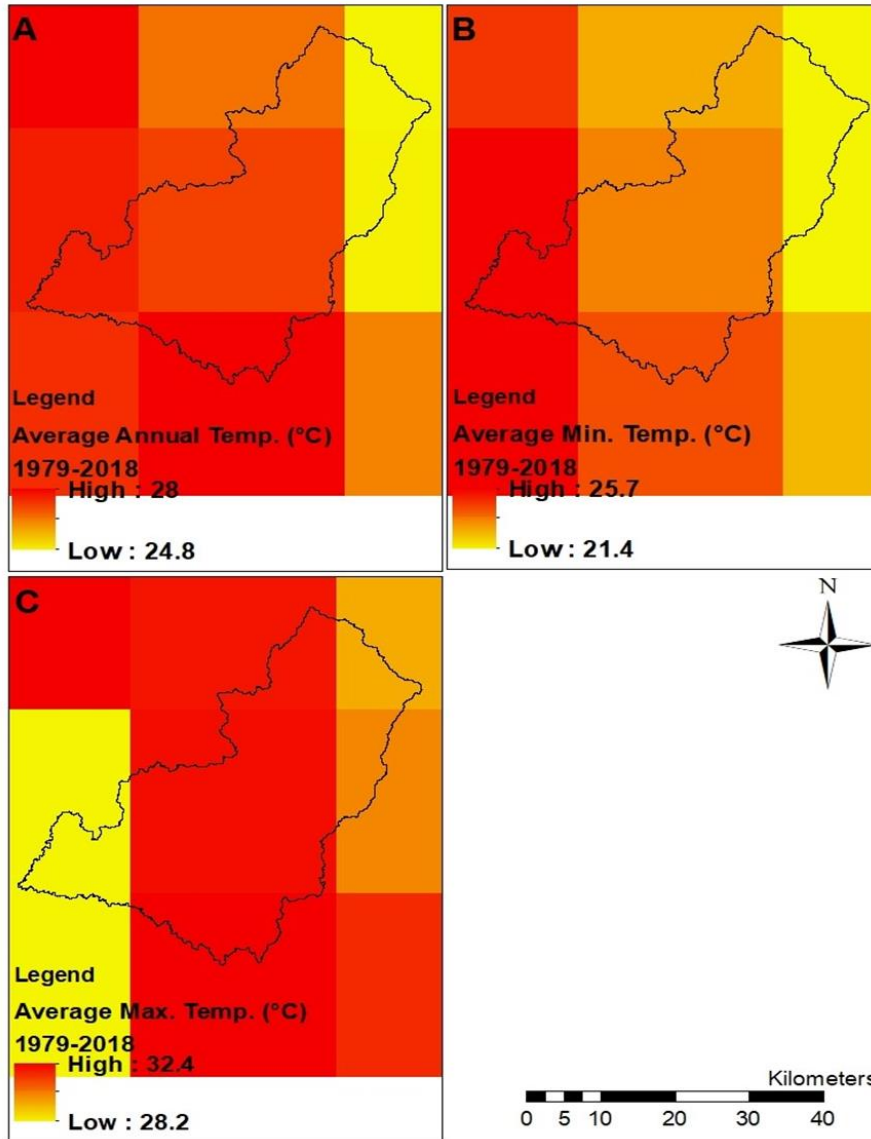


Figure 4.2-8: The Average Annual ERA5 Temperature For The Period 1979-2018.

The annual temperature trends, as presented in **Table 4.2-7**, unveils a pattern of statistically significant increasing trends across all grid points throughout the entire study period, including both the monsoon and inter-monsoon seasons. Only two grids in IntM1 and IntM2 periods exhibit non-significant trends. Interestingly, no decreasing trends in mean temperature were observed in any of the periods analysed. The

Sen's slope estimator further underscores the magnitude of these changes, with most grid points registering an annual increase of 0.03°C per year.

Table 4.2-7: *The Annual And Seasonal Mean Temperature Trend.*

Grids	Annual		NEM		SWM		IntM1		IntM2	
	Test Z	Q								
Grid 1	4.72**	0.03	3.67**	0.02	5.46**	0.04	4*	0.03	4.16**	0.03
Grid 2	5**	0.03	3.93**	0.03	5.77**	0.03	4.46**	0.03	5.23**	0.04
Grid 3	2.06*	0.01	2.23*	0.01	2.09*	0.01	0.59	0	1.5	0.01
Grid 4	5.49**	0.03	5.07**	0.03	5.12**	0.03	4.67**	0.03	4.04**	0.03
Grid 5	6.21**	0.03	4.97**	0.03	6.77**	0.04	5**	0.03	5.60**	0.03
Grid 6	2.57*	0.01	2.92**	0.01	2.41*	0.01	0.43	0	2.32*	0.01
Grid 7	3.90**	0.03	3.60**	0.03	3.70**	0.03	2.53*	0.02	3.37**	0.03

** if trend at $\alpha = 0.01$ level of significance, * if trend at $\alpha = 0.05$ level of significance, + if trend at $\alpha = 0.1$ level of significance, if the cell is blank, the significance level is greater than 0.1.

➤ **TXx TREND**

The analysis of the TXx trend, representing the warmest days (**Table 4.2-8**), shows a primarily increasing trend across the majority of the study area's grids, spanning both annual and seasonal periods. The exception is noted in grids 1 and 2, located upstream in the Northern region of the basin, where a decreasing trend is observed. Notably, significant trends are predominantly detected during IntM2, with grid 3 being the sole exception, showing insignificance. No significant trend emerges during the NEM season across the entire study area. The rate of change in TXx closely parallels that of mean temperature, with the

most rapid increase observed during the SWM period at grid 1, reaching 0.04°C per year.

Table 4.2-8: The Annual And Seasonal Txx Trend.

Grids	Annual		NEM		SWM		IntM1		IntM2	
	Test Z	Q	Test Z	Q	Test Z	Q	Test Z	Q	Test Z	Q
Grid 1	0.5	0.01	-0.69	-0.01	2.39*	0.04	1.36	0.02	2.18*	0.02
Grid 2	0.15	0	-0.09	0	1.36	0.02	2.52*	0.03	3.09**	0.03
Grid 3	1.04	0	0.71	0.01	0.24	0	0.8	0	1.85+	0.01
Grid 4	2.34*	0.03	0.29	0.01	2.34*	0.03	2.27*	0.02	3.11**	0.03
Grid 5	0.9	0.01	0.34	0.01	3.18**	0.03	2.85**	0.03	3.95**	0.03
Grid 6	0.6	0	1.29	0.01	0.29	0	0.8	0.01	2.18*	0.01
Grid 7	1.64	0.02	0.01	0	0.92	0.01	0.57	0.01	2.3*	0.03

** if trend at $\alpha = 0.01$ level of significance, * if trend at $\alpha = 0.05$ level of significance, + if trend at $\alpha = 0.1$ level of significance, if the cell is blank, the significance level is greater than 0.1.

➤ **TNx TREND**

Similarly, the analysis of the TNx trend, which quantifies the warmest nights (**Table 4.2-9**), reveals a pattern of significant positive trends across most grids during all analysed periods. These trends are often significant at a 0.01 level of significance. The rate of change, as determined by the Sen's slope, mirrors both the mean temperature and the TXx trend, with the highest rate of change reaching 0.05°C per year. This collective evidence underscores the consistent warming of night time temperatures within the study area.

Table 4.2-9: The Annual And Seasonal Tnx Trend.

Grids	Annual		NEM		SWM		IntM1		IntM2	
	Test Z	Q								
Grid 1	5.37**	0.04	3.11**	0.03	5.58**	0.05	5.25**	0.04	5.39**	0.04
Grid 2	5.21**	0.04	3.69**	0.03	6.05**	0.05	4.84**	0.04	5.65**	0.04

Grid 3	2.53*	0.01	1.69+	0.01	2.32*	0.01	1.5	0.01	2.6**	0.02
Grid 4	5.7**	0.05	4.74**	0.04	5.79**	0.05	5.14**	0.03	5.21**	0.04
Grid 5	5.91**	0.04	4.7**	0.04	6**	0.04	5.04**	0.04	5.35**	0.04
Grid 6	2.2*	0.01	1.74+	0.01	2.02*	0.01	0.87	0.01	2.04*	0.02
Grid 7	4.53**	0.04	3.83**	0.03	4.19**	0.03	3.76**	0.03	4.36**	0.04

** if trend at $\alpha = 0.01$ level of significance, * if trend at $\alpha = 0.05$ level of significance, + if trend at $\alpha = 0.1$ level of significance, if the cell is blank, the significance level is greater than 0.1.

4.2.2.1 LAND SURFACE TEMPERATURE

The evaluation of land surface temperature dynamics over three distinct years (1999, 2006, and 2017) offers a valuable perspective on long-term trends (**Figure 4.2-9**). The observations reveal a clear increase in temperature and a corresponding upward shift in temperature range over the 18-year period, as previously noted by Azari et al., (2020). Specifically, temperatures ranged from 9.5°C to 31.2°C in 1999, 8.5°C to 35.7°C in 2006, and 12.1°C to 41.3°C in 2017. The most elevated temperatures are concentrated in urbanised regions in the Southern and central regions of the basin, while the lowest temperatures prevail in the natural vegetation dominated Northern areas.

Importantly, this analysis indicates a substantial increase in both minimum and maximum temperatures over the 18-year period, with maximum temperatures experiencing a significant rise of 10.1°C and minimum temperatures increasing by 2.6°C. This robust evidence underscores the direct influence of urbanisation on surface

temperatures, resulting in elevated and intensified thermal conditions within the Klang River basin.

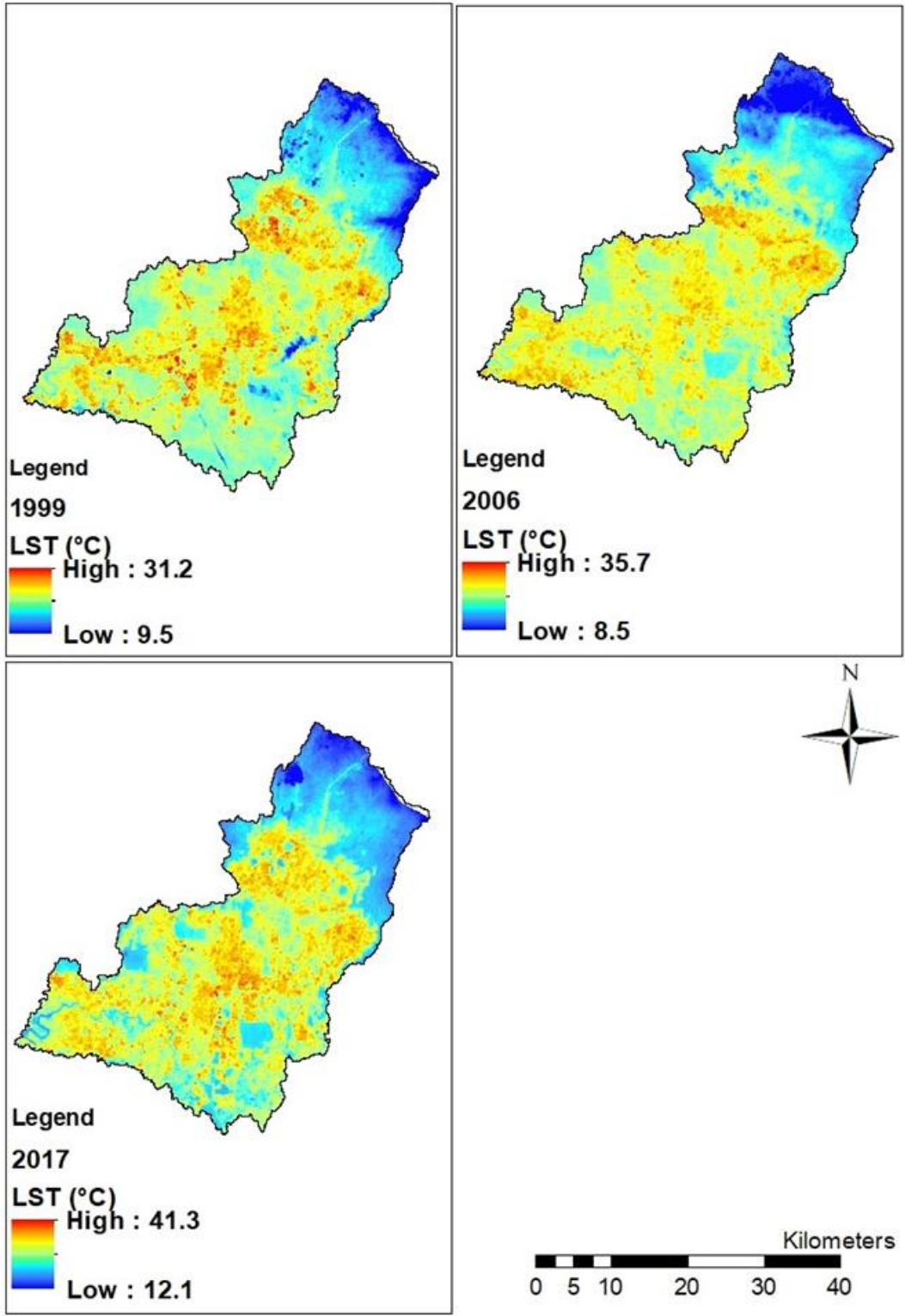


Figure 4.2-9: Land Surface Temperature For Year 1999, 2006 And 2017.

4.2.3 TRENDS IN FUTURE SCENARIOS

4.2.3.1 PRECIPITATION TREND

Table 4.2-10 illustrates the annual precipitation trends over the entire future period (2006-2099) and three distinct time periods: TP1 (2006-2039), TP2 (2040-2069), and TP3 (2070-2099) for the four different RCP scenarios. Across the entire period, all RCP scenarios exhibit positive trends, though RCP2.5 was not statistically significant. Projections suggest that annual precipitation will increase by 0.2% under RCP2.6, 3% under RCP4.5, 1.4% under RCP6, and 5.6% under RCP8.5 compared to baseline values. RCP8.5 exhibits the highest rate of change at 4.41 mm/year according to Sen's slope Q estimator, with RCP4.5 and RCP6 following at 2.48 mm/year and 1.84 mm/year, respectively.

For the TP1 period, all scenarios display positive trends, with only RCP4.5 exhibiting significance. On the other hand, TP2 and TP3 periods show no significant trends, and RCP6 even presents negative trends. The highest rate of change was detected for RCP4.5 during TP1 period, at rate of change of 6.05 mm/year.

Table 4.2-10: Annual Precipitation Trend For Future Climate Scenarios For The Period 2006-2099.

RCP Scenarios	2006-2099		TP1 (2006-2039)		TP2 (2040-2069)		TP3 (2070-2099)	
	Test Z	Q	Test Z	Q	Test Z	Q	Test Z	Q
RCP 2.6	0.84	0.55	1.22	3.74	0.82	3.45	0.11	0.35
RCP 4.5	3.66**	2.48	2.28*	6.05	1.75+	6.83	-0.04	-0.33
RCP 6	2.94**	1.84	0.56	1.62	-1.07	-4.67	-0.75	-2.65
RCP 8.5	5.45**	4.41	0.33	1.29	1.5	5.09	0.79	3.92

** if trend at $\alpha = 0.01$ level of significance, * if trend at $\alpha = 0.05$ level of significance, + if trend at $\alpha = 0.1$ level of significance, if the cell is blank, the significance level is greater than 0.1.

Monthly Precipitation Trends for the 4 RCP Scenarios for the entire future period (2006-2099) are presented in **Table 4.2-11**. Most trends are positive, with RCP2.6 and RCP6 having some negative trends, although a significant negative trend was detected in the month of April under RCP8.5 scenario. RCP8.5 shows significant positive trends in 8 out of 12 months. Notably, May, June, and November display positive significant trends for RCP4.5, RCP6, and RCP8.5. The month of April records the highest rate of change for RCP8.5 at 0.72 mm/year.

Table 4.2-11: Monthly Precipitation Trend For Future Climate Scenarios For The Period 2006-2099.

Month	Period 2006-2099							
	RCP 2.6		RCP 4.5		RCP 6		RCP 8.5	
	Test Z	Q	Test Z	Q	Test Z	Q	Test Z	Q
January	0.56	0.11	0.29	0.04	-0.76	-0.11	0.6	0.12
February	1.27	0.20	1.38	0.25	0.67	0.11	0.56	0.11
March	0.78	0.17	-0.32	-0.07	-0.25	-0.06	1.08	0.23
April	0.35	0.06	2.68**	0.50	-0.32	-0.07	3.90**	0.72
May	0.42	0.05	3.33**	0.40	4.74**	0.63	5.00**	0.68
June	-0.91	-0.05	2.35*	0.15	3.08**	0.22	4.32**	0.39
July	0.88	0.06	1.63	0.09	1.98*	0.16	2.82**	0.28
August	-1.08	-0.10	0.35	0.03	1.83+	0.18	4.19**	0.44
September	-1.03	-0.11	2.66**	0.24	1.27	0.14	3.25**	0.41

October	1.44	0.14	1.65+	0.21	2.22*	0.29	3.21**	0.45
November	-0.66	-0.10	2.49*	0.35	2.63**	0.42	2.34*	0.36
December	0.48	0.07	1.84+	0.25	0.46	0.06	1.42	0.25

** if trend at $\alpha = 0.01$ level of significance, * if trend at $\alpha = 0.05$ level of significance, + if trend at $\alpha = 0.1$ level of significance, if the cell is blank, the significance level is greater than 0.1.

The analysis of precipitation intensity indicators, SDII and R95p are presented in **Table 4.2-12** and **Table 4.2-13**, respectively. Across the entire future time frame from 2006 to 2099, both SDII and R95p exhibit noteworthy positive trends for the RCP4.5, RCP6, and RCP8.5 scenarios. However, it's worth noting that the most optimistic scenario, RCP2.6, does not display a significant trend in either indicator.

Examining the different time periods, a mix of upward and downward trends is observed. Of particular significance, the RCP4.5 scenario during period TP1 demonstrates a substantial upward trend for both SDII and R95p. However, negative trends become apparent in some scenarios. For instance, during TP3, SDII exhibits negative trends for RCP2.6, RCP4.5, and RCP6. In TP2, RCP6 also demonstrates a negative trend for SDII.

It's important to highlight that the rate of change for SDII remains minimal across the entire time span, registering at 0.01mm/day per year for RCP4.5, RCP6, and RCP8.5. On the other hand, R95p shows its highest rate of change for a significant trend in the RCP8.5 scenario, with a substantial increase of 2.63 mm per year.

Table 4.2-12: SDII Trend For Future Climate Scenarios.

RCP Scenarios	SDII							
	2006-2099		TP1 (2006-2039)		TP2 (2040-2069)		TP3 (2070-2099)	
	Test Z	Q	Test Z	Q	Test Z	Q	Test Z	Q
RCP 2.6	0.76	0.00	1.33	0.01	0.64	0.01	-0.18	0.00
RCP 4.5	3.64**	0.01	2.19*	0.02	1.71+	0.02	-0.36	0.00
RCP 6	3.12**	0.01	0.65	0.00	-0.79	-0.01	-0.79	-0.01
RCP 8.5	5.59**	0.01	0.44	0.00	1.78+	0.02	0.89	0.01

** if trend at $\alpha = 0.01$ level of significance, * if trend at $\alpha = 0.05$ level of significance, + if trend at $\alpha = 0.1$ level of significance, if the cell is blank, the significance level is greater than 0.1.

Table 4.2-13: R95p Trend For Future Climate Scenarios.

RCP Scenarios	R95p							
	2006-2099		TP1 (2006-2039)		TP2 (2040-2069)		TP3 (2070-2099)	
	Test Z	Q	Test Z	Q	Test Z	Q	Test Z	Q
RCP 2.6	1.31	0.60	1.16	2.44	1.14	3.23	0.29	0.56
RCP 4.5	3.60**	1.98	2.19*	5.29	0.89	1.99	0.75	2.47
RCP 6	2.23*	1.07	-0.65	-1.21	-0.25	-1.08	-0.82	-2.15
RCP 8.5	4.80**	2.63	-0.47	-0.99	1.64	5.70	1.5	6.06

** if trend at $\alpha = 0.01$ level of significance, * if trend at $\alpha = 0.05$ level of significance, + if trend at $\alpha = 0.1$ level of significance, if the cell is blank, the significance level is greater than 0.1.

4.2.3.2 TEMPERATURE TREND

Figure 4.2-10 presents the mean annual temperature projections for the period 2006-2099 under different RCP scenarios. All scenarios predict an increase in mean annual temperatures, with RCP8.5 showing the most substantial increase at 2.3°C compared to historical values. Average maximum temperatures are expected to decrease by 2.6°C for RCP2.6, 1.9°C for RCP4.5, and 1.6°C for RCP6 but increase by 0.5°C for RCP8.5.

In contrast, average minimum temperatures are projected to increase for all RCPs by approximately 4.7°C. **Table 4.2-14** outlines the changes in mean, maximum, and minimum temperatures relative to historical data for all time periods and RCP scenarios. Under RCP8.5, mean, maximum, and minimum temperatures are anticipated to increase by 3.8°C, 0.5°C, and 7.4°C, respectively, during the TP3 period.

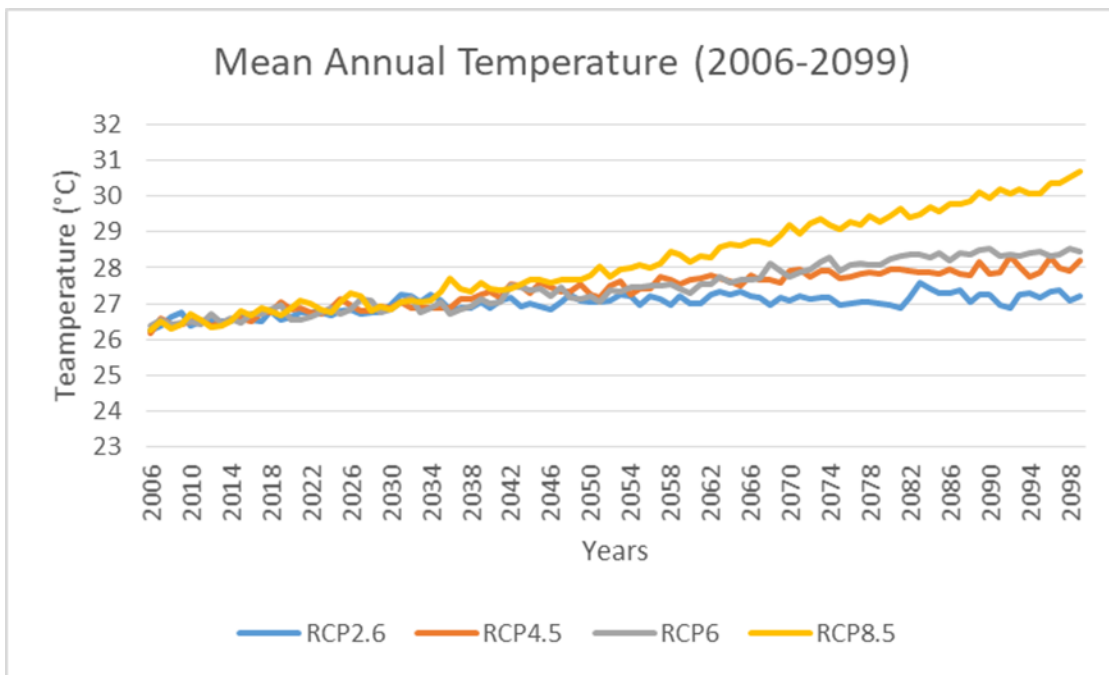


Figure 4.2-10: Mean Annual Temperature For Klang River Basin (2006-2099), Under Different RCP Scenarios.

Table 4.2-14: Change In Mean, Maximum, And Minimum Temperatures Under Different RCP Scenarios For All Time Periods Relative To Historical Data.

RCP Scenarios	TP1 (2006-2039)			TP2 (2040-2069)			TP3 (2070-2099)		
	Change (°C)			Change (°C)			Change (°C)		
	Mean	Max	Min	Mean	Max	Min	Mean	Max	Min
RCP2.6	0.9	-2.9	4.7	1.2	-2.8	5.3	1.3	-2.6	5.3
RCP4.5	0.9	-2.9	4.6	1.6	-2.4	5.6	2.0	-1.9	6.1
RCP6	0.9	-3.0	4.8	1.6	-2.1	5.4	2.4	-1.6	6.2
RCP8.5	1.0	-2.5	4.7	2.2	-1.3	5.8	3.8	0.5	7.4

** if trend at $\alpha = 0.01$ level of significance, * if trend at $\alpha = 0.05$ level of significance, + if trend at $\alpha = 0.1$ level of significance, if the cell is blank, the significance level is greater than 0.1.

Annual average temperature trends for the period 2006-2099 and the three time periods are presented in **Table 4.2-15**. All RCP scenarios show significant increasing trends for the entire period, with RCP8.5 displaying the highest rate of change at 0.05°C per year.

Table 4.2-15: Average Annual Temperature Trend For Future Climate Scenarios For The Period 2006-2099.

RCP Scenarios	2006-2099		TP1 (2006-2039)		TP2 (2040-2069)		TP3 (2070-2099)	
	Test Z	Q	Test Z	Q	Test Z	Q	Test Z	Q
RCP 2.6	7.71**	0.01	5.43**	0.02	2.28*	0.01	1.46	0.01
RCP 4.5	11.61**	0.02	5.46**	0.02	3.18**	0.01	1.68+	0.01
RCP 6	12.29**	0.02	4.89**	0.02	4.71**	0.02	5.00**	0.02
RCP 8.5	13.31**	0.05	6.02**	0.03	6.96**	0.05	6.57**	0.05

** if trend at $\alpha = 0.01$ level of significance, * if trend at $\alpha = 0.05$ level of significance, + if trend at $\alpha = 0.1$ level of significance, if the cell is blank, the significance level is greater than 0.1.

The trends in annual maximum and minimum temperatures, spanning the entire period from 2006 to 2099 and encompassing all climate scenarios, is presented in **Table 4.2-16** and **Table 4.2-17**. The analysis shows a significant increasing trend in both maximum and minimum temperatures for all scenarios. Notably, the RCP8.5 scenario exhibits the most pronounced rate of change, with temperatures rising by 0.05°C for both maximum and minimum temperatures. However, for specific time periods, this shows variations detected in these trends. During TP2, there is a nonsignificant decreasing trend in maximum temperatures for

the RCP4.5 scenario. Additionally, during TP3, a significant decreasing trend in minimum temperatures is observed for the RCP2.6 scenario.

Table 4.2-16: Annual Maximum Temperature Trend For Future Climate Scenarios For The Period 2006-2099.

RCP Scenarios	2006-2099		TP1 (2006-2039)		TP2 (2040-2069)		TP3 (2070-2099)	
	Test Z	Q	Test Z	Q	Test Z	Q	Test Z	Q
RCP 2.6	6.91**	0.01	3.59**	0.02	2.50*	0.015	1.93+	0.02
RCP 4.5	9.89**	0.02	3.50**	0.02	-0.14	-0.001	1.75+	0.01
RCP 6	10.62**	0.02	3.44**	0.02	2.43*	0.020	2.07*	0.01
RCP 8.5	12.44**	0.05	4.48**	0.03	6.49**	0.054	5.50**	0.05

** if trend at $\alpha = 0.01$ level of significance, * if trend at $\alpha = 0.05$ level of significance, + if trend at $\alpha = 0.1$ level of significance, if the cell is blank, the significance level is greater than 0.1.

Table 4.2-17: Annual Minimum Temperature Trend For Future Climate Scenarios For The Period 2006-2099.

RCP Scenarios	2006-2099		2006-2039		2040-2069		2070-2099	
	Test Z	Q						
RCP 2.6	6.20**	0.01	6.20**	0.02	0.89	0.00	-2.32*	-0.01
RCP 4.5	12.14**	0.02	6.64**	0.03	5.74**	0.02	1.46	0.00
RCP 6	12.86**	0.03	5.63**	0.02	5.92**	0.03	5.74**	0.03
RCP 8.5	13.69**	0.05	7.12**	0.03	7.00**	0.05	6.85**	0.05

** if trend at $\alpha = 0.01$ level of significance, * if trend at $\alpha = 0.05$ level of significance, + if trend at $\alpha = 0.1$ level of significance, if the cell is blank, the significance level is greater than 0.1.

4.2.4 RIVER DISCHARGE TRENDS

The average annual and monthly river discharge data for Batu Sentul station (3116434) and Jambatan Sulaiman station (3116430) are represented in **Figure 4.2-11**. Notably, November stands out as the month with the highest discharge rates at both stations, measuring 9.6 m³/s for Batu Sentul and 29 m³/s for Jambatan Sulaiman. This spike in discharge aligns with the period of high precipitation observed during the Northeast Monsoon (NEM) in November.

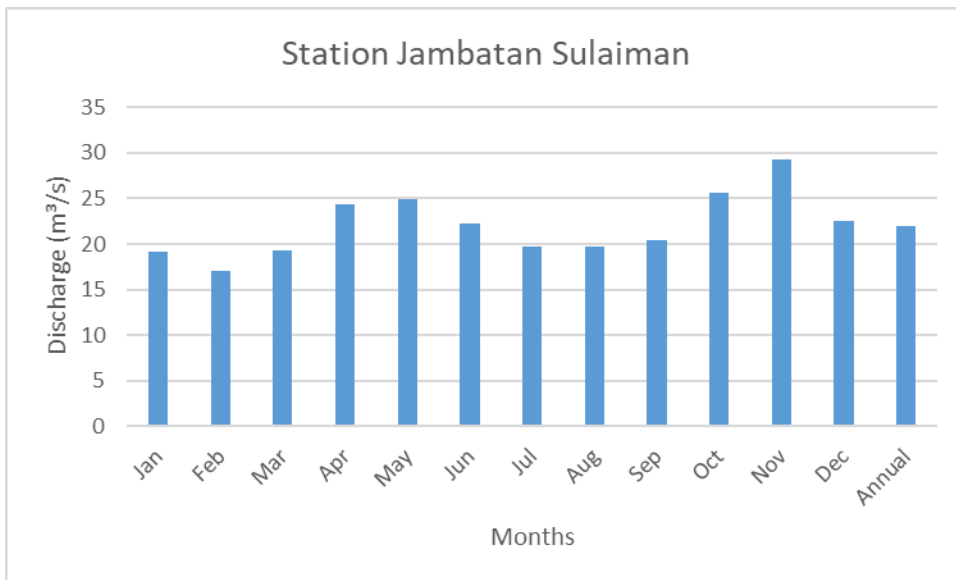
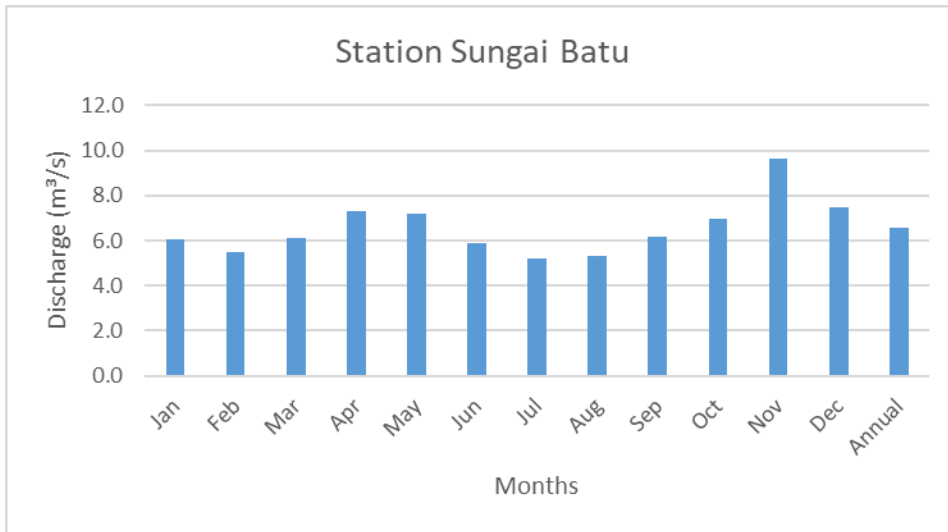


Figure 4.2-11: Average Annual And Monthly River Discharge At Stations Sungai Batu And Jambatan Sulaiman.

The analysis of the trends in annual and monthly discharge are presented in **Table 4.2-18**. The analysis reveals a consistent and statistically significant increasing annual trend in discharge for both stations. However, when assessing monthly trends, Batu Sentul station does not exhibit any statistically significant trends, while Jambatan

Sulaiman station demonstrates significant increases in discharge for 7 out of the 12 months. Notably, Jambatan Sulaiman station also boasts a higher annual rate of change, registering at 0.35 m³/s, compared to Batu Sentul station's 0.08 m³/s. When it comes to monthly rates of change, August emerges as the month with the most substantial increase, measuring 0.53 m³/s at Jambatan Sulaiman station.

Table 4.2-18: Annual And Monthly River Discharge Trends For Stations 3116430 And 3116434.

Date	Batu Sentul		Jambatan Sulaiman	
	Test Z	Q	Test Z	Q
January	0.93	0.04	3.16**	0.4
February	1.18	0.05	1.92+	0.25
March	1.70+	0.09	2.40*	0.29
April	0.94	0.05	2.19*	0.3
May	0.98	0.07	1.90+	0.34
June	0	0	2.82**	0.35
July	1.78+	0.07	3.41**	0.34
August	1.61	0.07	3.63**	0.53
September	1.05	0.05	2.55*	0.33
October	1.34	0.07	1.3	0.23
November	1.21	0.09	1.32	0.17
December	0.62	0.04	1.74+	0.3
Annual	2.09*	0.08	3.16**	0.35

** if trend at $\alpha = 0.01$ level of significance, * if trend at $\alpha = 0.05$ level of significance, + if trend at $\alpha = 0.1$ level of significance, if the cell is blank, the significance level is greater than 0.1.

4.2.5 DISCUSSION

In addition to LULC change, another important factor that impacts hydrological processes is climate parameters, in particular precipitation. Therefore, it is crucial to detect and understand the trends in hydro-meteorological parameters to comprehend the impacts of climate

change and LULC changes on hydrological processes. This section delves into the analysis of spatio-temporal trends in precipitation, temperature, and river discharge within the Klang River basin and addresses the question of what is the intensity and frequency of trends observed in these hydro-meteorological parameters.

In this study intensity in precipitation was presented by SDII and R95p indices and frequency was represented by R10mm and R30mm indices. Temperature trends were analysed using TXx and TNx indices, which represent warmest days and warmest nights, in addition to mean, maximum and minimum temperatures, as well as surface temperatures. The TXx and TNx reveal the extremeness of temperature patterns. Analysis of trend under future scenarios was based on data collected from global climate models for the period 2006 to 2099, under 4 Representative Concentration Pathway (RCP) scenarios, including RCP2.6, RCP4.5, RCP6, and RCP8.5, to account for various greenhouse gas emission trajectories and their potential impacts on the climate.

Precipitation data for 10 stations for a period of 40 years obtained from the Department of Irrigation and Drainage was utilised. However, for temperature due to lack of observed station data, the ERA 5 reanalysis data was utilised, plus thermal band of Landsat satellite images for surface temperatures. For discharge data for stations Batu Sentul and Jambatan Suliman was utilised. The ERA 5 data was assessed and

validated against 2 available data sets of observed station data spanning the period 1995 to 2018.

The validation demonstrated good correlation between the observed and ERA 5 dataset, and multiple studies have shown that ERA 5 can be a good substitute for observed station data, when there is lack of data, as it gives better representation of observed data and has less bias in temperature, precipitation and humidity data compared to other sources of data (Betts et al., 2019; Graham et al., 2019; Mahto and Mishra, 2019; Li, 2020).

Delving into the analysis of the precipitation trends, a pattern of upward trajectory over the Klang River basin is observed, with urban areas experiencing the most substantial increases. The intensity and frequency of precipitation mirrors these trends, with notable changes in central areas over urban land and declining trends in the upper forested land and lower parts of the basin.

The precipitation results obtained in this study for Klang River basin are comparable with results obtained for the neighboring Langat River basin by Amirabadizadeh et al., (2015), where increasing trend in annual precipitation was detected over urban areas, similarly the NEM showed increasing trend over urban areas for the period 1971 to 2011. This

illustrates that these changes in precipitation in the Klang River basin can be significantly influenced by change in climate at regional level.

The quantitative analysis of the precipitation trend illustrates that, with an average precipitation range of 2583 mm to 3368 mm urban areas in the Klang River basin experience the highest amount of precipitation. Of the five weather stations situated within these urban areas, four stations; namely 48648, 3117070, 3116006, and 3115079 have recorded an increase in precipitation during the period spanning from 1999 to 2017, with percentage increases of 0.4%, 2.2%, 0.7%, and 4.9%, respectively.

All four stations also exhibit statistically significant upward trends in annual precipitation, with station 3116006 displaying the most notable rate of change at 28.46 mm per year. Meanwhile, the average annual precipitation in both the upper and lower parts of the basin fall within the range of 2024 mm to 2583 mm. This highlights the spatial variability in precipitation, and that urban areas on average receive more rainfall than other areas in Klang River basin. This also highlights the assumption that increasing trend in precipitation has significant impact on hydrological processes in the Klang River basin, which shall be further analysed in **Section 4.3**.

The other important aspects of precipitation change are intensity and frequency, where more intense rainfall can culminate in more intense flooding and more frequent extreme precipitation can culminate in more frequent flooding events. Across the Klang River basin, the annual SDII, R10mm, R30mm, and R95p indices yield similar results to the observed precipitation amounts. Central parts of the basin experience increasing trends, while the upper and lower segments show decreasing trends. Positive trends are detected for all indices at stations 3116006 and 3115079, whereas negative trends are observed at stations 2616135, 3014084, and 3114085, all of which are located just outside the boundaries of the Klang River basin. Illustrating more intense and frequent extreme rainfall events occurring over urban areas.

Seasonality plays an important part in precipitation trends, particularly in Southeast Asia which experiences monsoon seasons. The seasonal trend in the Klang River basin exhibited a similar spatial pattern to annual trend, as illustrated by the trend maps in **Section 4.2.1.2**. Notably, a consistent increasing trend in the five weather stations situated within the urban areas of the basin was detected. Of particular significance is the SDII, which provides a measure of precipitation intensity, with station 48648 exhibiting the highest rate of change at 0.29 mm/day.

Significant increase in precipitation intensity and frequency is mostly detected during the NEM period, and the average monthly precipitation is highest in the month of November for all the stations. This indicates that NEM is the major contributing factor to the annual precipitation. This is similar to results found by Palizdan et al., (2014) that showed increasing trend for precipitation during NEM season in the Langat River basin.

As past studies have shown, temperatures can influence precipitation. Increase in temperatures leads to increase in evapotranspiration, which results in higher air moisture, hence it can lead to urban induced precipitation. As demonstrated by Ooi *et al.*, (2017), increase in urban heat intensity of 0.9°C during the day and a more severe increase of 1.9°C during the night in the Greater Kuala Lumpur, accelerated the moisture bearing sea breeze during the day and with the simultaneous vertical lifting created an environment for convective precipitation on the upwind of the region.

The patterns of temperature trends observed for the Klang River basin are similar to precipitation patterns, with land surface temperatures exhibiting higher values and intensity over urban areas. On the other hand, uptrends in mean temperature, TXx, and TNx observed across the basin align with broader global warming patterns, that have an increasing rate 0.08°C per decade since 1880 as report by NOAA,

(2020), with the maximum temperatures detected over urban areas. However, it is important to note that this temperature is 2m air temperature which represents ambient temperature and differs from surface temperature where during the day the ground temperature is higher than air temperature and at night when the ground releases heat to the atmosphere, the ground temperature is lower than air temperature.

The higher surface temperature can lead to higher evaporation and hence lead to induced precipitation, this point is further highlighted in the study by Li *et al.*, (2020) that observed increase in precipitation intensity by 35% over the period 1981 to 2011 due to UHI effect, which created a more unstable atmosphere, increased vertical uplift and moisture convergence .

In the Klang River basin, the increase in urban land in the period 1999 to 2017 resulted in an increase in maximum LST of about 10.1°C and minimum LST of about 2.6°C, over urban areas, creating the urban heat island effect over KL and conditions suitable for urban induced precipitation. This is in agreement with Harun *et al.*, (2020), that analysed the various factors that affect UHI in KL, and the results show that land cover is the main factor in increasing of temperatures compared to other factors like wind speed and humidity. The results

show that urban green spaces and water can reduce UHI by 6°C - 3°C compared to pure urban mid-rise building areas.

Similarly Yatim *et al.*, (2019) showcased increases in the annual daily mean temperature, daily mean maximum temperature, and daily mean minimum temperature in the Klang Valley by 0.07°C/year, 0.07°C/year and 0.08°C/year, respectively and that the annual TNx trend increased more than TXx at a rate of 0.11°C/year, which is similar to values found in this study.

To address the assumption that changes in LULC and precipitation in the Klang River basin have impact on hydrological processes, it's important to analyse the trend in these processes. Trend in river discharge was analysed to better understand the magnitude of the impacts from LULC and precipitation changes. The trend in river discharge at Batu Sentul and Jambatan Sulaiman stations mirrors that of precipitation and temperature trend, with an overall increasing trend detected at both stations with an annual rate of change of 0.08 m³/s and 0.35 m³/s respectively.

However, significant trend was only detected at station Jambatan Sulaiman, with 7 out of 12 months having significance, and the month of August having the highest rate of change at 0.53 m³/s. On the other hand, in the study by Kabiri *et al.*, (2015) on the assessment of climate

change impact on runoff and discharge in Klang River basin, observed river discharge at station Jambatan Sulaiman for the period 1975 to 2001, showed peak discharge in April and November, and lowest discharge in February and August. The reason for higher discharge in August in this study compared to the study by Kabiri et al., (2015) can be due to the increase in urban land and changes in precipitation after the year 2001. This highlights the effects of LULC change and precipitation changes on river discharge and hydrological processes.

The trend analysis of future precipitation and temperature under different climate change scenarios, can give better insight into the impacts of climate change in the future and help in better preparation and management of water resource for possible future conditions. Trend in future precipitation in Klang River basin illustrates by the end of the century, average annual precipitation will increase by 0.2%, 3%, 1.4% and 5.6% under RCP2.6, RCP4.5, RCP6 and RCP8.5 scenarios respectively, relative to the baseline precipitation. With RCP8.5 scenario having the highest intensity of change at a rate of 4.41 mm/year.

4.3 QUANTITATIVE ANALYSIS OF SPATIO-TEMPORAL HYDROLOGICAL MODELLING

4.3.1 SWAT MODEL PARAMETER SENSITIVITY ANALYSIS

The sensitivity analysis of model parameters identified eight parameters to be the most sensitive and influential in shaping the model's performance, as detailed in **Table 4.3-1**. The parameters include CH_K1 which affects the movement of water within the tributary channels, CH_K2 and CH_N2 which affect the movement of water within the main channel, SOL_AWC which affects the availability of water in the soil, SOL_K which affects the movement of water within the soil layer, ESCO which affects soil evaporation rate, SURLAG which affects the timing and movement of surface runoff and CN2 which affects the amount of surface runoff. Notably, CH_K1, CH_K2, and CH_N2 emerge as the most sensitive parameters, each demonstrating substantial statistical significance. These eight parameters are chosen for model calibration as they are the most sensitive parameters.

Table 4.3-1: Sensitivity Ranking Of Parameters Used In Simulation Of Water Discharge.

Ranking	Parameter	Description	t-Stat	P-Value
1	CH K1	Effective hydraulic conductivity in tributary channel alluvium (mm/h)	-37.2764	3.2E-114
2	CH K2	Effective hydraulic conductivity in main channel alluvium (mm/h)	-44.9951	2.6E-176
3	CH N2	Manning's n value for the main channel	10.79926	1.55E-24
4	SOL AWC	Soil available water capacity (mm H2O/mm soil)	-1.59938	0.11038

5	SOL K	Soil saturated hydraulic conductivity (mm/h)	1.542174	0.123675
6	ESCO	Soil evaporation compensation factor	0.52675	0.598605
7	SURLAG	Surface runoff lag time (days)	-0.37643	0.706758
8	CN2	Initial SCS runoff curve number for moisture condition II	-0.19705	0.843873

4.3.2 SWAT MODEL CALIBRATION AND VALIDATION

The model is calibrated for streamflow by calibrating the eight parameters identified during the sensitivity analysis. The parameter ranges used to calibrate the model is selected based on literature review and similar studies in Malaysia. The description and range of the parameters is presented in **Table 4.3-2**.

Table 4.3-2: SWAT Model Parameters Used To Calibrate Streamflow.

Parameter	Description	Initial range used in calibration	Calibrated value
r_CN2.mgt	SCS runoff curve number	-0.2 to 0.2	0.015
v_ESCO.bsn	Soil evaporation compensation factor	0 to 1	0.167
v_CH_K1.sub	Effective hydraulic conductivity in tributary channel alluvium (mm/hr)	0 to 300	0.166
v_CH_K2.rte	Effective hydraulic conductivity in main channel alluvium (mm/hr)	-0.01 to 500	1.748
r_SOL_AWC.sol	Available water capacity of the soil layer (mm H ₂ O/mm soil)	0 to 1	0.095
v_SOL_K.sol	Saturated hydraulic conductivity (mm/hr)	0 to 300	124.5
v_CH_N2.rte	Manning's "n" value for the main channel	0 to 0.3	0.027
v_SURLAG.bsn	Surface runoff lag time (days)	4 to 24	14.58

The p-factor, r-factor, R² and NS values that show the performance of the calibration and validation are presented in **Table 4.3-3**. While calibration attains a p-factor of 0.67 and an r-factor of 0.9, the R² and

NS values reveal room for improvement, standing at 0.33. During validation, the p-factor registers 0.7, and the r-factor 1.69, albeit with R2 at 0.31 and NS at 0.19. It is noteworthy that the model effectively captures base flow but occasionally underestimates peak flows, as observed in the 95PPU graphs for both calibration (Figure 4.3-1) and validation (Figure 4.3-2).

Table 4.3-3: The Calibration And Validation Fitting Metrics.

	Calibration (Daily)	Validation (Daily)
	1999-2002	2006-2008
p-factor	0.67	0.7
r-factor	0.9	1.69
R2	0.33	0.31
NS	0.33	0.19

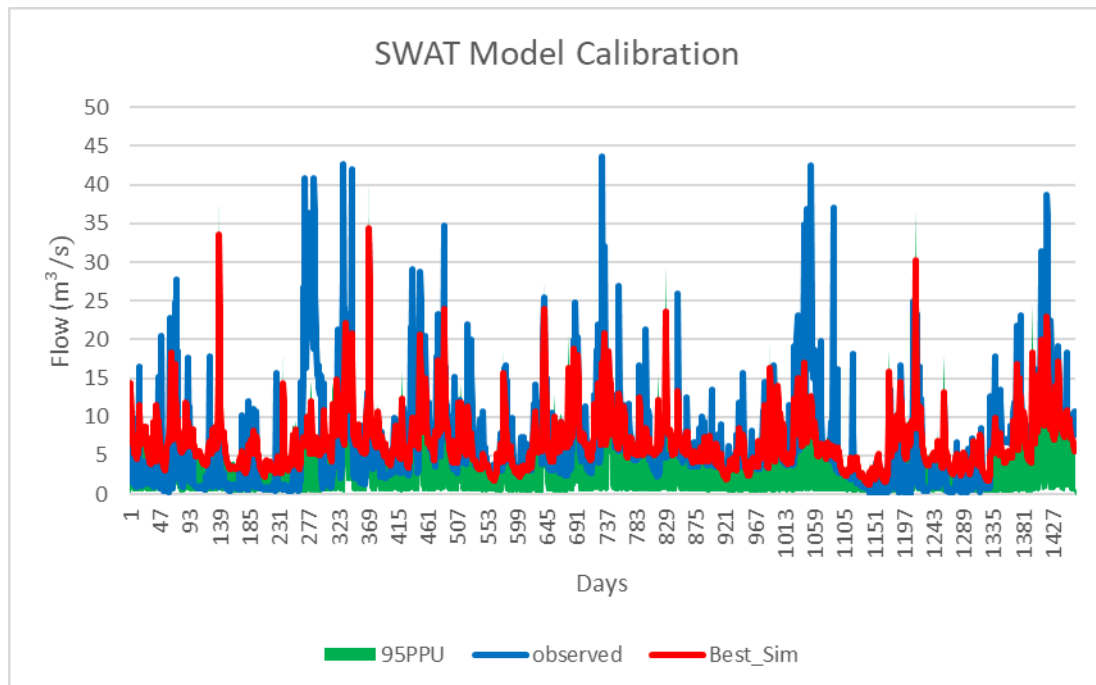


Figure 4.3-1: SWAT Model Calibration 95PPU.

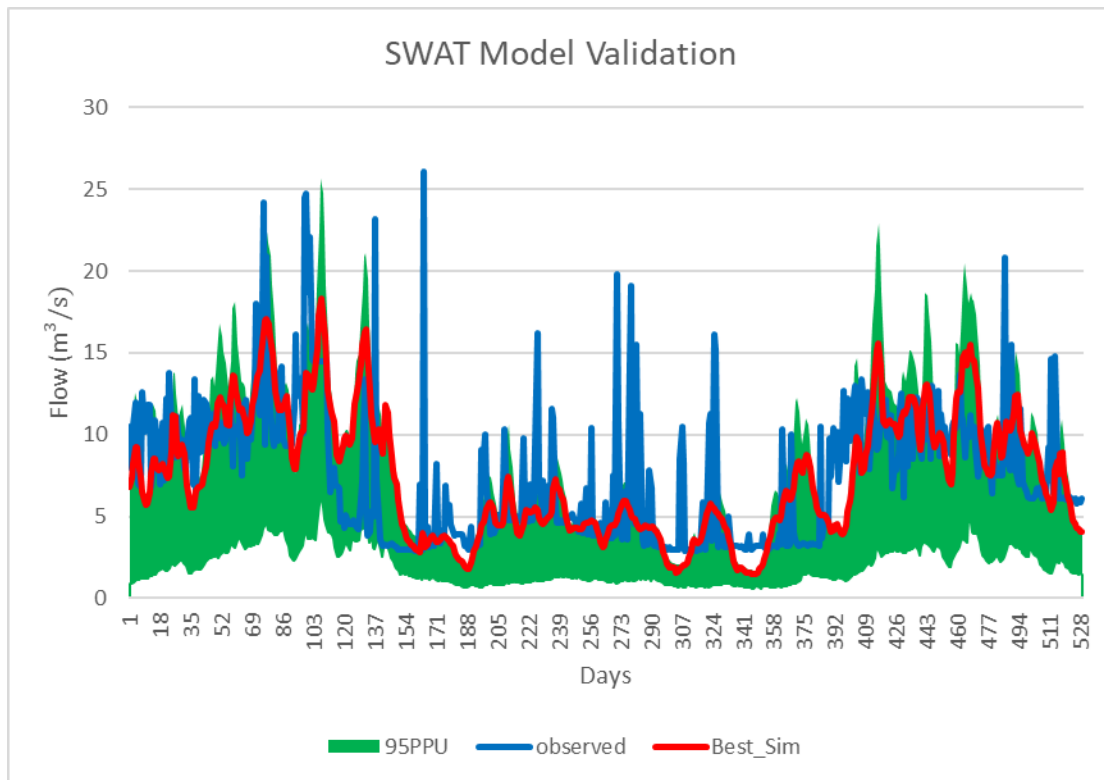


Figure 4.3-2: SWAT Model Validation 95PPU.

4.3.3 IMPACTS OF LAND USE AND LAND COVER AND PRECIPITATION

CHANGES ON SURFACE RUNOFF

Analysing the simulated surface runoff illustrates the intricate interplay of land use and land cover (LULC) and precipitation changes on hydrological dynamics of the Klang River basin. In 1999, the basin averaged 1327.3mm of surface runoff with a range of 437.5mm - 2479.1mm, and notable variations across subbasins, prominently affecting the middle and lower parts of the basin (**Figure 4.3-3**). By 2006, the basin average increased to 1640.6mm, with a range of 619.1mm – 3099.3mm, predominantly driven by urban land cover in

the middle part. In 2017, surface runoff ranged from 536.5mm to 2754.5mm, with a basin average of 1550.8mm, once again highlighting the most affected areas being the urbanised regions in the middle and lower parts of the basin.

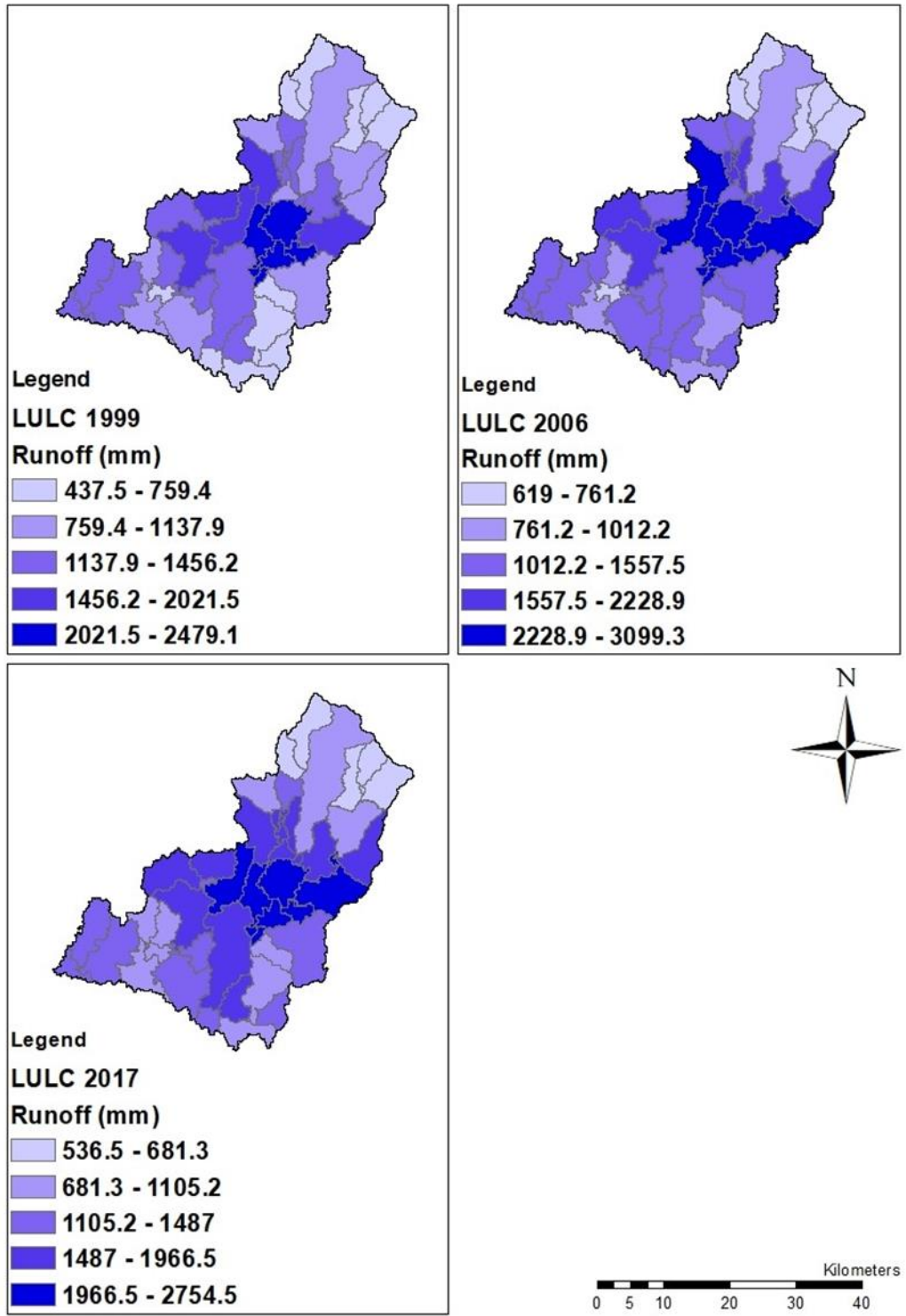


Figure 4.3-3: Surface Runoff For The Land-Use And Land Cover Maps Of 1999, 2006 And 2017.

4.3.3.1 IMPACTS UNDER FUTURE SCENARIOS

Three future LULC and climate change scenarios were considered in the analysis of future runoff. The first scenario with only LULC changing for the year 2030 and climate remaining the same, illustrates an increase in surface runoff by 71.8mm relative to 2017 values, although the basin average dips slightly compared to the 2006 LULC due to higher precipitation amounts in 2006. The simulated surface runoff ranged between 536.6mm to 2754.5mm, with the highest simulated runoff observed in the middle region of the basin as presented in **Figure 4.3-4**.

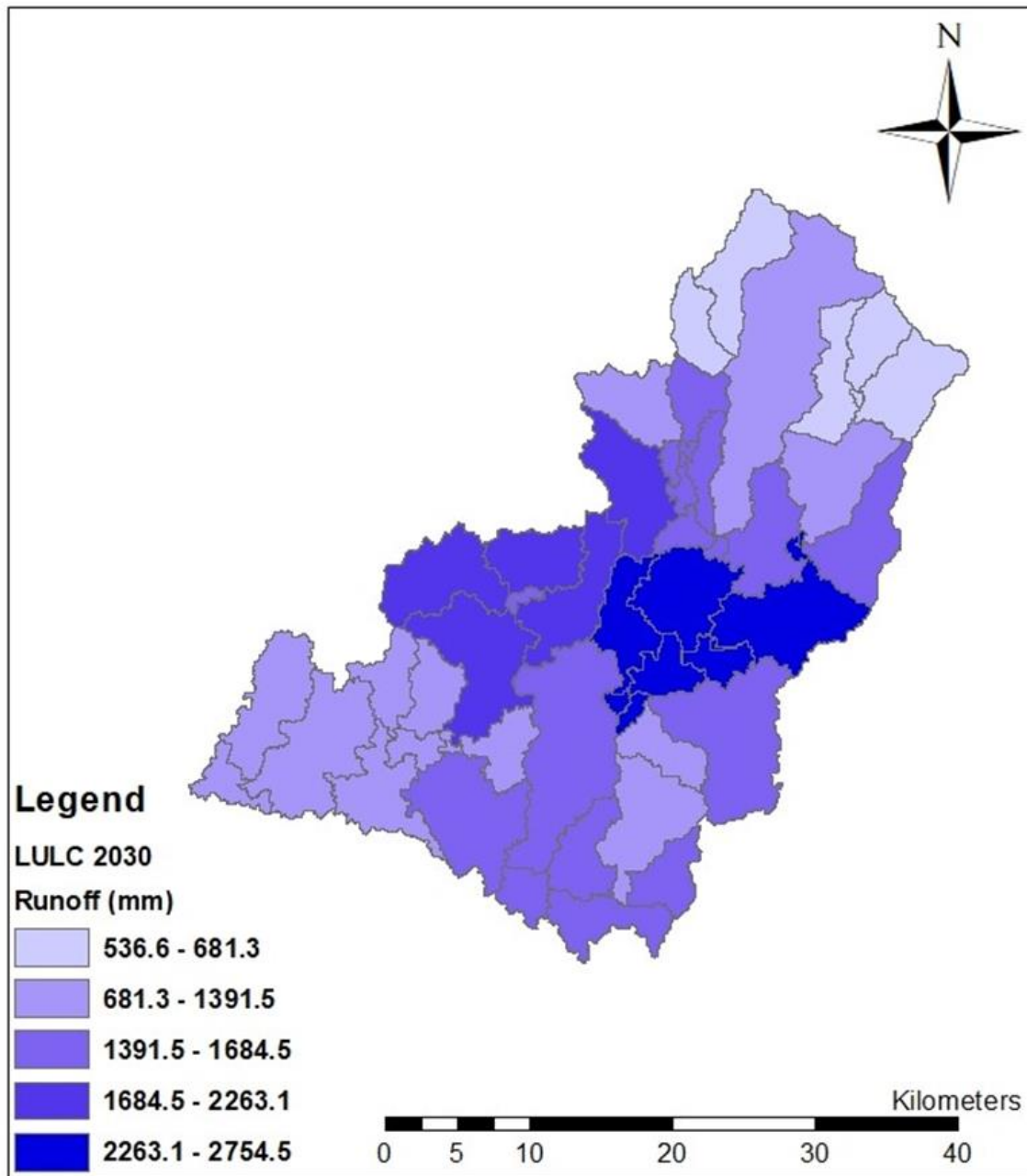


Figure 4.3-4: Simulated Surface Runoff For LULC 2030 Scenario.

Under the second scenario where LULC is unchanged and only climate variables, precipitation and temperature are changed under RCP8.5 and RCP4.5, surface runoff decreased compared to when only LULC is

changed. For the RCP4.5 scenario simulated runoff ranged between 196.5mm to 1053.3mm, with an average basin value of 771.9mm, with the highest runoff occurring in the central regions of the basin. Under the RCP8.5 scenario the simulated surface runoff exhibited a slightly higher range between 239.3mm and 1090.2mm and a slightly higher basin average of 757mm. However, compared to RCP4.5 scenario, most of the subbasins with high runoff are located at the lower regions of the basin, with a few in the middle part of the basin as shown in **Figure 4.3-5**.

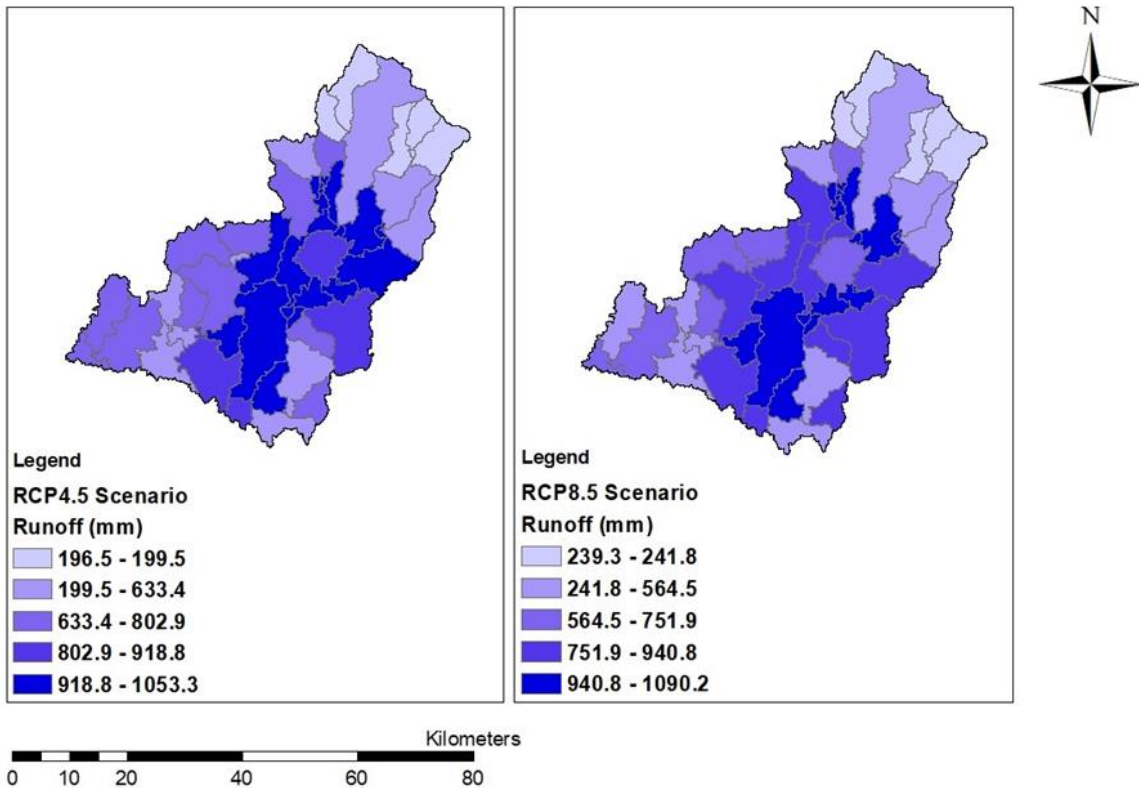


Figure 4.3-5: Simulated Surface Runoff For Climate Change Scenarios RCP4.5 And RCP8.5.

In the third scenario, both LULC and climate change are considered, under two conditions, one where LULC 2030 and climate scenario RCP8.5 is considered and one where LULC 2030 with climate scenario RCP4.5 is considered. The simulated surface runoff under both conditions illustrates a higher range of runoff compared to the scenario when only climate change was considered, but lower range compared to the scenario when LULC was considered. The range of runoff for combined LULC 2030 and RCP4.5 scenario is between 196.5mm to 1053.3mm with a basin average of 860.7mm, and the range of runoff for the combined LULC 2030 and RCP8.5 scenario is between 237.9mm to 1088.2mm, with a basin average of 832.7mm as shown in **Figure 4.3-6**. In both cases the subbasins experiencing the highest runoff are located mostly in the middle region of the basin, some parts of the lower basin and some parts on the east of the basin.

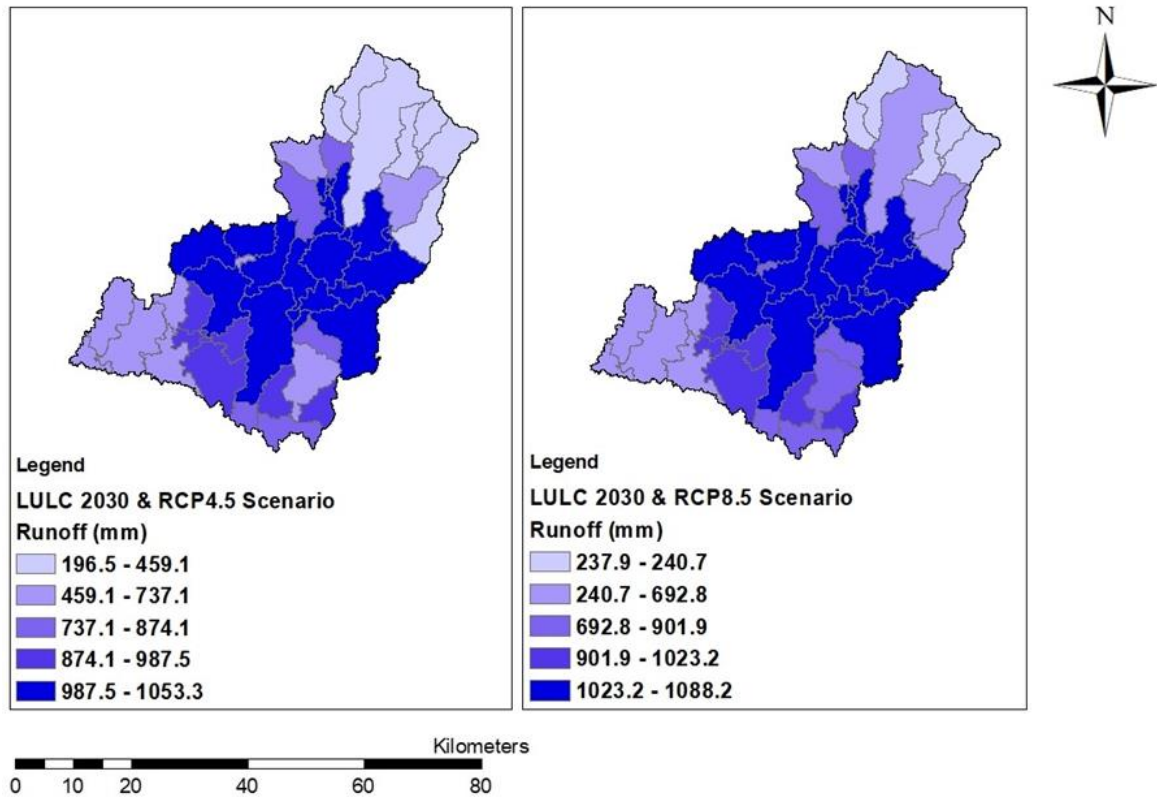


Figure 4.3-6: Simulated Surface Runoff For Combined LULC 2030 And RCP4.5 Scenario, And LULC 2030 And RCP8.5 Scenario.

4.3.4 IMPACTS OF LAND USE AND LAND COVER AND PRECIPITATION

CHANGES ON RIVER DISCHARGE UNDER FUTURE SCENARIOS

River discharge was simulated under both LULC and climate change scenarios at Batu Sentul station. Examining the simulated river discharge across different time periods underscores noteworthy trends. Significant increasing trend was detected under the RCP4.5 scenario and the combined LULC 2030 and RCP4.5 scenario, with a rate of increase of 0.04 m³/s per year during TP1 and TP2 periods. However,

significant trend was not detected for other scenarios as shown in **Table 4.3-4**.

On the other hand, the average annual river discharge illustrates higher discharges for all scenarios during the period (TP3) from 2070 to 2099, compared to TP1 and TP2, with TP1 having the lowest discharges as shown in **Table 4.3-5**. However, all the discharges for all these scenarios are lower than the scenario when only LULC was changed, which exhibited an average annual discharge of 11.5m³/s.

Table 4.3-4: Trend For Simulated River Discharge For Future LULC And Climate Change Scenarios.

Scenarios	TP1 (2010-2039)		TP2 (2040-2069)		TP3 (2070-2099)	
	Test Z	Q	Test Z	Q	Test Z	Q
RCP4.5	2.21*	0.04	1.82+	0.04	0.05	0.00
RCP8.5	0	0.00	1.48	0.03	0.87	0.03
LULC 2030 and RCP4.5	2.21*	0.04	1.96*	0.04	-0.07	0.00
LULC 2030 and RCP8.5	0	0.00	1.48	0.03	0.89	0.02

** if trend at $\alpha = 0.01$ level of significance, * if trend at $\alpha = 0.05$ level of significance, + if trend at $\alpha = 0.1$ level of significance, if the cell is blank, the significance level is greater than 0.1.

Table 4.3-5: Simulated Average Annual River Discharge For Future LULC And Climate Change Scenarios At Sg. Batu Sentul Station.

Scenarios	Average Annual River Discharge (m ³ /s)		
	TP1 (2010-2039)	TP2 (2040-2069)	TP3 (2070-2099)
RCP4.5	9.29	9.73	9.89
RCP8.5	9.35	9.97	10.44
LULC2030 RCP4.5	9.29	9.73	9.88
LULC2030 RCP8.5	9.35	9.97	10.44

4.3.5 DISCUSSION

The SWAT model has been instrumental in simulating surface runoff and river discharge for both historical and future LULC and climate change scenarios. The sensitivity analysis of the hydrological parameters revealed the eight most sensitive parameters in model calibration. Among these, CH_K1, CH_K2, and CH_N1 stood out as the most sensitive parameters. CH_K1 and CH_K2 play a pivotal role in determining the hydraulic conductivity of the main channel and tributaries, thereby influencing the movement of water between the channels and groundwater.

Meanwhile, CH_N1 represents Manning's roughness coefficient for the main channel, affecting water flow characteristics within the channel. The calibration value of 0.027 for CH_N1, reflects the relative uniform and straight nature of the channels, which is common in urbanised watersheds characterised by artificial channels and river channelisation (Chow, 1959). This highlights the impact of urbanisation and land use change on the morphology of the basin, which ultimately affects river discharge.

Model calibration achieved a p-factor of 0.67 and an r-factor of 0.9, indicating a reasonable fit of the model to the observed hydrological processes. It is important to note that the model occasionally

underestimated peak flows, possibly due to a lack of operational and release data for upstream structures like the Batu dam and Batu retention pond, which affect the flow patterns at the observed station. During the model validation, the p-factor improved to 0.7, while the r-factor increased to 1.69, suggesting a more robust performance in capturing the hydrological dynamics. Despite these slight underestimations in peak flows, we can conclude that the model has been effectively calibrated and validated for the study area.

The model is used to analyse the complex interactions between LULC changes and climate variations and their impact on surface runoff and river discharge within the Klang River basin. Surface runoff was initially simulated for the years 1999, 2006, and 2017 to assess the influence of LULC modifications. It was observed that, as urban land cover increased, surface runoff also exhibited a corresponding increase. In particular, the year 2006 recorded the highest average basin runoff, primarily attributed to higher annual precipitation levels during that period.

This is in agreement with the study by Saadatkhan and Kassim, (2017), that analysed the impacts of land use change on flood events in the Hulu Kelang River basin, which covers the Northern and Northeastern parts of the Klang River basin. The study observed that urban and agricultural land contributed to around 50% of runoff volume in 1994 and that this number increased to more than 60% in 2013 as the area of urban and

agricultural land increased, whereas natural forests and secondary forests contributed to only 20% and 15% in 1994 and 2013 respectively.

In a similar study in Kelantan River basin, the agricultural and developed land areas during the period 1988 to 2013, were observed to have resulted in enhanced flood volumes compared to other land use classes (Asmat et al., 2016). This illustrates significant impact of LULC change on surface runoff, where the change from forest to urban and agricultural land increases imperviousness and reduces canopy cover, hence less water is trapped by the canopy and less water is infiltrated by the surface.

Subsequent simulations considering future scenarios with three distinct combinations: changes in LULC only, changes in climate variables only (under RCP4.5 and RCP8.5), and the combined effect of LULC and climate scenarios was carried out. The results illustrated that LULC changes have a significant impact on future surface runoff. Specifically, under the combined influence of LULC changes and climate scenarios, surface runoff levels surpassed those resulting from climate changes alone. This indicates that LULC change is expected to have a higher impact on future hydrological processes than climate change.

In terms of spatial variability, the middle region of the basin, which is predominantly urbanised, consistently experienced the highest surface

runoff throughout the study period. However, under future climate scenarios, some parts of the lower basin began to exhibit increased surface runoff, potentially reflecting shifts in precipitation patterns and the interplay with urban development.

On the other hand, the analysis of river discharge under various future scenarios at the Batu Sentul station revealed the most significant increase in river discharge was observed under the RCP4.5 scenario and the combined LULC 2030 and RCP4.5 scenario during TP1 and TP2 periods. However, these significant trends were not detected in other scenarios. The average annual river discharge for TP3 (2070-2099) was consistently higher across all scenarios, compared to TP1 and TP2, similar to the results presented by Kabiri et al., (2015), where mean annual discharge for the 2080s under A2 scenario increased by 3.4% within the Klang River basin.

However, it's important to indicate that Kabiri et al., (2015) did not consider the potential impact of LULC change in their study, and this study illustrates the importance of LULC change where it showcases changes in LULC have a substantial impact, resulting in higher average annual discharge compared to scenarios where only climate variables were altered. As illustrated under the LULC 2030 scenario with current climate conditions, where the average annual river discharge at Batu Sentul was projected to be 11.15 m³/s, significantly higher than the

discharge under RCP4.5 and the combined LULC 2030 and RCP4.5 scenarios during TP1, which registered average annual discharges of 9.29 m³/s.

Overall, the outcome of the study illustrates the significant correlation with LULC and climate change with changes in hydrological processes. And the pivotal role both LULC change and the changes in precipitation play in influencing hydrological processes. Although LULC change has a more significant impact on hydrological processes, it is important to consider both LULC and climate change in planning and policy making decisions.

4.4 SUMMARY OF RESULTS AND DISCUSSION

The summary of all the results and discussion is presented in **Table 4.4-1**.

Table 4.4-1: Summary Of Results And Discussion.

Objective	Results	Discussion
To analyse spatio-temporal trends in land-use and land cover.	<ul style="list-style-type: none"> Increase in Built-up by 147.5 km² (11.8%) and decrease in agricultural by 36.71 km² (2.9%), and natural vegetation by 73.4 km² (5.9%) from 1999 - 2017. Projected increase in built-up land by 120.6 km² (9.7%), decrease in agricultural by 9.11 km² (0.7%) and natural vegetation by 109.5 km² (8.7%) from 2017 to 2030. 	<ul style="list-style-type: none"> High magnitude of urban expansion in the period 1999 to 2017 at the expense of natural vegetation. Urbanisation increased at a rate of 0.6% per year in the period 1999 to 2017. It is expected urban land use to continue to expand until 2030 with expansion taking place in protected forest reserves and urban green spaces.

		<ul style="list-style-type: none"> • Accessibility and proximity to urban areas, are major factors that contribute to this expansion. • This Urban expansion can have significant impact on hydrological processes in Klang River basin.
<p>To analyse spatio-temporal trends in Precipitation, and temperature.</p>	<ul style="list-style-type: none"> • Mean annual precipitation highest in urban areas ranging from 3010mm to 3368mm. • Significant trend in mean annual precipitation detected. • Increasing trend in precipitation intensity and frequency observed over urban areas. • Seasonal trend is similar to annual trend. • Increasing trend also detected for land surface temperature (LST) over urban areas. • Maximum LST increased by 10.1°C and minimum temperatures increasing by 2.6°C in the period 1999 to 2017. • Increasing trend in precipitation and temperature predicted under future scenarios. • Significant increasing trend in river discharged was detected most at station Jambatan Sulaiman. 	<ul style="list-style-type: none"> • Precipitation showed increasing trend, with urban areas experiencing the most significant increases. • Central urban areas exhibit the most intense and frequent precipitation. • Temperature trends in the Klang River basin align with broader global warming patterns, with urban areas having higher land surface temperatures. • NEM period has the highest influence on annual precipitation. • The analysis of river discharge trends at Batu Sentul and Jambatan Sulaiman stations mirrors precipitation and temperature trends, with an overall increasing trend. • Significant trends are observed at Jambatan Sulaiman, emphasising the impacts of LULC and precipitation changes on river discharge.
<p>To develop an integrated spatio-temporal hydrological model, with land use and climate models.</p>	<ul style="list-style-type: none"> • 8 parameters identified as the most sensitive. • CH_K1, CH_K2, and CH_N2 were the most sensitive parameters. • Calibration with p-factor of 0.67 and r-factor of 0.9, with R2 and NS of 0.33. • Validation with p-factor of 0.7 and r-factor of 1.69, with R2 of 0.31 and NS of 0.19. 	<ul style="list-style-type: none"> • CH_K1, CH_K2 and CH_N2, illustrate the movement of water in main channel and tributaries, showcasing the impact of urbanisation on morphology of the basin. • The model underestimated some peak flows. • Calibration and validation were satisfactory.

<p>To measure quantitative effects of both LULC and precipitation changes on surface runoff and river discharge.</p>	<ul style="list-style-type: none"> • Increase in surface runoff from 1999 to 2017. • In the year 1999 average basin runoff at 1327.3mm, year 2006 at 1640.6mm, year 2017 at 1550.8mm. • Under future scenario for only LULC change, runoff increased by 71.8mm relative to 2017 value. • Under RCP 4.5 and RCP8.5 only scenarios runoff is less, compared to LULC change only scenario, with average basin runoff at 771.9mm and 757mm respectively. • Under combined LULC change and RCP climate change scenarios, runoff is higher compared to only RCP scenarios but less than only LULC change scenario at 860.7mm, and 832.7mm. • Significant river discharge trend detected during TP1 period under RCP4.5 only scenario and under combined RCP4.5 and LULC 2030 scenario. • Highest average annual discharge during TP3 period. • Highest annual discharge detected when only LULC 2030 scenario used at 11.15 m³/s. 	<ul style="list-style-type: none"> • Model was able to successfully integrate LULC change and climate change variables. • With increase in urbanisation surface runoff also increased in the period 1999 to 2017. • The year 2006 had the highest surface runoff, partly due to high precipitation amount in that year. • Similar findings observed by Saadatkah and Kassim, (2017). • Under future scenarios, LULC changes have higher significant impact on future surface runoff. • Spatially the middle region of the basin which are highly urbanised, experience higher runoff. • Significant increase in river discharge was observed under the RCP4.5 and the combined LULC 2030 and RCP4.5 scenarios during TP1 and TP2 periods. • Highest river discharge was observed under the LULC 2030 only scenario, indicating the significant of LULC change on river discharge.
--	--	---

CHAPTER 5: CONCLUSION

This chapter presents the conclusion of the study on the impacts of spatio-temporal changes in land use and land cover, and precipitation on surface runoff and river discharge in the Klang River basin.

5.1 CONCLUSION

This study was conducted with the main aim of assessing the combined effects of land use and land cover change and change in precipitation on surface runoff and river discharge within the Klang River basin, with a focus on projecting these effects under future scenarios. To achieve this aim, several specific objectives were outlined.

The first objective of the study was to analyse the spatial and temporal trends in LULC change, precipitation, and temperature. To achieve this objective, a combination of methods was utilised, including maximum likelihood algorithm for land use classification, and the Decision Forest – Markov Chain model for land use change modelling. Additionally historical data was examined to detect trends in precipitation and temperature, using the Mann-Kendall and Sen’s slope statistics.

The findings revealed significant trends detected in land use and land cover, particularly an increase in urbanisation, which was concentrated in the central part of the Klang River basin in the period 1999 to 2017. These trends are consistent with previous studies and highlight the

urban expansion of Kuala Lumpur and its surrounding areas. And due to the urban expansion, natural vegetation and other land use classes have been on the decline. The future scenarios show, these trends to continue, with urban areas expanding in the remaining urban green spaces and forests.

As for precipitation, trends show an upwards trajectory in the basin, particularly in urban areas. Increasing trend in precipitation intensity and frequency was detected among urban stations, although Simple Day Intensity Index (SDII) exhibited decreasing trend in most of the stations. Similarly, increasing trends were detected in seasonal precipitation, with the most significant increasing trends detected during the NEM period. Temperature patterns also exhibited similarities to precipitation, with higher surface temperatures observed in urban areas, potentially contributing to urban-induced precipitation.

The assessment of precipitation and temperature under future climate scenarios illustrates an increasing trend in both precipitation and temperature for the period 2006 to 2099. Overall, we can conclude that increasing trend in both LULC and climate variables is detected within Klang River basin, with variability in spatial trend, and under future scenarios it is expected that these trends will continue.

The second objective of this study involves the development of an integrated hydrological model that combines land use and climate models, to assess the impacts of LULC and climate changes on hydrological processes. The SWAT model was utilised to achieve this objective. The calibration and validation of the SWAT model demonstrates its effectiveness and reliability in modelling hydrological processes in the Klang River basin. However, the model can be improved to better capture peak flow with additional operational and release data for upstream structures.

The final objective of the study aimed to measure the quantitative effects of both LULC and precipitation changes on surface runoff and river discharge. The results showed that LULC change has a significant impact on surface runoff and river discharge, particularly urban land use. The increase in urban land use has resulted in increasing impervious surfaces, reduction in infiltration and hence increase in surface runoff.

Notably, the study illustrates that LULC change has a higher impact on hydrological processes, than changes in climate variables alone. Although, the combined impact of LULC change and changes climate scenarios resulted in high surface runoff levels, emphasising the importance of considering both factors in planning and policy-making decisions.

Overall, the results of this study illustrate the significance of understanding the impacts of LULC change and changes in climate variables on the hydrological processes of the Klang River basin. The combined impact of urbanisation and changes in precipitation properties can have a great effect on surface runoff and river discharge, potentially increasing the risk of flooding in the Klang River basin.

This research has contributed to the body of knowledge regarding the dynamic relationship between land use, climate variables and hydrological processes. Highlighting the importance of sustainable land use practices and urban planning in the face of current urbanisation and climate change. The outcomes of this study can better inform policymakers and stakeholders in making decisions that ensure the resilience and sustainability of the Klang River basin in the future.

5.2 STUDY LIMITATIONS

While this study contributes valuable insights into the combined impacts of LULC change and changes in precipitation on hydrological processes in the Klang River basin, it is essential to acknowledge the limitations of the study.

Data limitations were a challenge faced in the study, where availability and quality of the input data for the hydrological model and runoff data for model calibration and validation was an issue. The lack of data for

some of the weather parameters, like temperature, humidity, wind speed and solar radiation added further uncertainty to the model. Secondly gaps and missing values in the data added further limitations to the study. This is a common limitations within hydrological studies, as stated in a review of SWAT model studies in Southeast Asia by Tan *et al.*, (2019), which revealed one of the major limitations most hydrological studies in Southeast Asia face is poor data reliability and availability.

Another limitation the study faced is the limitation of the models used. The SWAT model has limited options for treatment of artificial pathways (sewers, storm water systems, channels etc.) and since urbanised watersheds are highly channelised and have many artificial pathways, it is difficult to incorporate some of these aspects of the urban watershed in the model, which increases the model uncertainty.

5.3 RECOMMENDATIONS

5.3.1 RECOMMENDATIONS FOR FUTURE RESEARCH

Future research could consider integrating socio-economic variables in LULC change modelling, such as population growth, economic development, and policy changes. Understanding how these factors influence land use decisions can help to improve model accuracy.

Future studies could also integrate more sources of hydro-climatic data, to reduce the gap and missing values of the data and improve the quality of input data for modelling. These sources of data include weather radar, climate model outputs and satellite data.

Lastly, future research could utilise and integrate urban hydrological models with other hydrological models, for watersheds that are highly urbanised. This can improve the accuracy of the outputs by considering the urban hydrological infrastructure. Examples of urban hydrological models include SWMM, MIKE Urban, and URBS-MO.

5.3.2 RECOMMENDATIONS FOR POLICY MAKERS AND STAKEHOLDERS

Policy makers should consider the long-term impacts of urbanisation on LULC and hydrological processes and prioritise sustainable urban planning. Emphasis should be given to preserving urban green spaces, forests, and natural vegetation to mitigate the adverse effects of urban sprawl.

Secondly, policy makers and stakeholders should promote and prioritise investment in green infrastructure, such as green roofs, urban forest, and permeable surfaces. Green infrastructure can help improve water retention, infiltration and reduce surface runoff.

Lastly, policy makers and stakeholders should incorporate climate change into decision-making and policy development. This can be done

through the implementation of more climate resistant infrastructure. Such as, designing drainage systems capable of handling more intense rainfall and integrating climate adaptation strategies into urban development plans.

References

- Abas, A. A. and Hashim, M. (2014) 'Change detection of runoff-urban growth relationship in urbanised watershed', *IOP Conference Series: Earth and Environmental Science*, 18(1), p. 012040. doi: 10.1088/1755-1315/18/1/012040.
- Abbaspour, K. C., Johnson, C. A. and van Genuchten, M. T. (2004) 'Estimating Uncertain Flow and Transport Parameters Using a Sequential Uncertainty Fitting Procedure', *Vadose Zone Journal*, 3(4), pp. 1340–1352. doi: 10.2136/vzj2004.1340.
- Abbaspour, K. C., Yang, J., Maximov, I., Siber, R., Bogner, K., Mieleitner, J., Zobrist, J. and Srinivasan, R. (2007) 'Modelling hydrology and water quality in the pre-alpine/alpine Thur watershed using SWAT', *Journal of Hydrology*, 333(2–4), pp. 413–430. doi: 10.1016/j.jhydrol.2006.09.014.
- Abbaspour, K. C. (2012) 'Swat-Cup2: SWAT Calibration and Uncertainty Programs Manual Version 2, Department of Systems Analysis, Integrated Assessment and Modelling (SIAM) Eawag', *Swiss Federal Institute of Aquatic Science and Technology, Duebendorf, Switzerland. 106 p., Swiss Federal Institute of Aquatic Science and Technology. Duebendorf, Switzerland.*
- Abbaspour, K. C., Rouholahnejad, E., Vaghefi, S., Srinivasan, R., Yang, H. and Kløve, B. (2015) 'A continental-scale hydrology and water quality model for Europe: Calibration and uncertainty of a high-resolution large-scale SWAT model', *Journal of Hydrology*, 524, pp. 733–752. doi: 10.1016/j.jhydrol.2015.03.027.
- Abbaspour, K. C., Vaghefi, S. A. and Srinivasan, R. (2017) 'A guideline for successful calibration and uncertainty analysis for soil and water assessment: A review of papers from the 2016 international SWAT conference', *Water*

(Switzerland). doi: 10.3390/w10010006.

- Abbaspour, K. C., Vaghefi, S. A., Yang, H. and Srinivasan, R. (2019) 'Global soil, landuse, evapotranspiration, historical and future weather databases for SWAT Applications', *Scientific Data*, 6(1), pp. 1–11. doi: 10.1038/s41597-019-0282-4.
- Abdulkareem, J. H., Pradhan, B., Sulaiman, W. N. A. and Jamil, N. R. (2018) 'Review of studies on hydrological modelling in Malaysia', *Modeling Earth Systems and Environment*, pp. 1577–1605. doi: 10.1007/s40808-018-0509-y.
- Abdulkareem, J. H., Pradhan, B., Sulaiman, W. N. A. and Jamil, N. R. (2019) 'Long-term runoff dynamics assessment measured through land use/cover (LULC) changes in a tropical complex catchment', *Environment Systems and Decisions*, 39(1), 16–33. <https://doi.org/10.1007/s10669-018-9696-3>.
- Abdullah, S. A. and Hezri, A. A. (2008) 'From forest landscape to agricultural landscape in the developing tropical country of Malaysia: Pattern, process, and their significance on policy', *Environmental Management*, 42(5), pp. 907–917. doi: 10.1007/s00267-008-9178-3.
- Aburas, M. M., Abdullah, S. H., Ramli, M. F., Ash'aari, Z. H. and Ahamad, M. S. S. (2018) 'Simulating and monitoring future land-use trends using CA-Markov and LCM models', *IOP Conference Series: Earth and Environmental Science*, 169(1), p. 012050. doi: 10.1088/1755-1315/169/1/012050.
- Adnan, N. A. and Atkinson, P. M. (2018) 'Disentangling the effects of long-term changes in precipitation and land use on hydrological response in a monsoonal catchment', *Journal of Flood Risk Management*, 11, pp. S1063–S1077. doi: 10.1111/jfr3.12294.
- Agarwal, C., Green, G. M., Grove, J. M., Evans, T. P. and Schweik, C. M. (2002) 'A Review and Assessment of Land-Use Change Models: Dynamics of Space, Time, and Human Choice', *Apollo The International Magazine Of Art And*

Antiques, p. 62. Available at:
<http://citeseerx.ist.psu.edu/viewdoc/download?doi=10.1.1.86.2775&rep=rep1&type=pdf>.

- Aisyah, A., Shahrul, A., Zulfahmie, M., Sharifah Mastura, S. and Mokhtar, J. (2015) 'DEFORESTATION ANALYSIS IN SELANGOR, MALAYSIA BETWEEN 1989 AND 2011', *Journal of Tropical Forest Science*, 27(1), pp. 3–12.
- Ajami, H. (2021) *Geohydrology: Global Hydrological Cycle*. 2nd edn, *Encyclopedia of Geology*. 2nd edn. Edited by D. Alderton and S. A. Elias. Academic Press. doi: 10.1016/B978-0-12-409548-9.12387-5.
- Ajmal, M., Moon, G. woo, Ahn, J. hyun and Kim, T. woong (2015) 'Investigation of SCS-CN and its inspired modified models for runoff estimation in South Korean watersheds', *Journal of Hydro-Environment Research*, 9(4), pp. 592–603. doi: 10.1016/j.jher.2014.11.003.
- Alaghmand, S., Abdullah, R., Abustan, I. and Vosoogh B. (2012) 'The Effects of Rainfall Event and Land Use Characteristics on River Basin Hydrological Response: A Case of Sg. Kayu Ara, Malaysia', *Pertanika Journal of Science & Technology*, 20(2), 205–219.
- Al-sharif, A. A. A. and Pradhan, B. (2014) 'Monitoring and predicting land use change in Tripoli Metropolitan City using an integrated Markov chain and cellular automata models in GIS', *Arabian Journal of Geosciences*, 7(10), pp. 4291–4301. doi: 10.1007/s12517-013-1119-7.
- Al-sharif, A. A. A. and Pradhan, B. (2015) 'A novel approach for predicting the spatial patterns of urban expansion by combining the chi-squared automatic integration detection decision tree, Markov chain and cellular automata models in GIS', *Geocarto International*, 30(8), pp. 858–881. doi: 10.1080/10106049.2014.997308.
- Alkama, R. and Cescatti, A. (2016) 'Biophysical climate impacts of recent

changes in global forest cover', *Science*, 351(6273), pp. 600–604. doi: 10.1126/science.aad7270.

- Allen, M. R., Dube, O. P., Solecki, W., Aragón-Durand, F., Cramer, W., Humphreys, S., Kainuma, M., Kala, J., Mahowald, N., Mulugetta, Y., Perez, R., M. Wairiu, A. and Zickfeld, K. (2018) 'Framing and Context. In: Global Warming of 1.5°C. An IPCC Special Report on the impacts of global warming of 1.5°C above pre-industrial levels and related global greenhouse gas emission pathways, in the context of strengthening the global response to the', [Masson-Delmotte, V., P.Zhai, H.-O. Pörtner, D. Roberts, J. Skea, P.R. Shukla, A.Pirani, W. Moufouma-Okia, C. Péan, R. Pidcock, S. Connors, J.B.R. Matthews, Y. Chen, X.Zhou, M.I. Gomis, E. Lonnoy, T. Maycock, M.Tignor, and T. Waterfield (eds.)]. *In Press*. doi: 10.5194/nhess-16-2189-2016.
- Almdhun, H. M., Mallak, S. K., Aburas, M. M., Md Said, M. A. and Ghadiri, S. M. (2018) 'Measuring and predicting urban growth patterns and trends in Putrajaya, Malaysia', *IOP Conference Series: Earth and Environmental Science*, 169(1). doi: 10.1088/1755-1315/169/1/012114.
- Amanollahi, J., Tzani, C., Ramli, M. F. and Abdullah, A. M. (2016) 'Urban heat evolution in a tropical area utilizing Landsat imagery', *Atmospheric Research*, 167, pp. 175–182. doi: 10.1016/J.ATMOSRES.2015.07.019.
- Amin, I. M. Z. bin M., Ercan, A., Ishida, K., Kavvas, M. L., Chen, Z. Q. and Jang, S. H. (2019) 'Impacts of climate change on the hydro-climate of peninsular Malaysia', *Water*, 11(9). <https://doi.org/10.3390/w11091798>.
- Amirabadizadeh, M., Huang, Y. F. and Lee, T. S. (2015) 'Recent Trends in Temperature and Precipitation in the Langat River Basin, Malaysia', *Advances in Meteorology*, 2015, pp. 1–16. doi: 10.1155/2015/579437.
- Amisigo, B. A., McCluskey, A. and Swanson, R. (2015) 'Modeling impact of climate change on water resources and agriculture demand in the Volta Basin

and other basin systems in Ghana', *Sustainability*, 7(6), 6957–6975.
<https://doi.org/10.3390/su7066957>.

- Apollonio, C., Balacco, G., Novelli, A., Tarantino, E., and Piccinni, A. F. (2016) 'Land use change impact on flooding areas: The case study of Cervaro Basin (Italy)', *Sustainability (Switzerland)*, 8(10), 996–1014.
<https://doi.org/10.3390/su8100996>
- Arneth, A. and et. al (2019) 'Framing and Context. in Climate Change and Land: An IPCC Special Report on Climate Change, Desertification, Land Degradation, Sustainable Land Management, Food Security, and Greenhouse Gas Fluxes in Terrestrial Ecosystems', (eds. Shukla, P. R. et al.) Ch. 1.
- Arnold, J. G., Allen, P. M. and Bernhardt, G. (1993) 'A comprehensive surface-groundwater flow model', *Journal of Hydrology*, 142(1–4), pp. 47–69. doi: 10.1016/0022-1694(93)90004-S.
- Arnold, J. G., Srinivasan, R., Muttiah, R. S. and Williams, J. R. (1998) 'Large area hydrologic modeling and assessment part I: Model development', *Journal of the American Water Resources Association*, 34(1), pp. 73–89. doi: 10.1111/j.1752-1688.1998.tb05961.x.
- Arnold, J. G., Moriasi, D. N., Gassman, P. W., Abbaspour, K. C., White, M. J., Srinivasan, R., Santhi, C., Harmel, R. D., Griensven, A. van, Liew, M. W. Van, Kannan, N. and Jha, M. K. (2012) 'SWAT: Model Use, Calibration, and Validation', *Transactions of the ASABE*, 55(4), pp. 1491–1508. doi: 10.13031/2013.42256.
- Asmat, A., Mansor, S., Saadatkah, N., Adnan, N. A. and Khuzaimah, Z. (2016) 'Land Use Change Effects on Extreme Flood in the Kelantan Basin Using Hydrological Model', in *ISFRAM 2015*. Springer, Singapore, pp. 221–236. doi: 10.1007/978-981-10-0500-8_18.
- Asnawi, N. H. and Choy, L. K. (2016) 'Analysis of land use and land cover

changes in Gombak, Selangor using remote sensing data', *Sains Malaysiana*, 45(12), pp. 1869–1877. doi: 10.17576/JSM-2016-4512-11.

- Avdan, U. and Jovanovska, G. (2016) 'Algorithm for automated mapping of land surface temperature using LANDSAT 8 satellite data', *Journal of Sensors*, 2016. doi: 10.1155/2016/1480307.
- Azari, M., Billa, L. and Chan, A. (2020) 'Modelling of Land-Use/Land-Cover Change and Its Impact on Local Climate of Klang River Basin', *IOP Conference Series: Earth and Environmental Science*, 489(1). doi: 10.1088/1755-1315/489/1/012017.
- Baiya, B. and Hashim, M. (2020) 'Modelling Catchment Land Use Changes against Water Yield with Satellite Multi-Temporal Data', *IOP Conference Series: Earth and Environmental Science*, 540(1), p. 12060. <https://doi.org/10.1088/1755-1315/540/1/012060>.
- Bakar, M. A. A., Ariff, N. M., Jemain, A. A. and Nadzir, M. S. M. (2020) 'Cluster Analysis of Hourly Rainfalls Using Storm Indices in Peninsular Malaysia', *Journal of Hydrologic Engineering*, 25(7), pp. 1–11. doi: 10.1061/(ASCE)HE.1943-5584.0001942.
- Balamurugan, G. (1991) 'Sediment balance and delivery in a humid tropical urban river basin: The Kelang River, Malaysia', *Catena*, 18(3–4), pp. 271–287. doi: 10.1016/0341-8162(91)90026-T.
- Bari, M. A., Alam, L., Alam, M. M., Rahman, L. F. and Pereira, J. J. (2021) 'Estimation of losses and damages caused by flash floods in the commercial area of Kajang, Selangor, Malaysia', *Arabian Journal of Geosciences*, 14(3), p. 195. doi: 10.1007/s12517-021-06503-x.
- Bell, V. *et al.* (2020) 'Flood Impacts across Scales: towards an integrated multi-scale approach for Malaysia', in *4th European Conference on Flood Risk Management*. doi: 10.3311/floodrisk2020.9.6.

- Betts, A. K., Chan, D. Z. and Desjardins, R. L. (2019) 'Near-Surface Biases in ERA5 Over the Canadian Prairies', *Frontiers in Environmental Science*, 7. <https://doi.org/10.3389/fenvs.2019.00129>.
- Beven, K. (2012) *Rainfall-Runoff Modelling: The Primer, 2nd Edition*, Wiley-Blackwell. Wiley-Blackwell. Available at: <https://www.wiley.com/en-gb/Rainfall+Runoff+Modelling%3A+The+Primer%2C+2nd+Edition-p-9780470714591> (Accessed: 11 April 2022).
- Bhatta, B., Shrestha, S., Shrestha, P. K. and Talchabhadel, R. (2019) 'Evaluation and application of a SWAT model to assess the climate change impact on the hydrology of the Himalayan River Basin', *Catena*, 181(October 2018), p. 104082. doi: 10.1016/j.catena.2019.104082.
- Bhuiyan, T. R., Hasan Reza, M. I., Choy, E. A. and Pereira, J. J. (2018) 'Direct impact of flash floods in Kuala Lumpur City: Secondary data-based analysis', *ASM Science Journal*, 11(3), pp. 145–157.
- Blunden, J., Arndt, D. S. and Dunn, R. J. H. (2020) 'State of the Climate in 2019', *Bulletin of the American Meteorological Society*. American Meteorological Society, p. SI-S429. doi: 10.1175/2020BAMSSTATEOFTHECLIMATE.1.
- Bonneau, J., Fletcher, T. D., Costelloe, J. F. and Burns, M. J. (2017) 'Stormwater infiltration and the "urban karst" – A review', *Journal of Hydrology*. Elsevier, pp. 141–150. doi: 10.1016/j.jhydrol.2017.06.043.
- Boori, M. S., Netzband, M., Choudhary, K. and Voženílek, V. (2015) 'Monitoring and modeling of urban sprawl through remote sensing and GIS in Kuala Lumpur, Malaysia', *Ecological Processes*, 4(1), pp. 1–10. doi: 10.1186/s13717-015-0040-2.
- Borrelli, P., Robinson, D. A., Fleischer, L. R., Lugato, E., Ballabio, C., Alewell, C., Meusburger, K., Modugno, S., Schütt, B., Ferro, V., Bagarello, V., Oost, K. Van, Montanarella, L., & Panagos, P. (2017) 'An assessment of the global

impact of 21st century land use change on soil erosion', *Nature Communications*, 8(1), pp. 1–13. <https://doi.org/10.1038/s41467-017-02142-7>.

- Boulet, G., Jarlan, L., Oliosio, A. and Nieto, H. (2020) 'Evapotranspiration in the Mediterranean region', in *Water Resources in the Mediterranean Region*. Elsevier, pp. 23–49. doi: 10.1016/B978-0-12-818086-0.00002-9.
- Bradshaw, C. J. A., Sodhi, N. S., Peh, K. S. H. and Brook, B. W. (2007) 'Global evidence that deforestation amplifies flood risk and severity in the developing world', *Global Change Biology*, 13(11), pp. 2379–2395. doi: 10.1111/j.1365-2486.2007.01446.x.
- Briak, H., Mrabet, R., Moussadek, R. and Aboumaria, K. (2019) 'Use of a calibrated SWAT model to evaluate the effects of agricultural BMPs on sediments of the Kalaya river basin (North of Morocco)', *International Soil and Water Conservation Research*, 7(2), pp. 176–183. doi: 10.1016/j.iswcr.2019.02.002.
- Brirhet, H. and Benaabidate, L. (2016) 'Comparison Of Two Hydrological Models (Lumped And Distributed) Over A Pilot Area Of The Issen Watershed In The Souss Basin, Morocco', *European Scientific Journal, ESJ*, 12(18), p. 347. doi: 10.19044/esj.2016.v12n18p347.
- Bruch, S., Pfeifer J. and Guillame-bert, M. (2020) 'Learning Representations for Axis-Aligned Decision Forests through Input Perturbation', *arXiv:2007.14761 [cs.LG]*.
- Calijuri, M.L., Castro, J.S., Costa, L.S., Assemany, P.P. and Alves, J.E.M. (2015) 'Impact of land use/land cover changes on water quality and hydrological behavior of an agricultural subwatershed', *Environmental Earth Sciences*, 74, pp. 5373–5382. doi.org/10.1007/s12665-015-4550-0.
- Chao, Z., Wang, L., Che, M. and Hou, S. (2020) 'Effects of Different

Urbanization Levels on Land Surface Temperature Change: Taking Tokyo and Shanghai for Example', *Remote Sensing*, 12(12), p. 2022. doi: 10.3390/rs12122022.

- Chen, Y., Marek, G. W., Marek, T. H., Porter, D. O., Brauer, D. K. and Srinivasan, R. (2021) 'Simulating the effects of agricultural production practices on water conservation and crop yields using an improved SWAT model in the Texas High Plains, USA', *Agricultural Water Management*, 244(August 2020), p. 106574. doi: 10.1016/j.agwat.2020.106574.
- Choi, G., Collins, D., Ren, G., Trewin, B., Baldi, M., Fukuda, Y., Afzaal, M., Pianmana, T., Gomboluudev, P., Huong, P. T. T., Lias, N., Kwon, W. T., Boo, K. O., Cha, Y. M. and Zhou, Y. (2009) 'Changes in means and extreme events of temperature and precipitation in the Asia-Pacific Network region, 1955-2007', *International Journal of Climatology*, 29(13), pp. 1906–1925. doi: 10.1002/joc.1979.
- Chow, V. Te (1959) 'Open-channel hydraulics', *New York: McGraw-Hill*.
- Colkesen, I. and Kavzoglu, T. (2019) 'Comparative Evaluation of Decision-Forest Algorithms in Object-Based Land Use and Land Cover Mapping', 499-517. doi: 10.1016/B978-0-12-815226-3.00023-5.
- Crochemore, L., Isberg, K., Pimentel, R., Pineda, L., Hasan, A. and Arheimer, B. (2019) 'Lessons learnt from checking the quality of openly accessible river flow data worldwide', *Hydrological Sciences Journal*, 65(5), pp. 699–711. doi: 10.1080/02626667.2019.1659509.
- Deng, X., Zhao, C. and Yan, H. (2013) 'Systematic modeling of impacts of land use and land cover changes on regional climate: A review', *Advances in Meteorology*, 2013. doi: 10.1155/2013/317678.
- Depetris, P. J. (2021) 'The Importance of Monitoring River Water Discharge', *Frontiers in Water*, 3. <https://doi.org/10.3389/frwa.2021.745912>.

- Devia, G. K., Ganasri, B. P. and Dwarakish, G. S. (2015) 'A Review on Hydrological Models', *Aquatic Procedia*, 4, pp. 1001–1007. doi: 10.1016/j.aqpro.2015.02.126.
- Dhanesh, Y., Bindhu, V. M., Senent-Aparicio, J., Brighenti, T. M., Ayana, E., Smitha, P. S., Fei, C. and Srinivasan, R. (2020) 'A comparative evaluation of the performance of CHIRPS and CFSR data for different climate zones using the SWAT model', *Remote Sensing*, 12(18), p. 3088. doi: 10.3390/RS12183088.
- Díaz, S. et al. (2019) *Summary for policymakers of the global assessment report on biodiversity and ecosystem services of the Intergovernmental Science-Policy Platform on Biodiversity and Ecosystem Services, Secretariat of the Intergovernmental Science-Policy Platform on Biodiversity and Ecosystem Services*. Bonn, Germany. Available at: https://www.ipbes.net/sites/default/files/downloads/spm_unedited_advance_for_posting_htn.pdfhttp://www.scielo.br/scielo.php?script=sci_arttext&pid=S1676-06032016000100010&lng=en&tlng=en.
- Döll, P. and Schmied, H. M. (2012) 'How is the impact of climate change on river flow regimes related to the impact on mean annual runoff? A global-scale analysis', *Environmental Research Letters*, 7(1). <https://doi.org/10.1088/1748-9326/7/1/014037>.
- Dwarakish, G. S. and Ganasri, B. P. (2015) 'Impact of land use change on hydrological systems: A review of current modeling approaches', *Cogent Geoscience*, 1(1), p. 1115691. doi: 10.1080/23312041.2015.1115691.
- Ebrahimian, M., Nuruddin, A. A., Mohd Soom, A. M., Mohd Sood, A. and Juneng, L. (2017) 'Hydrological Responses to Climate and Land Use Change at Watershed Scale - Malaysia', *Pertanika Journal of Scholarly Research Reviews*, 2(3), 10–32. <http://www.pjsrr.upm.edu.my/>.
- Elias, S. A. (2021) 'Introduction to Paleoclimates', in *Encyclopedia of Geology*.

Academic Press, pp. 288–298. doi: 10.1016/b978-0-08-102908-4.00013-8.

- Elsayed, I. S. M. (2012) 'A Study on the Urban Heat Island of the City of Kuala Lumpur , Malaysia', *Journal of King Abdulaziz University: Metrology , Environment and Arid Land Agricultural Sciences*, 23(2), pp. 121–134. doi: 10.4197/MET.23-2-8.
- Estoque, R. C., Murayama, Y. and Myint, S. W. (2017) 'Effects of landscape composition and pattern on land surface temperature: An urban heat island study in the megacities of Southeast Asia', *Science of The Total Environment*, 577, pp. 349–359. doi: 10.1016/J.SCITOTENV.2016.10.195.
- Ezechi, E. H. and Muda, K. (2019) 'Overview of trends in crude palm oil production and economic impact in Malaysia', *Sriwijaya Journal of Environment*, 4(1), pp. 19–26. doi: 10.22135/sje.2019.4.1.19.
- Fan, J., Rosenfeld, D., Yang, Y., Zhao, C., Leung, L. R. and Li, Z. (2015) 'Substantial contribution of anthropogenic air pollution to catastrophic floods in Southwest China', *Geophysical Research Letters*, 42(6066–6075), p. pg 175 of 649. doi: doi:10.1002/2015GL064479.
- FAO (2020) 'Global Forest Resources Assessment 2020: Main report', Rome. doi: <https://doi.org/10.4060/ca9825en>.
- Findell, K. L., Berg, A., Gentine, P., Krasting, J. P., Lintner, B. R., Malyshev, S., Santanello, J. A., & Shevliakova, E. (2017) 'The impact of anthropogenic land use and land cover change on regional climate extremes', *Nature Communications*, 8(1), pp. 1–10. <https://doi.org/10.1038/s41467-017-01038-w>.
- Flato, G., Marotzke, J., Abiodun, B., Braconnot, P., Chou, S. C., Collins, W., Cox, P., Driouech, F., Emori, S., Eyring, V., Forest, C., Gleckler, P., Guilyardi, E., Jakob, C., Kattsov, V., Reason, C. and M. Rummukaine (2013) *Evaluation of Climate Models. In: Climate Change 2013: The Physical Science Basis.*

Contribution of Working Group I to the Fifth Assessment Report of the Intergovernmental Panel on Climate Change, Cambridge University Press. Cambridge, United Kingdom and New York, NY, USA.

- Foster, G. and Rahmstorf, S. (2011) 'Global temperature evolution 1979–2010', *Environmental Research Letters*, 6(4), 044022. <https://doi.org/10.1088/1748-9326/6/4/044022>.
- Friedlingstein, P. et al. (2019) 'Global carbon budget 2019', *Earth System Science Data*, 11(4), pp. 1783–1838. doi: 10.5194/ESSD-11-1783-2019.
- Gambo, J., Mohd Shafri, H. Z., Shaharum, N. S. N., Abidin, F. A. Z. and Rahman, M. T. A. (2018) 'Monitoring and Predicting Land Use-Land Cover (Lulc) Changes Within and Around Krau Wildlife Reserve (Kwr) Protected Area in Malaysia Using Multi-Temporal Landsat Data', *Geoplanning: Journal of Geomatics and Planning*, 5(1), p. 17. doi: 10.14710/geoplanning.5.1.17-34.
- Gassman, P. ., Reyes, M. ., Green, C. . and Arnold, J. . (2007) 'The Soil and Water Assessment Tool: Historical Development, Applications, and Future Research Directions', *Transactions of the ASABE*, 50(4), pp. 1211–1250. doi: 10.13031/2013.23637.
- Gaur, A. and Simonovic, S. P. (2019) 'Chapter 4 - Introduction to Physical Scaling: A Model Aimed to Bridge the Gap Between Statistical and Dynamic Downscaling Approaches', in Ramesh, T. (ed.) *Trends and Changes in Hydroclimatic Variables*. Elsevier, pp. 199–273. doi: 10.1016/B978-0-12-810985-4.00004-9.
- Glavan, M. and Pintar, M. (2012) 'Strengths, Weaknesses, Opportunities and Threats of Catchment Modelling with Soil and Water Assessment Tool (SWAT) Model', in Nayak, P. D. (ed.) *Water Resources Management and Modeling*. InTech, pp. 39–64. doi: DOI: 10.5772/34539.
- Good, S. P., Noone, D. and Bowen, G. (2015) 'Hydrologic connectivity

constrains partitioning of global terrestrial water fluxes', *Science*, 349(6244), pp. 175–177. doi: 10.1126/SCIENCE.AAA5931.

- Gordon, L. J., Peterson, G. D. and Bennett, E. M. (2008) 'Agricultural modifications of hydrological flows create ecological surprises', *Trends in Ecology and Evolution*, 23(4), pp. 211–219. doi: /10.1016/j.tree.2007.11.011.
- Graham, R. M., Hudson, S. R. and Maturilli, M. (2019) 'Improved Performance of ERA5 in Arctic Gateway Relative to Four Global Atmospheric Reanalyses', *Geophysical Research Letters*, 46(11), 6138–6147. <https://doi.org/10.1029/2019GL082781>.
- Hafoud, S., Boutoial, K., Oussama, A., Mahjoubi, F. and Kzaiber, F. (2020) 'Urbanisation and Its Impact on Land Surface Temperature Changes Using Landsat Image in Dakhla City, Morocco', *International Journal of Advanced Research in Engineering and Technology*, 11(6), pp. 143–155. Available at: https://papers.ssrn.com/sol3/papers.cfm?abstract_id=3644315 (Accessed: 8 March 2021).
- Haines, A., Kovats, R. S., Campbell-lendrum, D. and Corvalan, C. (2006) 'Climate change and human health: Impacts, vulnerability and public health *', pp. 585–596. doi: 10.1016/j.puhe.2006.01.002.
- Hamad, R., Balzter, H. and Kolo, K. (2018) 'Predicting land use/land cover changes using a CA-Markov model under two different scenarios', *Sustainability (Switzerland)*, 10(10), pp. 1–23. doi: 10.3390/su10103421.
- Haque, M. I. and Basak, R. (2017) 'Land cover change detection using GIS and remote sensing techniques: A spatio-temporal study on Tanguar Haor, Sunamganj, Bangladesh', *Egyptian Journal of Remote Sensing and Space Science*, 20(2), pp. 251–263. doi: 10.1016/j.ejrs.2016.12.003.
- Harun, Z., Reda, E., Abdulrazzaq, A., Abbas, A. A., Yusup, Y. and Zaki, S. A. (2020) 'Urban heat island in the modern tropical Kuala Lumpur: Comparative

weight of the different parameters', *Alexandria Engineering Journal*, 59(6), pp. 4475–4489. doi: 10.1016/j.aej.2020.07.053.

- Hasan, A. R. and Nair, P. L. (2014) 'Urbanisation and growth of metropolitan centres in Malaysia', *Malaysian Journal of Economic Studies*, 51(1), pp. 87–101.
- Hegazy, I. R. and Kaloop, M. R. (2015) 'Monitoring urban growth and land use change detection with GIS and remote sensing techniques in Daqahlia governorate Egypt', *International Journal of Sustainable Built Environment*, 4(1), pp. 117–124. doi: 10.1016/j.ijbsbe.2015.02.005.
- Hirsch, A. L., Guillod, B. P., Seneviratne, S. I., Beyerle, U., Boysen, L. R., Brovkin, V., Davin, E. L., Doelman, J. C., Kim, H., Mitchell, D. M., Nitta, T., Shiogama, H., Sparrow, S., Stehfest, E., van Vuuren, D. P. and Wilson, S. (2018) 'Biogeophysical Impacts of Land-Use Change on Climate Extremes in Low-Emission Scenarios: Results From HAPPI-Land', *Earth's Future*, 6(3), pp. 396–409. doi: 10.1002/2017EF000744.
- Hrachowitz, M., Stockinger, M., Coenders-Gerrits, M., van der Ent, R., Bogen, H., Lücke, A. and Stump, C. (2020) 'Deforestation reduces the vegetation-accessible water storage in the unsaturated soil and affects catchment travel time distributions and young water fractions', *Hydrology and Earth System Sciences Discussions*, pp. 1–43. doi: 10.5194/hess-2020-293.
- Hua, A.K. (2017) 'Land Use Land Cover Changes in Detection of Water Quality: A Study Based on Remote Sensing and Multivariate Statistics', *Journal of Environmental and Public Health*, pp. 1-12. doi.org/10.1155/2017/7515130.
- Huang, B., Hu, X., Fuglstad, G.-A., Zhou, X., Zhao, W. and Cherubini, F. (2020) 'Predominant regional biophysical cooling from recent land cover changes in Europe', *Nature Communications* 2020 11:1, 11(1), pp. 1–13. doi: 10.1038/s41467-020-14890-0.

- Huang, Y., Yang, B., Wang, M., Liu, B. and Yang, X. (2020) 'Analysis of the future land cover change in Beijing using CA-Markov chain model', *Environmental Earth Sciences*, 79(2), pp. 1–12. doi: 10.1007/s12665-019-8785-z.
- Ibrahim, W. Y. W. and Ludin, A. N. M. (2016) 'SPATIOTEMPORAL LAND USE AND LAND COVER CHANGE IN MAJOR RIVER BASINS IN COMPREHENSIVE DEVELOPMENT AREA', *Journal of the Malaysian Institute of Planners*, (Iv), pp. 225–242.
- Idso, C. D., Carter, R. M. and Singer, S. F. (2013) *Climate Change Reconsidered II: Physical Science*. Chicago, IL: Sebastian Lüning. Available at: www.heartland.org (Accessed: 25 April 2022).
- Ihlen, V. and Zanter, K. (2019) 'Landsat 7 (L7) Data Users Handbook', *USGS Landsat User Services*, 7(November), p. 151.
- IPCC (2007) *Climate Change 2007: The Physical Science Basis. Contribution of Working Group I to the Fourth Assessment Report of the Intergovernmental Panel on Climate Change*, Cambridge University Press. Cambridge, United Kingdom and New York, NY, USA,. doi: 10.1256/wea.58.04.
- IPCC (2014) *Climate Change 2014: Synthesis Report. Contribution of Working Groups I, II and III to the Fifth Assessment Report of the Intergovernmental Panel on Climate Change*, *Ipcc*. Geneva, Switzerland. Available at: https://ar5-syr.ipcc.ch/topic_futurechanges.php (Accessed: 23 May 2022).
- IPCC (2019) 'Climate Change and Land: an IPCC special report', *Climate Change and Land: an IPCC special report on climate change, desertification, land degradation, sustainable land management, food security, and greenhouse gas fluxes in terrestrial ecosystems*, pp. 1–864. Available at: <https://www.ipcc.ch/srccl/>.
- Jamaludin, N. and Izma, N. (2015) 'Thermal Comfort of Residential Building in

Malaysia at Different Micro-Climates', *Procedia - Social and Behavioral Sciences*, 170, pp. 613–623. doi: 10.1016/j.sbspro.2015.01.063.

- Jang, S. S., Ahn, S. R. and Kim, S. J. (2017) 'Evaluation of executable best management practices in Haean highland agricultural catchment of South Korea using SWAT', *Agricultural Water Management*, 180, pp. 224–234. doi: 10.1016/j.agwat.2016.06.008.
- Jia, G., Shevliakova, E., Artaxo, P., Ducoudré, N. D. N., Houghton, R., House, J., Kitajima, K., Lennard, C., Popp, A., Sirin, A., Sukumar, R. and Verchot, L. (2019) *Land–climate interactions. In: Climate Change and Land: an IPCC special report on climate change, desertification, land degradation, sustainable land management, food security, and greenhouse gas fluxes in terrestrial ecosystems.*
- Jubb, I., Canadell, P. and Dix, M. (2013) 'Representative Concentration Pathways', *AUSTRALIAN CLIMATE CHANGE SCIENCE PROGRAM*, pp. 1–3.
- June, T., Meijide, A., Stiegler, C., Kusuma, A. P. and Knohl, A. (2018) 'The influence of surface roughness and turbulence on heat fluxes from an oil palm plantation in Jambi, Indonesia', *IOP Conference Series: Earth and Environmental Science*, 149, p. 12048. doi: 10.1088/1755-1315/149/1/012048.
- Kabiri, R., Ramani Bai, R. and Chan, A. (2013) 'Regional precipitation scenarios using a spatial statistical downscaling approach for Klang watershed, Malaysia', *Journal of Environmental Research And Development*, 8(1), pp. 126–134.
- Kabiri, R., Ramani Bai, R. and Chan, A. (2015) 'Assessment of hydrologic impacts of climate change on the runoff trend in Klang Watershed, Malaysia', *Environmental Earth Sciences*, 73, pp. 27–37. doi.org/10.1007/s12665-014-3392-5.
- Kamarudin, M. K. A., Gidado, K. A., Toriman, M. E., Juahir, H., Umar, R., Abd

- Wahab, N., Ibrahim, S., Awang, S. and Maulud, K. N. A. (2018) 'Classification of land use/land cover changes using GIS and remote sensing technique in Lake Kenyir Basin, Terengganu, Malaysia', *International Journal of Engineering and Technology(UAE)*, 7(3.14 Special Issue 14), pp. 12–15. doi: 10.14419/ijet.v7i3.14.16854.
- Kamusoko, C. and Gamba, J. (2015) 'Simulating Urban Growth Using a Random Forest-Cellular Automata (RF-CA) Model', *ISPRS International Journal of Geo-Information*, 4(2), pp. 447–470. doi: 10.3390/ijgi4020447.
 - Karimi, F., Sultana, S., Babakan, A. S. and Suthaharan, S. (2019) 'Urban expansion modeling using an enhanced decision tree algorithm', *GeoInformatica*. doi: 10.1007/s10707-019-00377-8.
 - Karimi, H., Jafarnejhad, J., Khaledi, J. and Ahmadi, P. (2018) 'Monitoring and prediction of land use/land cover changes using CA-Markov model: a case study of Ravansar County in Iran', *Arabian Journal of Geosciences*, 11(19). doi: 10.1007/s12517-018-3940-5.
 - Kendall, M. G. (Maurice G. (1975) *Rank correlation methods*. London: Griffin.
 - Khaleghi, M. R. (2017) 'The influence of deforestation and anthropogenic activities on runoff generation', *Journal of Forest Science*, 63(6), pp. 245–253. doi: 10.17221/130/2016-JFS.
 - Khanna, J., Medvigy, D., Fueglistaler, S. and Walko, R. (2017) 'Regional dry-season climate changes due to three decades of Amazonian deforestation', *Nature Climate Change*, 7(3), pp. 200–204. doi: 10.1038/nclimate3226.
 - Khanna, J. and Medvigy, D. (2014) 'Strong control of surface roughness variations on the simulated dry season regional atmospheric response to contemporary deforestation in Rondônia, Brazil', *Journal of Geophysical Research: Atmospheres*, 119(23), pp. 13,067–13,078. doi: 10.1002/2014JD022278.

- Khawaldah, H. A., Farhan, I. and Alzboun, N. M. (2020) 'Simulation and prediction of land use and land cover change using GIS, remote sensing and CA-Markov model', *Global Journal of Environmental Science and Management*, 6(2), pp. 215–232. doi: 10.22034/gjesm.2020.02.07.
- Khwairakpam, E., Khosa, R., Gosain, A. and Nema, A. (2019) 'Monitoring and modelling water quality of Loktak Lake catchment', *SN Applied Sciences*, 1(5), pp. 1–15. doi: 10.1007/s42452-019-0517-1.
- Klein Tank, A. M. G., Zwiers, F. W. and Zhang, X. (2009) 'Guidelines on Analysis of extremes in a changing climate in support of informed decisions for adaptation', <http://www.clivar.org/organisation/etccdi/etccdi.php>.
- Konapala, G., Mishra, A. K., Wada, Y. and Mann, M. E. (2020) 'Climate change will affect global water availability through compounding changes in seasonal precipitation and evaporation', *Nature Communications*, 11(1). <https://doi.org/10.1038/s41467-020-16757-w>.
- Konrad, C. P. (2003) 'Effects of Urban Development on Floods', *U.S. Geological Survey*, pp. 1–4.
- Kushwaha, K., Singh, M. M., Singh, S. K. and Patel, A. (2021) 'Urban growth modeling using earth observation datasets, Cellular Automata-Markov Chain model and urban metrics to measure urban footprints', *Remote Sensing Applications: Society and Environment*, p. 100479. doi: 10.1016/j.rsase.2021.100479.
- Laban, O. N., Maghanga, C. M. and Joash, K. (2019) 'Determination of the Surface Roughness Parameter and Wind Shear Exponent of Kisii Region from the On-Site Measurement of Wind Profiles', *Journal of Energy*, 2019, pp. 1–12. doi: 10.1155/2019/8264061.
- Lal, M., Mishra, S. K. and Pandey, A. (2015) 'Physical verification of the effect of land features and antecedent moisture on runoff curve number', *Catena*,

133, pp. 318–327. doi: 10.1016/j.catena.2015.06.001.

- Lambin, E. (2006) 'Land Cover Assessment and Monitoring', in *Encyclopedia of Analytical Chemistry*. John Wiley & Sons, Ltd. doi: 10.1002/9780470027318.a2311.
- Legdou, A., Chafik, H., Amine, A., Lahssini, S. and Berrada, M. (2020) 'A random forest-cellular automata modeling approach to predict future forest cover change in middle atlas morocco, under anthropic, biotic and abiotic parameters', in *Lecture Notes in Computer Science (including subseries Lecture Notes in Artificial Intelligence and Lecture Notes in Bioinformatics)*. Springer, pp. 91–100. doi: 10.1007/978-3-030-51935-3_10.
- Lejeune, Q., Seneviratne, S. I. and Davin, E. L. (2017) 'Historical land-cover change impacts on climate: Comparative assessment of LUCID and CMIP5 multimodel experiments', *Journal of Climate*, 30(4), pp. 1439–1459. doi: 10.1175/JCLI-D-16-0213.1.
- Li, H., Harvey, J. and Kendall, A. (2013) 'Field measurement of albedo for different land cover materials and effects on thermal performance', *Building and Environment*, 59, pp. 536–546. doi: 10.1016/J.BUILDENV.2012.10.014.
- Li, Y., Zhao, M., Motesharrei, S., Mu, Q., Kalnay, E. and Li, S. (2015) 'Local cooling and warming effects of forests based on satellite observations', *Nature Communications*, 6(1), pp. 1–8. doi: 10.1038/ncomms7603.
- Li, Y., Zhao, M., Mildrexler, D. J., Motesharrei, S., Mu, Q., Kalnay, E., Zhao, F., Li, S. and Wang, K. (2016) 'Potential and Actual impacts of deforestation and afforestation on land surface temperature', *Journal of Geophysical Research: Atmospheres*, 121(24), pp. 14,372–14,386. doi: 10.1002/2016JD024969.
- Li, M., Cui, Y., Fu, Y., Li, N., Tang, X., Liu, X. and Run, Y. (2020) 'Simulating the potential sequestration of three major greenhouse gases in China's natural ecosystems', *Forests*, 11(2), p. 128. doi: 10.3390/f11020128.

- Li, Y., Fowler, H. J., Argüeso, D., Blenkinsop, S., Evans, J. P., Lenderink, G., Yan, X., Guerreiro, S. B., Lewis, E. and Li, X. F. (2020) 'Strong Intensification of Hourly Rainfall Extremes by Urbanisation', *Geophysical Research Letters*, 47(14), p. e2020GL088758. doi: 10.1029/2020GL088758.
- Li, X. X. (2020) 'Heat wave trends in Southeast Asia during 1979–2018: The impact of humidity', *Science of The Total Environment*, 721, 137664. <https://doi.org/10.1016/J.SCITOTENV.2020.137664>.
- Liang, P. and Ding, Y. (2017) 'The long-term variation of extreme heavy precipitation and its link to urbanisation effects in Shanghai during 1916–2014', *Advances in Atmospheric Sciences*, 34(3), pp. 321–334. doi: 10.1007/s00376-016-6120-0.
- Liang, S., Li, X. and Wang, J. (2012) 'Land Cover and Land use Changes', in *Advanced Remote Sensing*. Academic Press, pp. 703–772. doi: 10.1016/B978-0-12-385954-9.00024-1.
- Lin, C. Y., Chen, W. C., Chang, P. L. and Sheng, Y. F. (2011) 'Impact of the urban heat island effect on precipitation over a complex geographic environment in northern Taiwan', *Journal of Applied Meteorology and Climatology*, 50(2), pp. 339–353. doi: 10.1175/2010JAMC2504.1.
- Liu, J., Zhang, C., Kou, L. and Zhou, Q. (2017) 'Effects of Climate and Land Use Changes on Water Resources in the Taoer River', *Advances in Meteorology*, 2017, pp. 1–13. doi: 10.1155/2017/1031854.
- Liu, J. and Niyogi, D. (2019) 'Meta-analysis of urbanisation impact on rainfall modification', *Scientific Reports*, 9(1), p. 7301. doi: 10.1038/s41598-019-42494-2.
- Lo, C. P. and Quattrochi, D. A. (2003) 'Land-Use and Land-Cover Change, Urban Heat Island Phenomenon, and Health Implications: A Remote Sensing Approach', *Photogrammetric Engineering & Remote Sensing*, 69(9), pp. 1053–

1063.

- Lu, D., Mausel, P., Brondízio, E. and Moran, E. (2004) 'Change detection techniques', *International Journal of Remote Sensing*, 25(12), pp. 2365–2407. doi: 10.1080/0143116031000139863.
- Luyssaert, S. *et al.* (2014) 'Land management and land-cover change have impacts of similar magnitude on surface temperature', *Nature Climate Change*, 4(5), pp. 389–393. doi: 10.1038/nclimate2196.
- Mahamud, M. A., Samat, N., Tan, M. L., Chan, N. W. and Tew, Y. L. (2019) 'PREDICTION of FUTURE LAND USE LAND COVER CHANGES of KELANTAN, MALAYSIA', *International Archives of the Photogrammetry, Remote Sensing and Spatial Information Sciences - ISPRS Archives*, 42(4/W16), pp. 379–384. doi: 10.5194/isprs-archives-XLII-4-W16-379-2019.
- Mahowald, N. M., Randerson, J. T., Lindsay, K., Munoz, E., Doney, S. C., Lawrence, P., Schlunegger, S., Ward, D. S., Lawrence, D. and Hoffman, F. M. (2017) 'Interactions between land use change and carbon cycle feedbacks', *Global Biogeochemical Cycles*, 31(1), pp. 96–113. doi: 10.1002/2016GB005374.
- Mahto, S. S. and Mishra, V. (2019) 'Does ERA-5 Outperform Other Reanalysis Products for Hydrologic Applications in India?', *Journal of Geophysical Research: Atmospheres*, 124(16), 9423–9441. <https://doi.org/10.1029/2019JD031155>.
- Majid, N. A., Rainis, R. and Mohamed, A. F. (2018) 'Spatial analysis of development pressure in the Langat Basin, Selangor, Malaysia', *IOP Conference Series: Earth and Environmental Science*, 169(1). doi: 10.1088/1755-1315/169/1/012016.
- Malaysian Meteorological Department. (2009) 'Climate change scenarios for Malaysia, 2001 – 2099'.

- Mann, B. H. (1945) 'Nonparametric Tests Against Trend', *Econometrica*, 13(3), pp. 245–259. Available at: <http://www.jstor.com/stable/1907187>.
- Mansour, S., Al-Belushi, M. and Al-Awadhi, T. (2020) 'Monitoring land use and land cover changes in the mountainous cities of Oman using GIS and CA-Markov modelling techniques', *Land Use Policy*, 91(November 2019), p. 104414. doi: 10.1016/j.landusepol.2019.104414.
- Mao, W., Lu, D., Hou, L., Liu, X. and Yue, W. (2020) 'Comparison of Machine-Learning Methods for Urban Land-Use Mapping in Hangzhou City, China', *Remote Sensing*, 12(17), p. 2817. doi: 10.3390/rs12172817.
- Masum, K. M., Mansor, A., Sah, S. A. M. and Lim, H. S. (2017) 'Effect of differential forest management on land-use change (LUC) in a tropical hill forest of Malaysia', *Journal of Environmental Management*, 200, 468–474. <https://doi.org/10.1016/j.jenvman.2017.06.009>.
- Mayowa, O. O., Pour, S. H., Shahid, S., Mohsenipour, M., Harun, S. Bin, Heryansyah, A. and Ismail, T. (2015) 'Trends in rainfall and rainfall-related extremes in the east coast of peninsular Malaysia', *Journal of Earth System Science*, 124(8), pp. 1609–1622. doi: 10.1007/s12040-015-0639-9.
- McMichael, A. J., Woodruff, R. E. and Hales, S. (2006) 'Climate change and human health: Present and future risks', *Lancet*, 367(9513), pp. 859–869. doi: 10.1016/S0140-6736(06)68079-3.
- Megonigal, J. P. and Neubauer, S. C. (2019) 'Biogeochemistry of Tidal Freshwater Wetlands', in Perillo, G. M. . et al. (eds) *Coastal Wetlands: An Integrated Ecosystem Approach*. Elsevier, pp. 641–683. doi: 10.1016/B978-0-444-63893-9.00019-8.
- Memarian, H., Balasundram, S.K., Talib, J.B., Sung, C.T.B., Sood, A.M. and Abbaspour, K. (2012) 'Validation of CA-Markov for Simulation of Land Use and Cover Change in the Langat Basin, Malaysia', *Journal of Geographic Information*

System, 4(6), pp. 542–554. doi: 10.4236/jgis.2012.46059.

- Memarian, H., Balasundram, S. K., Abbaspour, K. C., Talib, J. B., Teh, C., Sung, C.T.B. and Sood, A. M. (2014) 'SWAT-based hydrological modelling of tropical land-use scenarios', *Hydrological Sciences Journal*, 59(10), pp. 1808–1829. doi: 10.1080/02626667.2014.892598.
- Mirici, M. E., Berberoglu, S., Akin, A. and Satir, O. (2017) 'Land Use/Cover Change Modelling in Mediterranean Rural Landscape Using Multi-Layer Perceptron and Markov Chain (MLP-MC)', *Applied Ecology and Environmental Research*, 16(1), pp. 467–486. doi: 10.15666/aeer/1601.
- Mishra, S. K., Pandey, A. and Singh, V. P. (2012) 'Special Issue on Soil Conservation Service Curve Number (SCS-CN) Methodology', *Journal of Hydrologic Engineering*, 17(11), pp. 1157–1157. doi: 10.1061/(ASCE)HE.1943-5584.0000694.
- Mohammed, K. S., Eltayeb Elhadary, Y. A. and Samat, N. (2016) 'Identifying Potential Areas for Future Urban Development Using Gis-Based Multi Criteria Evaluation Technique', *SHS Web of Conferences*, 23, p. 03001. doi: 10.1051/shsconf/20162303001.
- Mohammady, M., Moradi, H. R., Zeinivand, H., Temme, A. J. A. M., Yazdani, M. R. and Pourghasemi, H. R. (2017) 'Modeling and assessing the effects of land use changes on runoff generation with the CLUE-s and WetSpa models', *Theoretical and Applied Climatology*, pp. 1–13. <https://doi.org/10.1007/s00704-017-2190-x>.
- Mohd Jaafar, W. S. W., Maulud, K. N. A., Muhmad Kamarulzaman, A. M., Raihan, A., Sah, S. M., Ahmad, A., Maizah Saad, S. N., Mohd Azmi, A. T., Syukri, N. K. A. J. and Khan, W. R. (2020) 'The influence of deforestation on land surface temperature-A case study of Perak and Kedah, Malaysia', *Forests*, 11(6). doi: 10.3390/F11060670.

- Mohd, M. S. F., Mispan, M. R., Juneng, L., Tangang, F. T., Rahman, N. F. A., Khalid, K., Rasid, M. Z. A. and Haron, S. H. (2015) 'Assessment of impacts of climate change on streamflow trend in upper Kuantan watershed', *ARPN Journal of Engineering and Applied Sciences*, 10(15), pp. 6634–6642. Available at: <https://www.researchgate.net/publication/281264803> (Accessed: 18 April 2022).
- Moriasi, D. N., Arnold, J. G., Van Liew, M. W., Bingner, R. L., Harmel, R. D. and Veith, T. L. (2007) 'Model Evaluation Guidelines for Systematic Quantification of Accuracy in Watershed Simulations', *Transactions of the ASABE*, 50(3), pp. 885–900. doi: 10.13031/2013.23153.
- Moriasi, D. N., Wilson, B. N., Douglas-Mankin, K. R., Arnold, J. G. and Gowda, P. H. (2012) 'Hydrologic and water quality models: Use, calibration, and validation', *Transactions of the ASABE*, 55(4), pp. 1241–1247.
- Morris, K. I., Aekbal Salleh, S., Chan, A., Ooi, M. C. G., Abakr, Y. A., Oozeer, M. Y. and Duda, M. (2015) 'Computational study of urban heat island of Putrajaya, Malaysia', *Sustainable Cities and Society*, 19, pp. 359–372. doi: 10.1016/J.SCS.2015.04.010.
- Morris, K. I., Chan, A., Morris, K. J. K., Ooi, M. C. G., Oozeer, M. Y., Abakr, Y. A., Nadzir, M. S. M. and Mohammed, I. Y. (2017) 'Urbanisation and urban climate of a tropical conurbation, Klang Valley, Malaysia', *Urban Climate*, 19(October 2016), pp. 54–71. doi: 10.1016/j.uclim.2016.12.002.
- Munoth, P. and Goyal, R. (2020) 'Impacts of land use land cover change on runoff and sediment yield of Upper Tapi River Sub-Basin, India', *International Journal of River Basin Management*, 18(2), pp. 177–189. doi: 10.1080/15715124.2019.1613413.
- Nader, S. and Azman, K. (2017) 'Land use Changes Impact on extreme flood events in the Hulu Kelang River Basin, Malaysia', *Journal of Geotechnical*

Geology, 13(1), pp. 73–86.

- Namugize, J.N., Jewitt, G. and Graham, M. (2018) 'Effects of land use and land cover changes on water quality in the uMngeni river catchment, South Africa', *Physics and Chemistry of the Earth*, 105, pp. 247 - 264.
- Nazari-Sharabian, M., Taheriyoun, M., Ahmad, S., Karakouzian, M. and Ahmadi, A. (2019) 'Water quality modeling of Mahabad Dam watershed-reservoir system under climate change conditions, using SWAT and system dynamics', *Water*, 11(2), pp. 1–16. doi: 10.3390/w11020394.
- Ndhlovu, G. Z. and Woyessa, Y. E. (2020) 'Modelling impact of climate change on catchment water balance, Kabompo River in Zambezi River Basin', *Journal of Hydrology: Regional Studies*, 27, pp. 100650. doi: 10.1016/j.ejrh.2019.100650.
- Neitsch, S. L., Arnold, J. G., Kiniry, J. R., Srinivasan, R. and Williams, J. R. (2000a) 'Soil and Water Assessment Tool User's Manual, Version 2000', Temple, Texas.
- Neitsch, S. L., Arnold, J. G., Kiniry, J. R., Williams, J. R. and King, K. W. (2000b) 'Soil and Water Assessment Tool, Theoretical Documentation Version 2000', Temple, Texas.
- Neitsch, S. L., Arnold, J. G., Kiniry, J. R. and Williams, J. R. (2011) 'Soil and Water Assessment Tool Theoretical Documentation Version 2009', *Science of the Total Environment*. Texas. doi: 10.1016/j.scitotenv.2015.11.063.
- Ngai, S. T., Juneng, L., Tangang, F., Chung, J. X., Salimun, E., Tan, M. L. and Amalia, S. (2020) 'Future projections of Malaysia daily precipitation characteristics using bias correction technique', *Atmospheric Research*, 240, p. 104926. doi: 10.1016/j.atmosres.2020.104926.
- Niyogi, D., Lei, M., Kishitawal, C., Schmid, P. and Shepherd, M. (2017) 'Urbanisation impacts on the summer heavy rainfall climatology over the

eastern United States', *Earth Interactions*, 21(5). doi: 10.1175/EI-D-15-0045.1.

- NOAA (2020) *Global Climate Report - Annual 2020 | National Centers for Environmental Information (NCEI)*. Available at: <https://www.ncdc.noaa.gov/sotc/global/202013> (Accessed: 19 January 2022).
- NOAA (2021) *State of the Climate: Global Climate Report for Annual 2020, National Center for Environmental Information*. Available at: <https://www.ncei.noaa.gov/access/monitoring/monthly-report/global/202013> (Accessed: 31 March 2022).
- Noori, N., Kalin, L. and Isik, S. (2020) 'Water quality prediction using SWAT-ANN coupled approach', *Journal of Hydrology*, 590(December 2019), p. 125220. doi: 10.1016/j.jhydrol.2020.125220.
- Nourqolipour, R., Shariff, A. R. B. M., Balasundram, S. K., Ahmad, N. B., Sood, A. M., Buyong, T. and Amiri, F. (2015a) 'A GIS-based model to analyse the spatial and temporal development of oil palm land use in Kuala Langat district, Malaysia', *Environmental Earth Sciences*, 73(4), pp. 1687–1700. doi: 10.1007/s12665-014-3521-1.
- Nourqolipour, R., Shariff, A. R. B. M., Ahmad, N. B., Balasundram, S. K., Sood, A. M., Buyong, T. and Amiri, F. (2015b) 'Multi-objective-based modeling for land use change analysis in the South West of Selangor, Malaysia', *Environmental Earth Sciences*, 74(5), pp. 4133–4143. doi: 10.1007/s12665-015-4486-4.
- Nourqolipour, R., Shariff, A. R. B. M., Balasundram, S. K., Ahmad, N. B., Sood, A. M. and Buyong, T. (2016) 'Predicting the Effects of Urban Development on Land Transition and Spatial Patterns of Land Use in Western Peninsular Malaysia', *Applied Spatial Analysis and Policy*, 9(1), pp. 1–19. doi: 10.1007/s12061-014-9128-9.

- De Oliveira, V. A., De Mello, C. R., Viola, M. R. and Srinivasan, R. (2018) 'Land-use change impacts on the hydrology of the upper grande River Basin, Brazil', *Cerne*, 24(4), pp. 334–343. doi: 10.1590/01047760201824042573.
- Ooi, M. C. G., Chan, A., Ashfold, M. J., Morris, K. I., Oozeer, M. Y. and Salleh, S. A. (2017) 'Numerical study on effect of urban heating on local climate during calm inter-monsoon period in greater Kuala Lumpur, Malaysia', *Urban Climate*, 20, pp. 228–250. doi: 10.1016/j.uclim.2017.04.010.
- Othman, J., Sharifah Mastura, S.A. and Mohd Sood, A. (2009) 'Land Use and Deforestation Modelling of River Catchments in Klang Valley, Malaysia', *Sains Malaysiana*, 38(5), pp. 655-664.
- Palizdan, N., Falamarzi, Y., Huang, Y. F., Lee, T. S. and Ghazali, A. H. (2014) 'Regional precipitation trend analysis at the Langat River Basin, Selangor, Malaysia', *Theoretical and Applied Climatology*, 117(3–4), pp. 589–606. doi: 10.1007/s00704-013-1026-6.
- Pang, J., Zhang, H., Xu, Q., Wang, Yujie, Wang, Yunqi, Zhang, O. and Hao, J. (2020) 'Hydrological evaluation of open-access precipitation data using SWAT at multiple temporal and spatial scales', *Hydrology and Earth System Sciences*, 24(7), pp. 3603–3626. doi: 10.5194/hess-24-3603-2020.
- Patil, N. S., & Nataraja, M. (2020) 'Effect of land use land cover changes on runoff using hydrological model: a case study in Hiranyakeshi watershed', *Modeling Earth Systems and Environment*, 6(4), pp. 2345–2357. <https://doi.org/10.1007/s40808-020-00808-8>.
- Paudel, M. (2010) 'An Examination of Distributed Hydrologic Modeling Methods as Compared with Traditional Lumped Parameter Approaches', *Brigham Young University*. Available at: <https://scholarsarchive.byu.edu/etd> (Accessed: 11 April 2022).

- Pechlivanidis, Ilias G., Jackson, B. M., McIntyre, N. R. and Wheeler, H. S. (2011) 'Catchment scale hydrological modelling: A review of model types, calibration approaches and uncertainty analysis methods in the context of recent developments in technology and applications', *Global Nest Journal*, 13(3), pp. 193–214. doi: 10.30955/gnj.000778.
- Peña-Arancibia, J. L., Bruijnzeel, L. A., Mulligan, M. and van Dijk, A. I. J. M. (2019) 'Forests as "sponges" and "pumps": Assessing the impact of deforestation on dry-season flows across the tropics', *Journal of Hydrology*, 574, pp. 946–963. doi: 10.1016/j.jhydrol.2019.04.064.
- Peng, S., Piao, S., Ciais, P., Friedlingstein, P., Oettle, C., Bréon, F.-M., Nan, H., Zhou, L. and Myneni, R. B. (2012) 'Surface Urban Heat Island Across 419 Global Big Cities', *Environmental Science and Technology*, 46(2), pp. 696–703. doi: 10.1021/ES2030438.
- Perkins, S. (2019) 'Core Concept: Albedo is a simple concept that plays complicated roles in climate and astronomy', *Proceedings of the National Academy of Sciences of the United States of America*, 116(51), pp. 25369–25371. doi: 10.1073/pnas.1922493117.
- Pielke, R. A., Marland, G., Betts, R. A., Chase, T. N., Eastman, J. L., Niles, J. O., Niyogi, D. and Running, S. (2002) 'The influence of land-use change and landscape dynamics on the climate system- relevance to climate change policy beyond the radiative effect of greenhouse gases', *Philosophical Transactions of the Royal Society A*, 360, pp. 1705–1719.
- Plecher, H. (2020) *Malaysia - urbanisation 2009-2019* | Statista. Available at: <https://www.statista.com/statistics/455880/urbanisation-in-malaysia/> (Accessed: 8 February 2021).
- Pontius, R. G. and Millones, M. (2011) 'Death to Kappa: Birth of quantity disagreement and allocation disagreement for accuracy assessment',

International Journal of Remote Sensing. Taylor and Francis Ltd., pp. 4407–4429. doi: 10.1080/01431161.2011.552923.

- Pontius, R. G., Peethambaram, S. and Castella, J. C. (2011) 'Comparison of three maps at multiple resolutions: A case study of land change simulation in cho don district, Vietnam', *Annals of the Association of American Geographers*, 101(1), pp. 45–62. doi: 10.1080/00045608.2010.517742.
- Powers, R.P. and Jetz, W. (2019) 'Global habitat loss and extinction risk of terrestrial vertebrates under future land-use-change scenarios', *Nature Climate Change*, 9(4), pp. 323 - 329.
- Prevedello, J. A., Winck, G. R., Weber, M. M., Nichols, E. and Sinervo, B. (2019) 'Impacts of forestation and deforestation on local temperature across the globe', *PLOS ONE*, 14(3), p. e0213368. doi: 10.1371/JOURNAL.PONE.0213368.
- Qiu, J., Yang, X., Cao, B., Chen, Z. and Li, Y. (2020) 'Effects of Urbanisation on Regional Extreme-Temperature Changes in China, 1960–2016', *Sustainability*, 12(16), p. 6560. doi: 10.3390/su12166560.
- Quinta Shegwe, T., Destain Yungsi, W., Erika Suh, S., Christian Brice, T., Kohtem Lebga, A., Mbi Bienvenu Magloire, T., Ngouanet, C. and Mbi Bienvenu, T. (2021) 'Land Use / Land Cover Change in the Western Highlands of Cameroon: Case of the Sabga-Bamunka Area (1980-2020)', *American Journal of Remote Sensing*, 9(1), pp. 55–64. doi: 10.11648/j.ajrs.20210901.17.
- Razaai, N. H., Abdullah, S. A. and Hasan Reza, M. I. (2020) 'Identifying factors and predicting the future land-use change of protected area in the agricultural landscape of Malaysian peninsula for conservation planning', *Remote Sensing Applications: Society and Environment*, 18, p. 100298. doi: 10.1016/j.rsase.2020.100298.
- Rahman, N. A. A. S., Ridzuan, M. R., Hidayat, N. and Manas, N. B. (2020) 'The Aftermath of Unsustainable Urbanisation In South East Asia Countries',

International Journal of Humanities Technology and Civilisation, 1(9), pp. 57–68.

- Rashid, M. B. and Hossain, S. S. (2018) 'Statistical downscaling of global climate model (GCM) outputs for climate change impact assessment of mean temperature of the winter season over Bangladesh', *The Journal of NOAMI*, 35(1–2), pp. 45–58. Available at: <https://www.researchgate.net/publication/348916418> (Accessed: 1 May 2022).
- Ravindran, S. and Rajendra, E. (2020) 'Green lung under threat', *Thestar.Com.My*. <https://www.thestar.com.my/metro/metro-news/2020/02/18/green-lung-under-threat>.
- Rawat, J. S. and Kumar, M. (2015) 'Monitoring land use/cover change using remote sensing and GIS techniques: A case study of Hawalbagh block, district Almora, Uttarakhand, India', *Egyptian Journal of Remote Sensing and Space Science*, 18(1), pp. 77–84. doi: 10.1016/j.ejrs.2015.02.002.
- Rosni, N. A., Noor, N. M. and Abdullah, A. (2016) 'Managing urbanisation and urban sprawl in Malaysia by using remote sensing and GIS applications', *Planning Malaysia*, 4(Special Issue 4), pp. 17–30. doi: 10.21837/pmjournal.v14.i4.145.
- Rumph Frederiksen, R. and Molina-Navarro, E. (2021) 'The importance of subsurface drainage on model performance and water balance in an agricultural catchment using SWAT and SWAT-MODFLOW', *Agricultural Water Management*, 255(May), p. 107058. doi: 10.1016/j.agwat.2021.107058.
- Saadatkah, N., Tehrani, M.H., Mansor, S., Khuzaimah, Z., Kassim, A. and Saadatkah R. (2016) 'Impact assessment of land cover changes on the runoff changes on the extreme flood events in the Kelantan River basin', *Arabian Journal of Geosciences*, 9(687). <https://doi.org/10.1007/s12517-016-2716-z>.

- Saadatkah, N. and Kassim, A. (2017) 'Land use Changes Impact on extreme flood events in the Hulu Kelang River Basin, Malaysia', *Journal of Geotechnical Geology*, 13(1), 73–86.
- Sa'adi, Z., Shahid, S., Ismail, T., Chung, E. S. and Wang, X. J. (2019) 'Trends analysis of rainfall and rainfall extremes in Sarawak, Malaysia using modified Mann–Kendall test', *Meteorology and Atmospheric Physics*, 131(3), pp. 263–277. doi: 10.1007/s00703-017-0564-3.
- Saade, J., Atieh, M., Ghanimeh, S. and Golmohammadi, G. (2021) 'Modeling impact of climate change on surface water availability using swat model in a semi-arid basin: Case of el kalb river, lebanon', *Hydrology*, 8(3). doi: 10.3390/HYDROLOGY8030134.
- Salazar, A., Baldi, G., Hirota, M., Syktus, J., & McAlpine, C. (2015) 'Land use and land cover change impacts on the regional climate of non-Amazonian South America: A review', *In Global and Planetary Change*, 128, pp. 103–119. <https://doi.org/10.1016/j.gloplacha.2015.02.009>.
- Salmi, T., Maatta, A., Anttila, P., Ruoho-Airola, T. and Amnell, T. (2002) *Detecting Trends of Annual Values of Atmospheric Pollutants by the Mann-Kendall Test and Sen's Solpe Estimates the Excel Template Application MAKESENS*, Finnish Meteorological Institute, Air Quality Research.
- Samardžić-petrović, M., Dragičević, S., Bajat, B. and Kovačević, M. (2015) 'Exploring the Decision Tree Method for Modelling Urban Land Use Change', *GEOMATICA*, 69(3). doi: dx.doi.org/10.5623/cig2015-305.
- Samardžić-Petrović, M., Dragičević, S., Kovačević, M. and Bajat, B. (2016) 'Modeling Urban Land Use Changes Using Support Vector Machines', *Transactions in GIS*, 20(5), pp. 718–734. doi: 10.1111/TGIS.12174.
- Samat, N., Mahamud, M. A., Tan, M. L., Tilaki, M. J. M. and Tew, Y. L. (2020) 'Modelling land cover changes in peri-urban areas: A case study of George town

conurbation, malaysia', *Land*, 9(10), pp. 1–16. doi: 10.3390/land9100373.

- Samsuri, N., Abu Bakar, R. and Unjah, T. (2018). 'Flash Flood Impact in Kuala Lumpur – Approach Review and Way Forward', *International Journal of the Malay World and Civilisation*, 6(1), pp. 69 - 76. doi.org/10.17576/jatma-2018-06SI1-10.
- Sanderson, M., Arbuthnott, K., Kovats, S., Hajat, S. and Falloon, P. (2017) 'The use of climate information to estimate future mortality from high ambient temperature: A systematic literature review', *PLoS ONE*. Public Library of Science. doi: 10.1371/journal.pone.0180369.
- Sani, S. (1972) 'Some aspects of urban micro-climate in Kuala Lumpur West Malaysia', *Akademika*, 1, pp. 85–92. Available at: <https://ejournal.ukm.my/akademika/article/view/410> (Accessed: 15 July 2021).
- Santhi, C., Arnold, J. G., Williams, J. R., Dugas, W. A., Srinivasan, R. and Hauck, L. M. (2001) 'Validation of the SWAT model on a large river basin with point and nonpoint sources', *Journal of the American Water Resources Association*, 37(5), pp. 1169–1188. doi: 10.1111/j.1752-1688.2001.tb03630.x.
- Schmid, P. E. and Niyogi, D. (2017) 'Modeling urban precipitation modification by spatially heterogeneous aerosols', *Journal of Applied Meteorology and Climatology*, 56(8), pp. 2141–2153. doi: 10.1175/JAMC-D-16-0320.1.
- Seino, N., Aoyagi, T. and Tsuguti, H. (2018) 'Numerical simulation of urban impact on precipitation in Tokyo: How does urban temperature rise affect precipitation?', *Urban Climate*, 23, pp. 8–35. doi: 10.1016/j.uclim.2016.11.007.
- Sen, P. K. (1968) 'Estimates of the Regression Coefficient Based on Kendall's Tau', *Journal of the American Statistical Association*, 63(324), pp. 1379–1389.

doi: 10.1080/01621459.1968.10480934.

- Shadeed, S. and Almasri, M. (2010) 'Application of GIS-based SCS-CN method in', *Water Science and Engineering*, 3(1), pp. 1–13. doi: 10.3882/j.issn.1674-2370.2010.01.001.
- Shaharuddin, A., Noorazuan, M. H., Takeuchi, W. and Noraziah, A. (2014) 'The effects of Urban Heat Islands on Human Comfort: A case of Klang Valley Malaysia', *Global Journal on Advances Pure and Applied Sciences*, 2, pp. 1–8. Available at: <http://archives.un-pub.eu/index.php/paas/article/view/3099> (Accessed: 15 July 2021).
- Shawul, A. A. and Chakma, S. (2020) 'Trend of extreme precipitation indices and analysis of long-term climate variability in the Upper Awash basin, Ethiopia', *Theoretical and Applied Climatology*, 140(1–2), pp. 635–652. doi: 10.1007/s00704-020-03112-8.
- Shepherd, J. M. (2005) 'A review of current investigations of urban-induced rainfall and recommendations for the future', *Earth Interactions*, 9(12). doi: 10.1175/EI156.1.
- Shi, Z. H., Chen, L. D., Fang, N. F., Qin, D. F. and Cai, C. F. (2009) 'Research on the SCS-CN initial abstraction ratio using rainfall-runoff event analysis in the Three Gorges Area, China', *Catena*, 77(1), pp. 1–7. doi: 10.1016/j.catena.2008.11.006.
- Shiferaw, H., Gebremedhin, A., Gebretsadkan, T. and Zenebe, A. (2018) 'Modelling hydrological response under climate change scenarios using SWAT model: the case of Ilala watershed, Northern Ethiopia', *Modeling Earth Systems and Environment*, 4(1), pp. 437–449. doi: 10.1007/s40808-018-0439-8.
- Singh, V. and Qin, X. (2020) 'Study of rainfall variabilities in Southeast Asia using long-term gridded rainfall and its substantiation through global climate indices', *Journal of Hydrology*, 585(October 2019). doi:

10.1016/j.jhydrol.2019.124320.

- Sinha, R. K. and Eldho, T. I. (2018) 'Effects of historical and projected land use/cover change on runoff and sediment yield in the Netravati River basin, Western Ghats, India', *Environmental Earth Sciences*, 77(3), 1–19. <https://doi.org/10.1007/s12665-018-7317-6>.
- Sitterson, J., Knightes, C., Parmar, R., Wolfe, K., Muche, M. and Avant, B. (2017b) 'An Overview of Rainfall-Runoff Model Types An Overview of Rainfall-Runoff Model Types', *United States Environmental Protection Agency*, pp. 0–29. Available at: www.epa.gov/research (Accessed: 11 April 2022).
- Sleeter, B. M., Loveland, T. R., Domke, G. M., Herold, N., Wickham, J. and Wood, N. J. (2018) *Land Cover and Land Use Change. Impacts, Risks, and Adaptation in the United States: The Fourth National Climate Assessment, Volume II*. Washington, DC. doi: 10.7930/NCA4.2018.CH5.
- Sobrino, J. A., Jiménez-Muñoz, J. C. and Paolini, L. (2004) 'Land surface temperature retrieval from LANDSAT TM 5', *Remote Sensing of Environment*, 90(4), pp. 434–440. doi: 10.1016/j.rse.2004.02.003.
- Soesbergen, A. van (2016) 'a Review of Land', Available at: https://www.unep-wcmc.org/system/comfy/cms/files/files/000/000/802/original/Land_Use_Change_Models_2016_WEB.pdf.
- Solomon, N., Pabi, O., Annang, T., Asante, I. K. and Birhane, E. (2018) 'The effects of land cover change on carbon stock dynamics in a dry Afromontane forest in northern Ethiopia', *Carbon Balance and Management*, 13(1), p. 14. doi: 10.1186/s13021-018-0103-7.
- Son, N. T., Chen, C. F. and Chen, C. R. (2020) 'Urban expansion and its impacts on local temperature in San Salvador, El Salvador', *Urban Climate*, 32, p. 100617. doi: 10.1016/j.uclim.2020.100617.
- Soulis, K. X. and Valiantzas, J. D. (2012) 'SCS-CN parameter determination

using rainfall-runoff data in heterogeneous watersheds-the two-CN system approach', *Hydrology and Earth System Sciences*, 16(3), pp. 1001–1015. doi: 10.5194/hess-16-1001-2012.

- Srinivasan, M. S., Gérard-Marchant, P., Veith, T. L., Gburek, W. J. and Steenhuis, T. S. (2005) 'Watershed scale modeling of critical source areas of runoff generation and phosphorus transport', *Journal of the American Water Resources Association*, 41(2), pp. 361–377. doi: 10.1111/j.1752-1688.2005.tb03741.x.
- Sultana, S. and Satyanarayana, A. N. V. (2020) 'Assessment of urbanisation and urban heat island intensities using landsat imageries during 2000 – 2018 over a sub-tropical Indian City', *Sustainable Cities and Society*, 52, p. 101846. doi: 10.1016/j.scs.2019.101846.
- Sun, L., Wei, J., Duan, D. H., Guo, Y. M., Yang, D. X., Jia, C., & Mi, X. T. (2016) 'Impact of Land-Use and Land-Cover Change on urban air quality in representative cities of China', *Journal of Atmospheric and Solar-Terrestrial Physics*, 142, pp. 43–54. <https://doi.org/10.1016/j.jastp.2016.02.022>.
- Syahmi Armain, M. Z., Hassan, Z., Zainol, M. R. R. M. A., Harun, S., Kamarudzaman, A. N. and Makhtar, S. M. Z. (2021) 'Analysis impact of climate change on hydrological trend in Kelantan River Basin using HEC-HMS coupled with SDSM', in *5th International Conference on Water Resources*. Johor Bahru. Available at: https://www.researchgate.net/publication/356617308_Analysis_impact_of_climate_change_on_hydrological_trend_in_Kelantan_River_Basin_using_HEC-HMS_coupled_with_SDSM (Accessed: 23 May 2022).
- Tabari, H. (2020) 'Climate change impact on flood and extreme precipitation increases with water availability', *Scientific Reports*, 10(1), pp. 1–10. doi: 10.1038/s41598-020-70816-2.

- Tamm, O., Maasikamäe, S., Padari, A. and Tamm, T. (2018) 'Modelling the effects of land use and climate change on the water resources in the eastern Baltic Sea region using the SWAT model', *Catena*, 167(April), pp. 78–89. doi: 10.1016/j.catena.2018.04.029.
- Tan, M. L., Ibrahim, A. L., Yusop, Z., Duan, Z. and Ling, L. (2015) 'Impacts of land-use and climate variability on hydrological components in the Johor River basin, Malaysia', *Hydrological Sciences Journal*, 60(5), pp. 873–889. doi: 10.1080/02626667.2014.967246.
- Tan, M. L., Gassman, P. W., Srinivasan, R., Arnold, J. G. and Yang, X. Y. (2019) 'A review of SWAT studies in Southeast Asia: Applications, challenges and future directions', *Water (Switzerland)*. MDPI AG. doi: 10.3390/w11050914.
- Tan, M. L., Juneng, L., Tangang, F. T., Chan, N. W. and Ngai, S. T. (2019) 'Future hydro-meteorological drought of the Johor River Basin, Malaysia, based on CORDEX-SEA projections', *Hydrological Sciences Journal*, 64(8), pp. 921–933. doi: 10.1080/02626667.2019.1612901.
- Tang, K. H. D. (2019) 'Climate change in Malaysia: Trends, contributors, impacts, mitigation and adaptations', *Science of the Total Environment*. Elsevier, pp. 1858–1871. doi: 10.1016/j.scitotenv.2018.09.316.
- Tölle, M. H., Breil, M., Radtke, K. and Panitz, H.-J. (2018) 'Sensitivity of European Temperature to Albedo Parameterization in the Regional Climate Model COSMO-CLM Linked to Extreme Land Use Changes', *Frontiers in Environmental Science*, 6(123), pp. 1–15. doi: 10.3389/FENVS.2018.00123.
- Trlica, A., Hutyra, L. R., Schaaf, C. L., Erb, A. and Wang, J. A. (2017) 'Albedo, Land Cover, and Daytime Surface Temperature Variation Across an Urbanised Landscape', *Earth's Future*, 5(11), pp. 1084–1101. doi: 10.1002/2017EF000569.
- Trzaska, S. and Schnarr, E. (2014) *A review of downscaling methods for climate*

change projections. Burlington, Vermont.

- Tuo, Y., Duan, Z., Disse, M. and Chiogna, G. (2016) 'Evaluation of precipitation input for SWAT modeling in Alpine catchment: A case study in the Adige river basin (Italy)', *Science of the Total Environment*, 573, pp. 66–82. doi: 10.1016/j.scitotenv.2016.08.034.
- Ullah, S., Noman, M., Rahimi, M., Stanikzai, A. G., Ayub, S., Din, Z. U., Emiliya, H., Esmati, S., Zahoor, F. and Khan, S. (2021) 'A Comprehensive Review of Climate Change Impacts on Water Resources: A Global perspective', *IOSR Journal of Environmental Science, Toxicology and Food Technology*, 15(3), pp. 43–48. doi: 10.9790/2402-1503034348.
- Varentsov, M., Wouters, H., Platonov, V. and Konstantinov, P. (2018) 'Megacity-induced mesoclimatic effects in the lower atmosphere: A modeling study for multiple summers over Moscow, Russia', *Atmosphere*, 9(2). doi: 10.3390/atmos9020050.
- Vaze, J., Jordan, P., Beecham, R., Frost, A., Summerell, G. and Vaze, J., Jordan, P., Beecham, R., Frost, A., Summerell, G. (2012) 'Guidelines for rainfall-runoff modelling Towards best practice model application', *eWater Cooperative Research Center*.
- Verburg, P. H., Soepboer, W., Veldkamp, A., Limpiada, R., Espaldon, V. and Mastura, S. S. A. (2002) 'Modeling the spatial dynamics of regional land use: The CLUE-S model', *Environmental Management*, 30(3), pp. 391–405. doi: 10.1007/s00267-002-2630-x.
- van der Esch, S., ten Brink, B., Stehfest, E., Bakkenes, M., Sewell, A., Bouwman, A., Meijer, J., Westhoek, H. and van den Berg, M. (2017) 'Exploring future changes in land use and land condition and the impacts on food, water, climate change and biodiversity: Scenarios for the Global Land Outlook', Hague.
- van Liew, M. W., Arnold, J. G. and Garbrecht, J. D. (2003) 'Hydrologic

simulation on agricultural watersheds: Choosing between two models', *Transactions of the American Society of Agricultural Engineers*, 46(6), pp. 1539–1551. doi: 10.13031/2013.15643.

- van Vuuren, D. P., Edmonds, J., Kainuma, M., Riahi, K., Thomson, A., Hibbard, K., Hurtt, G. C., Kram, T., Krey, V., Lamarque, J. F., Masui, T., Meinshausen, M., Nakicenovic, N., Smith, S. J. and Rose, S. K. (2011) 'The representative concentration pathways: An overview', *Climatic Change*, 109(1), pp. 5–31. doi: 10.1007/s10584-011-0148-z.
- Wang, K., Aktas, Y. D., Stocker, J., Carruthers, D., Hunt, J. and Malki-Epshtein, L. (2019) 'Urban heat island modelling of a tropical city: case of Kuala Lumpur', *Geoscience Letters*, 6(1), pp. 1–11. doi: 10.1186/S40562-019-0134-2.
- Wang, Y., Liu, Y. and Jin, J. (2018) 'Contrast effects of vegetation cover change on evapotranspiration during a revegetation period in the Poyang Lake Basin, China', *Forests*, 9(4), p. 217. doi: 10.3390/f9040217.
- Welde, K., & Gebremariam, B. (2017) 'Effect of land use land cover dynamics on hydrological response of watershed: Case study of Tekeze Dam watershed, northern Ethiopia', *International Soil and Water Conservation Research*, 5(1), pp. 1–16. <https://doi.org/10.1016/j.iswcr.2017.03.002>.
- Williams, J. R. (1995) 'The EPIC Model, Computer Models of Watershed Hydrology', *Computer models of watershed hydrology*, pp. 909–1000.
- Winchell, M., Srinivasan, R., Di Luzio, M. and Arnold, J. . (2007) *ArcSWAT interface for SWAT2005 - User's Guide*. Temple, Texas.
- Winckler, J., Reick, C. H. and Pongratz, J. (2017) 'Robust identification of local biogeophysical effects of land-cover change in a global climate model', *Journal of Climate*, 30(3), pp. 1159–1176. doi: 10.1175/JCLI-D-16-0067.1.
- Winkler, K., Fuchs, R., Rounsevell, M. and Herold, M. (2021) 'Global land use changes are four times greater than previously estimated', *Nature*

Communications, 12(1), pp. 1–10. doi: 10.1038/s41467-021-22702-2.

- Wong, C. L., Liew, J., Yusop, Z., Ismail, T., Venneker, R. and Uhlenbrook, S. (2016) 'Rainfall characteristics and regionalisation in peninsular Malaysia based on a high resolution gridded data set', *Water (Switzerland)*, 8(11). doi: 10.3390/w8110500.
- World Bank Group. (2015) 'East Asia's Changing Urban Landscape : Measuring a Decade of Spatial Growth', *Urban Development, Washington, DC, World Bank*. <http://hdl.handle.net/10986/21159>.
- Wu, M., Luo, Y., Chen, F. and Wong, W. K. (2019) 'Observed link of extreme hourly precipitation changes to urbanisation over coastal South China', *Journal of Applied Meteorology and Climatology*, 58(8), pp. 1799–1819. doi: 10.1175/JAMC-D-18-0284.1.
- Wu, Y., Tao, Y., Yang, G., Ou, W., Pueppke, S., Sun, X. and Chen, G. (2019) 'Land Use Policy Impact of land use change on multiple ecosystem services in the rapidly urbanising Kunshan City of China: Past trajectories and future projections', 85(October 2018), pp. 419–427. doi: 10.1016/j.landusepol.2019.04.022.
- Xiao, B., Wang, Q. H., Fan, J., Han, F. P. and Dai, Q. H. (2011) 'Application of the SCS-CN model to runoff estimation in a small watershed with high spatial heterogeneity', *Pedosphere*, 21(6), pp. 738–749. doi: 10.1016/S1002-0160(11)60177-X.
- Yan, J., Gao, S., Xu, M. and Su, F. (2020) 'Spatial-temporal changes of forests and agricultural lands in Malaysia from 1990 to 2017', *Environmental Monitoring and Assessment*, 192(12). doi: 10.1007/s10661-020-08765-6.
- Yang, J., Han, X., Huang, J. and Pan, Q. (2003) 'Effects of land use change on carbon storage in terrestrial ecosystem', *Chinese Journal of Applied Ecology*, 14(8), pp. 1385–1390. Available at:

<https://pubmed.ncbi.nlm.nih.gov/14655381/> (Accessed: 17 July 2021).

- Yang, P., Ren, G. and Yan, P. (2017) 'Evidence for a strong association of short-duration intense rainfall with urbanisation in the Beijing urban area', *Journal of Climate*, 30(15), pp. 5851–5870. doi: 10.1175/JCLI-D-16-0671.1.
- Yatim, A. N. M., Latif, M. T., Ahamad, F., Khan, M. F., Nadzir, M. S. M. and Juneng, L. (2019) 'Observed Trends in Extreme Temperature over the Klang Valley, Malaysia', *Advances in Atmospheric Sciences*, 36(12), pp. 1355–1370. doi: 10.1007/s00376-019-9075-0.
- Yu, M., Liu, Y. and Miao, S. (2020) 'Impact of urbanisation on rainfall of different strengths in the Beijing area', *Theoretical and Applied Climatology*, 139(3–4), pp. 1097–1110. doi: 10.1007/s00704-019-03035-z.
- Yusuf, Y. A., Pradhan, B. and Idrees, M. O. (2014) 'Spatio-temporal Assessment of Urban Heat Island Effects in Kuala Lumpur Metropolitan City Using Landsat Images', *Journal of the Indian Society of Remote Sensing*, 42(4), pp. 829–837. doi: 10.1007/S12524-013-0342-8.
- Zang, W., Liu, S., Huang, S., Li, J., Fu, Y., Sun, Y. and Zheng, J. (2019) 'Impact of urbanisation on hydrological processes under different precipitation scenarios', *Natural Hazards*, 99(3), pp. 1233–1257. doi: 10.1007/s11069-018-3534-2.
- Zhan, X. and Huang, M. L. (2004) 'ArcCN-Runoff: An ArcGIS tool for generating curve number and runoff maps', *Environmental Modelling and Software*, 19(10), pp. 875–879. doi: 10.1016/j.envsoft.2004.03.001.
- Zhang, G., Su, X., Ayantobo, O. O., Feng, K. and Guo, J. (2020) 'Evaluation of open access precipitation and temperature products using SWAT in Shiyang river basin, Northwest China', *Preprints*, (March). doi: 10.20944/preprints202003.0294.v1.
- Zhang, L., Nan, Z., Xu, Y. and Li, S. (2016) 'Hydrological impacts of land use

change and climate variability in the headwater region of the Heihe River Basin, northwest China', *PLoS ONE*, 11(6). doi: 10.1371/journal.pone.0158394.

- Zhang, Y. and Liang, S. (2018) 'Impacts of land cover transitions on surface temperature in China based on satellite observations', *Environmental Research Letters*, 13(2). doi: 10.1088/1748-9326/aa9e93.
- Zhong, S., Qian, Y., Zhao, C., Leung, R., Wang, H., Yang, B., Fan, J., Yan, H., Yang, X. Q. and Liu, D. (2017) 'Urbanisation-induced urban heat island and aerosol effects on climate extremes in the Yangtze River Delta region of China', *Atmospheric Chemistry and Physics*, 17(8), pp. 5439–5457. doi: 10.5194/acp-17-5439-2017.
- Zhou, S., Wang, K., Yang, S., Li, W., Zhang, Y., Zhang, B., Fu, Y., Liu, X., Run, Y., Chubwa, O. G., Zhao, G., Dong, J. and Cui, Y. (2020) 'Warming effort and energy budget difference of various human land use intensity: Case study of Beijing, China', *Land*, 9(9), p. 280. doi: 10.3390/LAND9090280.
- Zope, P. E., Eldho, T. I. and Jothiprakash, V. (2016) 'Impacts of land use-land cover change and urbanisation on flooding: A case study of Oshiwara River Basin in Mumbai, India', *Catena*, 145, pp. 142–154. doi: 10.1016/j.catena.2016.06.009.
- Zou, M., Niu, J., Kang, S., Li, X. and Lu, H. (2017) 'The contribution of human agricultural activities to increasing evapotranspiration is significantly greater than climate change effect over Heihe agricultural region', *Scientific Reports*, 7(1), pp. 1–14. doi: 10.1038/s41598-017-08952-5.

Appendix

Appendix A – Definition of the ETCCDI indices.

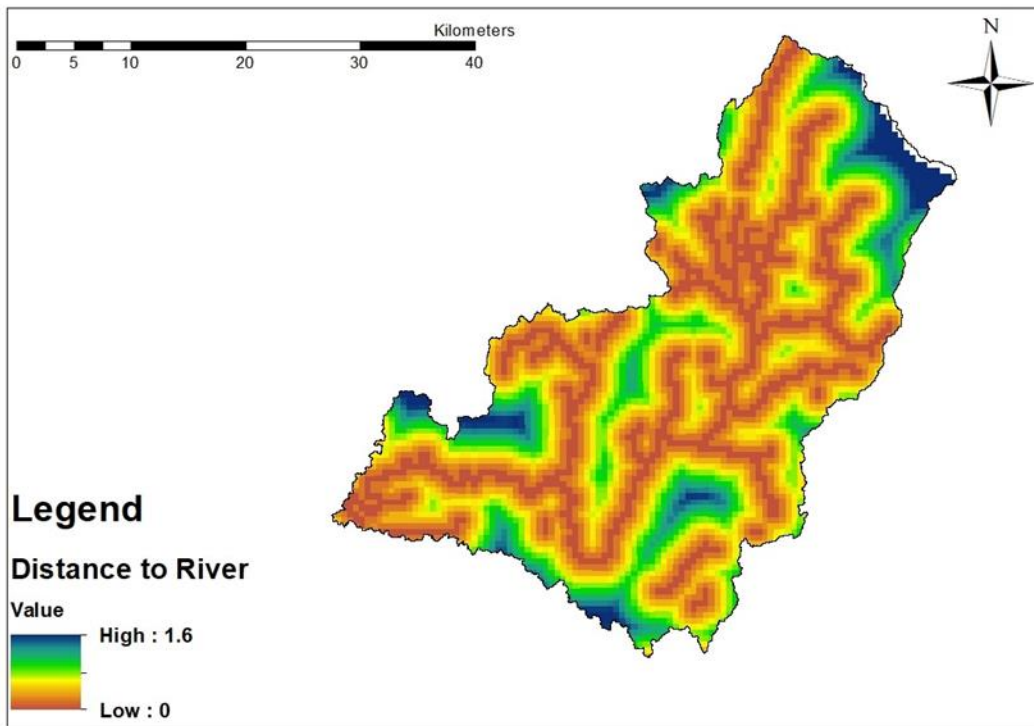
Indices	Name	Indices Calculation	Definition	Unit
FD	Frost days	$TN_{ij} < 0^{\circ}\text{C}$	Annual count of days when TN (daily minimum temperature) $< 0^{\circ}\text{C}$	Days
SU	Summer days	$TX_{ij} > 25^{\circ}\text{C}$	Annual count of days when TX (daily maximum temperature) $> 25^{\circ}\text{C}$	Days
ID	Icing days	$TX_{ij} < 0^{\circ}\text{C}$	Annual count of days when TX (daily maximum temperature) $< 0^{\circ}\text{C}$	Days
TR	Tropical nights	$TN_{ij} > 20^{\circ}\text{C}$	Annual count of days when TN (daily minimum temperature) $> 20^{\circ}\text{C}$	Days
GSL	Growing season length	$TG_{ij} > 5^{\circ}\text{C}$ $TG_{ij} < 5^{\circ}\text{C}$	Annual count between first span of at least 6 days with daily mean temperature $TG > 5^{\circ}\text{C}$ and first span after July 1st (Jan 1st in SH) of 6 days with $TG < 5^{\circ}\text{C}$.	Days
TXx,	Warmest day	$TXx_{kj} = \max(TXx_{kj})$	Monthly maximum value of daily maximum temperature	$^{\circ}\text{C}$

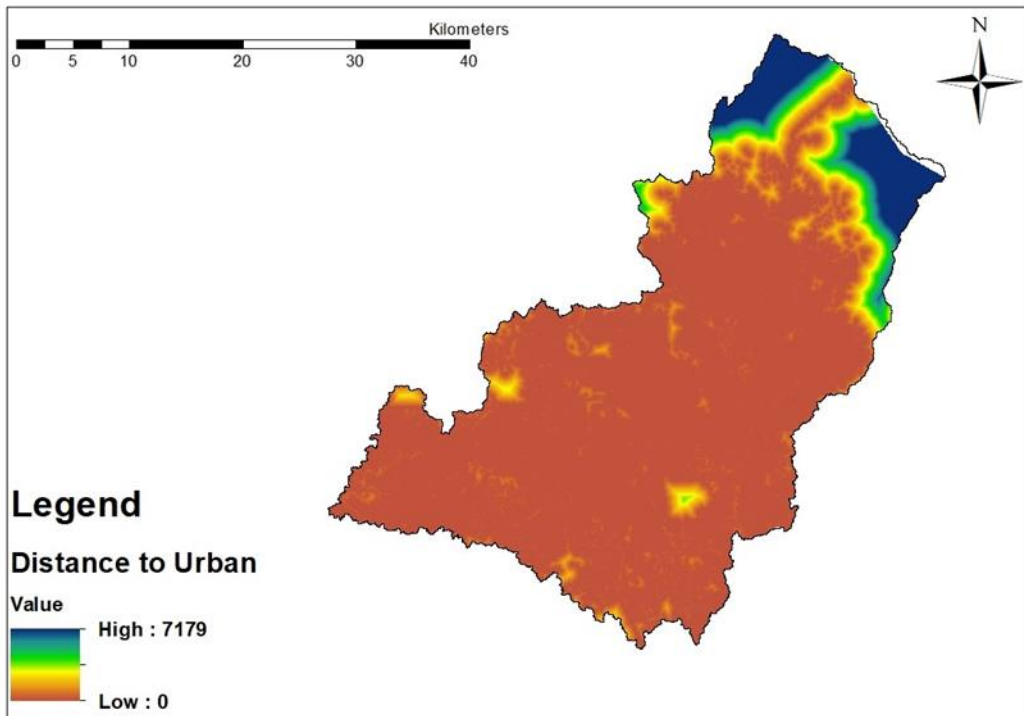
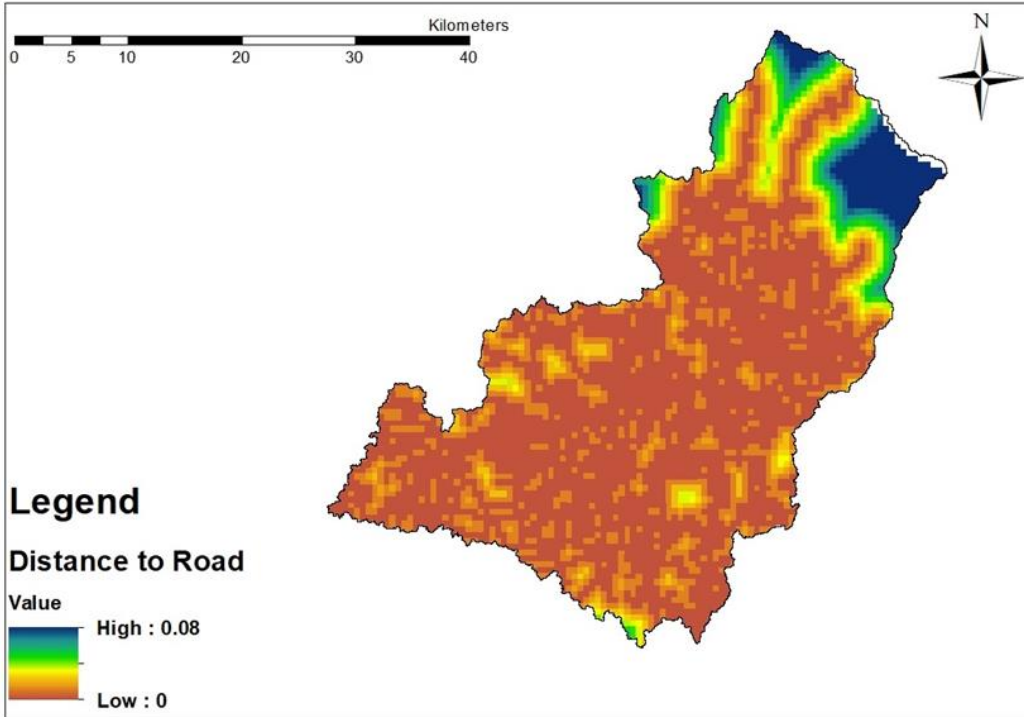
TNx	Warmest night	$TNx_{kj} = \max(TNx_{kj})$	Monthly maximum value of daily minimum temperature	°C
TXn	Coolest day	$TXn_{kj} = \min(TXn_{kj})$	Monthly minimum value of daily maximum temperature	°C
TNn	Coolest night	$TNn_{kj} = \min(TNn_{kj})$	Monthly minimum value of daily minimum temperature	°C
TN10p	Cold nights	$TN_{ij} < TN_{in10}$	Percentage of days when TN < 10th percentile	% days
TX10p	Cold daytimes	$TX_{ij} < TX_{in10}$	Percentage of days when TX < 10th percentile	% days
TN90p	Warm nights	$TN_{ij} > TN_{in90}$	Percentage of days when TN > 90th percentile	% days
TX90p	Warm daytime	$TX_{ij} > TX_{in90}$	Percentage of days when TX > 90th percentile	% days
WSDI	Warm spell duration index	$TX_{ij} > TX_{in90}$	Annual count of days with at least 6 consecutive days when TX > 90th percentile	days
CSDI	Cold spell duration index	$TN_{ij} < TN_{in10}$	Annual count of days with at least 6 consecutive days when TN < 10th percentile	days

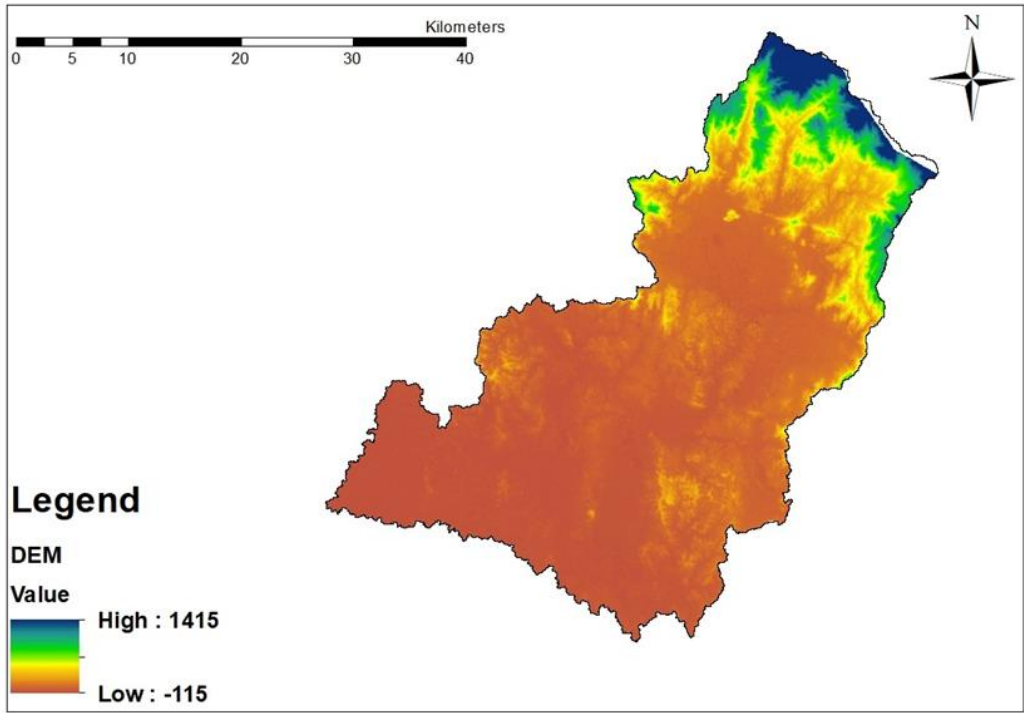
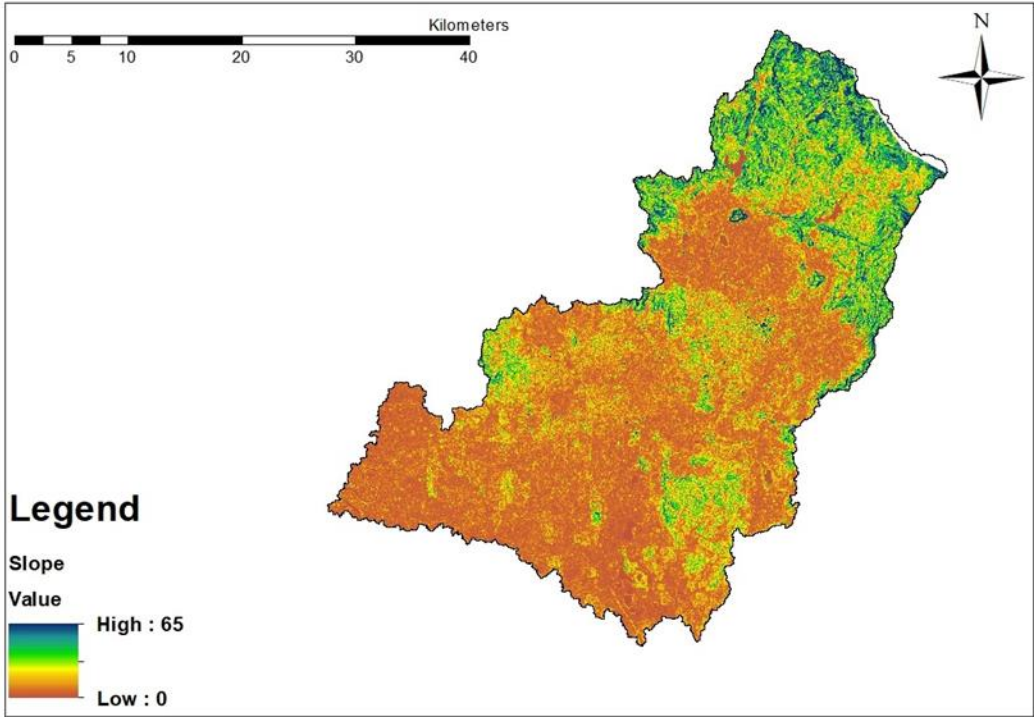
DTR	Daily temperature range	$DTR_j = \frac{\sum_{i=1}^I (Tx_{ij} - Tn_{ij})}{I}$	Monthly mean difference between TX and TN	°C
Rx1day	Monthly maximum one-day precipitation	$Rx1day_j = \max (RR_{ij})$	-	mm
Rx5day	Monthly maximum consecutive 5-day precipitation	$Rx5day_j = \max (RR_{kj})$	-	mm
SDII	Simple daily intensity index	$SDII_j = \frac{\sum_{W=1}^W RR_{wj}}{W}$	Annual mean rainfall when PRCP ≥ 1 mm	Mm/day
R10mm	Number of low to rainfall days	$RR_{ij} \geq 10$	Annual count of days when PRCP ≥ 10 mm	Days
R20mm	Number of moderate rainfall days	$RR_{ij} \geq 20mm$	Annual count of days when PRCP ≥ 20mm	Days
Rnnmm (30mm)	The number of rainfall days for user defined threshold. In this case ≥ 30mm	$RR_{ij} \geq nn$	Annual count of days when PRCP ≥ nnmm, nn is user defined threshold	Days
CDD	Maximum length of dry spell	$RR_{ij} < 1mm$	Maximum number of consecutive days with RR < 1mm	Days
CWD	Maximum length of wet spell	$RR_{ij} \geq 1mm$	Maximum number of consecutive days with RR ≥ 1mm	Days

R95p	Very wet days	$R95p_j = \sum_{W=1}^W RR_{wj}$	Annual total rainfall when RR > 95 percentile	mm
R99p	Extreme wet days	$R99p_j = \sum_{W=1}^W RR_{wj}$	Annual total rainfall when RR > 95 percentile	mm
PRCPTOT	Annual total precipitation in wet days	$PRCPTOT_j = \sum_{i=1}^I RR_{ij}$	-	mm

Appendix B - LULC Modelling Driver variables

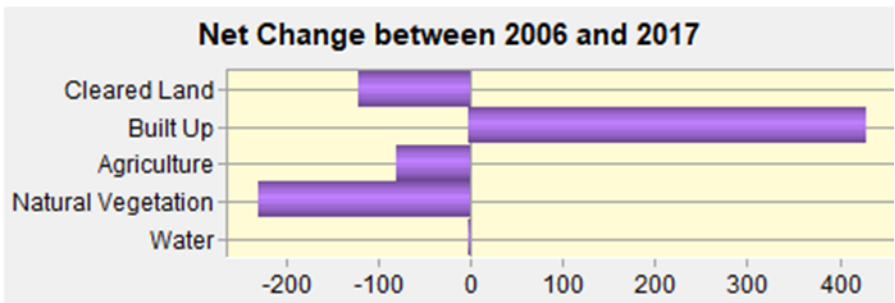
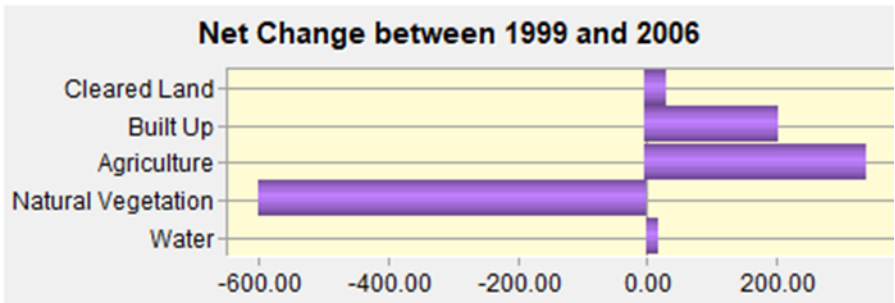
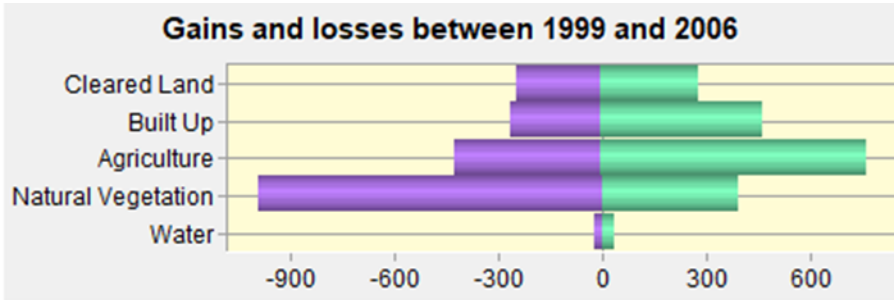






Appendix C – The Gains and Losses and Net Gain for The Year 1999-2006 And

2006-2017



Appendix D – Average Monthly Precipitation

